Change of address (with 15 days advance notice) and letters regarding subscriptions and payments should be mailed to the Secretary of the IRE, 1 East 79 Street, New York 21, N. Y.

PROCEEDINGS OF THE IRE®

Published Monthly by

The Institute of Radio Engineers, Inc.

VOLUME 45 — *January, 1957* — NUMBER 1

CONTENTS

ADVERTISING SECTION

THE COVER—A row of mechanically resonant metal disks, terminated at each end by an electromechanical transducer, forms a mechanical filter which can be used in electrical circuits. At frequencies below one megacycle, mechanical filters can be designed to have a more nearly rectangular frequency response curve than can conventional electrical filters, as demonstrated by the respective red and dotted-white curves. This feature makes the mechanical filters especially well suited for such demanding tasks as separating a series of carrier-system channels only 4 kilocycles wide, as depicted in the background. An excellent survey of mechanical filters starts on page 5 of this issue.

John T. Henderson

PRESIDENT, 1957

John T. Henderson was born on December 9, 1905, in Montreal, Canada. He received the B.S. and M.S. degrees in engineering physics at McGill University in 1927 and 1928, respectively, and the Ph.D. degree from the University of London in 1932. He carried out ionospheric experiments during the total solar eclipse in Canada in 1932, and studied further in Munich, Germany until 1933.

In 1933 Dr. Henderson joined the staff of the National Research Council of Canada in Ottawa. As head of the radio section he participated in direction-finding experiments on atmospherics in Ontario and Manitoba which gave rise to the development of a shortwave cathode-ray direction finder, widely used by the Royal Canadian Navy during World War II.

In 1939 Dr. Henderson represented Canada at the first official disclosure of British radar to the Commonwealth countries. He returned to Ottawa to start similar work at the Council, directed the development of radar equipment for the armed services, and contributed in organizing the radar division of Research Enterprises Limited, a Crown company for quantity manufacture of the Council's wartime developments.

From 1942 to 1946 Dr. Henderson served as an officer in the Royal Canadian Air Force, where he was concerned with the installation and operation of the early warning radar chain in Nova Scotia, Newfoundland, and Labrador. He later served overseas.

Returning to the National Research Council, Dr. Henderson was the Canadian delegation's scientific advisor to the United States Atomic Energy Commission. Back in Ottawa, he headed a group studying the application of radar to surveying, and succeeded in evolving methods now used extensively in northern Canada by the Dominion Geodetic Survey and Royal Canadian Air Force. In 1949 he took charge of the Council's electricity laboratory to expand its scope and set up new absolute electrical standards for Canada in conformity with international agreements.

Dr. Henderson joined the IRE in 1928 as an Associate, became a Senior Member in 1947, and was elected Fellow in 1951. A member of the Ottawa Section, he was Vice-Chairman in 1949–1950, Chairman in 1950–1951, and Director of the IRE Canadian Region from 1953 to 1956

Notices

Obituaries

Photographs

Poles and Zeros

Professional Groups

Report of Secretary

Scanning the Issue

Sections and Subsections

Poles and Zeros

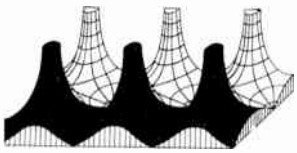

Staff. January being the traditional time for taking statistical stock, we present this month a brief resume of publications activity during the past year and an introduction to the members of the staff who have handled the editorial load at Headquarters. During 1956 the Institute published 96 issues of its publications: 12 PROCEEDINGS, 4 Student Quarterlies, the Directory, the IRE CONVENTION RECORD in 9 parts, and 70 Professional Group TRANSACTIONS. This is a two-foot shelf comprising over 13,000 pages and no fewer than eight million words, not counting illustrations. This huge random-access memory is IRE's contribution to the all-industry professional computer—160,000,000 bits, in fact.

Responsibility for this massive editorial output is shared by two groups, the volunteers and the staff. The volunteers, the IRE members who write and review papers, prepare standards, admit members and bestow awards—are recognized in bylines and committee lists. But the staff members, to whom are entrusted the myriad details of correspondence, proofreading, and contact with the printer, have with few exceptions labored anonymously.

The picture below is presented to correct this situation. Shown are Managing Editor E. K. Gannett, Assistant Editor Helene Samuels, and the 23 other members of the Headquarters Editorial Staff. Gannett, besides acting as grand vizier for the most attractive staff in professional journalism, accepts or rejects PROCEEDINGS papers on the reviewers' recommendations. He writes "Scanning the Issue" (he reads *all* the technical papers); he assembles special issues, procures review and tutorial papers, determines print runs, costs and schedules, and he is the HQ liaison officer with the editors of the TRANSACTIONS.

Miss Samuels is responsible for the editorial functioning and staffing of the department, and in particular directs the editing and production of the letterpress division, which produces the PROCEEDINGS, 13 TRANSACTIONS and special publications.

The offset division (offset is the method of photographic reproduction of typewritten copy, in use by 10 of the TRANSACTIONS), is supervised by Anita Mason. The Directory division, headed by Isabella Lewine, operates all year preparing 50,000 questionnaires, handling some 30,000 additions, deletions and corrections, and reading proof. Four members comprise the office staff, outside these three divisions; they maintain the direct contact with authors and reviewers and keep track of the 1000-plus manuscripts that arrive at Headquarters in the course of a year.

The wonder is that the staff, so heavily of the distaff persuasion, has mastered this highly technical operation. What confusion there is is confined to such cases as the missing author: after a long search, one of the editorial assistants reported that she could find the paper by J. J. Jones, but she could *not* locate the manuscript by Mr. Jones and his co-author, G. E. Syracuse.—D.G.F.

Front row, left to right—Diana Shapiro, Mignonne Snyder, Patricia Penick, Anita Mason, Isabella Lewine, E. K. Gannett, Helene Samuels, Dolores Asensio, Lorrain Isaac, and Emanuela Formica. *Back row, left to right*—Sandra Linkoff, Ruth Brown Sturm, Maryan Malone, Caroline Goetzel, Joan Hamlett, Dorothy Gordon, Elenor Johanson, Violet Krupansky, Ruth Meyerson, Charlotte Wagner, Carmella Scafidi, Leda McNally, Nancy Gilligan, Kathryn Hamill, and Dolores Sherwood.

Scanning the Issue

Survey of Mechanical Filters and Their Applications (Hathaway and Babcock, p. 5)—The first paper in the issue reviews a circuit element that has become of increasing importance in the last ten years as a highly selective filter in the 50 to 1000 kc range, especially in IF circuits. The mechanical filter consists of a series of mechanically resonant metal plates, rods or disks, which are coupled to the electrical circuit by means of electromechanical transducers. Because of the extremely high Q of the mechanical elements, these filters can be designed to have much narrower bandwidths and sharper cutoffs than electrical filters, characteristics which make them especially well suited for carrier systems and single sideband circuits.

Phase-Shift Radio Teletype (Costas, p. 16)—A teletype transmission system is described in which "mark" and "space" signals are indicated by reversing the phase of the carrier, instead of shifting its frequency as is usually done. A phase-sensitive detector is then employed at the receiving end to extract the mark-space information from the signal. This detection process requires that the phase of the receiver oscillator be locked to the phase of the carrier. Since the received signal contains no carrier component to lock to (it is actually a suppressed-carrier AM signal), the author resorts to a novel synchronizing technique reported in the Single Sideband Issue last month, in which carrier phase information is derived from the sideband components of the signal. This method of using the signal itself to obtain phase control eliminates the need for maintaining an extremely precise control of frequency in both the transmitting and receiving equipment, resulting in a system comparable to others in performance and superior in respect to simplicity and cost of equipment.

The Vernier Time-Measuring Technique (Baron, p. 21)—An ingenious method is presented for measuring with greater accuracy the time interval between two random, nonrepetitive occurrences by making use of vernier measuring techniques. By using a continuously running master "clock" and counting the number of "ticks" that occur between two random pulses, the time interval between the two pulses can be measured to the nearest number of ticks. Still unmeasured, however, is the small extra interval that transpires between the first pulse and the first tick and between the last tick and the second pulse. Therefore two vernier clocks are added to the system which are triggered respectively by the first and second pulse, and which run a little faster than the master clock. The number of ticks each vernier clock takes to catch up to the ticking of the slower-running master clock provides a measure of the extra intervals at the beginning and end. This technique, which has proven accurate to ten millimicroseconds, extends substantially the accuracy of previous methods of timing random events.

Measurements of Instantaneous Frequency with a Microwave Interferometer (Raabe, p. 30)—A technique for measuring instantaneous frequency is described which makes use of the fact that the nodes of a standing wave squeeze together or spread out as frequency changes. A probe placed on a transmission line, containing a wave pattern set up by the wave under study, will see frequency variations as changes in amplitude caused by the shifting nodes. Since any change in the amplitude of the input wave itself will give a false indication of frequency variation, the author has devised a two-probe arrangement that greatly reduces this source of error. The resulting device provides a useful tool for studying the operation of microwave equipment, such as magnetrons and radar systems, and at the same time presents an interesting contribution toward making FM detectors more immune to AM.

Surface Leakage Current in Silicon Fused Junction Diodes (Cutler and Bath, p. 39)—This paper presents a study of the effects of surface leakage currents on the behavior of silicon junction diodes. The author develops a simplified model for analyzing the forward and reverse currents in terms of a junction current and a channel leakage current. A comparison of theoretical and experimental results shows that the model provides a useful first-order approximation for explaining a number of puzzling features of silicon diodes.

On the Mechanisms of Radar Sea Clutter (Katzin, p. 44)—Considerable effort has been made during the past decade to understand more fully radar reflections from the sea, since this effect frequently limits the ability of radar to detect targets on or near the surface of the sea. This understanding has been made quite difficult because of the complicating effects of the depression angle of the beam, polarization, frequency and condition of the sea surface. This study makes substantial progress toward reducing the discrepancies that have existed between theory and observed results, primarily by taking into account secondary reflections which have already proved to be important in analyzing reflections from surface targets but which have not heretofore been applied to the sea clutter problem.

Measured Statistical Characteristics of VLF Atmospheric Radio Noise (Watt and Maxwell, p. 55)—The great variety in the types of radio facility currently in use has created a need for a more accurate description of the world's noise field than is now available. This is particularly true at vlf, the domain of very-long-range navigational systems, where noise is greatest. This study of the statistical characteristics of atmospheric noise will be immediately useful to those engaged in system planning and in studies of information transfer; but it will also be important to the basic science of propagation, which has already profited greatly from the work on atmospherics. The authors report new and interesting observations —their work is the first to show the effect of latitude upon the noise statistics—and presentation of their results will be important both educationally and as a stimulus to further research.

IRE Standards on Electron Tubes: Physical Electronic Definitions (p. 63)—This important Standard defines terms which relate to basic physical properties and characteristics associated with electron tubes, and includes such fundamental terms as "electronics."

Confined Electron Flow in Periodic Electrostatic Fields of Very Short Periods (Chang, p. 66)—A new and potentially important method of focusing electron beams is disclosed which utilizes electrostatic rather than magnetic fields as a focusing force. By making use of the centrifugal force of rotating electrons as a restoring force to balance the strong focusing action caused by the electrostatic field, a focusing system results that is considerably more stable than previous ones. This development offers the possibility of a light weight focusing system that may result in a major simplification of traveling-wave tubes.

Signal-Flow Graphs and Random Signals (Huggins, p. 74) —In this novel discussion the author shows how methods that have been developed to solve circuit theory problems can be applied to solving some fairly difficult problems that arise in probability and statistical communication theory. The circuit theorist's tool he uses is the signal-flow graph. Important relationships between stochastic processes and familiar circuit concepts are illustrated by calculating the probabilities associated with four coin-tossing experiments, and from there he moves on to determining expressions for the power spectra and correlation functions of signals arising from Markoffian processes. Readers will find this a well written and stimulating study.

Survey of Mechanical Filters and Their Applications*

J. C. HATHAWAY†, MEMBER, IRE, AND D. F. BABCOCK†, SENIOR MEMBER, IRE

The following paper is one of a planned series of invited papers, in which men of recognized standing will review recent developments in, and the present status of, various fields in which noteworthy progress has been made.—*The Editor*

Summary—Since the inception of mechanical filters several years ago, their many desirable features have resulted in many applications. As filtering requirements have become more stringent, the improved performance of mechanical filters has become more pronounced. *Q*'s in the order of a hundred times better than those of comparable electrical circuits are possible. These high *Q*'s allow the use of lossless filter design for narrow bandwidth flat-top filters with more than one section. The mechanical filter allows compact design which is consistent with the miniaturization of modern equipment.

Although numerous mechanical filters structures have been built, three types have found the most application. These are the ladder type with resonant plates interconnected by fine wires, the cylindrical rod structure machined to produce alternate necks and slugs, and a cylindrical arrangement with disk resonators interconnected by coupling wires. The center frequency, bandwidth, and filter skirt selectivity are a function of element sizes, spacing, and number of elements used. Proper selection of resonator size and shape, and proper arrangement of driving and coupling elements will suppress spurious responses, which are a major problem in mechanical filter design. Transducers used with mechanical filters provide for the converting of electrical to mechanical energy or mechanical to electrical energy and impedance matching of the filter. Of the four kinds of transducers that have been employed—electromagnetic, electrostatic, magnetostrictive, and piezoelectric—the magnetostrictive have been the most promising in regard to high frequency of operation, stability, efficiency, and economy.

Mechanical filters are especially applicable to carrier systems and single-sideband equipment, and are equally useful in band-pass filtering in high-performance communications receivers. Filters used in carrier systems have proved beneficial in providing improved performance in selecting channels and carriers with dependable, compact design. In single-sideband transmission and reception, mechanical filters are very effective in rejecting the carrier frequency and the undesired sideband. The use of mechanical filters will often eliminate an extra stage of conversion. Simplicity of design is afforded in receivers when mechanical filters are employed by eliminating the need for many IF stages to obtain the desired selectivity. A selective bandwidth arrangement is possible which occupies no more room than one conventional IF shield can. Mechanical filters may be employed in nearly any environmental condition where other filters are used. Filter designs are sufficiently rugged for application in portable and mobile equipment. Also, they are not subject to appreciable change with temperature variations. Mechanical filters have revolutionized electrical equipment design and with new design and fabrication techniques, they will continue to exert an accelerated influence in the field.

Introduction

THE APPLICATION of mechanical elements to electrical filtering problems has been receiving an increasing amount of study in recent years. As filtering requirements have become more and more stringent and the shortcomings of electrical elements have become a limiting factor in filter designs, mechanical elements have shown desirable properties. The losses and instability of electrical resonant elements have placed a definite lower limit on the fractional bandwidth of intermediate frequency electrical filters. The development of metal alloys with exceedingly low loss and very good temperature stability has added impetus to the development of mechanical filtering elements. Moreover, the increased demand for smaller size in components associated with electronic circuitry has made the small size of the mechanical filters look very desirable.

The development of constant modulus alloys suitable for use in mechanical filters can be traced to early work done by Guillaume[1] and Chevenard.[2] The alloys which have been of greatest importance have been those of iron and nickel. The range of investigation has been primarily between 30 and 50 per cent nickel with smaller amounts of other alloying elements. The alloy which has found frequent use in recent filter designs is Ni-Span C.[3] This is a heat treatable alloy with a nickel content of 42 per cent and small concentrations of chromium and titanium. With proper heat treatment this alloy has realized temperature coefficients of frequency less than three parts per million per degree over the range of −50°F to 150°F.

Early developments in the field of mechanical filtering dealt primarily with the use of isolated resonators as replacements for electrical resonant elements. This includes work by W. P. Mason,[4] R. V. L. Hartley,[5] H. A. Burgess,[6] and G. W. Pierce.[7] Although this work dealt with isolated resonators, it formed a background for later work in multiple section filter design. Since World War II, several organizations have pursued development of electromechanical filters for use in electronic circuitry. Among those who have developed multiple sec-

* Original manuscript received by the IRE, July 30, 1956.
† Collins Radio Co., Burbank, Calif.

[1] G. E. Guillaume, "Action des additions metallurgiques sur l'anomaliede dilatabilite desaciers au nickel," *Compt. Rend.*, vol. 170, pp. 1433–1435; June, 1920.
[2] M. P. Chevenard, "Etude de l'elastice de torsion des aciers au nickel a'haute teneur en chrome," *Compt. Rend.*, vol. 171, pp. 93–96; July, 1920.
[3] *Eng. Data Bull.*, H. A. Wilson Co., New York, N. Y.
[4] U. S. Patents 2,342,813; 2,345,491.
[5] U. S. Patent 1,654,123.
[6] U. S. Patent 1,666,681.
[7] U. S. Patents 1,750,124; 1,882,394; 1,882,396; 1,882,397.

tion electromechanical filters are R. Adler,[8] W. Van B. Roberts,[9] M. L. Doelz,[10] L. L. Burns Jr.,[11] M. L. Anthony,[12] R. M. Virkus,[12] and V. D. Landon.[13] Nearly all of this late work has been in the frequency range of 50 to 1000 kc using mechanical couplers, magnetostriction transducers, and alloy resonators.

The loss in resonant elements in the band-pass filter must be such that the fractional loss, or $1/Q$, be small with respect to the fractional bandwidth (bandwidth/center frequency) of the filter. It can be seen that, as the filter fractional bandwidth becomes 1 per cent or less, the requirements on the Q of the electrical elements become restrictive. Mechanical resonant sections commonly have Q's in the order of 10,000 or approximately a hundred times that realizable with electrical elements. This allows lossless filter theory to be used in designing narrow bandwidth filters with flat tops and with many sections having low insertion loss. An example of the comparison between a mechanical filter and a multiple section LC filter is shown in Fig. 1. These filters are compared on the basis of similar skirt characteristics. The 60-db bandwidth of the mechanical filter is 16 kc. The rounding of the LC filter response is obvious with the low Q obtainable from electrical elements. In narrower bandwidths this effect is even more pronounced. Typical mechanical filter selectivity curves are shown in Fig. 2 for bandwidths of 0.5 kc, 6 kc, and 35 kc at a center frequency of 455 kc.

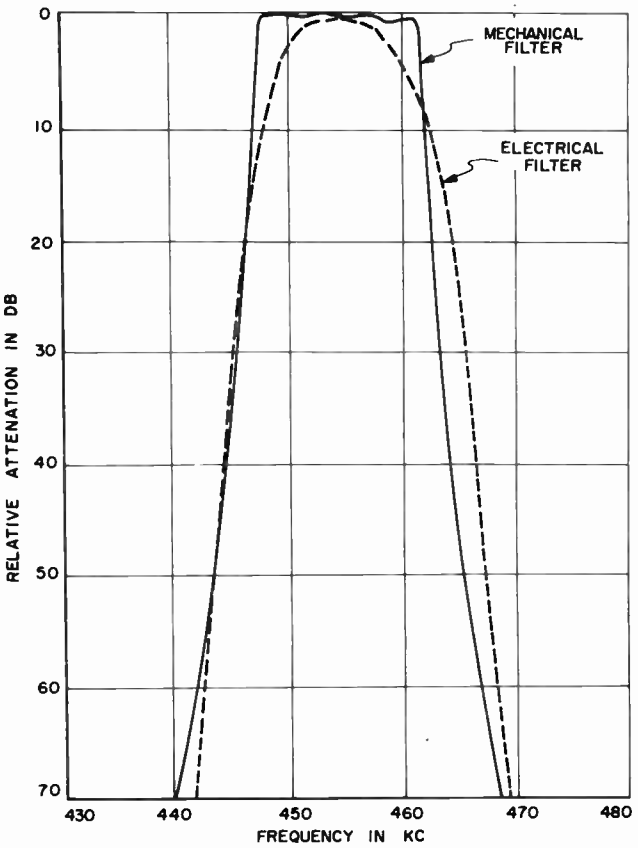

Fig. 1—Frequency response curves for mechanical and electrical LC filters.

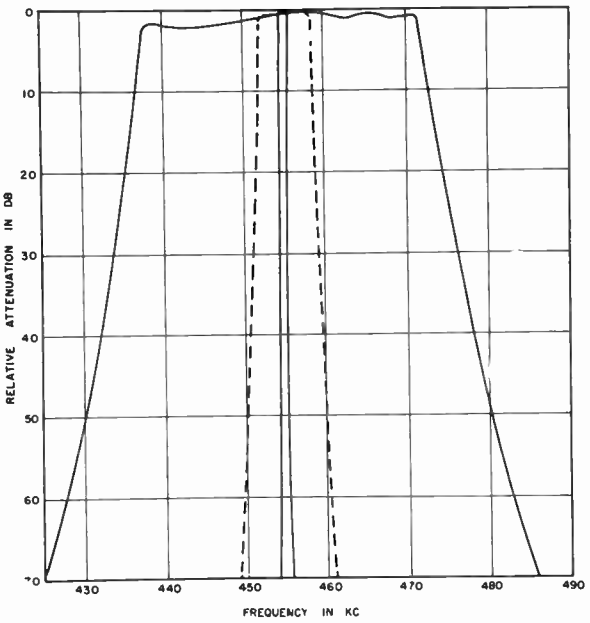

Fig. 2—Selectivity curves of 455-kc filters with nominal 6-db bandwidths of 0.5 kc, 6 kc, and 35 kc.

Filter Structures

This survey is concerned primarily with IF filters in which the selectivity characteristic is determined entirely by mechanical elements. Filters for low frequencies and those which include both electrical and mechanical elements, such as crystal lattices, are beyond the scope of this paper. Each mechanical filter has a number of resonators and couplers which form a central structure. The design of this structure is determined by center frequency, bandwidth, and selectivity requirements. Transducers located at each end of the filter provide coupling between the mechanical elements and the electrical circuit. They also provide the correct impedance for filter termination. This loading impedance is obtained from mechanical damping in the transducer and from resistance in the electrical circuit to which it is coupled.

A large number of structures have been proposed for use in mechanical IF filters. The arrangement of elements in the structure is determined largely by the choice of mechanical resonators. Of the many possible designs, three types are the most common. One employs a ladder type structure with resonant plates interconnected by fine wires. Another employs a cylindrical rod machined to produce alternate necks and slugs. In this case, either the necks or the slugs may be utilized as resonators. A third type of mechanical filter has a cylindrical arrangement with disk resonators interconnected by coupling wires. These three structures will be discussed in the following paragraphs.

[8] U. S. Patent 2,501,488.
[9] U. S. Patents 2,578,452; 2,617,882; 2,696,590; 2,647,948.
[10] U. S. Patent 2,615,981.
[11] U. S. Patent 2,647,949; 2,605,354.
[12] U. S. Patents 2,652,542; 2,652,543.
[13] U. S. Patent 2,660,712.

In 1947, Adler presented a practical design for a mechanical filter with half-wave longitudinal resonant plates.[14] A more recent model of this type has been discussed in an article by Lapin.[15] The filter structure consists of a series of flat plates interconnected by a pair of fine metal wires, as shown in Fig. 3. Each of the plates vibrates in an extensional mode with motion parallel to the long axis of the filter as shown. Resonant plates have Q's ranging from 2000 to 10,000. The two thin wires between each pair of plates expand and contract to provide elastic coupling. The center frequency of a filter is determined by the length of the plates, which must be a half-wave long at the center of the pass band. Bandwidth is a function of coupling wire diameter and length, as well as the position of wires on the plates. With a given length and position, bandwidth is approximately proportional to the cross sectional area or to the square of the diameter. The filter skirt selectivity on each side of the pass band is determined by the number of resonant plates in the structure.

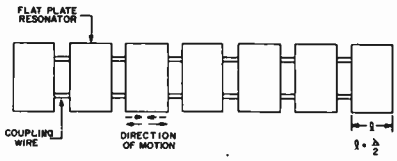

Fig. 3—Diagram of central structure—plate type filter.

Since resonators in mechanical filters are distributed elements, they have a number of natural vibration frequencies in addition to that utilized for operation of the filter. These undesired resonances give rise to spurious responses outside the pass band. Thus, the suppression of spurious responses is a major design problem. For all of the filters discussed here, spurious peaks have been minimized by proper selection of resonator size and shape, and by proper arrangement of driving and coupling elements. In recent plate type filters, spurious responses do not occur within 50 kc of the center frequency, and are more than 70 db down for all other frequencies.

A photograph of the plate type mechanical filter structure is shown in Fig. 4. This filter is designed for operation at 455 kc with a 6-db bandwidth of 10 kc. Each of the seven resonant plates is 0.250 inch by 0.398 inch by 0.010 inch. The two coupling wires between each pair of plates are $\frac{1}{8}$ wavelength, or about 0.055 inch long, with a diameter of 0.0055 inch. Filters have been constructed with up to 13 plates. The width of the central structure is approximately $\frac{3}{8}$ inch and the length slightly less than $1\frac{7}{8}$ inch. A photograph of the filter assembly is shown in Fig. 5. With this mounting, the central ladder structure is sandwiched between a

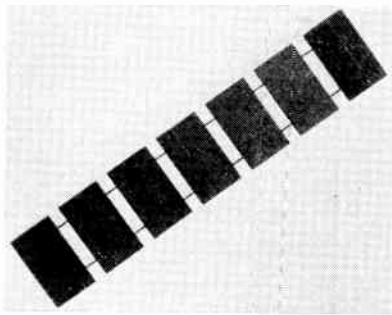

Fig. 4—Plate type filter structure. (Courtesy of Motorola, Inc.)

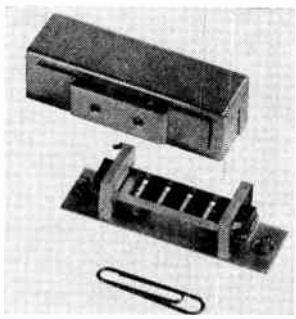

Fig. 5—Plate type filter assembly. (Courtesy of Motorola, Inc.)

bakelite retainer plate on the bottom and a cellulose retainer sponge on top. In this manner, it is protected against damage due to shock and vibration. The over-all case size is $2\frac{5}{8}$ inches by $\frac{3}{4}$ inch by $\frac{5}{8}$ inch.

In fabricating these filters, strips the width of the plates are first cut from sheets of Ni-Span C in a precision shear. These are then cut to the correct length in a micrometer shear. Wires are attached to plates by a spot welding technique. Special fixtures are employed to position and hold these elements during the welding operation. This operation is sufficiently uniform to preclude misadjustment of the elements during assembly.

Another type of mechanical filter, the neck-and-slug type, has been discussed in articles by Roberts, Burns, and George.[16–18] It is illustrated in Fig. 6. The neck-and-slug type filter may vibrate in either the longitudinal mode or the torsional mode. The longitudinal mode is illustrated in Fig. 6(a). This filter has a number of small diameter neck resonators, each one-half wavelength long. Resonators vibrate with motion parallel to the long axis of the filter. Slugs are provided between resonators for coupling. This filter differs from the others discussed here in that it employs mass coupling rather than spring coupling. The center of the pass band is determined by the length of each neck resonator. Also, for a given resonator diameter, bandwidth is determined by the length and diameter of the slugs. As on the other

[14] R. Adler, "Compact electromechanical filters," *Electronics*, vol. 20, pp. 100–105; April, 1947.
[15] S. P. Lapin, "Electromechanical filters," *Radio and Television News, Radio-Electronic Eng. Sec.*, vol. 50, pp. 9–11+; December, 1953. Also, *Proc. NEC*, vol. 9, pp. 353–362; February, 1954.
[16] R. W. George, "Electromechanical filters for 100-kc carrier and sideband selection," PROC. IRE, vol. 44, pp. 31–35; January, 1956. (See p. 34.)
[17] L. L. Burns and W. Van B. Roberts, "Mechanical filters for radio frequencies," *RCA Rev.*, vol. 10, pp. 348–365; September, 1949.
[18] L. L. Burns, "A band-pass mechanical filter for 100 kilocycles," *RCA Rev.*, vol. 13, pp. 34–36; March, 1952.

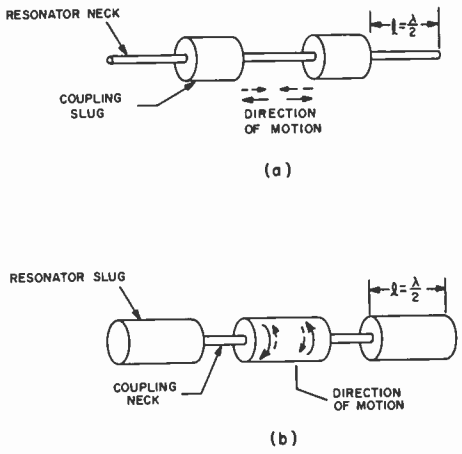

Fig. 6—Diagram of central structure, neck-and-slug type filter. (a) Longitudinal mode, slug coupled. (b) Torsional mode, neck coupled.

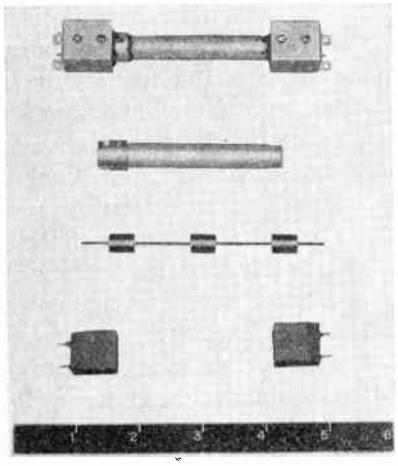

Fig. 7—Longitudinal mode, slug coupled filter. (Courtesy of Radio Corp. of America.)

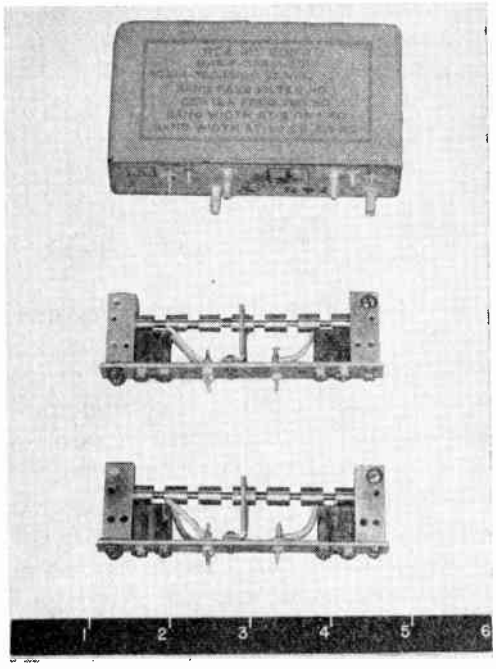

Fig. 8—Torsional mode, neck-coupled filter. (Courtesy of Radio Corp. of America.)

filters, skirt selectivity is determined by the number of resonant sections. The neck-and-slug type filter may also vibrate in the torsional mode, as illustrated in Fig. 6(b). Each large cylinder is a half-wave resonator tuned to the center of the pass band. At resonance, one end vibrates in rotation about the axis in the opposite direction to the motion of the other end. The small diameter quarter-wave sections provide spring coupling between resonators. Coupler length and the ratio of coupler neck diameter to resonator diameter determines the fractional bandwidth of the filter. For most applications, the torsional mode offers advantages over the longitudinal mode. Since the velocity of propagation for the torsional mode is about 60 per cent of the velocity for the extensional mode, the filter is more compact. Also, since the mechanical impedance of couplers is proportional to the fourth power of the diameter rather than to the square, a narrow-band torsional filter can be constructed without very great difference in diameter between the resonator and coupler portions.

An example of the longitudinal slug coupled filter is illustrated in Fig. 7. This has two half-wave resonators in the central structure as shown in the center of the figure. The three large cylinders are coupling slugs. The filter structure, consisting of neck resonators and coupling slugs, is mounted in the tubular case shown above it. Transducers at each end are inserted in coil mounting blocks at the bottom. The complete assembly is illustrated at the top of the photograph. This has over-all dimensions of approximately $\frac{5}{8}$ inch by $\frac{5}{8}$ inch by $4\frac{1}{8}$ inches. The filter is designed to have a center frequency of 105 kc and a 6-db bandwidth of 0.4 kc.

An example of the torsional neck coupled filter is illustrated in Fig. 8. This assembly employs two filters in a single case. Both have center frequencies of 200 kc. The unit at the bottom of the photograph has a 6-db bandwidth of 1 kc, and the unit in the center, a bandwidth of 3 kc. Each filter has seven half-wave torsional resonators coupled by six small diameter necks. The central structure of each filter is supported between two mounting blocks at the ends. Angle brackets are provided in the center to increase shock resistance. These two filters are mounted side by side in a case shown at the top of the picture. This has over-all dimensions of $1\frac{1}{4}$ inch by $2\frac{1}{16}$ inches by $3\frac{3}{16}$ inches.

Very narrow bandwidths may be obtained by employing multiple couplers between resonant sections. This is illustrated by the filter in Fig. 9. This model employs five half-wave resonant cylinders. These are located on each side of multiple couplers consisting of two quarter-wave necks separated by a quarter-wave slug, Fig. 10. With this arrangement, a very small coefficient of coupling can be achieved without employing extremely small diameter necks. The filter described here has a 6-db bandwidth of about 50 cycles at a center frequency of 100 kc.

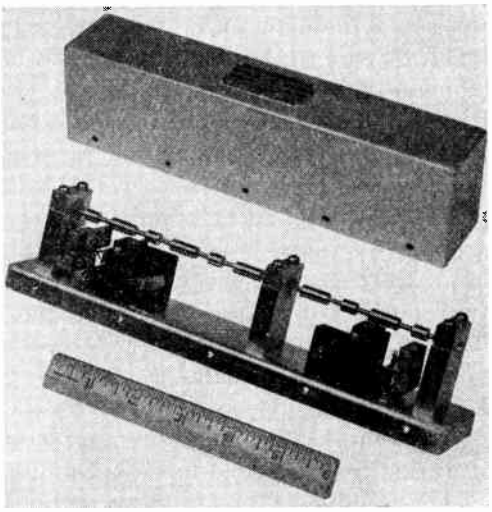

Fig. 9—Torsional neck-coupled filter with multiple couplers. (Courtesy of Radio Corp. of America.)

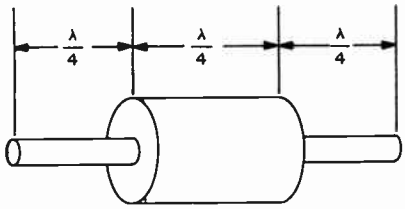

Fig. 10—Multiple coupler—neck-coupled filter.

The neck-and-slug type filter is fabricated by grinding necks in a solid rod of Ni-Span C. After grinding, resonators are individually tuned to the center frequency. During this operation, adjacent slugs are clamped, and the frequency of the resonator is determined by coupling into a coil and external measuring circuit. Frequency can be raised by removing material from a narrow band around the center or lowered by removing material from the ends. After each resonator has been tuned, the filter is securely clamped in the end supports.

A third type of mechanical filter employs Ni-Span C disks as high Q resonant elements. It has been discussed in articles by Doelz, Hathaway, and Brown.[19–21] This disk type filter is illustrated in Fig. 11. Resonators vibrate with motion perpendicular to the flat surface as shown by the two patterns in Fig. 12. Here, deflections are illustrated by cross sectional views and nodal circles by dashed lines on top views. In designing mechanical filters, a mode is selected to obtain the most convenient disk size. In most cases, the pattern with one circle is employed below 200 kc and the pattern with two circles from 200 kc to 600 kc. The resonant frequency of each disk may be varied by adjusting thickness and diameter. Disk resonators have Q's of about 10,000. Coupling in

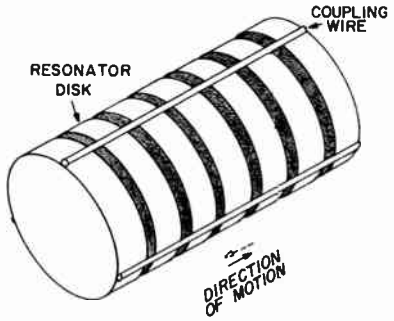

Fig. 11—Diagram of central structure—disk type filter.

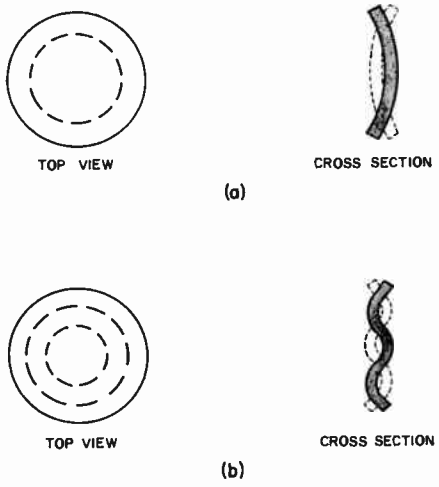

Fig. 12—Two normal modes of vibration for circular disks. (a) One nodal circle. (b) Two nodal circles.

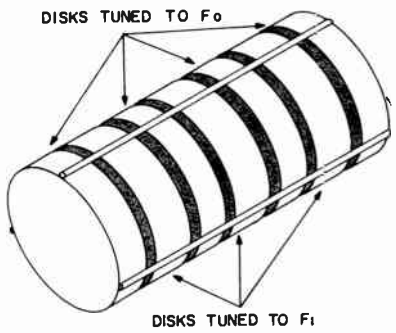

Fig. 13—Disk filter with multiple couplers.

the filter is provided by wires welded to the peripheries of disk resonators. Bandwidth varies approximately as the total area of the coupling wires, while selectivity is determined by the number of disks. With the disk type filter, spurious responses have been reduced 60 to 100 db below the pass band level. Here, as on the slug filter, it is possible to design ruggedized narrow-band models by employing multiple couplers between resonant sections as illustrtaed in Fig. 13. Four disks are tuned to the center frequency, F_0. while three alternate impedance matching disks are tuned to F_1, either above or below the pass band. Since detuned disks have a high mechani-

[19] M. L. Doelz and J. C. Hathaway, "How to use mechanical I-F filters," *Electronics*, vol. 26, pp. 138–142; March, 1953.
[20] E. M. Brown, "Using the Collins F455A-31 filters," *CQ*, vol. 9, pp. 13–19; March, 1953.
[21] E. M. Brown, "More on mechanical filters," *CQ*, vol. 9, pp. 34–36; October, 1953.

cal impedance at the center of the pass band, coupling is reduced between F_0 disks without employing small coupling wires.

Two examples of the disk type mechanical filter are illustrated in Fig. 14 and Fig. 15. Fig. 14 shows a filter with 3-kc bandwidth at 455-kc center frequency. This filter has a rigid tubular type arrangement of disks and wires. Each of the disk resonators has a diameter of 0.350 inch, and a thickness of 0.071 inch. They are separated by a space of 0.040 inch. Each of the three coupling wires attached to the disk peripheries has a diameter of 0.010 inch. The small wires attached between the end disk and adjacent disk are for the purpose of impedance matching. The central structure of the filter is supported by means of two brass tube assemblies, which also contain transducer coils. Since they do not resonate in the pass band, they have negligible effect on filter characteristics. The over-all length of the filter structure with its supporting tubes is 2 inches. Fig. 15 shows a filter with 8.5-kc bandwidth at a center frequency of 250 kc. Here, each disk resonator has a diameter of 0.630 inch and a thickness of 0.124 inch. Resonators are separated by a space of 0.050 inch. A total of 12 coupling wires 0.017 inch in diameter are required to obtain this relatively wide fractional bandwidth.

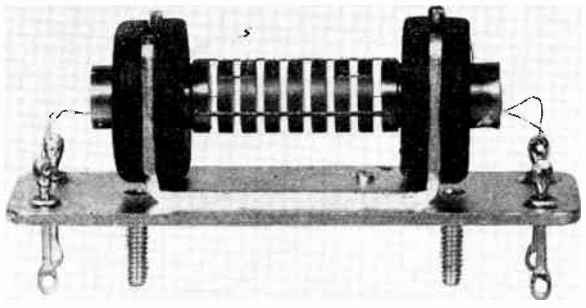

Fig. 14—Disk filter—455-kc center frequency.

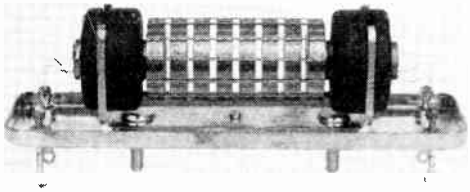

Fig. 15—Disk filter—250-kc center frequency.

Four different mechanical filter mounting cases are illustrated in Fig. 16. The filter on the right is designed for single-sideband operation at 250 kc. Its over-all dimensions are 1 inch by 1 inch by $3\frac{1}{2}$ inches. The two filters in the center are designed for AM or cw application at 455 kc. The bathtub has over-all dimensions of 1 inch by $1\frac{5}{16}$ inch by $2\frac{3}{16}$ inches, while the tubular arrangement has a diameter of $\frac{3}{4}$ inch and a length of $2\frac{5}{8}$ inches. The can on the left is a new tubular mounting with a diameter of $\frac{7}{16}$ inch and a length of $1\frac{3}{4}$ inch. It is especially desirable where miniaturization is important.

In fabricating disk type filters, resonators are cut from rods of Ni-Span C. They are then ground and lapped to a very fine tolerance. After grinding, disks are heat treated to relieve strains. Final tuning is accomplished by measuring the resonance of each disk and by grinding the required amount of material from the flat surface. Automatic equipment has been designed to perform this operation rapidly on large quantities of disks. Specially designed jigs and fixtures are employed for welding coupling wires to disks. By maintaining precise control of this operation, it is possible to obtain uniform characteristics in assembled filters without subsequent adjustment.

Fig. 16—Disk type filter mounting cases.

Electromechanical Transducers

In general there are four methods of electromechanical transduction available to the filter designer. These are electromagnetic, electrostatic, magnetostrictive, and piezoelectric. Electromagnetic and electrostatic transducers were used in several early filtering devices. Since these are lumped constant systems, their use has been restricted to the audio and ultrasonic range by parasitic resonances which limit their high-frequency performance. Magnetostrictive and piezoelectric transducers, however, are basically distributed constant systems, and may be employed at radio frequencies when proper dimensions are chosen. Transducers in mechanical filters perform a double function. They terminate the filter with the correct impedance, as well as converting electrical energy to mechanical (and vice versa). For minimum loss, it is desirable to terminate a filter with the reflected load which the transducer receives by coupling into the electrical circuit. Since electromechanical coupling is not always sufficient to provide this loading, it is frequently necessary to employ a terminating element with inherent mechanical dissipation, in addition to utilizing reflected resistance. A

transducer may be employed as the end resonator in a filter or it may be attached to the end resonator. Magnetostrictive transducers have been employed most frequently in mechanical filters because of their efficiency, economy, and stability.

Mechanical filters have been designed with magnetostrictive transducers employing either nickel-iron alloys[22] or ferrites. The principal requirements for these transducers are good magnetostrictive coupling and low temperature coefficient of frequency. A magnetic bias field is required for optimum magnetostrictive coupling. This is normally obtained from a permanent magnet located near the transducer. The signal input current is fed to a coil around the magnetostrictive element. The resulting ac field causes the transducer to expand and contract. This vibration is coupled directly to mechanical elements in the filter. Alloys have been employed as magnetostrictive transducers for many years. The principal advantage of alloy transducers is their ease of fabrication. Since they normally have high eddy current loss, it is not possible to obtain sufficient electromechanical coupling for termination of wide-band filters. Additional loading may be obtained by employing a dissipative metal, such as annealed nickel, or by coating the transducer with a viscous material, such as petroleum jelly or silicone oil. Magnetostrictive ferrites have very low eddy current loss. Filters constructed with transducers of the equimolar iron-nickel type have very small transmission loss values.[15,23] These filters have nearly constant coupling coefficients over a wide temperature range, as well as low temperature coefficients of frequency. Ferrites are particularly advantageous in providing low loss termination for wide-band filters.

Magnetostrictive drives have been employed in the three types of filter structures discussed above. The driving arrangement for a plate type filter is illustrated in Fig. 17. Here the transducer and first resonator plate are shown. The transducer plate is made of nickel or a magnetostrictive alloy. The coil provides an alternating magnetic field, causing the plate to vibrate as shown, while a ferrite permanent magnet furnishes the necessary bias. This method of coupling gives insertion loss values of 8 to 15 db per filter. Comparable inductance-capacitance filters have an insertion loss of 15 to 17 db. In a mechanical filter with high Q resonant sections, the insertion loss is concentrated almost entirely in the transducers. Thus, narrow-band multisection mechanical filters offer less loss than the corresponding electrical designs. The range of electrical termination impedance for the plate type filter discussed here is 1500 ohms to 8000 ohms.

[22] E. M. Wise, "Design of Nickel Magnetostrictive Transducers," The International Nickel Co.

[23] R. L. Harvey, "Ferrites and their properties at radio frequencies," *Proc. NEC*, vol. 9, pp. 287–299; February, 1954.

The torsional neck-and-slug type filter employs a composite end resonator for transduction, Fig. 18. A pair of longitudinal mode ferrite transducers are attached tangentially through connecting wires to a torsional resonator at one end of the filter. Two coils wound around this pair of resonators are connected to produce opposing fields. The ac field, together with the dc bias from the Alnico magnet, causes one transducer to become longer while the other becomes shorter, thereby exciting the torsional resonator. With this pair of balanced transducers, a minimum bending moment is applied to the filter. Thus objectional spurious modes are minimized. Magnetostrictive transducers have been fabricated from either a magnetostrictive alloy or a ferrite. With the ferrite, transmission loss is less than 2 db. Typical values of termination impedance range from 1500 ohms to 30,000 ohms.

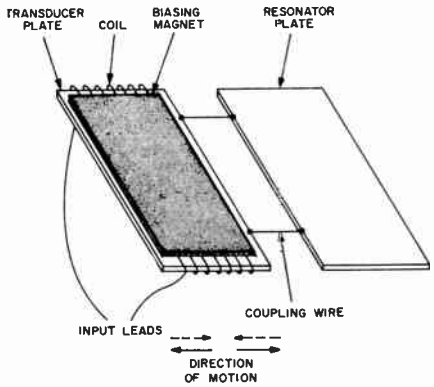

Fig. 17—Transducer for plate type filter.

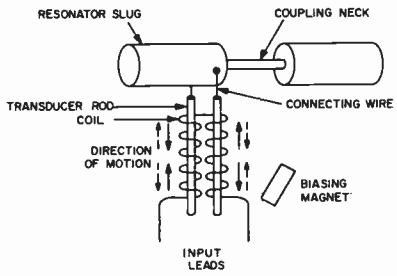

Fig. 18—Transducer for slug type filter.

Fig. 19 illustrates the transducer normally employed with disk type filters. A nickel-iron alloy wire is attached to the center of the first disk resonator. A coil is placed around the wire and a bias magnet located adjacent to the coil. Alternating fields cause the alloy wire to expand and contract with a longitudinal motion to drive the first disk. The wire is an odd multiple of a quarter wavelength long. Transducer elements may be seen in the exploded view in Fig. 20. In most filters, the transducer wire is attached to the center of the first active disk. This symmetrical drive minimizes objectionable spurious responses. A typical value of transmission loss with

high impedance load is 10 db. Here, transmission loss is equal to 20 $\log_{10} E_i/E_o$, where E_i and E_o are input and output voltages respectively. Filter input impedance may be obtained from a few hundred ohms to 50,000 ohms.

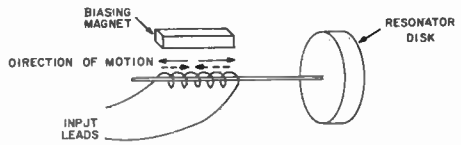

Fig. 19—Transducer for disk type filter.

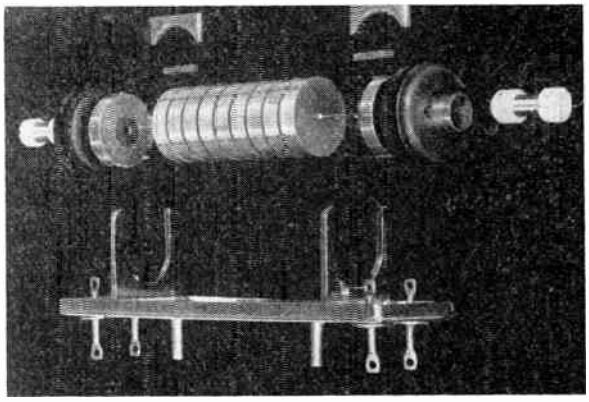

Fig. 20—Exploded view of disk filter showing transducer wire, coil, and magnet.

A special nickel-iron alloy has been developed for use in this application.[24] This material has good magnetostrictive characteristics together with a low value of Q. Thus it provides adequate impedance match for relatively wide-band filters. In addition, this material has a low temperature coefficient of frequency permitting filters to be operated over the range from −40°C. to +85°C. Transducer wires are fabricated from alloy ingots. These are rolled and drawn to the required diameter. Wire is then passed through a vertical furnace for the final anneal and straightening. As it emerges from this furnace, it is automatically sliced to the desired length. The short wires are then secured to the center of the first disk.

Most mechanical filter designs employ magnetostrictive transducers. However, it is also feasible to utilize piezoelectric elements for this application. A quartz transducer was employed to drive the plate type filter discussed above. This had a −18.5° X-cut quartz element with plating on the X-faces. Electromechanical conversion was good, but Q and impedance level were too high for satisfactory termination. Moreover, fabrication problems were more difficult than with the magnetostrictive plates. Polarized ceramic drivers, such as barium titanate, have more favorable impedance and Q values, but these have not been employed in standard designs because of difficulties with temperature coefficient and aging.

[24] U. S. Patent 2,719,084.

Filter Characteristics

The application of mechanical filters involves most of the same considerations observed in the use of electrical filters. The basic parameters of the filter are the selectivity and transfer characteristics. One essential difference in the case of mechanical filters is that the termination is only partly determined by the external electrical circuit, as some of the loading may be mechanical in the transducer. Various circuit parameters and environmental conditions which affect mechanical filter operation must be considered in order that the filter may operate in an optimum fashion.

Typical selectivity curves are shown in Fig. 21. The

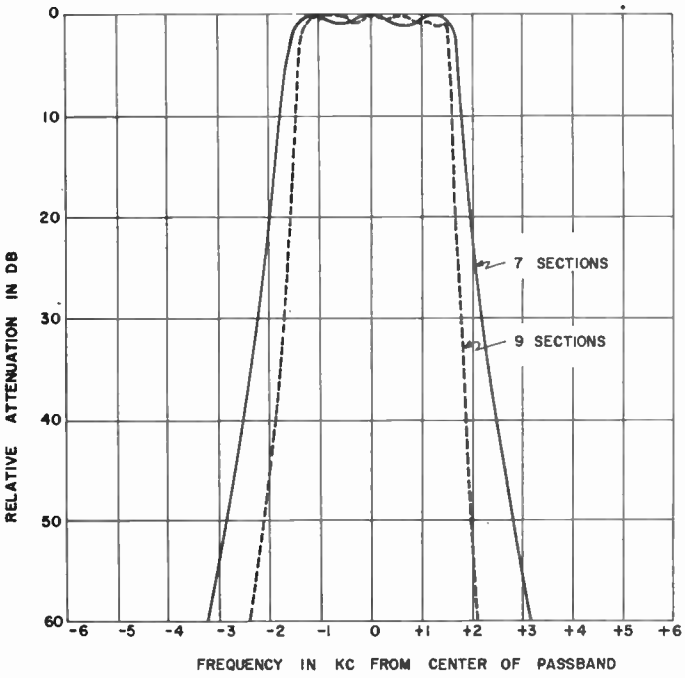

Fig. 21—Selectivity curves for filters with seven sections and nine sections.

steepness of the skirts is determined by the number of sections in each filter. The seven-section design has a 6-db bandwidth of 3.4 kc and a 60-db bandwidth of 6.3 kc. The ratio of these bandwidths, or shape factor, is 1.85 to 1. For the nine-section model, the 6-db bandwidth is 3.0 kc, and the 60-db bandwidth, 4.5 kc. This gives a shape factor of 1.5 to 1. A greater number of resonators would produce even steeper skirts. The ratio of maximum to minimum output level in the pass band is defined as ripple or peak-to-valley ratio. Here, pass band is the useful frequency range. For most applications, ripple amplitude must be 3 db or less. To produce mechanical filter designs having a minimum peak-to-valley ratio, it is essential that elements be accurately tuned and mechanical impedances be held within close limits. This requires precise control of materials and fabrication techniques. The problem is particularly critical for designs with a large number of sections. By accurate adjustment

of filter elements, it is possible to fabricate models with peak-to-valley ratio of less than 1 db.

In designing circuits with mechanical filters, it is important to consider the rated impedance and loss values. A circuit diagram of a mechanical filter network is shown in Fig. 22. In this diagram, R_s and R_0 are source and load

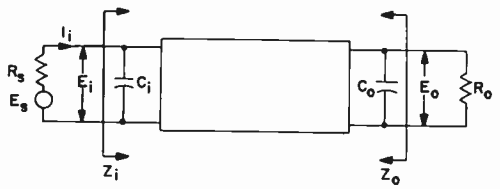

Fig. 22—Network parameters.

resistance, respectively. Since electrical loading affects the pass band ripple, it is important to employ rated values of R_s and R_0, especially with low-loss filters. The capacitors, C_i and C_o, are required to resonate input and output transducer coils. Since the coils reflect reactance back into the filter, it is necessary that the capacitance be maintained within a given tolerance to maintain the specified values of transmission loss and peak-to-valley ratio. Filter losses in the pass band have been defined in terms of insertion loss or transmission loss with open circuit load. Insertion loss values are useful for filters operated with matched impedances, while transmission loss values with open circuit load are useful in pentode IF amplifiers where both source and load impedance are much greater than filter impedances. Filter insertion loss values range from less than 2 db for ferrite transducers to 16 db for alloy transducers. Another useful parameter is the transfer impedance. The over-all gain of a pentode amplifier stage with a mechanical filter may be determined by multiplying the g_m of the tube by the transfer impedance of the filter. The input and output impedances, Z_i and Z_o, are measured across the parallel resonant capacitor and transducer coil. These impedances are largely resistive and have typical values ranging from 1000 ohms to 50,000 ohms. Filter characteristics are adversely affected by excessive dc, I_i and by excessive ac input voltage, E_i. Direct current affects the magnetic biasing field of the transducer. For minimum transmission loss and peak-to-valley ratio, this current must be maintained below a rated value. An excessive input voltage applied across the transducer coil causes nonlinear operation. Thus for minimum distortion, filter input voltage should be less than the rated value.

Mechanical filters are suitable for application in environments generally considered suitable for electrical filters. The elements in mechanical filters are fabricated from special alloys to minimize temperature changes. With Ni-Span C resonators it is possible to have frequency drift below 10 parts per million per degree centigrade. Also, with low temperature coefficient transducer alloys or ferrites, it is possible to minimize variations in peak-to-valley ratio. A typical operating range for a mechanical filter is −40°C. to +85°C. With mechanical structures fabricated from metal alloys, they are not damaged by extreme variations in temperature during storage. Also, with strain-relieved alloys, there is no observable drift with time.

The ability of mechanical filters to resist mechanical shock and vibration is a function of electrical design parameters. In general, wider bandwidth filters are more rugged. Filters with 3 kc and wider bandwidths have proven suitable for portable and mobile application in civilian and military equipment.

Applications

Mechanical filters may be employed for most bandpass filtering requirements in the frequency range from 50 to 500 kc. They are especially applicable to carrier systems and single-sideband equipment, as well as communications receivers with high performance requirements.

The characteristics of available filters greatly influence the design of carrier systems. The mechanical filter has been applied to these systems because of its improved performance and smaller size compared with electrical filters. Filters are used here for two purposes—channel separation and carrier selection.

In carrier system applications, it is often required that a family of separation filters be provided every 4 kc through the frequency range of the system. Fig. 23

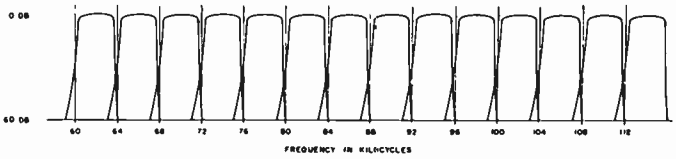

Fig. 23—Composite curves of family of mechanical channel filters designed for carrier systems.

shows a combined curve of a group of channel separation filters. In general this requirement is similar to the single-sideband requirement which will be mentioned later. However, since the carrier system signal may pass through many filters in tandem, the requirements on peak-to-valley ratio are more stringent. For optimum system performance, it is desirable that the pass band response variation be minimized.

To obtain satisfactory transmission of digital type signals through a carrier system, it is necessary to have minimum phase distortion. For no distortion, variation in phase shift β must be linear with respect to frequency, or the envelope delay, represented by $d\beta/d\omega$, must be constant. An envelope delay curve for a filter with ten sections is shown in Fig. 24. Sharp delay peaks at the edges of the pass band are associated with the very rapid cutoff on the attenuation characteristics. From theoretical analysis, it may be shown that envelope delay is related to the variation in amplitude response.[25]

[25] H. W. Bode, "Network Analysis and Feedback Amplifier Design," D. Van Nostrand Co., Inc., New York, N. Y., 1945.

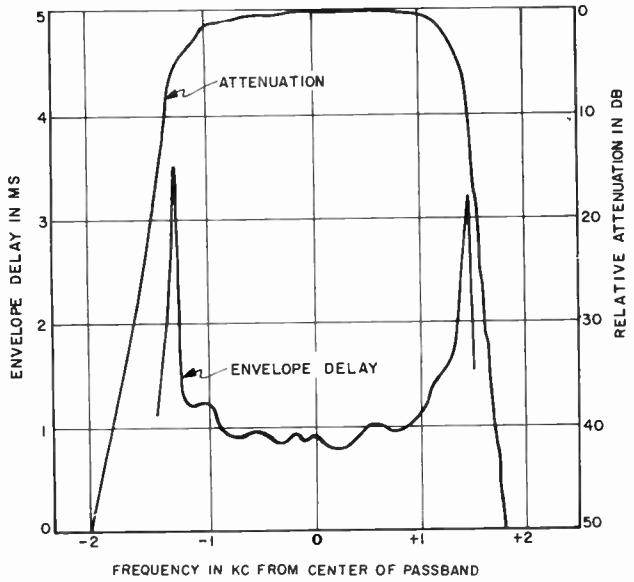

Fig. 24—Envelope delay and attenuation for ten-section filter.

In a frequency stabilized carrier system, it is also necessary to provide carrier selection filters whose function it is to select the injection carrier out of a spectrum of frequencies. A curve showing a family of these carrier selection filters is shown in Fig. 25. The compactness of mechanical filters simplifies the design of carrier frequency equipment, as shown in Fig. 26, a photograph of a carrier selector.

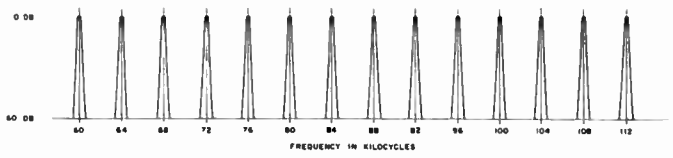

Fig. 25—Composite curves of mechanical carrier selector filters designed for carrier systems.

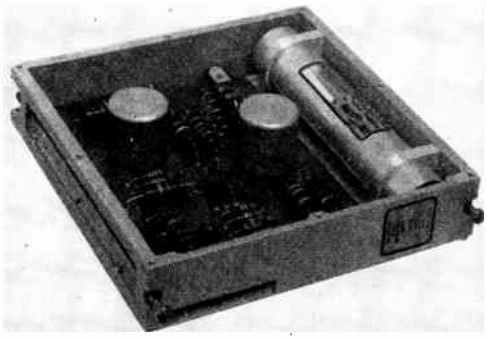

Fig. 26—Carrier system module with mechanical filter.

Mechanical filters find frequent application in single-sideband transmitters and receivers. In the transmitter, the single-sideband signal is generated at a low radio frequency where a filter of appropriate characteristics is available. This frequency should in general be as high as is practical considering the requirements of the filter. Electrical filters for this purpose have been used in the frequency range of 20 to 50 kc. Crystal lattice filters have in general been used at 100 kc. In the succeeding stages, the sideband signal is heterodyned to the final operating frequency. The low frequencies of electrical filters require one extra step of conversion. This is true because the ratio of the injection frequency to the signal frequency should always be maintained within the range of 5/1 to 10/1. This compromise is required in order to operate between the limits of spurious frequency generation and practical selectivity requirements.

A specification placed upon a filter in single-sideband applications requires a specific amount of carrier rejection. Since the filter must have very rapid cutoff from the lowest desired audio frequency to the carrier frequency, it is necessary that very high performance filters be used. In Fig. 27 are shown curves for a pair

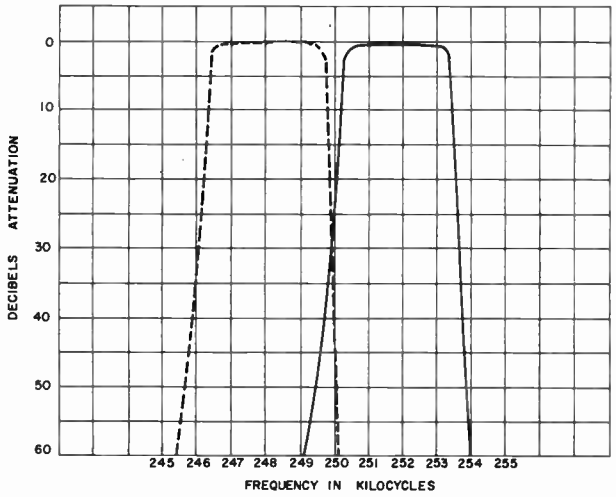

Fig. 27—Mechanical filter response curves for single sideband.

of 250-kc single-sideband filters which will provide 20 db of rejection of the carrier frequency. Since the curve of the filter is very steep in the region of the carrier, it is necessary that the temperature coefficient of frequency be small. For example, a change in frequency of the filter of 100 cps will result in a change of carrier rejection of 10 db. Also, a change in the corner of the filter will be directly translated as a change in the audio frequency response of the single-sideband transmitter. Another function of the mechanical filter in the single-sideband generator is to reject the undesired sideband. As is shown in Fig. 27, the filter will provide excellent sideband rejection.

In radio receiver applications, a mechanical filter fulfills the need for selectivity in a fashion superior to that usually provided by a multiplicity of IF transformers. Not only is the mechanical filter capable of providing

a flatter topped pass band and steeper skirts on the selectivity curve, but also its availability as a lumped selective network allows the designer considerably more freedom in providing an optimum receiver design. The problem of cross modulation or desensitization has always plagued the radio designer. The accepted ideal is to provide only enough gain ahead of the selectivity to overcome mixer noise. However, with distributed selectivity it is necessary to pick up some gain with each IF stage in order to keep the number of tubes from becoming too large. Comparison of the desensitization performance between the mechanical filter IF strip and a well-designed conventional IF transformer strip is shown in Fig. 28. By preventing overloading of the first and

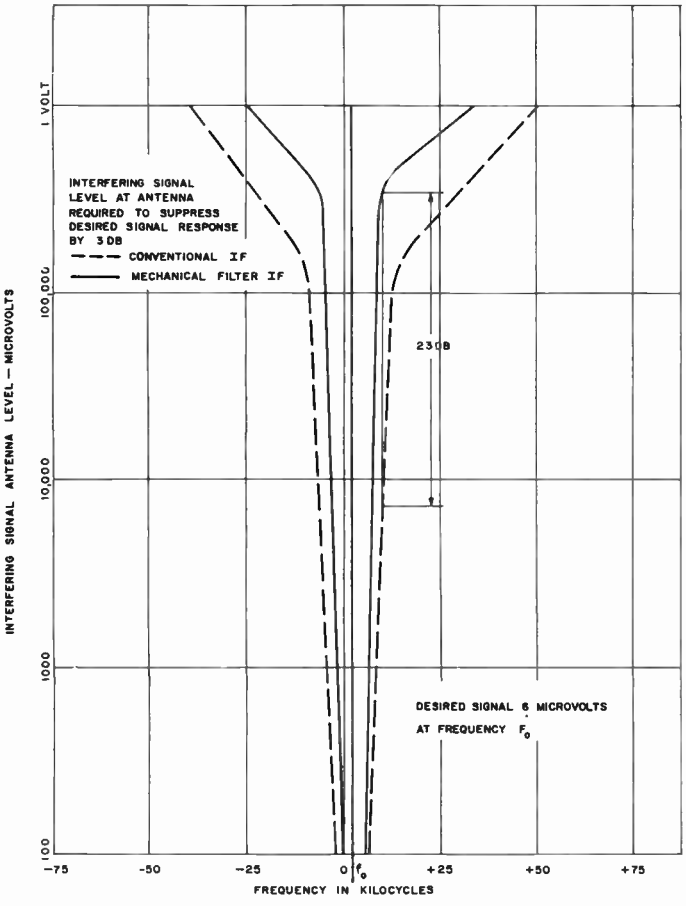

Fig. 28—Desensitization performance for mechanical filter IF strip and conventional IF strip.

second IF tubes, 23 db of improved protection is given by the mechanical filter IF strip. The use of selectivity in such concentrated form brings with it certain problems as well as certain advantages. If a high degree of selectivity is to be realized across the filter, it is necessary that the coupling be through the filter and not around it. In Fig. 29 is shown a schematic diagram of a mechanical filter stage indicating the paths by which unwanted signals may find their way around the filter.

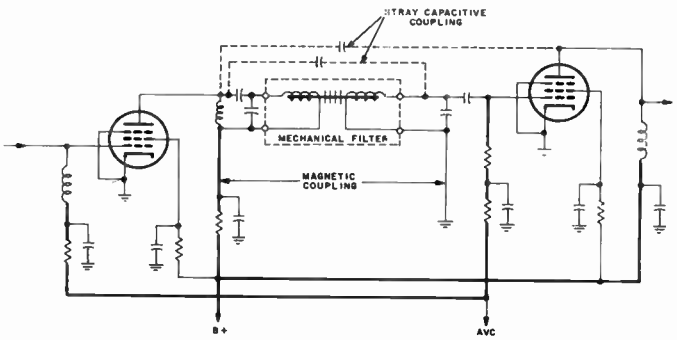

Fig. 29—Undesired coupling paths which must be reduced below 100 db for proper filter operation.

Since the filter will provide rejection band losses greater than 100 db, it is necessary that the shielding and decoupling be good to this value also.

The small size of the mechanical filter makes possible a selection of various bandwidths in very compact form. As an example of what can be done, Fig. 30 shows a four bandwidth turret which is not much larger than one conventional IF transformer. With bandwidths available from 500 cycles to 35 kc, the radio designer may easily provide whatever degree of selectivity he wants in very convenient fashion.

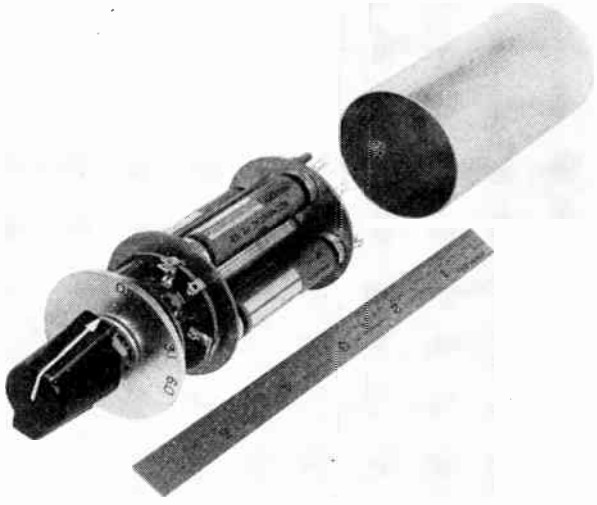

Fig. 30—Mechanical filter turret to provide selection of various bandwidths.

In the design of receivers which may be subjected to severe impulse noise interference, the response of the filters to impulses is an important consideration. Impulse response measurements are shown in Fig. 31 for filters with seven sections and ten sections. Both designs have bandwidths of 3 kc. The envelope of the response may be expressed approximately by the relation $\sin x/x$, where x is a direct function of time, for times greater than that of the main response. In the seven-section case, the impulse response rises to the first maximum 0.8

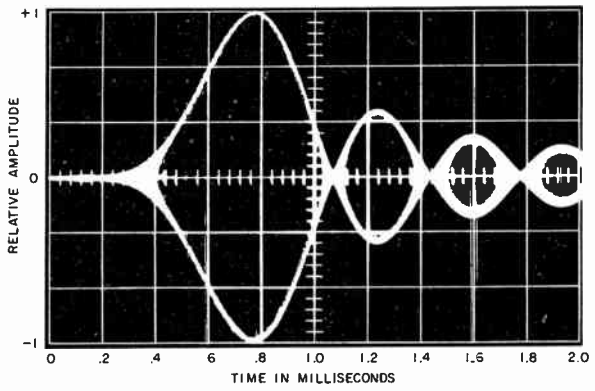

(a) Seven-section Filter.

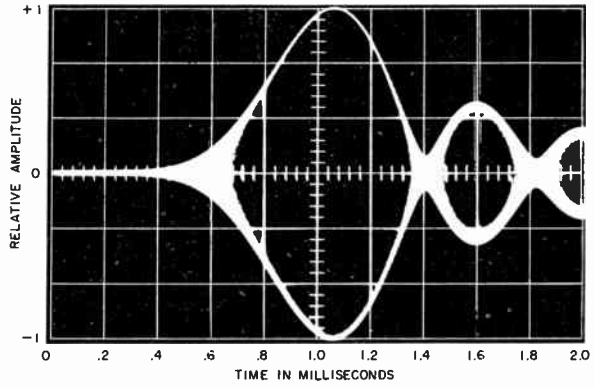

(b) Ten-section Filter.

Fig. 31—Impulse response for 3-kc bandwidth filters.

millisecond after the input pulse at $t=0$. In the ten-section case, the response is shifted with respect to time so that the maximum value occurs 1.05 milliseconds after $t=0$. The impulse response may be obtained for other bandwidths by changing the time scale. Thus, for a filter with 6-kc bandwidth, the horizontal scale in Fig. 31 would be halved.

Conclusion

Mechanical IF filters were first presented as a practical radio component nine years ago. Since that time, they have found wide application in equipment designs to provide improved performance over other types of filters. In addition to providing improved performance, mechanical filters have introduced new concepts in communication system design. It is reasonable to expect that further advancements in design and fabrication techniques will result in superior mechanical filters with an even greater range of applications.

Acknowledgment

The authors wish to express their appreciation to B. Niederman of Motorola, Inc., R. W. George of the RCA Laboratories Division, and P. D. Gerber and D. L. Lundgren of the RCA Victor Division for their kind assistance in supplying information for this paper. Thanks are also due to M. L. Doelz of the Collins Radio Company for his advice and suggestions.

Phase-Shift Radio Teletype*

JOHN P. COSTAS†, SENIOR MEMBER, IRE

Summary—**A method whereby teletype transmission is accomplished by phase-shift rather than frequency-shift keying a carrier signal is outlined. Reception methods involving coherent or synchronous detectors are presented. Results indicate that the synchronous system offers an ultimate gain of 12.5 db over FSK with 10.5 db advantage realizable in the practical case. The practical synchronous system also shows an advantage of about 2.5 db over the Predicted Wave Radio Teletype System described by Doelz and Heald.**

Introduction

THE transmission of teletype signals over radio links was originally accomplished by on-off keying for mark-space indication. It was later found that significant improvements could be obtained by carrier frequency shift for mark-space signal transmission. In one extensive test the FSK system showed an 11 db power gain over the on-off system. With these results in mind the question naturally arises as to whether FSK represents an ultimate system or whether still further improvements are possible. In a paper by Doelz and Heald[1] it is shown that FSK by no means represents the ultimate system and a Predicted Wave Radio Teletype (PWRT) system is described which shows an 8 db advantage over FSK. The PWRT system might be classed as an FSK system with the exception of the detection methods employed. Mark and space are transmitted by FSK methods, but, at the receiver, a semi-coherent detection and integration process is employed for both the mark and space channels. The larger integrator output determines the mark or space decision for a particular baud. The authors correctly point out

* Original manuscript received by the IRE, April 20, 1956.
† General Electric Co., Syracuse, N. Y.

[1] M. L. Doelz and E. T. Heald, "A predicted wave radio teletype system," 1954 IRE Convention Record, Part 8, pp. 63–69.

that by such a comparison process flat-fading can be accommodated without the use of limiting amplifiers.

Since the Doelz and Heald results will be used as a basis for comparison it will be convenient to assume a message structure similar to that employed in PWRT. The teletype output signal is retimed by storage methods into a 7 baud character of 156 ms duration with equal times assigned to each baud. This time is somewhat shorter than the shortest character time for 60 wpm teletype so that the transmission system stays ahead of the teletype at all times. On occasion, of course, a blank message will be transmitted due to higher transmission channel capacity. The retimed message structure is shown in Fig. 1. This retiming process may seem

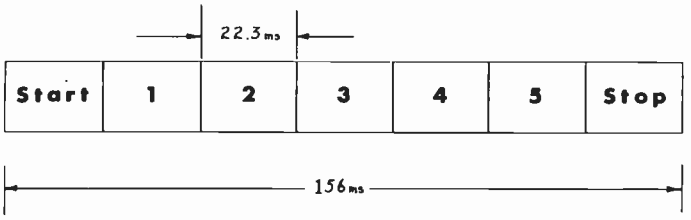

Fig. 1—Retimed teletype character.

somewhat awkward but it appears to be necessary in any advanced type transmission system. Retiming is a concession which must be made in order to realize available signal-to-noise advantages. The power gains which can be obtained should more than compensate for the required change in message structure.

Synchronous Techniques

The application of synchronous or coherent detection techniques has been a subject of considerable interest[2] for some time at the Electronics Laboratory of the General Electric Company, and much work has been done in applying these techniques to various communications problems. In this paper, however, we shall restrict the discussion to the radio teletype problem. One rather simple approach to synchronous techniques can be made by considering the ultimate situation which would result if the present trend in reducing the frequency deviation in FSK systems continues. Eventually the frequency shift becomes zero and, since something must be shifted or keyed for the transmission of intelligence, about the only thing left is phase. In other words, a carrier wave is used whose frequency remains unchanged but whose phase changes from zero to 180° with a mark-space transition. Detection of such a wave will of course require a coherent or phase-sensitive detector. A system which operates as described is shown in Fig. 2. For the present we may assume that the shaper output is a square wave of $\pm E$ volts so that the transmitted signal becomes $\pm E \cos \omega_s t$ (the + or − determined by mark or space). If the synchronous detector is assumed to oper-

[2] J. P. Costas, "Synchronous detection of AM signals," *Proc. NEC*, pp. 121–129; October, 1951.

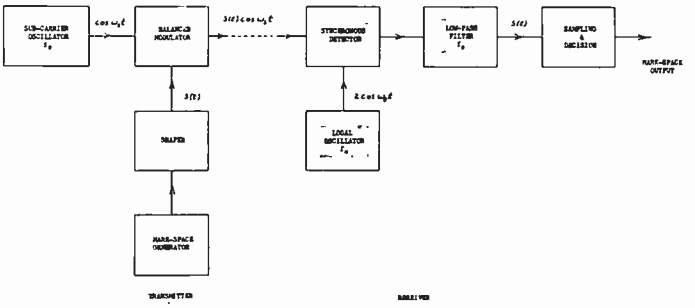

Fig. 2—Synchronous radio teletype system.

ate as a multiplier and if the low-pass filter cutoff frequency is adjusted to pass only the frequency band occupied by the $S(t)$ square wave it can be seen that $S(t)$ will appear at the low-pass filter output. This square wave is sampled and the appropriate mark-space decision is made. With this type of detector it should be noted that predetection filtering is not required since receiver selectivity is determined by the low-pass post-detector filter. It should further be noted that the low-pass filter output noise power is equal to the pre-detector noise power which falls in the frequency band $f_s - f_c$ to $f_s + f_c$. In the presence of noise the low-pass filter output is sampled at the center of each baud interval. If this sample is positive a mark decision is made; if negative the decision becomes space. In this manner flat-fading effects are eliminated (except for increased probability of error as the S/N ratio worsens which is inevitable in any system) without the use of limiting circuits. We are now in a position to examine the synchronous system in more detail.

The Ultimate Synchronous System

One question which immediately arises from the above discussion is the problem of required system bandwidth. The phase of a wave cannot be changed instantaneously without requiring infinite bandwidth and the same conditions apply to instantaneous amplitude and frequency changes. In the interest of bandwidth conservation, a shaper circuit and balanced modulator are employed at the transmitter of Fig. 2 to permit a phase transition of the transmitted signal between mark and space rather than an abrupt change. The shaper converts the mark-space generator output into a pulse train $S(t)$ composed of individual pulses $p(t)$. A positive $p(t)$ pulse results for mark and a negative $p(t)$ for space. Under these conditions the output of the balanced modulator will be a wave having both amplitude variations as well as phase reversals. In actual fact this wave is a suppressed-carrier AM signal whose modulation consists of the pulse train S(t). This prevents the use of class-C amplification of this type of signal but in most cases more than one teletype channel must be put through the main rf system. In the common multiplex operation class-C amplification would not be possible even if the individual subchannel signals were of the constant-amplitude phase-shifted variety. Thus

no practical advantage is lost by the shaping process and a bandwidth conservation per subchannel can be realized which will permit a closer spacing of subcarrier frequencies in multiplex operation. The bandwidth and power relationships of $S(t)$ as a function of pulse shape $p(t)$ are discussed in some detail in the Appendix. However, if the minimum bandwidth is to be used the pulse shape $p(t)$ must have the form

$$p(t) = E\frac{\sin \omega_c t}{\omega_c t}. \tag{1}$$

This pulse shape is the classical one which has no frequency components beyond f_c and permits independent sample values to be transmitted at a rate of $2f_c$. Thus, for a given mark-space transmission rate the pulse shape of (1) will result in the minimum bandwidth requirements. The term "ultimate" is used here in this sense. As a practical matter the choice of $p(t)$ made in (1) has certain disadvantages, one of which is the timing accuracy required for sampling at the receiver. However, it is interesting to consider this case as a limiting condition for the system of Fig. 2 and to note the loss in power gain which will result from a more practical choice of $p(t)$.

The message structure specified in Fig. 1 will require that f_c be made equal to 22.5 cycles per second and from the material in the Appendix it can be shown that the average rf signal power input to the receiver synchronous detector, $P_{\text{ave.}}$ will be given by

$$P_{\text{ave.}} = E^2/2. \tag{2}$$

If noise is present at the input to the synchronous detector the noise power at the low-pass filter output will be equal to the total predetector noise power falling within 22.5 cycles on either side of the local oscillator frequency. In other words, the receiver of Fig. 2 displays an effective predetector bandwidth of 45 cycles which is twice the cutoff frequency value of the low-pass filter.

Practical Synchronous System

The pulse-to-pulse time overlap which would result from the $p(t)$ function chosen in the section above presents a practical problem which could be overcome, but a choice of $p(t)$ will now be made which almost entirely avoids the problem. For the message structure assumed, the baud period lengths are about 22.2 ms. If some time overlap into adjacent baud periods (say 25 per cent) is assumed, each pulse could be permitted a duration of 1.5×22.2 ms or 33.3 ms. This would still leave the middle 50 per cent of each baud interval free of adjacent pulse voltages and the receiver sampling accuracy requirements would be reasonable. On this basis we may choose a pulse shape $p(t)$ of the form

$$p(t) = \frac{E}{2}(1 + \cos \omega_0 t), \quad \left(-\frac{T_0}{2} < t < \frac{T_0}{2}\right) \tag{3}$$

where

$$\omega_0 = \frac{2\pi}{T_0}, \qquad T_0 = 0.0333 \text{ sec.} \tag{4}$$

The pulse of (3) has a peak value of E volts and a duration of 33.3 ms. From the work in the Appendix it can be shown that a pulse train $S(t)$ made up of such pulses will require a baseband frequency of 60 cps and that the average rf signal power input to the receiver synchronous detector will be

$$P_{\text{ave.}} = 0.281E^2. \tag{5}$$

Since both the ultimate and practical systems produce a signal of E volts peak at their respective low-pass filter outputs, the practical system shows a power advantage of 1/0.562 or 2.51 db over the ultimate system. This advantage is lost, however, due to the increased bandwidth requirements of the practical system. Since a low-pass filter cutoff of 60 cycles must be used in the latter case a filter output noise power increase of 120/45 or 4.27 db will result. This leaves 4.27–2.51 or a 1.76 db S/N advantage for the ultimate system. Thus a practical design for the radio teletype system of Fig. 2 results in a system performance which is within 2 db of the theoretical limit. The question still remains as to the performance of the practical synchronous system relative to other systems such as FSK or PWRT.

Noise Considerations

If the noise at the input to the synchronous detector of Fig. 2 is of the usual "white-Gaussian" variety the low-pass filter output noise will also be Gaussian with a probability density distribution $W_1(y)$ given by

$$W_1(y) = \frac{1}{\sqrt{2\pi m_2}}\epsilon^{-y^2/2m_2} \tag{6}$$

where

$$\overline{y^2} = m_2 = \text{average noise power.} \tag{7}$$

It should be remembered that the average noise power m_2 at the output of the low-pass filter of cutoff frequency f_c is equal to the noise power at the receiver input which falls within the band $f_s - f_c$ to $f_s + f_c$. The noise power density in watts/cycle predetector is thus one-half the postdetector value. Since the signal (E volts peak in each case) plus noise output voltage of the low-pass filter is sampled, and since the mark-space decision is based on the sample being greater or less than zero volts, the probability of a correct baud decision $P_b(c)$ will be

$$P_b(c) = P(y < E) \tag{8}$$

or

$$P_b(c) = \frac{1}{2}\left[1 + I\left(\frac{E}{\sqrt{2m_2}}\right)\right] \tag{9}$$

where the probability integral I is defined by

$$I(x) = \frac{2}{\sqrt{\pi}} \int_0^x e^{-x^2} dx. \qquad (10)$$

Although Fig. 1 shows a character composed of 7 bauds, a little thought will show that character and baud timing in systems such as this or PWRT must be established by some independent means at the receiver. Thus the start-stop pulses should not be considered as a part of a given character. It is not obvious from the Doelz and Heald paper as to the exact number of baud decisions involved per character, but to avoid taking unfair advantage the maximum of 7 will be assumed for the synchronous system. Thus in any practical situation the synchronous system will provide better results than are indicated here.

On the basis of 7 baud decisions per character the probability of clearing an erroneous character $P_c(\epsilon)$ will be given by

$$P_c(\epsilon) = 1 - \left\{\frac{1}{2}\left[1 + I\left(\frac{E}{\sqrt{2m_2}}\right)\right]\right\}^7. \qquad (11)$$

These results were normalized to the 3100-cycle predetector bandwidth of the Doelz and Heald experiments and are shown plotted in Fig. 3. The PWRT and FSK curves are those of footnote 1. The FSK data are experimental while the PWRT data represent both experimental and computed data which are in good agreement. In the US and PS curves zero db represents equal average noise and rf signal powers in the 3100-cycle pass band. At the 0.1 per cent error lines the practical synchronous system shows a 10.5 db advantage over FSK and 2.5 db over PWRT. The ultimate and practical synchronous systems differ by the 1.76 db margin mentioned previously.

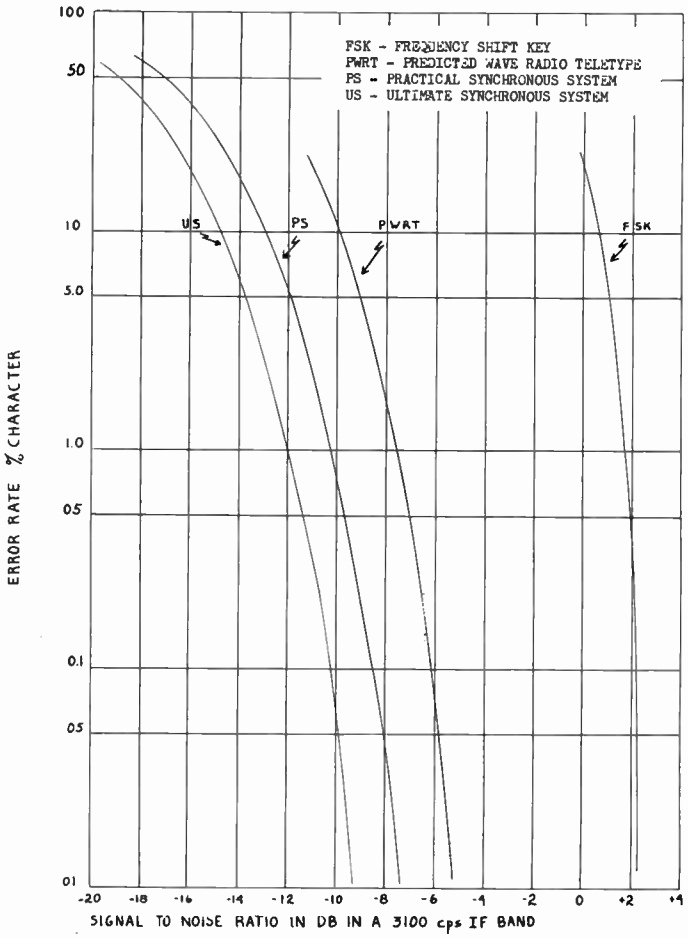

Fig. 3—Error rate vs predetection signal-to-noise ratio.

Results and Conclusions

The PWRT system represents an obvious advance in detection of FSK. The point of this paper is to show that even greater gains may be obtained by abandoning FSK as a transmission method entirely and using a phase-shift keyed (or more correctly suppressed-carrier AM keyed) signal and a synchronous or coherent detection receiver. If true coherent detection were employed with PWRT its performance would be as good in theory as that of the system described here. This still does not justify the extra bandwidth requirements of FSK as compared to phase-shift keying.

Very little has been said about actual equipment due to the nature of this paper. It might be well, however, to discuss the problem of receiver local oscillator phase control. Since the received signal contains no carrier component and since the local oscillator must be locked to carrier phase, a rather unusual phase-control scheme is called for. The carrier phase information can easily be derived from the sideband components of a suppressed-carrier AM signal by a method described in another paper.[3] This method provides a simple yet effective means for phase control and eliminates the need for frequency standards of extreme precision at the system terminals. This not only reduces system cost and complexity but provides for automatic correction of random phase variations which may arise in the transmission medium. This is not to say that no attention need be paid to oscillator stability but rather that the stabilities required are several of orders of magnitude less severe than would be required in a "clock-timed" system. Character and baud timing may be established at the receiver by similar techniques.

Physical realization of the basic system shown in Fig. 2 presents no serious problems and no unusual or critical circuits need be employed. The phase-shift radio teletype system can be implemented with a simplicity which cannot be found in other systems of comparable performance which have been disclosed to date.

[3] J. P. Costas, "Synchronous Communications," presented at the Symposium on Aeronautical Communications, Utica, N. Y.; October, 1956. Also, Proc. IRE, vol. 44, pp. 1713–1718; December, 1956.

Appendix

Pulse Shape-Bandwidth Considerations

Consider a signal voltage $S(t)$ composed of a train of pulses $p(t)$ falling at regular intervals. If the pulses $p(t)$ appear with equal probability of being positive or negative and if each pulse is independent of all other pulses, it can be shown that the autocorrelation function of $S(t)$, $\phi_{ss}(\tau)$, is given by

$$\phi_{ss}(\tau) = m\int_{-\infty}^{\infty} p(t)p(t+\tau)dt \tag{12}$$

where m is the pulse rate. Further, if the pulse is assumed to be of duration T_0 (12) may be written as

$$\phi_{ss}(\tau) = m\int_{-T_0/2}^{T_0/2} p(t)p(t+\tau)dt \tag{13}$$

where zero time represents the center of the pulse duration interval.

The power density spectrum of $S(t)$, $\Phi_{ss}(\omega)$ may be found by taking the Fourier Transform of the autocorrelation function $\phi_{ss}(\tau)$. This yields

$$\Phi_{ss}(\omega) = 2\pi m \left| P(\omega) \right|^2 \tag{14}$$

where $P(\omega)$ is the Fourier Transform of $p(t)$ as given by

$$P(\omega) = \frac{1}{2\pi}\int_{-\infty}^{\infty} p(t)\epsilon^{-j\omega t}dt \tag{15}$$

or, since the pulse is assumed to exist only for time T_0 we may write

$$P(\omega) = \frac{1}{2\pi}\int_{-T_0/2}^{T_0/2} p(t)\epsilon^{-j\omega t}dt. \tag{16}$$

In the interval $(-T_0/2, +T_0/2)$ if the pulse is symmetric about zero time $p(t)$ may be expressed as

$$p(t) = \frac{a_0}{2} + \sum_{n=1}^{\infty} a_n \cos n\omega_0 t \tag{17}$$

where

$$\omega_0 = 2\pi/T_0. \tag{18}$$

When (17) is substituted into (15) there results

$$P(\omega) = \frac{T_0}{4\pi}\left\{a_0\frac{\sin \omega T_{0/2}}{\omega T_{0/2}} + \sum_{n=1}^{\infty} a_n\left[\frac{\sin(\omega T_{0/2} - n\pi)}{(\omega T_{0/2} - n\pi)} + \frac{\sin(\omega T_{0/2} + n\pi)}{(\omega T_{0/2} + n\pi)}\right]\right\}. \tag{19}$$

Note that

$$P(n\omega_0) = T_0 a_n/4\pi \tag{20}$$

which means that

$$\Phi_{ss}(n\omega_0) = mT_0^2 a_n^2/8\pi. \tag{21}$$

Thus if the Fourier Series expansion for $p(t)$ is limited to N terms, the power density spectrum will be zero at $\omega = (N+1)\omega_0$ and for all n greater than $N+1$. The power spectrum will not be zero for frequencies between these points, but it can be shown that very little energy exists beyond $\omega = (N+1)\omega_0$ and that this frequency essentially specifies the bandwidth requirements for the pulse train. (There can be no absolute cutoff frequency since the train is made up of time limited pulses. A pulse which is limited in time cannot be also band-limited in frequency). This particular approach to the pulse shape-bandwidth problem can be quite useful since once the bandwidth is specified the designer may choose the non-zero a_n's for pulse-shaping to meet design requirements. Or in a different situation if certain demands are made on pulse shape the system bandwidth requirements can be determined. The details of this technique are beyond the scope of this paper.

Finally, once the pulse shape is specified the average power of $S(t)$ is of interest. This evaluation can be made by substituting (17) into (12) and letting τ be zero. The result is

$$P_{ave} = \frac{mT_0}{2}\left[\frac{a_0^2}{2} + \sum_{n=1}^{\infty} a_n^2\right]. \tag{22}$$

Correction

M. E. Van Valdenburg, author of "Special Case of a Bridge Equivalent of Brune Networks," which appeared on page 1621 of the November, 1956 issue of Proceedings of the IRE, has brought the following error to the attention of the editors.

Fig. 1 should have appeared as indicated opposite.

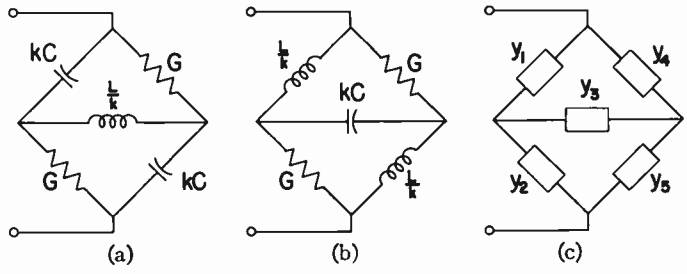

Fig. 1

The Vernier Time-Measuring Technique*

ROBERT G. BARON†, ASSOCIATE MEMBER, IRE

Summary—**This paper describes a measuring technique which is the electrical analog of the mechanical vernier scale. A system is presented that will measure the time between two pulses, which jitter relative to each other and occur at some random rate, accurate to 10 mμ sec. Pulse circuitry is employed to implement the system.**

Introduction

IT IS OFTEN necessary to measure accurately the time between two independent occurrences. When the usual methods of cathode-ray tube display or of division of the interval into quantized subintervals become inadequate due to the precision required, one must resort to other indirect methods of measurement. If the occurrences are repetitive and an average is permitted, then a counting technique may be used to integrate over a predetermined interval. However, when the interval is not repetitive or if a semi-instantaneous measurement is required, averaging techniques may not be adequate. This paper presents an extension of the accuracy of the direct method of measurement by which it is possible to measure a nonperiodic, asynchronous, and randomly jittering time interval to an accuracy of 10 mμsec.

The Vernier Technique

Consider two pulses that occur as shown in Fig. 1.

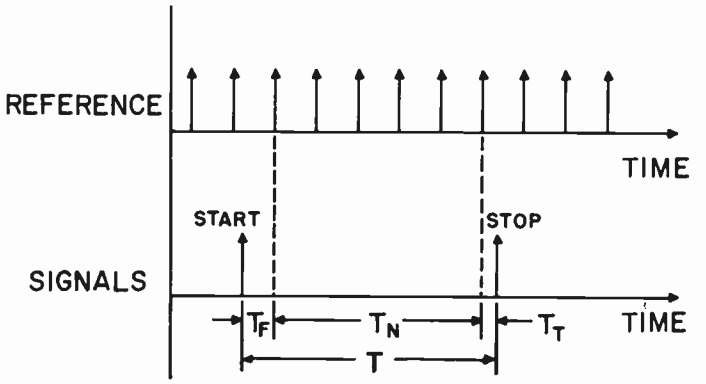

Fig. 1—Reference and signal pulses vs time.

The first signal pulse is denoted as the start pulse and the second as the stop pulse. The interval desired is the time (T) existing between the two pulses. Dividing the measurement into three parts and defining: the start interval which exists between the start pulse and the subsequent clock pulse is denoted as T_F, the number of clock references occurring between the start and stop pulses indicates the value of the coarse interval T_N, and the time between the last clock pulse within the interval and the stop pulse is denoted as the stop interval and shown as T_T. The sum of these quantities defines the total time interval, namely

$$T = T_F + T_N + T_T. \quad (1)$$

The determination of the start and stop quantities requires an additional scale. If the occurrence of a signal pulse generates a train of pulses (vernier), the period of which is less than the clock pulse period, each vernier pulse appears to advance in time on the preceding clock pulse by the difference between the pulse periods (see Fig. 2). When a vernier pulse becomes aligned with

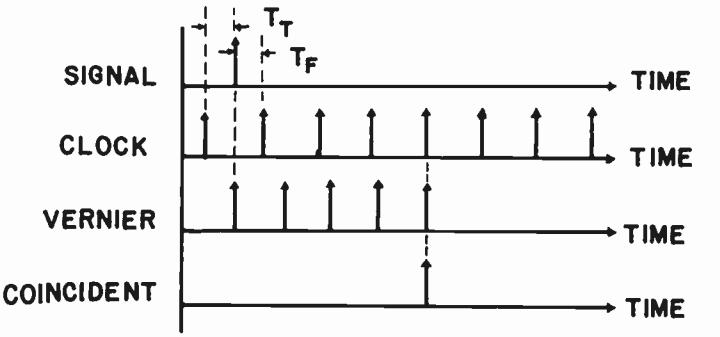

Fig. 2—Signal, clock, vernier, and coincident pulses vs time.

a clock pulse, coincidence is said to have occurred and the vernier pulses are inhibited. Since the vernier pulse period is less than the clock pulse period, the number of vernier pulses occurring before coincidence is proportional to the interval between the signal pulse and the preceding clock pulse or as defined above, the stop interval. The start interval can be determined simply by deducting the indication obtained by vernier action from the clock pulse period. A derivation which justifies the vernier count proportionality statement can be found in the subsequent text.

Combining the operations described above, the system may be diagrammatically implemented as shown in Fig. 3. The start pulse triggers the start vernier generator and opens the gate which permits the counting of clock pulses by the coarse counter. The start vernier generator and the clock generator energize the start coincident circuit, and the start vernier counter records the number of start vernier counts. At this instant, the vernier counter contains the start vernier count, and the coarse counter continues to record the coarse counts.

* Original manuscript received by the IRE, December 6, 1955; revised manuscript received, September 4, 1956. This research program was performed at Columbia University Electronics Res. Labs., New York, N. Y., for the G. L. Martin Co. under subcontract SC-53-2264-CP of prime contract AF33(038)-19639. A continuation of this work was permitted under contract AF30(635)-2815 with the Rome Air Development Center.

† International Business Machines, Airborne Computer Laboratory, Owego, N. Y.

The occurrence of a stop pulse energizes the stop vernier generator and closes the gate, thereby terminating the coarse count. In a similar manner, the stop vernier counter records the stop vernier count. The start, the coarse, and the stop indications are contained in their respective counters and the total time interval (T) is obtained by the appropriate application of (1).

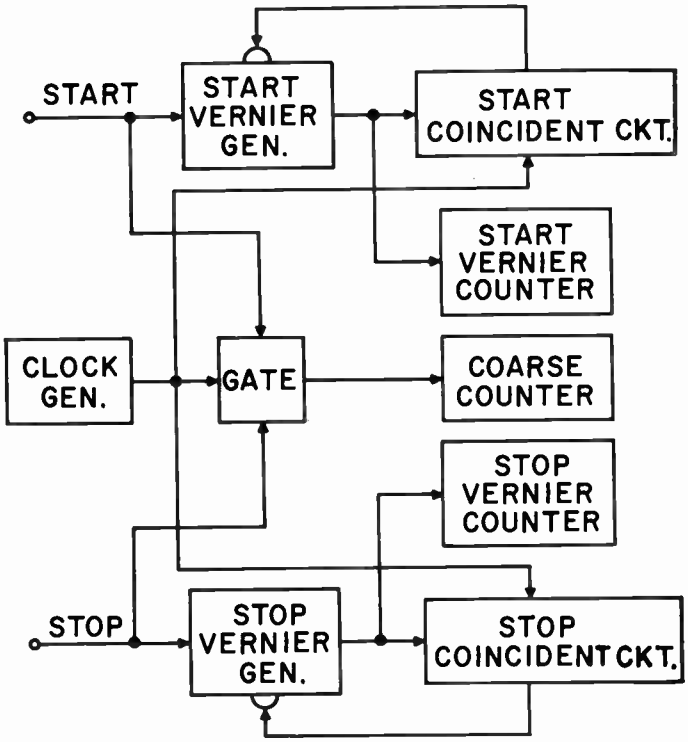

Fig. 3—Simplified system diagram.

Accuracy Considerations

In realizing the device described above, a number of details affecting the system accuracy should be considered. The important considerations are the system stability, the system resolution, and the coincident detection selectivity.

The system stability depends upon the absolute stability of the clock frequency during the coarse measurement, and the relative stability of the clock and vernier frequencies during the vernier measurements. Since the coarse interval is quantized to clock pulse periods, the clock frequency tolerance Δfc depends upon the duration of the interval under consideration. The clock frequency tolerance can be expressed as

$$\Delta fc = \pm \frac{1}{2}\left[\frac{1}{T_{C_2}} - \frac{1}{T_{C_1}}\right] \tag{2}$$

where T_{C_1} is the minimum clock period that yields the correct count minus one count and T_{C_2} is the maximum clock period that yields the correct count plus one count, as shown in Fig. 4. Expressing the periods T_{C_1} and T_{C_2} as functions of the number of clock pulses which define the coarse interval (T_N), and substituting in (2) we obtain

$$\Delta fc = \pm \frac{1}{T_N}. \tag{3}$$

If the maximum interval anticipated is 1.0 second, the stability tolerance of the clock pulse frequency should be limited to 1.0 cycle per second.

Since the vernier period (T_V) is selected less than the clock period (T_C), the system resolution (T_R) is defined as

$$T_R = T_C - T_V. \tag{4}$$

A relation between the clock and vernier periods exists (see Fig. 5), and can be expressed in general terms, namely

$$NT_V = (N-1)T_C, \tag{5}$$

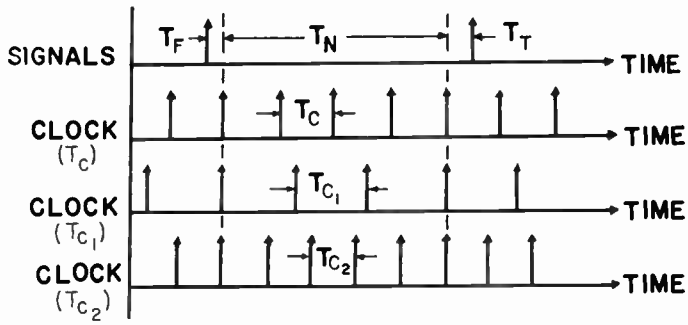

Fig. 4—Signal and clock pulses vs time (exemplifying clock frequency stability tolerance).

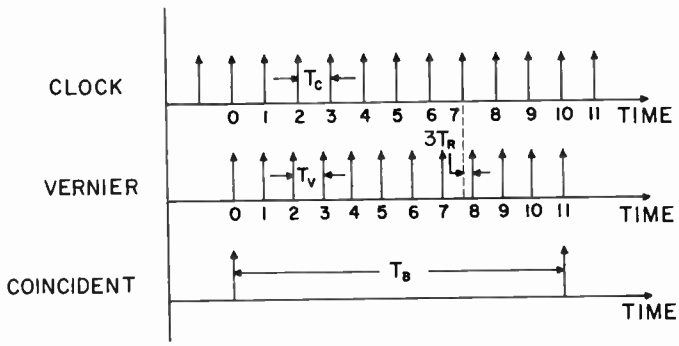

Fig. 5—Clock, vernier, and coincident pulses vs time.

where N is the maximum number of vernier pulses occurring before coincidence. Eqs. (4) and (5) determine the system resolution, the clock and vernier periods, and the maximum vernier count. For example, if the system resolution is to be 10 mμsec and the clock pulse frequency is selected as 2.0 megacycles, the vernier period should be 0.49 μsec and the maximum vernier count will be 50 vernier pulses.

To determine the vernier frequency stability required to preserve the system accuracy, consider the period of the difference beat frequency (T_B) of an ideal clock generator and a free running (uninhibited) vernier generator, as shown in Fig. 5. At the correct vernier frequency, coincidence occurs when the 0th and the Nth minus one $(N-1)$ clock pulses coincide with the 0th and the Nth vernier pulses respectively. Expressing the difference

beat frequency period as a function of the clock period, we have

$$T_B = (N - 1)T_C. \tag{6}$$

If the clock frequency is held constant and the vernier frequency varied, it is theoretically possible for coincidence to occur on any clock pulse. Letting T_{B_1} be the difference beat frequency period when coincidence occurs at the Nth clock pulse and the Nth plus one $(N+1)$ vernier pulse (see Fig. 6) and T_{B_2} be the difference beat frequency period when coincidence occurs at the Nth minus two $(N-2)$ clock pulse and the Nth minus one $(N-1)$ vernier pulse, the variation in the vernier frequency permitting the range of coincidence implied above can be found by taking the difference of the reciprocals of the periods, T_{B_1} and T_{B_2}. If the vernier frequency variation is limited to one-half the range specified above, coincidence always occurs at the Nth minus

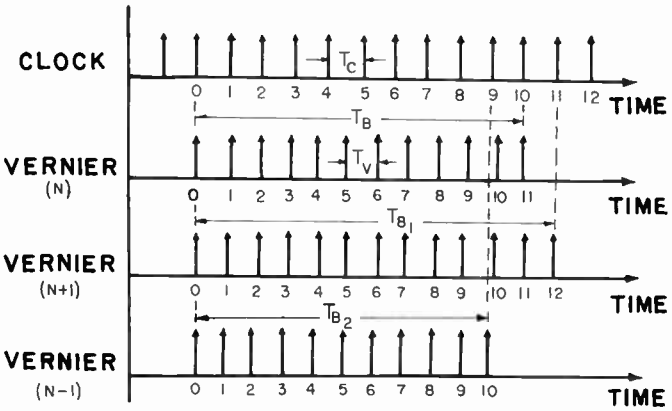

Fig. 6—Signal and vernier pulses vs time (exemplifying vernier frequency stability tolerance).

one $(N-1)$ clock pulse and the Nth vernier pulse. The vernier frequency tolerance (Δf_V) is obtained by dividing by two, so that

$$\Delta f_V = \pm \frac{1}{4}\left[\frac{1}{T_{B_2}} - \frac{1}{T_{B_1}}\right]. \tag{7}$$

Substituting for each beat frequency period the number of clock periods that define the interval, we obtain the general expression for the vernier frequency stability tolerance, namely

$$\Delta f_V = \pm \frac{f_C}{2N(N-2)} \tag{8}$$

where f_C is the clock pulse frequency. Using the numerics of a previous example, namely: a ten mμsec resolution and a clock frequency of 2.0 mc, the vernier frequency stability is approximately 400 cps or two hundred parts per million. Since a clock frequency stability tolerance of twenty parts per million presents little instrumentation difficulty, the assumption of a drift free clock frequency relative to the required vernier frequency stability appears reasonable when considering end interval measurement accuracies.

The remaining requirement concerns the coincident detection selectivity. Coincident detection is assumed to be a linear additive process in which an amplitude comparison permits a phase measurement. The clock and vernier pulses are summed and when the resulting signal exceeds a predetermined level, coincidence is said to have occurred. To specify performance, a measure of the pulse alignment and a measure of the threshold level tolerance require definition. The alignment time ϵ is defined as the time between the occurrence of the particular clock and vernier pulses that effect coincidence. In the range of interest, each alignment time defines a particular coincident pattern. For example, when the

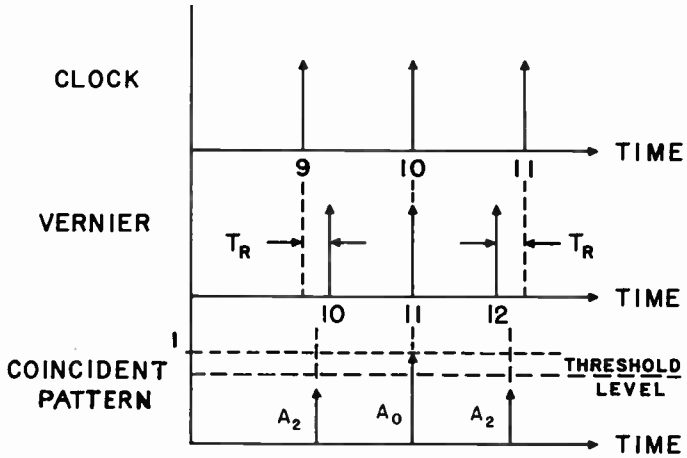

Fig. 7—Optimum coincident pattern.

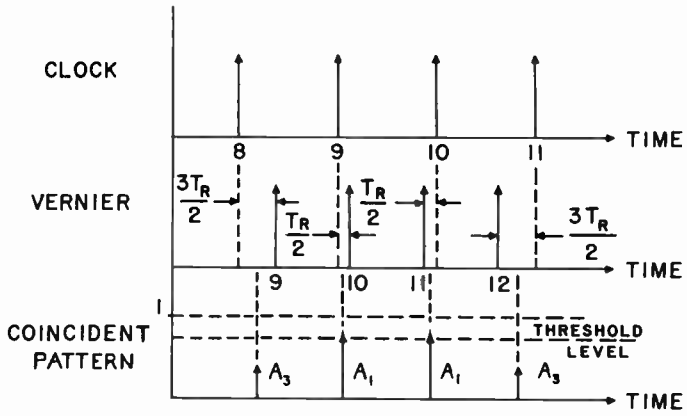

Fig. 8—Double-peak coincident pattern.

alignment time is zero a single-peaked pattern results (see Fig. 7); and when the alignment time is $T_R/2$ a doubly-peaked pattern results (see Fig. 8). Let A_1 represent the maximum amplitude of the coincident pattern when the alignment time is $T_R/2$ and A_2 the maximum amplitude of the coincident pattern when the alignment time is T_R. If the threshold level, A_L, is selected such that

$$A_L = \frac{A_1 + A_2}{2} \tag{9}$$

the error contribution of the coincident detection process will be less than the system resolution. The threshold level tolerance, ΔA_L, can then be defined as

$$\Delta A_L = \frac{A_1 - A_2}{2}. \tag{10}$$

Dividing (10) by (9), we obtain the threshold level tolerance ratio, namely

$$\frac{\Delta A_L}{A_L} = \frac{A_1 - A_2}{A_1 + A_2}. \tag{11}$$

Furthermore, the shape of each pulse in both the clock and vernier pulse trains effect the coincident detection process; and for the purposes of the following, the pulse shapes are assumed sinusoidal, as shown in Fig. 9. With input signal characteristics as specified

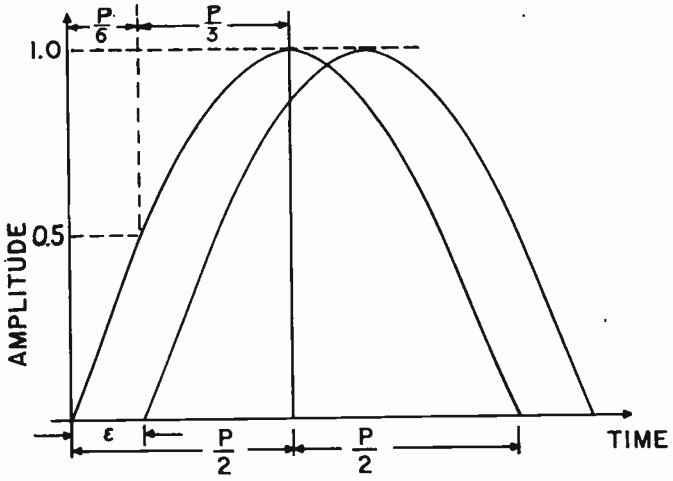

Fig. 9—Sinuosoidal pulse waveforms.

above, the coincident circuit output A can be expressed as

$$A = \sin \frac{\pi t}{P} + \sin \frac{\pi}{P}(t - \epsilon) \tag{12}$$

where P is the base pulse width. It can be shown that the maximum output signal occurs at

$$t = \frac{P + \epsilon}{2}. \tag{13}$$

By substituting in (12), the envelope of the maximum output A_m is found

$$A_m = 2 \cos \frac{\pi \epsilon}{2P}. \tag{14}$$

Using (14) to specify the maximum outputs at the alignment times T_R and $T_R/2$, and substituting into (11), the threshold tolerance ratio can be expressed as a function of the resolution-pulse width ratio T_R/P namely

$$\frac{\Delta A_L}{A_L} = \frac{\cos \frac{\pi T_R}{4P} - \cos \frac{\pi T_R}{2P}}{\cos \frac{\pi T_R}{4P} + \cos \frac{\pi T_R}{2P}}. \tag{15}$$

The plot of (15) is shown in Fig. 10. Assuming a conservative threshold tolerance, say 20 per cent, and imposing the condition that the system resolution be 10 mμsec, the maximum permissible pulse width is 17 mμsec. However, if the pulse peaks are presented to the coincident detection circuit, the effective pulse width is reduced. For example, by using only the upper one-half of the pulse, the width is effectively reduced by a factor of two-thirds (see Fig. 9). In numerics, a 30 mμsec wide pulse would appear to be 20 mμsec wide after amplification as specified above. Here, a system resolution of 10 mμsec requires the threshold tolerance be less than 12 per cent. When relatively wide clock and vernier pulses are employed, the repetitive application of pulse-peak amplification permits the accomplishment of a selective coincident detection at reasonable threshold tolerances.

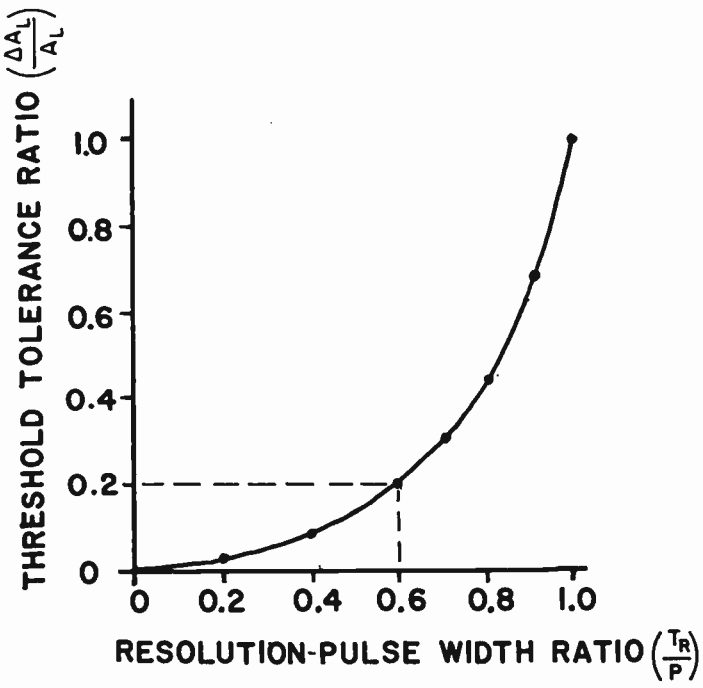

Fig. 10—Threshold tolerance ratio vs resolution-pulse width ratio.

System Description

The block diagram and the timing diagram of the system appear in Figs. 11 and 12 respectively and the subsequent discussion will be concerned with these diagrams.

It would be advantageous if the start and stop interval measurements previously described could be performed employing one vernier generator, one vernier counter, and one coincidence detector. If the vernier counter is reset to the maximum possible vernier count, and if the start end interval count is counted backward and the stop end interval count is counted forward, the resulting indication would represent the total vernier count. However, in precision time measuring systems, internal transmission delays are often not negligible.

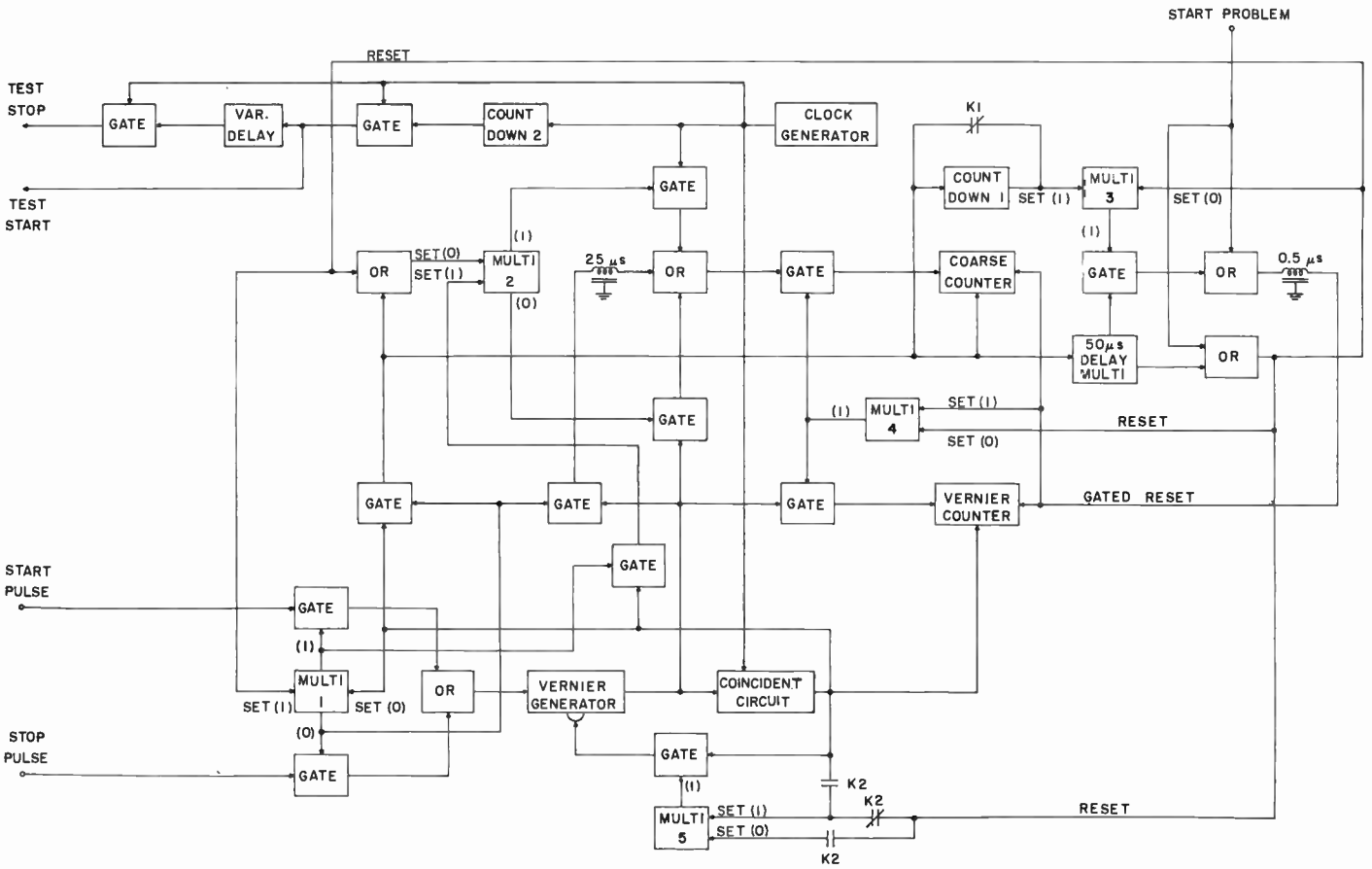

Fig. 11—Time interval measuring system block diagram.

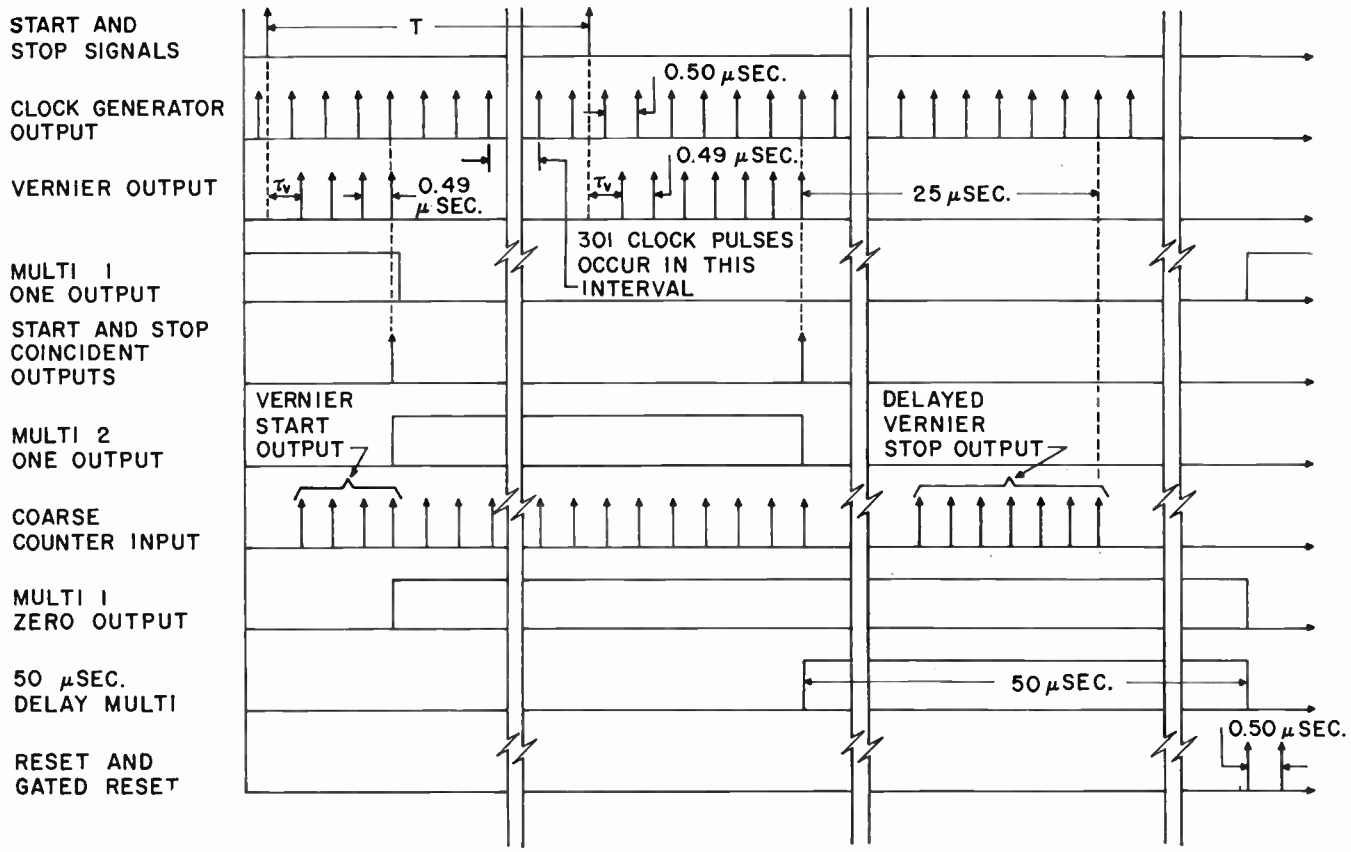

Fig. 12—Timing diagram.

Since it is hypothesized that the system employ one vernier generator and one coincidence detector, it is reasonable to assume the delays in the start and stop lines are equal. If N_{V_1} and N_{V_2} represent the number of start and stop interval counts respectively and τ_V denotes the inherent internal transmission delay, the vernier intervals shown in the timing diagram are

$$T_F = \tau_V - (N_{V_1} - 1)T_R \tag{16}$$

and

$$T_T = T_C - \tau_V + (N_{V_2} - 1)T_R. \tag{17}$$

Summing (16) and (17) and noting that the quantity $(T_F+T_T)/T_R$ represents the total vernier count, N_V, we obtain

$$N_V = \frac{T_C}{T_R} - N_{V_1} + N_{V_2}. \tag{18}$$

Hence, the bidirectional counting operation described above yields the correct vernier measurement as well as a measurement which is independent of inherent internal transmission delays.

The block diagram presents the instrumentation which mechanizes the operations described above. Application of a pulse to the start problem input causes a reset pulse which opens the gate energized by the [1] output of multivibrator 1. The occurrence of a start pulse energizes the vernier generator, and the vernier counter records the start vernier count. At coincidence, the coincident pulse inhibits the vernier generator, sets the vernier counter to count backward and opens the gate energized by the [0] output of multivibrator 1. When a stop pulse occurs, the vernier counter records the stop end interval; and the stop coincident pulse inhibits the vernier generator and excites the 50 μsec delay multivibrator, which determines the occurrence of the reset and gated reset pulses.

Since the start and stop signals occur asynchronously with respect to the internally generated clock references, either or both signals may occur on or between the clock pulses. If a signal pulse occurs in the vicinity of a clock pulse, a switching error of one count may appear in the coarse measurement. Since a known relation exists between the coincident clock pulse and the signal pulse, the coarse counter input is selected dependent upon coincidence. During the start vernier measurement, the start vernier pulses energize the coarse counter. At start coincidence the coarse counter input is switched to the clock line and clock pulses are counted until stop coincidence occurs. The stop coincident pulse sets the coarse counter to count the delayed stop vernier pulses backward; and the resulting count indicates the coarse interval independent of switching delays. The coarse count, N_C, may be expressed as

$$N_C = -2^\circ + N_{V_1} + N_S - N_{V_2} \tag{19}$$

where N_S is the number of clock pulses occurring between the start and stop coincident pulses.

Referring again to the block diagram, the gate energized by the [0] output of multivibrator 2 permits recording of the start vernier pulses in the coarse counter. The start coincident pulse sets multivibrator 1 to the [0] state and multivibrator 2 to the [1] state. Setting multivibrator 2 to the [1] state switches the coarse counter input from the vernier line to the clock line. The stop coincident pulse sets multivibrator 2 to the [0] state, thereby inhibiting the clock pulse input to the coarse counter, and sets the coarse counter to count backward. Since the gates energized by the [0] output of multivibrator 1 were opened by the start coincident pulse, the stop vernier pulses are allowed into the 25 μsec delay line (used for demonstrative purposes only), and the delayed stop vernier pulses are counted backward by the coarse counter.

If the vernier counter is reset to the maximum vernier count and the coarse counter is reset to the complement of zero counts, the constant terms in (18) and (19) are eliminated and the time interval is

$$T = N_V'T_R + N_C'T_C. \tag{20}$$

Using the example depicted by the timing diagram, the start vernier count is 4, the stop vernier count is 7, and 313 clock pulses exist between coincident pulses. The total vernier count, computed by (18), is 53 and the coarse count, computed by (19), is 309. Application of (20) yields a total time interval of 155.03 ± 0.01 μsec.

System Components

To provide the necessary equipment, a development program was undertaken. The clock pulse generator, the vernier generator, the coincident detection circuit, and the gates and counters which operationally set up and record the data represent the major component developments. A functional description of these units follows.

The clock pulse generator employs a crystal controlled oscillator as the system time reference. The oscillator emits a 2-mc wave, and subsequent stages of gain amplify and shape the signal. The unit will deliver a continuous train of pulses 20 volts in amplitude and 40 mμsec wide into a loaded 100-ohm coaxial cable. The rapid rise times and the narrow pulses required from this unit and others necessitated some amplifier experimentation. High perveance vacuum tubes operating into ferrite pot-core transformers proved adequate.

The vernier pulse generator is a circulating pulse amplifier[1] of distributed design,[2-5] having an input buffer stage, an inhibitor, and pulse amplifiers. The open

[1] Y. P. Yu, "Highly stable variable time-delay system," PROC. IRE, vol. 41, pp. 228–235; February, 1953.
[2] D. V. Payne, "Distributed amplifier theory," PROC. IRE, vol. 41, pp. 759–762; June, 1953.
[3] E. L. Ginston, W. R. Hewlett, J. H. Jasberg, and J. D. Noe, "Distributed amplification," PROC. IRE, vol. 36, pp. 956–969; August, 1948.
[4] A. P. Copson, "A distributed power amplifier," *Elec. Eng.*, vol. 69, pp. 893–898; October, 1950.
[5] W. H. Horton, J. H. Jasberb, and J. D. Noe, "Distributed amplifiers," PROC. IRE, vol. 38, pp. 748–753; July, 1950.

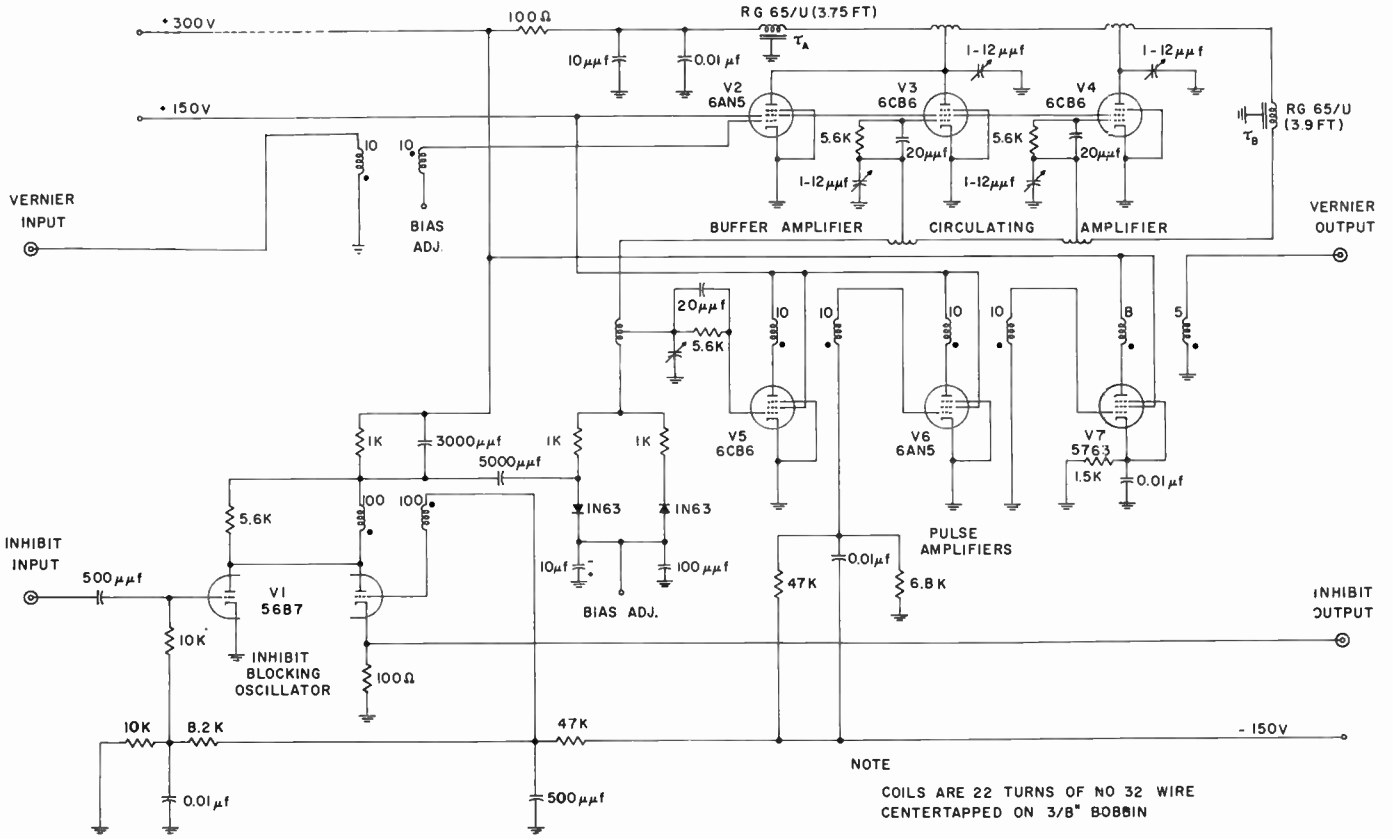

Fig. 13—Vernier generator schematic diagram.

loop gain is approximately 3 and the frequency response extends to 100 mc. The unit delivers a train of pulses and when driving a loaded 100-ohm coaxial cable, each pulse measures approximately 20 v in amplitude and 40 mμsec in width. The duration or the number of pulses in a given pulse train depends upon the occurrence of the coincident pulse. The inhibiting action is such that the unit can be retriggered with a minimum dead time between pulse trains of 5.0 μsec. The pulse to pulse period is 0.49 μsec and when continuously recirculating over a thirty minute interval, the frequency drift is less than 50 cps. The inherent internal delay is approximately 0.5 μsec.

A simplified schematic diagram of the vernier pulse generator is presented in Fig. 13. The unit accepts a positive pulse and after amplification a negative pulse appears at the plates of tubes V2 and V3. The negative pulse passes through the plate line and the delay line, τ_B, and is absorbed in the load. The negative pulse also passes through delay line, τ_A, is reflected as a positive pulse, passes through the plate line and the delay line, τ_B, and is also absorbed in the load. The grid line bias is set to amplify positive pulses and reject negative pulses. Amplification of the positive pulse on the grid line produces negative pulses at the plates of tubes V3 and V4. The resulting negative pulses distributively add at the late of tube V3 and the process repeats. Hence, the ernier pulse period expressed in terms of the delays, τ_A and τ_B, is

$$T_V = 2\tau_A + \tau_B. \tag{21}$$

At coincidence, the coincident pulse energizes the inhibit blocking oscillator, and the resulting negative grid line pulse increases the grid bias, thereby inhibiting circulation.

The coincident circuit, shown in Fig. 14, accomplishes a phase comparison of clock and vernier pulses. By setting the control grid biases high, the peaks of the applied pulses cause coincidence. After appropriate amplification the blocking oscillator, which is used as a comparator, delivers the coincident pulse. It was experimentally determined, using two pulse trains in which the pulses were 40 mμsec wide, that the 75 per cent voltage level (100 per cent occurring when the alignment time is zero) was obtained at a 5 mμsec alignment time and the 50 per cent level at a 10 mμsec alignment time.

The vernier counter is an eight-stage binary counter capable of counting gated pulses whose pulse to pulse period is less than 0.40 μsec. The unit counts forward or backward and resets to zero or fifty counts. The coarse counter is also a high-speed bidirectional binary counter and resets to the complement of zero counts. The number of coarse counter binary stages depends upon the maximum expected time interval and the expected rate of interval occurrence. A typical counter stage is shown

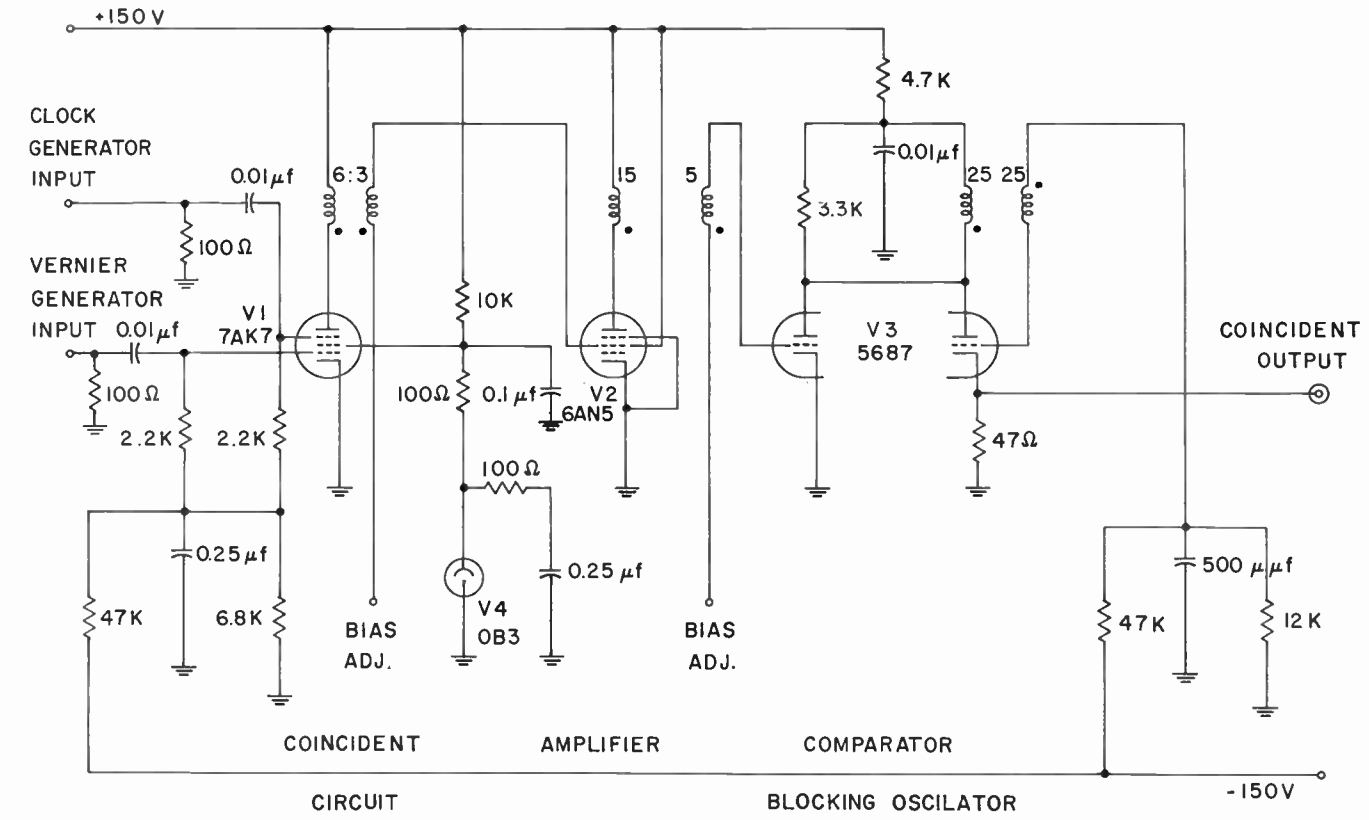

Fig. 14—Coincident circuit schematic diagram.

in Fig. 15. The binary plates are used to energize a digital recording device, and neon lights are available for the convenience of continuous indication.

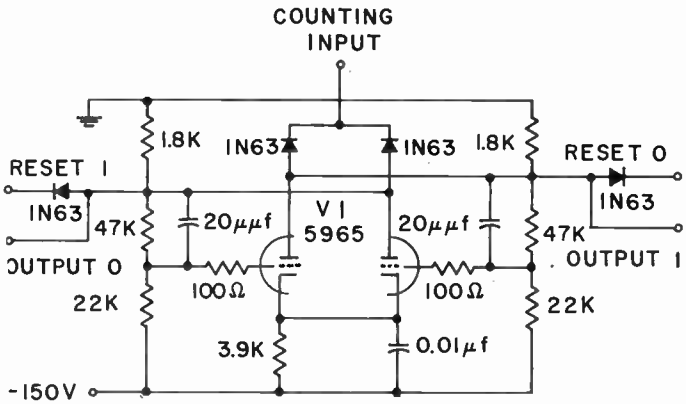

Fig. 15—Typical stage of the binary counters.

The gating circuitry employs threshold type "AND" gates driven directly from either bistable multivibrators or blocking oscillators. Since the gated pulses measure approximately 20 v in amplitude, the gating wave need swing only 20 v. The multivibrator-gate notation employed is defined as follows: when the multivibrator's set [1] input is energized, the [1] output is high and the [0] output is low; when the multivibrator's set [0] input is energized, the [0] output is high and [1] output is low. A gate energized by either the [0] or [1] output of a driver will pass a signal only when its control is up or high (*i.e.*, the gate is open).

Discussion

Measuring systems which have the capability of processing data rapidly often require high-speed recording equipment. Since the only recording equipment available at the time of system assembly was electromechanical in nature, additional circuitry is employed to permit the recording of selected measurements. If relay K1 (shown normally unenergized in the block diagram) is energized, count down circuit 1 controls the recording repetition frequency because the setting of multivibrator 3 to the [1] state permits generation of the gated reset pulse. The gated reset pulse resets both counters and sets multivibrator 4 to the [1] state thereby permitting inputs into both counters. Depending upon the design of the count down circuit, a wide range of ratios of signal occurrences to samples recorded may be obtained.

In precision measurements, a standard of comparison often presents a formidable problem. However, the system presented is particularly adaptable to the technique of self-calibration. After the clock frequency has been set by comparison (indirect) with the standard transmission signal (WWV), count down circuit 2 and its

associated gating deliver test signals which are, in fact, gated clock pulses. Since the test start and test stop signals are discretely variable and jitter free, system performance under test conditions can be predicted and readily verified. The coarse interval can be checked by an oscillograph and the vernier counter should indicate fifty counts since start and stop delays are assumed equal. If a calibrated delay line is inserted into one of the signal lines, the system accuracy can be determined.

The initial adjustment of the vernier frequency is somewhat tedious and requires explanation. After the vernier delay lines have been cut to the approximate length by employing heterodyne techniques, the system is set to receive and operate on stop pulses. If the vernier counter is reset to zero counts and allowed to count forward, the following sequence of events permits vernier calibration. Using the test stop signal as an input, the vernier counter records the stop circuitry transmission delay. When relay K2 is energized, the gating associated with multivibrator 5 permits vernier circulation until two coincident pulses occur. A test measurement which allows two coincident pulses records the stop circuit transmission delay plus the maximum vernier count. The correct vernier frequency is indicated by the maximum vernier count, which can be determined by differencing the vernier count when two coincident pulses occur and the vernier count when one coincident pulse occurs. For the clock frequency and system resolution cited above, the maximum count is 50 vernier pulses. Adjustments located on the vernier generator are available to vary the vernier frequency so that the correct count and hence the correct vernier frequency is obtained.

The photographs reproduced in Figs. 16–20 were taken with a Polaroid Land camera and a Tektronix type 517 oscillograph. The output waveshapes of the clock and vernier generators and the coincident detector are displayed in Figs. 16–19. The photograph presented in Fig. 20 is a composite of four photographs taken sequentially of the clock and vernier pulses resistively added. The first and second pulses shown are clock pulses and the third is a vernier pulse. The progression of the vernier pulses on the preceding clock pulses is demonstrated. Coincidence occurs on the next to last pulse, where the vernier and clock pulses appear aligned. The last pulse is a clock pulse, indicating the coincident pulse had inhibited the vernier generator. In this case the vernier count is seven, and the photograph represents the stop end measurement of the example presented in the timing diagram (see Fig. 12).

The range capability of the system depends upon the system characteristics and the signal repetition frequency. The maximum time to coincidence and the vernier generator recovery time determine the lower range limit; and the signal repetition frequency determines the upper range limit. For example, if the signal repetition frequency is 2000 cps, the system will measure a time interval ranging approximately from 30 μsec to 425 μsec.

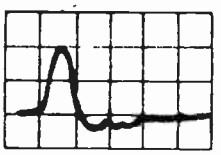

Fig. 16—Photograph of a clock generator pulse (abscissa 50 mμsec per division and ordinate 12 v per division).

Fig. 17—Photograph of a vernier generator pulse (abscissa 50 mμsec per division and ordinate 12 v per division).

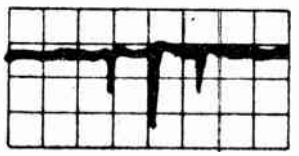

Fig. 18—Photograph of the optimum coincident pattern taken at the plate of the coincident circuit amplifier.

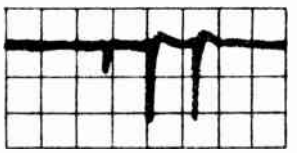

Fig. 19—Photograph of the double-peak coincident pattern taken at the plate of the coincident circuit amplifier.

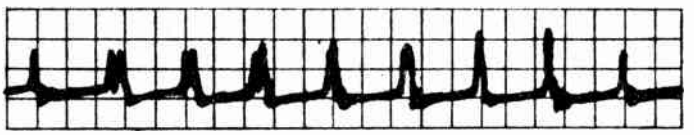

Fig. 20—Photograph of the vernier and clock pulses resistively added (corresponding to the stop measurement of Fig. 12).

The system described herein was fabricated, utilizing relay rack panel construction, and housed in a seven-foot cabinet. The machine was tested as indicated above and found to operate satisfactorily. A series of measurements was made and during this time the equipment operated reliably for over 300 hours. The detailed system block diagram is somewhat more complex than presented in this report; and for the sake of simplicity the interlocks, the fail-safe devices, the anti-lock up features, the digital recording equipment and the analog output instrumentation details have been omitted.

Conclusion

In discussing precision measuring devices, inquiries are often made relative to the ultimate system accuracy. Here, the precision can be improved simply by reducing the difference between the clock and vernier pulse periods. To improve the system accuracy an order of magnitude when operating at the same of lower clock frequency requires a more selective coincident detector, additional tolerances on the clock and vernier frequency stabilities, and the freedom to extend the end interval measurement times. At higher clock frequencies, the coincident selectivity and the mechanization of high frequency gated counters present a challenge. Although distributed amplification satisfies the bandwidth requirements as well as providing reasonable pulse amplification, the generation of triggered narrow pulses, the improvement of the coincident detection selectivity, the restriction imposed by the clock and vernier frequency stability tolerances, and the mechanization of economical and reliable high frequency gated counters should be evaluated relative to the particular system requirements.

Acknowledgment

The author wishes to acknowledge that L. Packer was instrumental in organizing and directing the original system studies and component developments relative to this program, and that W. Henn and R. Vogel participated actively in this project.

The author recognizes the fact that the Hughes Research and Development Laboratories, prior to the work described in this report, had fabricated a similar vernier measuring system.

Measurement of Instantaneous Frequency with a Microwave Interferometer*

HERBERT P. RAABE†, SENIOR MEMBER, IRE

Summary—**A microwave interferometer for the measurement of instantaneous frequency is described. It consists of a transmission line circuit used as a frequency modulation discriminator, and an indicator consisting of a microwave detector, video amplifier, and oscilloscope. The discriminator transforms the frequency variation during rf pulses, or that of continuous waves, to an amplitude variation at the input of the indicator. The characteristics of the discriminator are investigated theoretically and conditions are discussed for adjustment of the discriminator in order to minimize linear and nonlinear distortions. Since amplitude deviations of the input wave will simulate frequency variations, a technique which greatly reduces this effect is presented. Analysis and experiments indicate that this method provides a practical technique for measuring the frequency and its stability during a radar pulse.**

Introduction

THE MOST elementary formal description of a microwave signal might be an instantaneous time function, for example, the voltage-vs-time function. This function, of course, is not very useful. However, there are two other methods of accurately representing a microwave signal: 1) The Fourier spectrum, 2) the frequency- and amplitude-vs-time functions.

The Fourier spectrum is useful in determining the bandwidth of signals to which rf, IF, and video components and circuits must be adjusted in order to obtain high efficiency without loss of information. A suitable instrument to investigate the spectrum is a spectrum analyzer; however, this device is not able to provide complete information about the spectrum. The frequency and phase of single spectral components are not shown. It only presents a moderately accurate power spectrum envelope. Consequently, it is impossible to recover the modulation characteristics of the signal, let alone its instantaneous time function, from the spectrum as displayed by such an analyzer.

While amplitude-vs-time functions of microwave signals can easily be recorded, frequency-vs-time functions demand special attention, particularly if response is required to quick but small frequency changes which are common to pulse modulated signals. Knowledge of the instantaneous frequency is important for research and development work on magnetrons and other sources of microwave power, and for the investigation of the behavior of radar systems. For instance, the performance of moving target indication radar systems depends greatly on the pulse-to-pulse stability of the frequency-vs-time function during the rf pulse.

Analysis of the Discriminator

Definition of Amplitude and Frequency

The function of the instantaneous value vs time, $u(t)$, of a radar pulse can be presented as

$$u(t) = U_t \cos\left[\int \omega_t dt + \phi\right]. \quad (1)$$

* Original manuscript received by the IRE, April 14, 1956; revised manuscript received, September 24, 1956.

† General Mills, Inc., Minneapolis, Minn. Formerly with Aerial Reconnaissance Lab., Wright Air Dev. Ctr., Wright-Patterson AF Base, Ohio.

In this equation there are two empirical functions, the amplitude-time function U_t and the frequency-time function ω_t. These two functions are not uniquely determined by themselves. However, if either function is arbitrarily chosen, the other one will be determined. With regard to the practical use of these functions, the freedom of choice is limited. For instance, the usual connotation of the amplitude function of a pulse is an invariant function with respect to heterodyning and linear rectification. In other words, the amplitude function is scarcely affected by linear processes as they normally occur in radar receivers. This is true as long as the amplitude of the radio-frequency wave varies only slightly from cycle to cycle. Therefore, if only such amplitude functions are considered which form a smooth envelope around the peaks of the oscillating function $\cos[\int\omega_t dt+\phi]$ the freedom of choice of the amplitude function is rather limited.

The Circuit of the Discriminator

In order to obtain a signal which describes the frequency-vs-time function, it is necessary to convert the frequency modulation of the input wave into an amplitude modulation by means of a suitable discriminator. A circuit solving this problem is illustrated in Fig. 1.

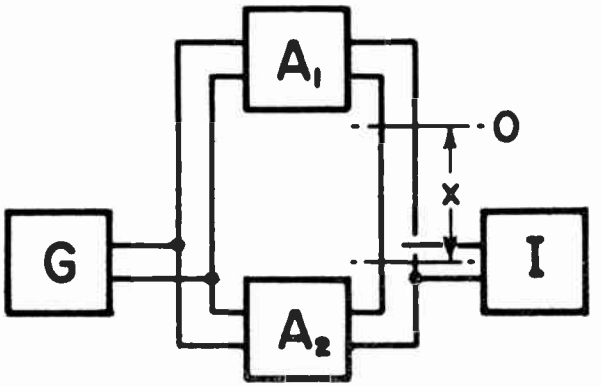

Fig. 1—The basic circuit of the discriminator for frequency modulation during a pulse. The pulse transmitted by the generator G is fed into a transmission line, which is connected in a loop. A_1 and A_2 are attenuators. The indicator I is coupled to the line at the distance x with respect to the point O which is equidistant from the feeding point.

The generator, G, feeds the oscillation into a closed uniform line. This line may be a coaxial line or a waveguide. Half of the energy travels clockwise through the attenuator, A_1, while the other half of the energy travels in the opposite direction through the attenuator, A_2. The total attenuation should be set high enough that signals traveling around the second time do not appreciably contribute to the original signal. The two waves coming from A_1 and A_2, respectively, arrive at the same time with equal sign at the point O, which is equidistant from the feeding point. Consequently, at this point the amplitude of the combined wave is always twice the amplitude of either of the contributing waves no matter what frequency might exist. At a certain distance, x, a probe picks up some energy from the line. The probe is connected to an indicator, I, consisting of a detector, video amplifier, and oscilloscope. Consequently, the indicator is able to show the amplitude-time function as it is at the position x of the probe. In the quasi-stationary case there is a standing wave pattern in the line. Nodes of the amplitude occur at all distances equal to an odd multiple of a half-wavelength from point O. Consequently, the amplitude is extremely sensitive to frequency variations in the neighborhood of these nodes, with a sensitivity increasing the farther the node is away from the balance point O. In order to obtain a perfect node, one of the two attenuators can be adjusted.

The Phasor Diagram of the Interferometer

The instantaneous voltage of the circuit at the point O may be determined by (1). Without losing generality ϕ can be set equal to zero. Therefore, the instantaneous voltage at the probe, being equal to the sum of the voltages of the two contributing waves, becomes

$$u = \frac{1}{2}U_{(t-x/w)}\cos\left[\int_0^{t-x/v}\omega_t dt\right] + \frac{1}{2}U_{(t+x/w)}\cos\left[\int_0^{t+x/v}\omega_t dt\right]. \quad (2)$$

In this equation v and w are the phase and group velocities, respectively. Assuming the change of amplitude of the pulse during the time x/w is negligible, the subsequent analysis is not affected by the amplitude modulation and we can set

$$U_{(t-x/w)} = U_{(t+x/w)} = U_t = U. \quad (3)$$

Furthermore we set

$$\int_0^{t\mp x/v}\omega_t dt = \int_0^{t\mp x/v}(\omega_m+\omega_d)dt = \omega_m\left(t\mp\frac{x}{v}\right)+\psi_{(t\mp x/v)} \quad (4)$$

so that (2) assumes the form

$$u = \frac{U}{2}\cos\left[\omega_m\left(t-\frac{x}{v}\right)+\psi_{(t-x/v)}\right] + \frac{U}{2}\cos\left[\omega_m\left(t+\frac{x}{v}\right)+\psi_{(t+x/v)}\right]. \quad (5)$$

In these equations ω_m is the average or unmodulated carrier angular frequency and ω_d the frequency deviation, while $\psi=\psi_{(t\mp x/v)}$ is the corresponding phase deviation.

Eq. (5) can be represented by the phasor diagram of Fig. 2. The first term in (5) describes the forward wave propagating in the direction of x and is represented by the phasor $^{+}\overline{U}$, while the second term or backward traveling wave is represented by the phasor $^{-}\overline{U}$. In the position $x=0$ the subscript 0 is attached to the right of the symbol as in $^{+}\overline{U}_0$. If the phasor describes a wave

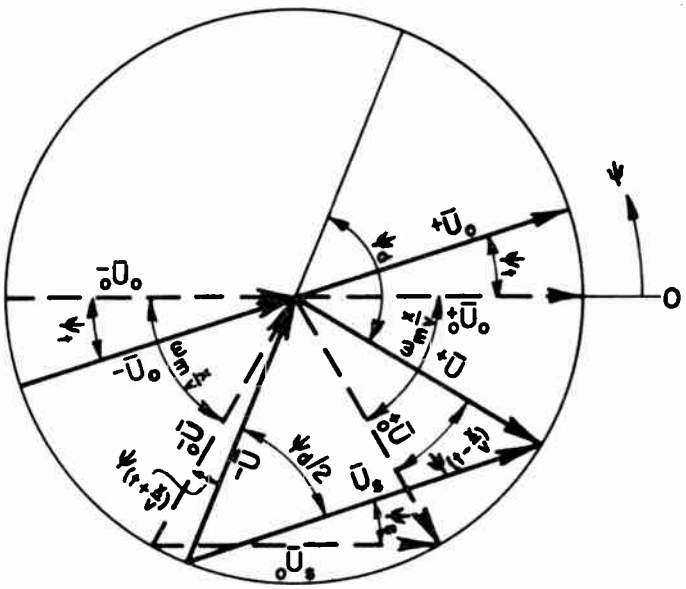

Fig. 2—The phasor diagram of the interferometer. The forward and backward waves are designated by symbols with a + sign and − sign respectively. In the unmodulated case the phasors are drawn as dashed lines.

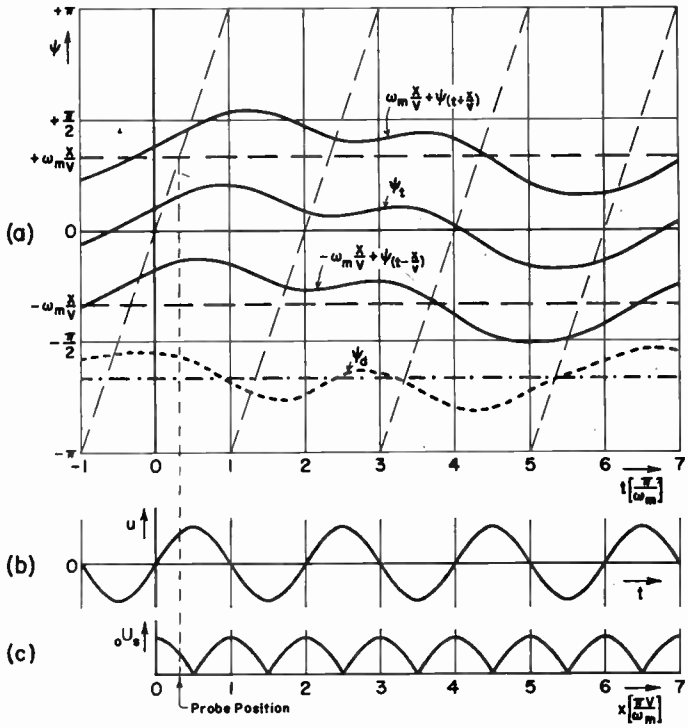

Fig. 3—The phase-vs-time graph. The original phase function ψ_t at $x=0$ shown in (a) undergoes a parallel displacement, both in phase and time, when observed at a probe position $x=0$. The phase difference ψ_d between the forward and backward waves approximately describes the frequency-vs-time function. The carrier is shown in (b) to furnish a time scale, while (c) shows the standing-wave pattern of the carrier with a scale normalized with respect to the propagation velocity v.

which is not frequency modulated the subscript 0 is attached to the left of the symbol so that the unmodulated waves at $x=0$ are represented by phasors in the positions ${}^{+}{}_{0}\overline{U}_{0}$ and ${}^{-}{}_{0}\overline{U}_{0}$ respectively. However, the frequency modulation of the wave causes a phase shift of ψ_t for both phasors, which are shown as $^{-}\overline{U}_{0}$ and $^{+}\overline{U}_{0}$. It is evident that the phasor sum $\overline{U}_{s0}=^{-}\overline{U}_{0}+^{+}\overline{U}^{0}$, which would be picked up by the probe at $x=0$, does not show any amplitude variation as a result of the frequency modulation.

With increasing x phasor $^{-}\overline{U}$ will turn counterclockwise, while phasor $^{+}\overline{U}$ will turn clockwise. For the unmodulated carrier waves the angular turns will be $\mp\omega_m x/v$, so that the positions designated by ${}^{-}{}_{0}\overline{U}$ and ${}^{+}{}_{0}\overline{U}$ result. Therefore, it is obvious that the amplitude of the sum of the unmodulated phasors varies as $\cos \omega_m x/v$ while the phase shift alternates between zero and π, which describes a standing wave pattern on the line as was anticipated. Frequency modulation causes additional phase shifts of $\psi_{(t-x/v)}$ and $\psi_{(t+x/v)}$, respectively, so that the amplitude of the phasor sum $\overline{U}_s=^{-}\overline{U}+^{+}\overline{U}$ will show a slightly different value, revealing a frequency discriminating effect of this circuit.

The relation between frequency and amplitude modulation can be illustrated much better if a phase-vs-time plot, to be used in combination with the phasor diagram is added. This plot is shown on Fig. 3(a). An arbitrary phase-time function ψ_t is shown in the diagram. The phasors in the positions of Fig. 2 for $x\neq 0$ were both shifted by $\omega_m x/v$. In the unmodulated case two straight horizontal lines shown as dashed lines result. However, the time shift corresponding to the new position causes a lag of the forward wave and an equivalent lead of the backward wave. In other words the new positions of the modulated phase functions are obtained by a combined lateral and longitudinal displacement, following a slanting line which progresses 2π for every period of the carrier wave. The carrier wave is plotted in Fig. 3(b) as a sine wave. In Fig. 3(c) the standing-wave function of the unmodulated wave is shown in a scale which matches propagation time and distance so that the probe position can be graphically related to the phase shift.

From the phase-time functions of $^{+}\overline{U}$ and $^{-}\overline{U}$ the phase difference can be obtained

$$\psi d = -\omega_m \frac{x}{v} + \psi_{(t-x/v)} - \omega_m \frac{x}{v} - \psi_{(t+x/v)}$$

$$= -2\omega_m \frac{x}{v} + \psi_e,$$

or

$$\psi_e = \psi_{(t-x/v)} - \psi_{(t+x/v)}. \tag{6}$$

The deviation ψ_e of the phase function ψ_d from the average of $-2\omega_m x/v$ is nearly proportional to the first derivative of the phase-time function of the original wave at $x=0$. Consequently, ψ_e will become approximately proportional to the frequency deviation ω_d. This is proved as follows. From (4) and (6) we derive

$$\psi_e = \int_0^{t-x/v} \omega_d dt - \int_0^{t+x/v} \omega_d dt = -\int_{-x/v}^{+x/v} \omega_d dt. \tag{7}$$

If the integration range $2x/v$ is small enough the tangent

at $x=0$ can be substituted for the function ω_d so that the integral becomes

$$\psi_d \cong -2\omega_d \frac{x}{v}, \tag{8}$$

thus showing proportionality between frequency and phase deviation.

The Linear Response of the Interferometer

Eq. (8) indicates that a large x/v factor increases the effectiveness of the discriminator which evidently will result in a loss of detail or linear distortion. To show this effect quantitatively the time function ω_d of (4) may be replaced by a Fourier series,

$$\omega_d = \sum_1^N \omega_n \cos(\Omega_n t + \Phi_n). \tag{9}$$

In this equation ω_n represents the amplitude of the nth Fourier component, while Ω_n and Φ_n are the frequency and phase, respectively, of that component.

Actually, for a pulsed signal, the frequency-time function, which is an empirical one, is defined during the pulses only. Therefore, some interpolation must be made for this function between the pulses. The number of the Fourier terms N and their amplitudes ω_n will depend largely on this interpolation. Therefore, ω_d represents a continuous function which approximates the empirical function during the pulses and defines the interval between pulses in such a way that the number N of the Fourier terms is minimized. Thus, pulsed signals are treated in the same way as continuous signals. Referring to (4), (5), and (9) we can set

$$\psi_{(t\mp x/v)} = \int_0^{t\mp x/v} \sum_1^N \omega_n \cos(\Omega t + \Phi_n)dt. \tag{10}$$

After integration we have

$$\psi_{(t\mp x/v)} = \sum_1^N \frac{\omega_n}{\Omega_n}\left\{\sin\left[\Omega_n\left(t \mp \frac{x}{v}\right) + \Phi_n\right] - \sin\Phi_n\right\}. \tag{11}$$

Hence, the phase differential according to (6) becomes

$$\psi_s = \sum_1^N \frac{\omega_n}{\Omega_n}\left\{\sin\left[\Omega_n\left(t - \frac{x}{v}\right) + \Phi_n\right] - \sin\left[\Omega_n\left(t + \frac{x}{v}\right) + \Phi_n\right]\right\}. \tag{12}$$

This equation can be reduced to

$$\psi_s = -2\sum_1^N \omega \frac{x}{v} \cdot \frac{\sin \Omega_n \frac{x}{v}}{\Omega_n \frac{x}{v}} \cdot \cos(\Omega_n t + \Phi_n),$$

or

$$\psi_s = \sum_1^N \psi_n \cos(\Omega_n t + \Phi_n). \tag{13}$$

Eq. (13) defines the linear response of the interferometer. It is the product of three functions. While the third function defines wave frequencies and phases, the first function which agrees with (8) states that sensitivity is linear with ω_n and increases with the probe distance x, and the second function describes the sensitivity response with respect to the modulating frequency. According to this function high sensitivity exists at low frequencies where $\sin \Omega_n x/v \approx \Omega_n x/v$. A drop of 3 db is reached at $\sin \Omega_n x/v = \sqrt{2}\Omega_n x/v$ or $\Omega_n x/v = 1.39$ so that the frequency range of the interferometer becomes

$$0 \leqq \Omega_n \leqq 1.39 \frac{v}{x},$$

or

$$0 \leqq \frac{\Omega_n}{2\pi} = F_n \leqq 0.221 \frac{v}{x}. \tag{14}$$

The Nonlinear Response of the Interferometer

The effect of the phase function ψ_d on the amplitude of the phasor $\overline{U}_s$ can be derived from the phasor triangle formed by $^-\overline{U}$, $^+\overline{U}$, and $\overline{U}_s$. The magnitudes of the phasors are related by

$$U_s^2 = {}^-U^2 + {}^+U^2 - 2{}^-U \cdot {}^+U \cdot \cos(\pi - \psi_d). \tag{15}$$

Since

$$^-U = {}^+U = \tfrac{1}{2}U_{so}, \tag{16}$$

$$U_{so} = U_o \cos\frac{\psi_d}{2}. \tag{17}$$

If we introduce the phase difference ψ_s as defined in (6), (17) becomes

$$U_s = U_{so} \cos\left(\omega_m \frac{x}{v} - \frac{\psi_s}{2}\right). \tag{18}$$

Hence

$$U_s = U_{so}\left(\cos \omega_m \frac{x}{v} \cdot \cos\frac{\psi_s}{2} + \sin \omega_m \frac{x}{v} \cdot \sin\frac{\psi_s}{2}\right). \tag{19}$$

This equation can be expanded into a series and becomes

$$U_s \cong U_{so}\left(\cos \omega_m \frac{x}{v} + \frac{1}{2}\sin \omega_m \frac{x}{v} \cdot \psi_s - \frac{1}{8}\cos \omega_m \frac{x}{v} \cdot \psi_s^2 - \frac{1}{48}\sin \omega_m \frac{x}{v} \cdot \psi_s^3\right). \tag{20}$$

In this series equation which describes the nonlinear response of the interferometer the first term determines a dc bias, the second one represents the desired linear transformation of the phase deviation into an amplitude variation, while the following terms indicate nonlinear distortion. Since these terms converge to zero very fast if $\psi_s < 1$, only the second and third-order terms are of interest.

Eq. (20) also shows that maximum sensitivity repeats periodically with the factor $\sin \omega_m x/v$. At these points the second-order term vanishes, while the third-order term, although assuming a maximum, is insignificant for most applications. It may be noted, however, that the dc bias also vanishes.

If the spectrum of (13) is substituted for ψ_e in (20) a rather complex pattern of frequencies results, the usefulness of which appears rather doubtful. However, a single component of the form

$$\psi_e = \psi_n \cdot \cos (\Omega_n t + \Phi_n) \tag{21}$$

may show some interesting facts. Since

$$\psi_e^2 = \frac{\psi_n^2}{2} + \frac{\psi_n^2}{2} \cos 2(\Omega_n t + \Phi_n) \tag{22}$$

and

$$\psi_e^3 = \frac{3\psi_n^3}{4} \cos (\Omega_n t + \Phi_n) + \frac{\psi_n^3}{4} \cos 3(\Omega_n t + \Phi_n), \tag{23}$$

we obtain

$$\begin{aligned} U_s \cong U_{so} \Bigg[& \left(1 - \frac{\psi_n^2}{16}\right) \cos \omega_m \frac{x}{v} \\ & + \frac{\psi_n}{2} \left(1 - \frac{\psi_n^2}{32}\right) \sin \omega_m \frac{x}{v} \cdot \cos (\Omega_n t + \Phi_n) \\ & - \frac{\psi_n^2}{16} \cos \omega_m \frac{x}{v} \cdot \cos 2(\Omega_n t + \Phi_n) \\ & - \frac{\psi_n^3}{192} \sin \omega_m \frac{x}{v} \cdot \cos 3(\Omega_n t + \Phi_n) \Bigg]. \end{aligned} \tag{24}$$

This equation determines the bias, the desired first harmonic, and the distorting second and third harmonics of the modulating wave.

Effect on Frequency Modulation

To complete the information on the rf signal at the probe the phase shift of the phasor sum at the position x with respect to the position $x=0$ must still be determined. This phase shift ψ_x is defined by

$$\psi_x = \psi_s - \psi_t. \tag{25}$$

From Fig. 2 we obtain the following relation:

$$\psi_x = \omega_m \frac{x}{v} + \psi_{(t+x/v)} - \frac{\psi_d}{2} - \psi_t. \tag{26}$$

With ψ_d from (6):

$$\psi_x = \frac{\psi_{(t+x/v)}}{2} + \frac{\psi_{(t-x/v)}}{2} - \psi_t. \tag{27}$$

Hence with (11) and after reduction of the trigonometric terms we obtain

$$\psi_x = -\sum_1^N \frac{\omega_n}{\Omega_n} \left(1 - \cos \Omega_n \frac{x}{v}\right) \sin (\Omega_n t + \Phi_n). \tag{28}$$

This equation indicates a second-order loss of frequency modulation when compared with (11) when $x=0$.

Detection Methods

The characteristics of the circuit which is connected to the probe and detects the amplitude of the microwave signal or demodulates it, is of major importance. While it may be assumed that the linear characteristic or bandwidth can be easily controlled to match the bandwidth of the interferometer, the nonlinear characteristic of the demodulator can be combined with that of the interferometer to minimize nonlinear distortions.

Demodulation with Added Carrier

If the probe is placed in the position of maximum sensitivity and linearity of the interferometer, (24) would assume the form

$$\begin{aligned} U_s \cong U_{so} \Bigg[& \frac{\psi_n}{2} \left(1 - \frac{\psi_n^2}{32}\right) \cos (\Omega_n t + \Phi_n) \\ & - \frac{\psi_n^3}{192} \cos 3(\Omega_n t + \Phi_n) \Bigg]. \end{aligned} \tag{29}$$

Since ψ_n is a bipolar signal any rectification would be extremely harmful as it would "fold up" the negative values to the positive side. Fig. 3(c) may serve as an illustration of this situation as the probe would occupy a node of the standing wave. The problem is related to the demodulation of communication signals with suppressed carrier. It can be solved by adding the carrier. Of course it is necessary that the phasor of the carrier remains parallel to the phasor of the sum of the sidebands at all times in order to produce an amplitude modulated carrier. With certain limitations this carrier is available at the position $x=0$ of the interferometer. As (28) shows, the angle between the phasors stays near zero for small values of x due to the second order function $1-\cos \Omega_n x/v$. The angle is also proportional to the frequency modulation swing due to the first factor. During a complete cycle of the amplitude modulation a complete cycle of frequency modulation would be accomplished. This is shown by the phasor diagram of Fig. 4 where $\overline{U}_{so}$ is shown in its position relative to $\overline{U}_s$

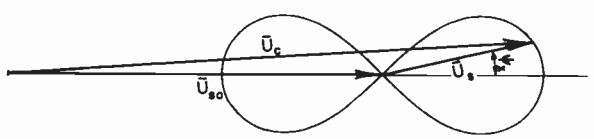

Fig. 4—Diagram of the phasor of a sinusoidally frequency modulated voltage picked up in a node of the carrier, in relation to the phasor of the original signal.

the position of which is fixed. The locus of $\overline{U}_{so}$ is a loop resembling the figure 8. At small values of x the loop narrows down to a line parallel with $\overline{U}_s$. It is obvious that broad loops as obtained at larger values of x will cause distortion of the amplitude modulation of phasor $\overline{U}_c = \overline{U}_s + \overline{U}_{so}$.

The Single Probe Detector

The most practicable detection device for microwaves is a crystal detector whose characteristic at low signal level is that of a square law. Therefore, for such a detector, the dc output of the probe becomes proportional to the square of (17):

$$U_{ss} = 2sU_{so}^2 \cos^2 \frac{\psi_d}{2} = sU_{so}^2(1 + \cos \psi_d). \quad (30)$$

With ψ_d as defined in (6) and after trigonometric transformation we obtain

$$U_{ss} = sU_{so}^2\left(1 + \cos 2\omega_m \frac{x}{v} \cdot \cos \psi_e + \sin 2\omega_m \frac{x}{v} \cdot \sin \psi_e\right). \quad (31)$$

Expansion into a series leads to

$$U_{ss} \cong sU_{so}^2\left[1 + \cos 2\omega_m \frac{x}{v} + \sin 2\omega_m \frac{x}{v} \cdot \psi_e - \frac{1}{2} \cos 2\omega_m \frac{x}{v} \cdot \psi_e^2 - \frac{1}{6} \sin 2\omega_m \frac{x}{v} \cdot \psi_e^3\right]. \quad (32)$$

In this equation the first two terms form a dc bias, the third term describes the linear response, while the fourth and fifth term determine the second and third-order distortions respectively. In order to maximize the linear response of the system the probe must be positioned so that a zero response of the second and fourth term results. This still leaves a bias due to the first term, while the fifth term, which also maximizes, requires attention. Under this condition (32) reduces to

$$U_{ss} \cong sU_{so}^2\left[1 \pm \left(\psi_e - \frac{\psi_e^3}{6}\right)\right],$$

$$2\omega_m \frac{x}{v} = \frac{\pi}{2}, \frac{3\pi}{2}, \frac{5\pi}{2}, \cdots. \quad (33)$$

In comparison with (20) the higher-order terms do not converge as fast unless the phase deviation is reduced to one half, which requires a probe distance only half as great as in the case of linear detection.

On a single sinusoidal component as of (21) the system response becomes

$$U_{ss} \cong sU_{so}^2\left[1 + \left(1 - \frac{\psi_n^2}{4}\right) \cos 2\omega_m \frac{x}{v} + \left(\psi_n - \frac{\psi_n^3}{8}\right) \sin 2\omega_m \frac{x}{v} \cdot \cos (\Omega_n t + \Phi_n) - \frac{\psi_n^2}{4} \cos 2\omega_m \frac{x}{v} \cdot \cos 2(\Omega_n t + \Phi_n) - \frac{\psi_n^3}{24} \sin 2\omega_m \frac{x}{v} \cdot \cos 3(\Omega_n t + \Phi_n)\right]. \quad (34)$$

In this equation the dc bias, linear response, and second and third harmonics are easily recognized. For the optimum probe position this equation becomes

$$U_{ss} \cong sU_{so}^2\left\{1 \pm \left[\left(\psi_n - \frac{\psi_n^3}{8}\right) \cos (\Omega_n t + \Phi_n) - \frac{\psi_n^3}{24} \cos 3(\Omega_n t + \Phi_n)\right]\right\}. \quad (35)$$

The Double Probe Detector

The two detection devices mentioned above can be assembled with commercially available microwave components. The single probe detector, especially, is very simple and easy to set up. However, both devices have a severe disadvantage. Since the dc bias is mixed with the desired signal, they are strongly affected by amplitude modulation of the original wave. Amplitude modulation of the dc term will be added to the amplitude modulation caused by the discriminating effect of the interferometer and thus produce an error. Of course, the amplitude modulation of the original wave will also show up on the desired first order term as crossmodulation, but this error is of a smaller magnitude and will increase proportionally with the desired signal rather than form a constant additive error. It may be noted that any pulsed signal is an amplitude modulated wave in this sense and causes undesirable effects. Because of the delay of one of the pulses with respect to the other one, a leading and trailing part of the pulse is not subjected to the discriminating effect of the interferometer. This does not mean a restriction of the analysis because the delay time is only $2x/v$, while the period of the highest frequency component of the modulation function as obtainable from (14) is $2\pi x/1.39$, or 2.26 times the delay time. However, these leading and trailing parts of the pulse cause excessive amplitude and transient phenomena which make it difficult to properly interpret the interferometer output.

The elimination of such error signals is based on the fact that they show up with the same sign regardless of the probe position, while the desired signal alternates in sign periodically. In the case of the single probe detector it is necessary to move the probe one quarter of the standing wavelength to reverse the sign of the discriminating effect. If the response to a repeatable signal is taken consecutively in two such positions and subtracted, only the desired signal, with doubled amplitude, will remain.

This is a tedious method and does not work with aperiodic signals. Therefore, these two signals must be taken and subtracted instantaneously. This requires the special design of a double probe assembly, with the probes mounted on the same carriage a quarter-wavelength apart. Each probe is connected to a square law rectifier and the video outputs subtracted electrically prior to amplification and recording. A schematic diagram is shown in Fig. 5. Actually the video signals from the two probes are added and divided by 2 in this bridge

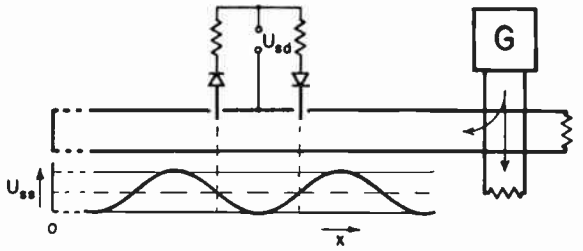

Fig. 5—The circuit of the double probe and its proper positioning with respect to the standing-wave pattern of the carrier. The pulse transmitted by the generator G is coupled into a shorted transmission line by means of a directional coupler.

type circuit, however, the signs of the video components are reversed by the opposite position of the detectors. Therefore, the output of the double probe is

$$U_{sD} = \tfrac{1}{2}(U_{ss1} + U_{ss2}). \tag{36}$$

If the single probe responses are taken from (32) we obtain

$$U_{sD} \cong sU_{so}^2\left[\cos 2\omega_m \frac{x}{v} + \sin 2\omega_m \frac{x}{v}\cdot\psi_e - \frac{1}{2}\cos 2\omega_m \frac{x}{v}\cdot\psi_e^2 - \frac{1}{6}\sin 2\omega_m \frac{x}{v}\cdot\psi_e^3\right]. \tag{37}$$

For the optimum position of the double probe we will get

$$U_{sD} \cong \pm sU_{so}^2\left(\psi_e - \frac{\psi_e^3}{6}\right). \tag{38}$$

For a single sinusoidal component of the Fourier spectrum the response can be derived from (34) and (35):

$$U_{sD} \cong sU_{so}^2\left[\left(1 - \frac{\psi_n}{4}\right)\cos 2\omega_m \frac{x}{v} + \left(\psi_n - \frac{\psi_n^3}{8}\right)\sin 2\omega_m \frac{x}{v}\cdot\cos(\Omega t + \Phi_n) - \frac{\psi_n^2}{4}\cos 2\omega_m \frac{x}{v}\cdot\cos 2(\Omega_n t + \Phi_n) - \frac{\psi_n^3}{24}\sin 2\omega_m \frac{x}{v}\cdot\cos 3(\Omega_n t + \Phi_n)\right] \tag{39}$$

and

$$U_{sD} \cong \pm sU_{so}^2\left[\left(\psi_n - \frac{\psi_n^3}{8}\right)\cos(\Omega_n t + \Phi_n) - \frac{\psi_n^3}{24}\cos 3(\Omega_n t + \Phi_n)\right]. \tag{40}$$

Experimental Data

A perfect balance of the amplitudes of the two waves at the position of the probe in the circuit of Fig. 1 is not necessary for practical measurements, as the excess voltage of one wave will result only in an additional dc bias in the probe. Therefore, a much simpler circuit may consist of a slotted waveguide section to which a shorted piece of waveguide is connected on one side, while a sample of the pulses, reduced in amplitude by a directional coupler, is fed into the other end of the slotted section. If the short circuit is at a distance x from the probe, the delay of the reflected wave is equivalent to the delay between the waves in the circuit of Fig. 1. This simpler circuit which was used in the experiments is especially suitable for the double probe, because this probe does not transmit any dc bias. It is shown in Fig. 5.

The basic parameters used in the experiments are as follows:

Transmission line:	Rectangular waveguide $a=0.9$ inch, $b=0.4$ inch
Probe position:	$x=245$ cm
Transmitter tube:	Magnetron 4J52
Radar frequency:	$f_m=9375$ mcps
Pulse length:	$\tau=0.4$ μs
Pulse repetition frequency:	$f_p=1300$ cps.

From these parameters we derive:

Wavelength in space: $\lambda = c/f_m = 3.2$ cm

Cutoff wavelength of guide: $\lambda_c = 2a = 4.572$ cm

Wavelength in guide:

$$\lambda_g = \frac{\lambda}{\sqrt{1 - \left(\frac{\lambda}{\lambda_c}\right)^2}} = 4.475 \text{ cm}$$

Phase velocity: $v = f_m \cdot \lambda_g = 41960 \cdot 10^6$ cm/s

$$v = f_m \cdot \lambda_g = 41960 \cdot 10^6 \text{ cm/s}$$

Bandwidth of discriminator (14):

$$\Omega_N = 1.39v/x = 238 \cdot 10^6 \text{ rad/s}$$

$$F_N = \frac{\Omega_N}{2\pi} = 38 \text{ mcps.}$$

The specially designed double probe is illustrated in Fig. 6. Two short waveguide sections are positioned side by side across the slotted section. Two probes whose depths are adjustable couple energy from the slotted waveguide into each of the other waveguide sections. The distance between the probes is fixed and equals $\frac{1}{4}\lambda_g = 7/16$ inch. In order to tune the probes an adjustable plunger is mounted to one side of each of the waveguide sections while a crystal head is mounted to the other end of these sections. The crystal heads are designed in such a way that crystals can be inserted in either direction. Therefore, a high degree of electrical symmetry can be obtained except for the asymmetry due to the opposite polarity of the two rectifiers. However, standard crystal mounts may be used if reversible crystals (Philco CRX-3) are available. While the lower ends of the crystals are grounded the other ends are connected to a coaxial outlet through two balanced resistors of 1000 ohms. Although by the choice of a balanced pair of crystals and by means of the probe and plunger adjustments a perfect dc balance can be ob-

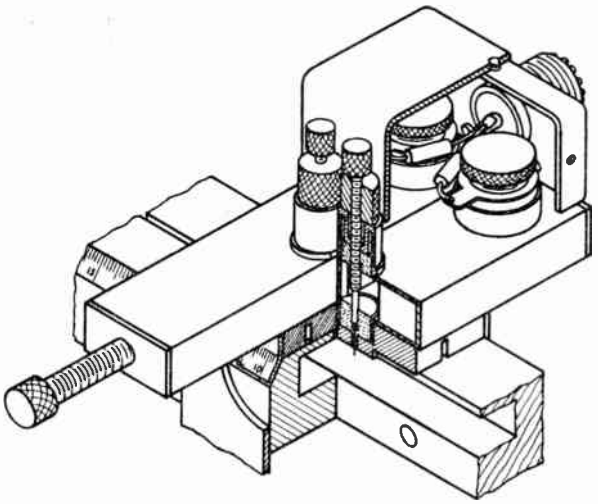

Fig. 6—Design of the double waveguide probe shown in isometric projection. Inside waveguide dimensions are 0.4 inch by 0.9 inch. Parts of the waveguides and of the shield are cut out to show details.

tained, it is also necessary to balance the transient response. It was found that the positions of the probes very close to the walls of the two waveguide sections caused unbalanced transients. There are two contributing factors. First, the coupling factor for the basic mode, H_{10}, was too low. Second, the higher mode, H_{20}, was generated due to the presence of spectral components above 13,000 mc. Diaphragms which reduced the apertures of the waveguides to one-half at the probe positions solved this problem.

Calibration of the oscillographs was obtained in a simple way. If we assume an incremental frequency deviation, Δf, the oscillograph trace will deviate by an amount Δa. This incremental amplitude deviation can also be produced by an incremental change of the position of the probe Δx. Therefore, the linear approximation $\Delta x = m\Delta f$ is sought. The operating position of the probe x is equal to n guide wavelengths, therefore

$$n = \frac{x}{\lambda_g} \cdot \tag{41}$$

If the frequency changes by the incremental amount Δf which establishes the wavelength λ_{g1} the incremental amplitude change Δa can be compensated by moving the probe by an incremental amount Δx so that

$$\Delta x = x - x_1 = x - n\lambda_{g1}. \tag{42}$$

With (41) we get

$$\Delta x = x\left(1 - \frac{\lambda_{g1}}{\lambda_g}\right). \tag{43}$$

The guide wavelength is determined by the velocity of light and by the operating and cutoff frequencies of the waveguide as in this equation.

$$\lambda_g = \frac{c}{\sqrt{f^2 - f_c^2}} \tag{44}$$

Hence (43) becomes

$$\Delta x = x\left[1 - \sqrt{\frac{f^2 - f_c^2}{(f + \Delta f)^2 - f_c^2}}\right]. \tag{45}$$

The linear coefficient m equals the first derivative of Δx with respect to Δf for $\Delta f = 0$ which is

$$m = x\frac{f}{f^2 - f_c^2} \cdot \tag{46}$$

Hence we have

$$\Delta x = x\frac{f}{f^2 - f_c^2}\Delta f. \tag{47}$$

With the parameters mentioned above the coefficient m becomes

$$m = 0.51 \text{ mm} \cdot \text{s/mc}. \tag{48}$$

Therefore, increasing the probe distance by a convenient incremental amount moves the trace on the oscillograph vertically a distance equivalent to a corresponding frequency increase. For example, in order to obtain a displacement equivalent to 2 mcps increase of frequency the probe must be moved 1.02 mm.

Fig. 7 shows three traces with a probe position x nearly zero, so that practically no frequency discrimination takes place. The upper and lower traces are the contributions of the two probes which were obtained individually by disconnecting the crystal in the other probe. Therefore, these traces show the amplitude-vs-time function of the pulse. With both crystals connected the center trace was obtained indicating very good balance of the two probes. Selection of crystals and careful adjustment of probe length and plunger position is necessary to obtain this condition.

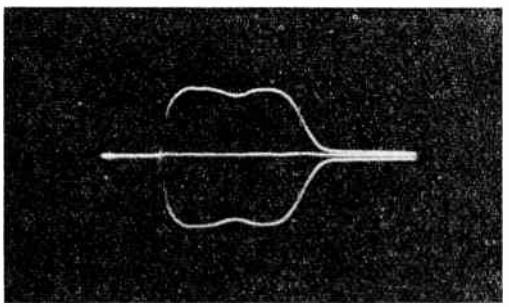

Fig. 7—Amplitude-vs-time functions taken with individual probes (positive and negative traces) and with both probes (middle trace).

Figs. 8 and 9 show single probe operation. While Fig. 8 is taken on a positive slope, Fig. 9 is taken on an adjacent negative slope. The weaker trace in Fig. 8 calibrates the discrimination effect, as it corresponds to a frequency decrease of 2 mcps. In both figures the spikes at the front and rear end of the pulses due to the delay time in the discriminator are conspicuous and make it difficult to properly interpret the oscillograph.

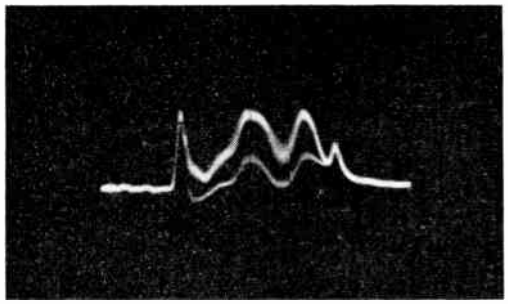

Fig. 8—Frequency-vs-time function taken with the positive probe on a positive discriminator characteristic. Weak trace affords calibration mark on 2 mcps.

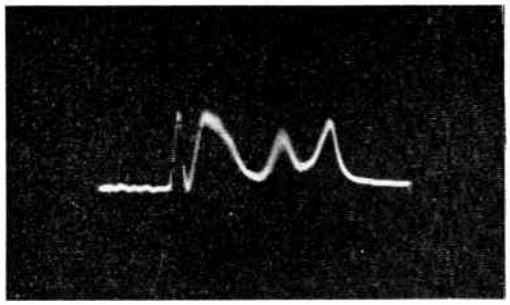

Fig. 9—Frequency-vs-time function taken with the positive probe on a negative discriminator characteristic.

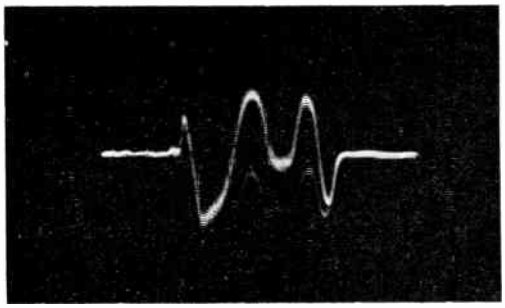

Fig. 10—Frequency-vs-time function taken with the double probe on a positive discriminator characteristic. Weak trace affords calibration mark of 2 mcps.

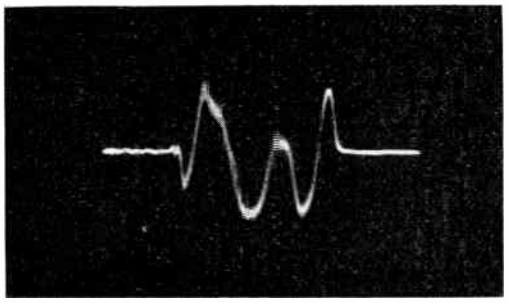

Fig. 11—Frequency-vs-time function taken with the double probe on a negative discriminator characteristic.

The frequency discrimination afforded by the double probe is illustrated in Figs. 10 and 11. Again these oscillographs were taken at a positive and the adjacent negative slope. The weak trace affords a 2-mcps calibration mark. The signals are bipolar, no spikes due to the delay in the discriminator are present. The spikes which can actually be seen are part of the frequency function as indicated by the fact they reverse their polarity with the rest of the signal. The symmetry of the positive and negative signals is very good. A slight frequency instability may also be noted. Comparison of the double probe signals with the respective single probe signals indicates considerable improvement afforded by the double probe. An improved double probe may consist of two separate probe carriages operated by two control knobs. One knob would control the relative distance between the probes while the other knob would control the position of the two carriages as a whole. This way the probe could be used over a wider frequency band and adjusted to other than square law characteristics of the detectors.

Not only is the double probe a very useful tool in microwave interferometers, but whenever phase measurements are to be taken it can be used in preference to a single probe. Because of the square law characteristic of crystals, phase measurements are usually taken at half-peak amplitude points. With a single probe this requires two successive settings with the possibility of inaccuracies due to amplitude variations. The double probe establishes at once the position of the zero amplitude with high accuracy.

Acknowledgment

The author is very grateful to Ralph Overholt, Jr. of Wright Air Development Center for his suggestion to explore the possibilities of the microwave interferometer for frequency measurements and his keen interest in the progress of the work.

Surface Leakage Current in Silicon Fused Junction Diodes*

M. CUTLER† AND H. M. BATH†

Summary—**The forward and reverse current of fused junction silicon diodes are compared with the predicted equations arising from a simplified model for surface leakage. It is found that analysis of the forward current in the "exponential" region leads to resolution of the contributions of the junction and the leakage path. The activation energies of the parameters describing these two contributions were determined; the former agrees with the value of the band gap. The implications and deficiencies of the model are discussed.**

Introduction

INVESTIGATIONS of surface properties of germanium and silicon, in the past few years, have led to the development of explanations of surface behavior in terms of the surface barrier, surface states, conductance in inversion regions, electronic transitions in surface recombination centers, and other phenomena.[1–4] Many of the investigations have centered on the behavior of "channels" on germanium surfaces, as influenced by the presence of different ambient gases.[5,6]

The purpose of this paper is to present a study of surface leakage currents from the point of view of their effect on device behavior. To do this, a comparison is made of experimental data with what seems to be the simplest possible theory.[7] The theory is based on a model which contains two elements: a leakage path on the surface of one side of a p-n junction, which is an electrical contact with the material on the other side of the junction, and a surface barrier separating the leakage path from the bulk region underneath. These seem to be the basic elements in surface leakage, and their reality is substantiated by experimental and theoretical information. To simplify the problem, it is assumed that the conductivity of the leakage path is a constant, and that the flow of current across the surface barrier is described by the simple diode equation. This is admittedly crude, but it avoids the complications introduced by the consideration of the distribution of surface states, and other details of the electronic structure of the surface which are incompletely understood.

The resulting equations are found to agree fairly well with the experiment, and provide explanations of many puzzling features of silicon diodes. Hence, the simplified theory seems to provide a useful first approximation to the behavior of junction diodes. The effects of further refinements will be discussed to some extent later.

Equations for Surface Leakage

The model for surface leakage is shown in Fig. 1. In addition to the junction current I_1 crossing the p-n junction, a leakage current I_2 crosses the surface barrier at all points x in which there is a bias, accumulates in the channel, and flows to the junction boundary ($x=0$). For purposes of deriving the equations, it is not necessary to stipulate which side of the p-n junction has the surface leakage path.

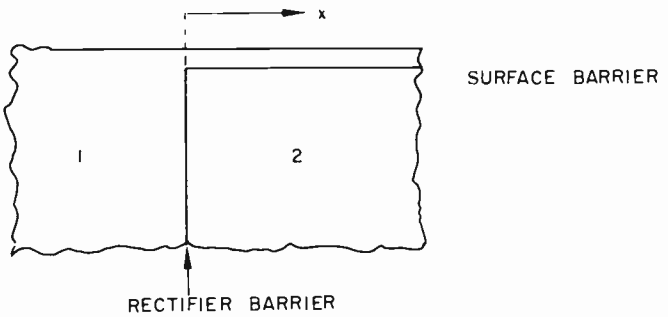

Fig. 1—Diagram of the model for surface leakage.

The change in voltage $V'(x)$ in the surface leakage path is given by Ohm's law:

$$dV'/dx = -I'/\sigma L \qquad (1)$$

where I' is the cumulative current at distance x, σ is the two dimensional conductivity of the leakage path, and L is the width of the path at the distance x.

The diode equation describes the change in $I'(x)$ due to flow across the surface barrier:

$$dI'/dx = -I_s L[\exp(qV'/kT) - 1], \qquad (2)$$

where I_s is the saturation current per unit area for the surface barrier. The boundary conditions are $I'=0$ at $x=\infty$, and $V'=0$ at $x=\infty$; the total leakage current I_2 is determined by the required value of I' at $x=0$, for a given $V'=V$ at $x=0$.

* Original manuscript received by the IRE, May 21, 1956; revised manuscript received, August 30, 1956. This paper was presented at the IRE-IEE Semiconductor Device Research Conference, Philadelphia, Pa., June, 1955.

† Semiconductor Lab., Hughes Aircraft Co., Culver City, Calif.

[1] W. H. Brattain and H. Bardeen, "Surface properties of germanium," *Bell Sys. Tech. J.*, vol. 32, p. 1; January, 1953.
[2] S. R. Morrison, "Changes in surface conductivity of germanium," *J. Phys. Chem.*, vol. 57, p. 860; November, 1953.
[3] W. L. Brown, "N-type surface conductivity on p-type germanium," *Phys. Rev.*, vol. 91, p. 518; August 1, 1953.
[4] R. H. Kingston, "Water-vapor induced n-type surface conductivity on p-type germanium," *Phys. Rev.*, vol. 98, p. 1766; June 15, 1955.
[5] A. L. McWhorter and R. H. Kingston, "Channels and excess reverse current in grown germanium p-n junction diodes," PROC. IRE, vol. 42, pp. 1376–1380; September, 1954.
[6] H. Cristensen, "Surface conduction channel phenomena in germanium," PROC. IRE, vol. 42, pp. 1371–1376; September, 1954.
[7] M. Cutler and H. M. Bath, "Surface leakage current in rectifiers," *J. Appl. Phys.*, vol. 25, p. 1440; November, 1954.

A solution for I_2 which is limited to the reverse direction can be obtained by assuming V' is large and negative. This was derived by Aigrain for a radial geometry.[8] For the one dimensional problem, with L independent of x, it is possible to derive a more complete solution by eliminating dx and integrating:

$$I_2^2 = I_L^2(e^v - v - 1), \tag{3}$$

where

$$I_L^2 = 2\sigma L^2 I_s kT/q. \tag{4}$$

We shall find it convenient to use v for qV/kT. It will be shown later that (3) is applicable also for radial geometry, if one has a forward bias.

The total current is the sum of the junction component I_1 and leakage components I_2:

$$I = I_j(e^v - 1) \pm I_L(e^v - v - 1)^{1/2}, \tag{5}$$

where the plus and minus signs are taken, respectively, for forward and reverse bias. I_j is the saturation current for the junction.

The qualitative difference in the behavior of the two functions of v is of interest. Fig. 2 shows plots on a log-log scale of (e^v-1) and $(e^v-v-1)^{1/2}$. The ordinate is converted to current by shifting each set of curves vertically by the amount log I_j or log I_L. In the reverse direction, the leakage component increases as $(-V)^{1/2}$, whereas the junction component becomes constant at a low reverse bias (about 0.1 volt). On the other hand, the junction component increases as exp (qV/kT) in the forward direction, whereas the leakage component increases as the square root of this function, exp $(qV/2kT)$. It is clear that for any ratio of values of I_j and I_L, the junction component will ultimately be dominant, given a large enough forward bias, and the leakage component will be significant at a large enough negative bias. The limits of validity of these equations, within the constraints of the model, are, in the forward direction, at currents large enough to give a base voltage drop ($\gtrsim$0.1 ma), and at a reverse bias large enough to lead to a junction breakdown.

For purposes of discussion, we shall present also the solution for the length of the leakage path, that is, the distance x_1 in which the voltage and current drop essentially to zero. This is obtained by substituting the solution for $I'(V')$, which is of the same form as $I_2(V)$ in (3), back into (1), and integrating. This gives

$$x_1 = \pm \frac{1}{2} \lambda \int_{qV/kT}^{\pm 1} (e^v - v - 1)^{-1/2} dv, \tag{6}$$

where

$$\lambda = (2kT\sigma/qI_s)^{1/2}. \tag{7}$$

The upper limit in the integral of (6) was chosen arbitrarily, since V approaches zero asymptotically with increasing x, and reaches zero only at $x = \infty$.

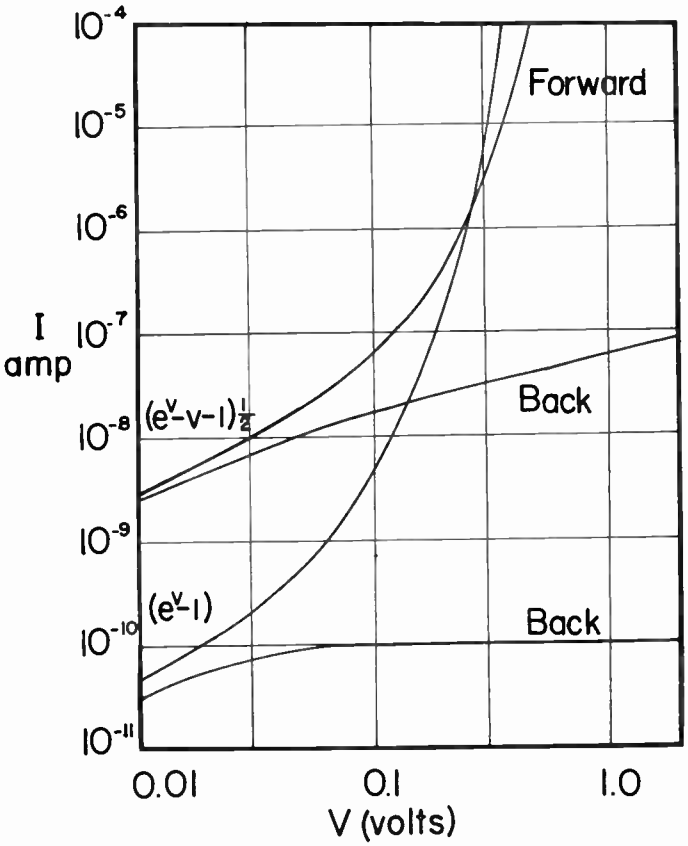

Fig. 2—Plots of theoretical junction and leakage current components for $I_j = 10^{-10}$ a, $I_L = 10^{-8}$ a.

Eq. (6) can be integrated numerically, but it suffices for our purpose to consider two approximations:

$$x_1 = \lambda e^{-v/2} \qquad \text{for } v \gg 0 \tag{8}$$

$$x_1 = \lambda(-v - 1)^{1/2} \qquad \text{for } v \ll 0 \tag{9}$$

One sees that x_1 becomes small rapidly with an increasing forward bias, and increases as the square root of reverse bias. Its magnitude is characterized by the distance parameter λ. It is apparent then, that as one increases the forward bias, not only is the leakage current less important compared to the junction current, but the leakage path becomes negligibly small; it is biased out. Since one can use one-dimensional equations even with radial geometry, provided that x_1 is small compared to the radius of the junction, the solution in equations (3) and (5) is valid in the forward direction for radial geometry. In this case, L is the circumference. We note here, for later reference, that the radial solution in the reverse direction predicts that I_2 will increase with increasing bias more rapidly than is indicated by (3).[8]

It should be recognized that changes in the "length" x_1 of the leakage path, as predicted by this model, would occur instantaneously on application of a bias. Phenomena involving time dependent changes would require that σ or I_s be functions of time.

[8] P. R. Aigrain, "Phenomena of rectification and transistance in germanium," *Ann. Phys.*, vol. 7, p. 140; January–February, 1952.

Experimental Results

The data reported here were obtained by extensive measurements of four silicon diodes, which were chosen at random from some production samples. The diodes were made by fusion on *n*-type silicon. The resistivities ranged between 0.3 and 10 ohm-cm. All of them showed the same qualitative behavior. Less extensive measurements on other silicon-fused junction diodes, including some prepared at another laboratory, also showed results similar to the ones reported here. Table I shows the pertinent data for the four diodes and the constants computed by analysis of the current voltage curves, measured at a number of temperatures, in the light of (5). The analysis is described in the following paragraphs.

TABLE I

Diode number	Probable resistivity range ohm-cm	I_j at 25°C 10^{-15} a	I_L at 25°C 10^{-10} a	Activation energy for I_j ev	Activation energy for I_L ev
1	1–2	5.7	1.0	1.25	0.61
2	4–10	5.6	1.5	1.25	0.64
3	2.5–5	11.8	1.8	1.26	0.64
4	0.3–0.8	3.2	1.0	1.27	0.61

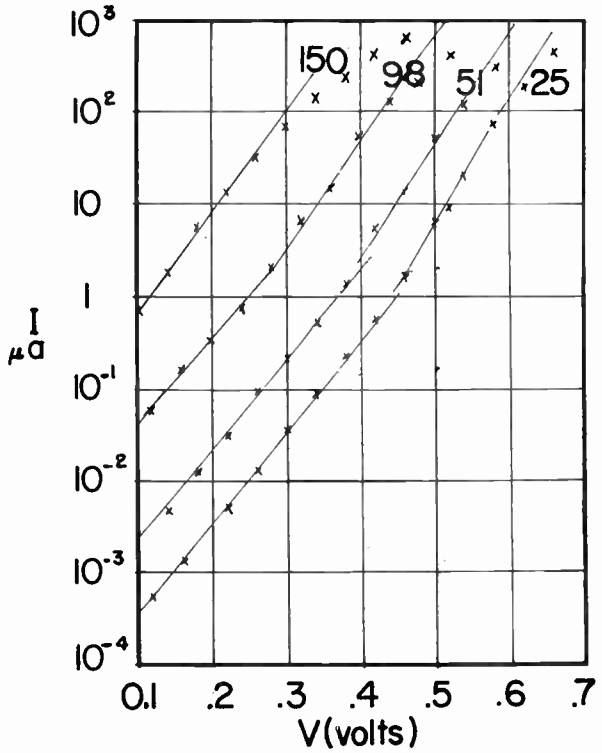

Fig. 3—Plots of ln$I$ vs V for diode no. 3 at 25°C., 51°C., 98°C., and 150°C.

Fig. 3 shows forward current plots for one of the diodes of log I vs V. When data are obtained with sufficient accuracy, (V is measured by means of a potentiometer) the curve shows a distinct break between two straight line regions. The lower part has a slope somewhat larger than $q/2kT$, and the upper part has a slope somewhat smaller than q/kT. The effect of the voltage drop in the base becomes apparent where the current is larger than 10^{-4} amperes. The curves are consistent with (5), and suggest that the two parts correspond, respectively, to the leakage current and the junction current. Rather than extrapolate to obtain the values of I_L and I_j, a more accurate procedure is used, as follows.

If one divides both sides of (5) by the leakage current function, one obtains for the forward direction

$$I(e^v - v - 1)^{-1/2} = I_L + I_j[(e^v - 1)/(e^v - v - 1)^{1/2}]. \quad (6)$$

The left-hand expression, computed from experimental data, plotted against the bracketed function in the second term on the right should be a straight line with slope I_j and intercept I_L. Fig. 4 shows a plot of this sort for a silicon diode at room temperature. Table I includes the room temperature values of I_L and I_j.

Fig. 5 (next page) shows plots of ln I_L and ln I_j as functions of $1/T$. It was found, for all diodes examined in this way, that the I_j points fell very well on a straight line with a slope that corresponds to an activation energy near 1.26 ev. When correction is made for the anticipated dependence of I_j on T^3 the slope was 1.20 ev; this is in fair agreement with the width of the forbidden band in silicon.

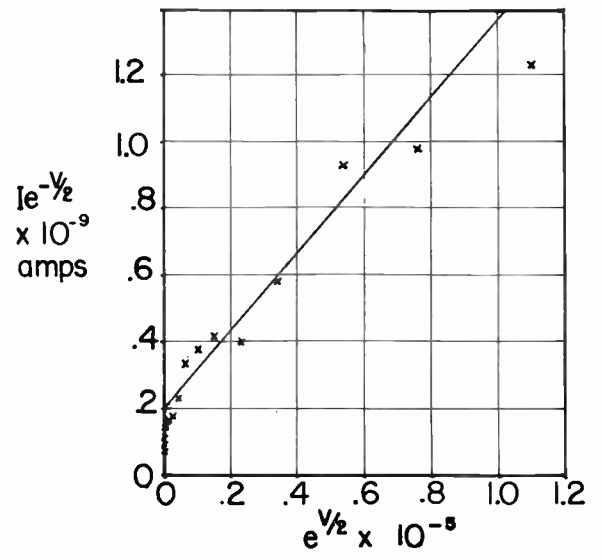

Fig. 4—Linear plot for analysis of I_j and I_L for diode no. 3 at 25°C. $I_j = 1.18 \times 10^{-14}$ a, $I_L = 1.8 \times 10^{-10}$ a.

The points for I_L lie on a straight line, but with larger deviations than I_j. The data for different diodes seem to show a similar deviation from a straight line, so that it seems likely that they represent a curve rather than scatter about a straight line. (It may be a linear plot with a break. The data are insufficient to tell.) The slope of the curve corresponds to an activation energy of 0.62 ev.

So far, the discussion of the experimental results has indicated good agreement with theory. There are further

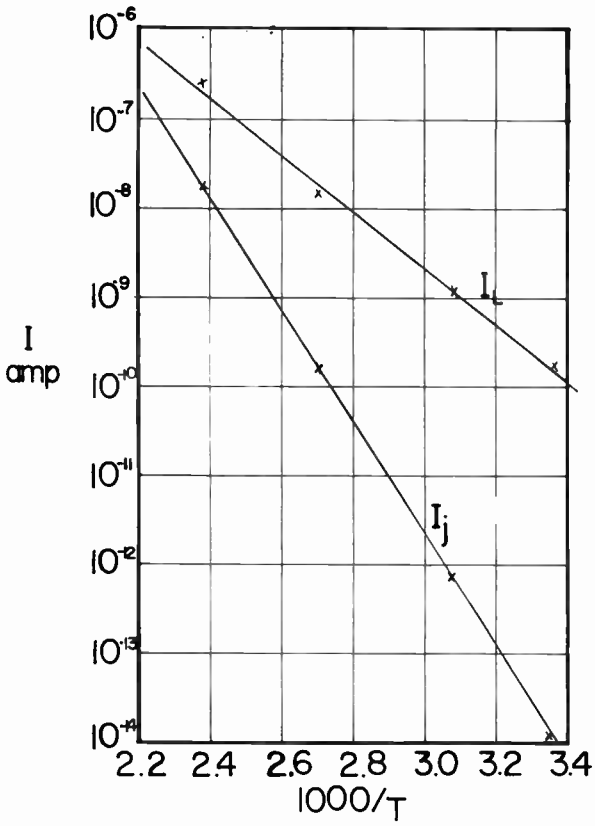

Fig. 5—Activation energy plots of I_j and I_L for diode no. 3.

observations which contain greater ambiguity. The data for low voltages, when plotted in Fig. 4, should all fall at the intercept, since $(e^v-1)(e^v-v-1)^{-1/2}$ is negligible on this scale, and $I(e^v-v-1)^{-1/2}$ should be constant and equal to I_L. It is not constant, however, and $I(e^v-v-1)^{-1/2}$ shows a steady decrease to a value of the order of one third of the extrapolated value of I_L. This is another way of saying that at these voltages the junction component of the current is negligible, and the leakage component is observed to deviate from the form of (3). However, in view of the fact that I changes by many orders of magnitude, whereas the change in $I(e^v-v-1)^{-1/2}$ is relatively small, (3) seems to be a good first-order approximation.

This discrepancy extends into the reverse bias region, where $-I$ should vary, theoretically, as $(-v-1)^{1/2}$. Fig. 6 shows a typical plot of the forward and reverse branch of $\ln I$ vs $\ln V$. It is seen that the slope of the reverse branch is usually smaller in magnitude than 0.5, and is not generally constant. This deviation cannot be explained by the fact that radial geometry exists instead of linear geometry, since the former would lead to a slope that is larger in magnitude than 0.5. The deviations are probably the result of deficiencies in the theoretical model, and will be discussed later.

The magnitude of the leakage current is of interest. The value at room temperature is of the order of 10^{-8} a. The reverse current, at any bias, represents the product of the saturation current density for the surface barrier and the area over which the leakage path extends at the bias. There is evidence that the length of the path in silicon is very short.[9] But even if it had the magnitude of the dimensions of the diode, the surface saturation current density is too large to be accounted for by generation of minority carriers in the bulk. The conclusion, then, is that the surface barrier is low enough so that the emission of majority carriers from the top of the barrier is dominant.

It is of interest to compare the measured values of I_j with the theoretical junction saturation current $q(D_p/L_p)p_0A$. The value of A is $1\text{–}2\times10^{-3}$ cm^2, and the resistivities are known only to a factor of 2 or 3. Using these numbers, it is found that τ_p must be at least the order of milliseconds. This is undoubtedly large by a factor of 100, indicating that the measured I_j are smaller than the theoretically expected ones by factors of ten or more.

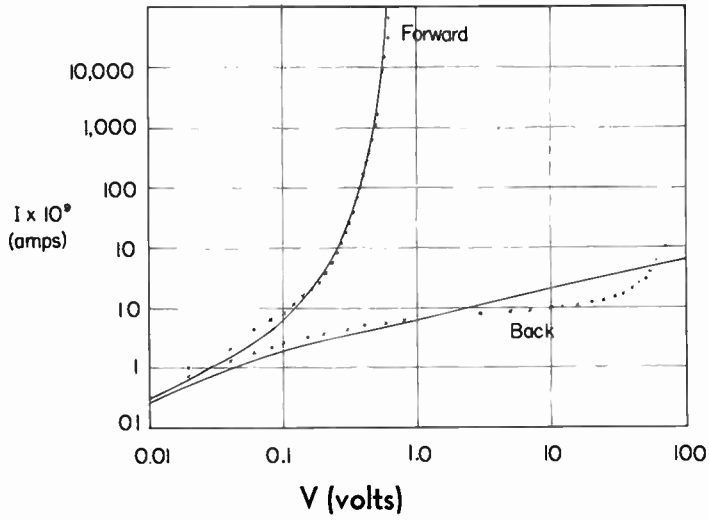

Fig. 6—Experimental points and theoretical curve for diode no. 1 at room temperature. The equation of the theoretical curve is $I=5.7\times10^{-15}(e^v-1)+1.0\times10^{-10}(e^v-v-1)^{1/2}$.

Conclusion

The general agreement with experiment, noted above, shows that the model is a useful first approximation for understanding and analyzing surface leakage currents in silicon diodes. The observed discrepancies, on the other hand, indicate the need for refinements in the model.

The improved model should take into account the dependence of the surface conductivity on the field, and the possible change in σ and I_s with bias, as the result of shifts in the field at the surface. It is known that the conductance of an inversion layer decreases if one has a larger field at the surface. This is in the proper direc-

[9] R. Gudmundsen (personal communication). His observations were made with an optical microprobe. He found that the leakage path is on the n-type side.

tion to account for the apparent decrease in I_k with decreasing forward bias. McWhorter and Kingston have derived the equation for leakage current in the reverse direction where I_s is constant but σ is inversely proportional to V.[5] The shape of this theoretical curve seems to be closer to the experimental ones, but it cannot be fitted accurately.

It is worth noting that the certain features of the behavior of I_2 as given in (3) are probably general ones, and independent of the details or degree of refinement of the model. These consist in the facts that I_2 varies, in the forward direction, roughly as exp. $(qV/2kT)$, and in the back direction as some power of qV/kT. This can be deduced from considerations that follow.

In the general case, σ in (1) and I_s in (2) may be functions of the bias V' at any point. Therefore, one derives the following equation instead of (3):

$$I_2^2 = \frac{2kT}{q} L^2 \int_0^v \sigma(y) I_s(y)(e^v - 1)dy, \qquad (7)$$

where the variable of integration y is qV'/kT. It is clear that if σ and I_s are slowly varying functions of V', then I_2 could be expressed as

$$I_2 = F(v)e^{v/2}. \qquad (8)$$

$F(v)$ will change slowly with v, compared to $e^{v/2}$; it could be interpreted as roughly corresponding to I_L of (4), with the values of σ and I_s appropriate for that value of v.

In the reverse direction, on the other hand, the exponential term in the integral is not significant, and the dependence of σ and I_s on V' will play an important part in the nature of the integral:

$$I_2 = -G(v) \qquad (9)$$

where G will be a relatively slowly varying function of v.

If one grants that the above model is necessary and sufficient in its basic elements to explain the behavior of silicon diodes, then several implications are indicated. which are of interest in developing a more comprehensive understanding of what may have been considered as diverse phenomena.

1) The discrepancy of the behavior of reverse currents and their dependence on temperature with the theory for p-n junctions was one of the main instigating reasons for this work. The conclusions are self-evident and consist in a dissociation of the observed phenomena from the predictions of simple p-n junction theory.

2) The fact that the surface leakage current may constitute most or all of the current, has important implications in the study of noise. The "$1/f$" power dependence of noise observed in back currents of diodes has long been associated with surface phenomena. The obvious procedure, of dividing the observed current into junction and surface components, and separating the noise contributions of the two, is being approached in recent work in this field.

3) As the length of the leakage path is increased by decreasing the bias, the area of the effective junction is increased. This would cause the capacitance of the diode to decrease less rapidly than what is predicted by p-n junction theory. The importance of this effect will depend on the relative magnitude of the area of the effective leakage path (x_1L) and that of the junction. This effect is probably negligible in silicon, which seems to have a small leakage path. It may, however, be significant in germanium.

4) The possibility that the leakage path may be on the regrown region of a fused junction is an important consideration in device fabrication. If this happens, the impedance of the surface leakage path will have a maximum value, achieved when the bias is sufficient to cause the effective path x_1 to extend across the entire regrown region. Since the latter may be very small, this could seriously limit the reverse impedance of a diode.

The current-voltage curves which were observed in a number of silicon diodes prepared by fusion on p-type material seem to be affected by this limitation. A typical such curve is shown in Fig. 7. It is noted that $I(v)$ becomes linear in the neighborhood of the origin over a large range of voltage, compared to kT/q. The fact that the impedance does continue to increase in the reverse direction, even though it does so slowly compared to n-type diodes, can be explained, as before, by a decrease in the conductivity of the leakage path. If this explanation is correct, of course, one concludes that the leakage in silicon is on the n-type surface. This conclusion has been substantiated by observations noted.[9]

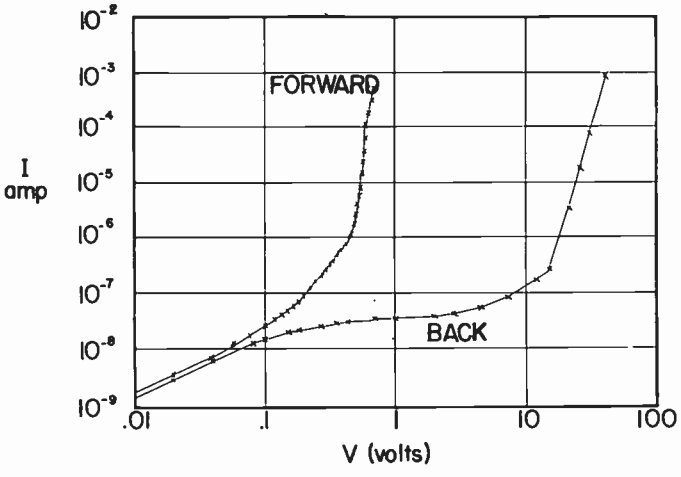

Fig. 7—Experimental curve for p-type silicon diode.

ACKNOWLEDGMENT

We would like to acknowledge the assistance of Ruth Rawa, who made the measurements upon which most of this work is based.

On the Mechanisms of Radar Sea Clutter*

MARTIN KATZIN†, FELLOW, IRE

Summary—Experimental data on radar sea clutter are described and discussed with reference to the physical principles involved. It is shown that the scattering elements are illuminated by a combination of direct and indirect fields, the latter being "reflected" by surface elements closer to the radar. At small depression angles these interfere destructively, giving rise to the so-called "critical angle," polarization dependence, "spikiness," and steeper frequency dependence.

A theory is developed in which the elemental scatterers are taken to be the small patches, or "facets," of the surface. It is found that the facets which back scatter most effectively at small depression angles are those whose dimensions are of the order of the wavelength, and that the frequency dependence of the scattering parameter σ^0 at small depression angles is determined by the size distribution of the facets. If the size and slope distributions of the facets are independent of each other, then, below a high-frequency limit, σ^0 has essentially the same frequency dependence at low angles and high angles. The high-angle variation of σ^0 with angle is determined mainly by the slope distribution of the facets. With the slope distribution determined from optical measurements by Cox and Munk, σ^0 is approximately proportional to wind speed at small depression angles, but inversely proportional to wind speed at vertical incidence. Using measured values of σ^0, the facet mechanism accounts for scattering by the entire surface of the sea.

Introduction

SEA CLUTTER, which is back scattering from the sea surface itself, frequently limits the ability of airborne and shipborne radar to detect targets, especially targets on or near the surface. In an effort to find ways of minimizing it, a number of investigations into its properties were carried out during World War II. Goldstein, who was perhaps the first to study the phenomenon systematically in a quantitative way, has given a thorough discussion of the results of these investigations.[1]

The sea clutter phenomenon is complicated by its dependence on a number of parameters, principally the depression angle (angle below the horizontal at which the sea is viewed), the polarization, the frequency, and the condition of the sea surface. In order to describe the back-scattering properties of the surface quantitatively, Goldstein[2] introduced a dimensionless quantity σ^0, the back-scattering cross section per unit area of the sea. From measurements of this quantity, he found the following characteristics:

1) There is a "critical angle" below which σ^0 decreases rapidly with decreasing angle, and above which it rises much more slowly, or remains constant. Furthermore, the critical angle decreases with increasing frequency.

2) There is a pronounced polarization dependence of σ^0, which, in turn, depends on the roughness of the sea. In calm seas, horizontal polarization gives much less clutter than vertical polarization, but the difference between the two polarizations substantially disappears in rough seas, or may even reverse somewhat.

3) The frequency dependence of σ^0 varies between about λ^{-4} in calm seas to about λ^0 in rough seas.

4) At times the area-extensive characteristic of sea clutter breaks down. On a radar with a pulse short enough to resolve individual waves, the scattering appears to be concentrated in the vicinity of the wave tops. This gives an *A*-scope presentation of the clutter a "spiky" appearance.

Goldstein was unable to find a satisfactory theory to explain the above characteristics. The polarization dependence could be explained very well by a surface reflection phenomenon, which led to the supposition that water droplets thrown up from the surface were the basic scattering elements. However, this led to violent disagreement with the frequency dependence.

More recently, Davies[3] has given a statistical analysis of the problem involving the autocorrelation of the surface irregularities. This gave fair agreement with the shape of the experimental curve for large depression angles, but violent disagreement at low angles. Furthermore, his model gives no frequency dependence.

This paper will discuss the results of an investigation of the characteristics of sea clutter made by the Naval Research Laboratory, and continued subsequently by the author. The results show that a reflection interference phenomenon, such as had been found to be important in the case of surface targets, also is important in the sea clutter phenomenon. This reflection phenomenon explains the critical angle, and the polarization dependence. It also explains the "spiky" appearance of clutter on an *A*-scope at very small depression angles.

From the existence of the reflection phenomenon and the observed frequency dependence, the basic scattering is suggested as being due to the small facets which overlie the main large-scale wave pattern, or swell. The theory of this mechanism is developed, and it is found that the facets which back scatter most effectively at small depression angles are those whose dimensions are of the order of the wavelength, and that the frequency dependence of σ^0 at small depression angles is determined by the size distribution of the facets. Furthermore, if the size and slope distributions of the facets are

* Original manuscript received by the IRE, March 19, 1956; revised manuscript received August 13, 1956.

† Electromagnetic Res. Corp., Washington, D. C.; formerly at the Naval Res. Lab., Washington, D. C.

[1] D. E. Kerr, Ed., "Propagation of Radio Waves," M.I.T. Radiation Lab. Ser., McGraw-Hill Book Co., Inc., New York, N. Y., vol. 13, pp. 481–587; 1951.

[2] H. Goldstein, "Frequency dependence of the properties of sea echo," *Phys. Rev.*, vol. 70, pp. 938–946; December 1 and 15, 1946.

[3] H. Davies, "The reflection of electromagnetic waves from a rough surface," *Proc. IEE*, part IV, vol. 101, pp. 209–214; August, 1954.

independent, then, below a high-frequency limit, σ^0 has essentially the same frequency dependence at low and high angles. The high-angle variation is found to be determined mainly by the slope distribution of the facets. Making use of slope distributions determined from optical measurements, σ^0 is found to be approximately proportional to wind speed at small depression angles, but inversely proportional to wind speed at vertical incidence. Using measured values of σ^0, the facet mechanism accounts for scattering by the entire surface of the sea.

Finally, the limitations imposed by the assumptions introduced in the theory are discussed, and suggestions are made for further development of the subject.

Reflection Interference Phenomenon

In 1950, the Naval Research Laboratory made rather extensive measurements of sea clutter on airborne radars. Three radars, operating at wavelengths of 3.2, 9.1, and 24 cm, were operated simultaneously in a single aircraft, and were arranged to view a fixed location on the sea. The measurements were made in the vicinity of the island of Bermuda, B.W.I., because this area give comsparatively uniform oceanographic conditions and is quite free of surface traffic and flotsam. Runs were made at altitudes from 200 to 10,000 feet upwind, downwind, and crosswind, with the antennas generally pointed along the ground track of the aircraft. Ocean wave heights were made simultaneously from a surface vessel, which also served to define the fixed location on the surface viewed by the radars.

The results of a typical run, at a wavelength of 3.2 cm, are shown on Fig. 1. This is a plot of received clutter

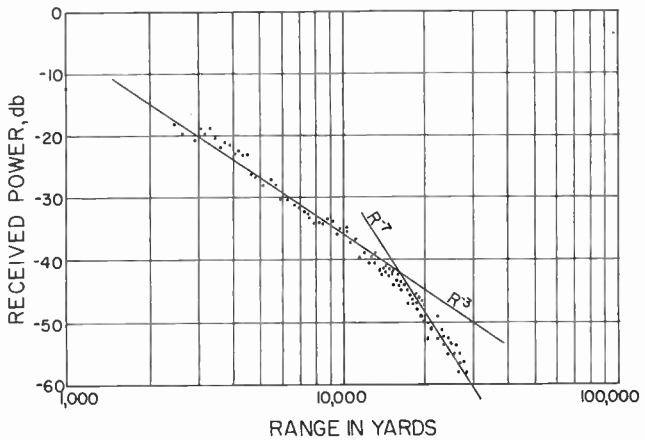

Fig. 1—Received sea-clutter power vs range. $\lambda = 3.2$ cm, altitude 1000 feet. The two lines drawn through the measured points represent R^{-3} and R^{-7} variations, respectively.

power, on a linear decibel scale, against range, on a logarithmic scale. Each dot represents the tenth highest peak on an A-scope photograph of about 300 consecutive pulses (over a time interval of about 1 second).[4]

[4] From simultaneous pulse-to-pulse photographs, it was found that this level was 8 to 10 db above the median level.

The experimental points can be fitted satisfactorily by two straight lines, corresponding to range variations of R^{-3} and R^{-7}, respectively.

This type of variation is strikingly suggestive of the type of power-vs-range plot obtained on a surface craft, where the two straight lines correspond to R^{-4} and R^{-8} laws, respectively. This division into two regimes, which we have termed near and far zones, respectively, has been shown[5] to be due to an interference phenomenon caused by reflection from the surface of the water. In the far zone the target is wholly below the lowest lobe of the interference pattern, so that the illumination of the target is less than the free-space value, and becomes progressively less as the target moves out in range. In the near zone, on the other hand, the target subtends one or more lobes, so that, in effect, it integrates the varying illumination over it, with the result that the deep ripples of the lobe pattern are almost completely smoothed out.

In the case of pulsed radar viewing an area-extensive target, such as sea clutter, the aximuthal extent of the surface which is illuminated is equal to $R\Phi$, where Φ is the azimuthal beamwidth, and so increases directly with range. Hence, in the case of an area-extensive target, the reflection phenomenon described above yields an R^{-3} range variation in the near zone and an R^{-7} range variation in the far zone.

The reflection theory outlined above is based on a flat reflecting surface. In most cases the effect of the earth's curvature is negligible in sea clutter measurements.

Transition Range

The transition between the near and far zones is a smooth one, and occurs near the angle of the first lobe. If the transition range, R_t, is defined as the intersection of the R^{-3} and R^{-7} lines, then, for a target uniformly distributed in height,

$$R_t \approx \frac{hH}{0.2\lambda}, \tag{1}$$

where h is the radar height and H the height of the top of the "target." For a given target, then, the transition range will be directly proportional to the frequency, and to the radar height. This relation, therefore, can be used to test the existence of the reflection phenomenon. For measurements which are made under the same sea conditions, the values of clutter power at various altitudes, on a given frequency, should give a family of curves such as shown in Fig. 2. These curves should join together smoothly into a single curve if the various branches of Fig. 2 are "slid" along the R^{-3} line until their transition ranges coincide. This is attained by using as abscissa the quantity $\log(R/R_t)$, and as ordinate, $\log(\sigma R_t^{-3})$. Furthermore, if σ^0 is independent of frequency, then the graphs on the several frequencies, after normalization to constant beamwidth, should

[5] Kerr, *op. cit.*, pp. 472–481.

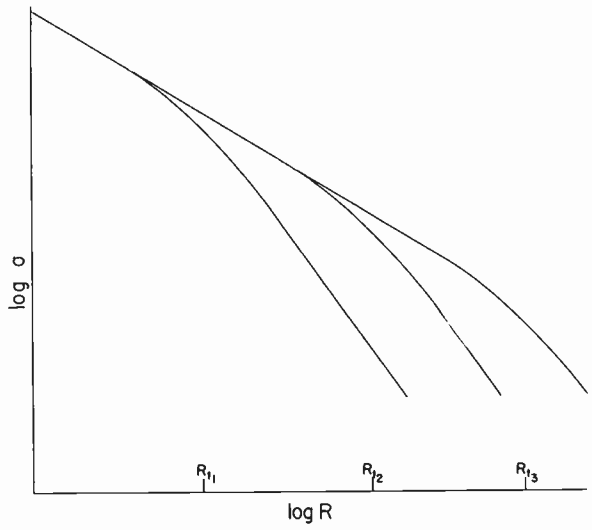

Fig. 2—Illustrating form of σ vs R curves obtained on a given radar at various altitudes.

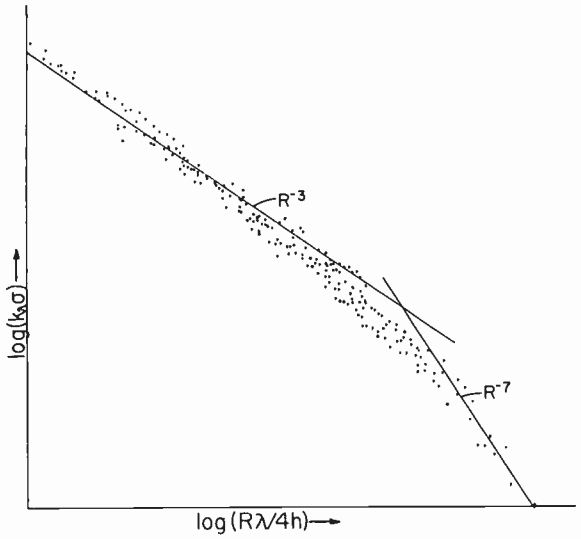

Fig. 3—Composite plot of sea-clutter power at three frequencies and six altitudes from 200 to 10,000 feet. Coordinates normalized to test interference mechanism.

match when superimposed; any adjustment *vertically* (without shift of abscissa) required to produce a match is then due to the variation of σ^0 with frequency.

Fig. 3 shows the result of such a superposition of the results for the three wavelengths (3.2, 9.1, and 24 cm) and for six altitudes from 200 to 10,000 feet. This is a composite plot of 17 different runs. The agreement with the type of behavior expected on the basis of the reflection mechanism is satisfactory, especially in view of the fact that some wind speed variations occurred during the time required to make the measurements (approximately $2\frac{1}{2}$ hours). From this it is concluded that the reflection mechanism does indeed exist.

If the effective target height H is calculated from the transition ranges, it is found to be much less than the measured wave height. This indicates that the reflection takes place above the wave troughs.

Illumination Factor

Because of the variation in illumination of the surface, produced by the reflection process, the radar equation normally used needs to be modified. This can be done by affixing an illumination factor $\overline{F}$,

$$\overline{F} = \frac{1}{H}\int_0^H \sigma F^4 dh,$$

where F represents the interference between direct and reflected fields, σ is the radar area of a scattering element (a function of height, h, above the reflecting level, in general) and H the height of the highest scattering element. The appropriate radar equation then becomes

$$P_r = P_t G^2 \lambda^2 \sigma^0 A \overline{F}/(4\pi)^3 R^4,$$

where A is the area of sea illuminated.

For a uniform distribution of σ with height, and a reflection coefficient of -1, $\overline{F}$ may be approximated by two values, corresponding respectively to the near and far zones. In the near zone,

$$\overline{F} = 6, \qquad R < R_t,$$

while in the far zone,

$$\overline{F} = 6(R_t/R)^4, \qquad R > R_t.$$

Thus, under the conditions assumed, the reflection phenomenon increases the back scattering by six times (7.8 db) in the near zone.

Frequency Dependence

In virtue of the reflection mechanism, it is evident that the frequency dependence of σ^0 should be deduced only from near-zone (R^{-3}-region) measurements. Otherwise the intrinsic frequency dependence of the backscattering mechanism would be "contaminated" by the interference phenomenon, which is also frequency-dependent.

Goldstein found the apparent frequency dependence of σ^0 to vary between about λ^{-4} in calm seas to about λ^0 in rough seas. Since sea roughness (in the sense of gross wave height) varies the transition range [see (1)], it follows that Goldstein's results indicate an intrinsic frequency dependence of about λ^0, *i.e.*, that σ^0 is independent of frequency. The NRL measurements at Bermuda gave values of σ^0 at the three frequencies used, which scattered, in varying degrees, about a best-fitting straight line. This line corresponds to a wavelength dependence close to λ^{-1}. The implications of this dependence with respect to the scattering mechanism will be discussed later.

Polarization Dependence

Goldstein[6] showed that the observed polarization dependence of σ^0 is explained completely by the reflection interference phenomenon discussed above. This led him

[6] *Ibid.*, pp. 522–526.

to consider spray droplets thrown upwards from the waves as the scattering elements, but this gave the wrong frequency dependence. Goldstein apparently did not appreciate that reflection interference could take place for elements of the surface itself.

Spikiness

It will be noted that the transition from the R^{-3} to the R^{-7} region in Fig. 3 is a gradual one. This indicates that the scattering elements are distributed over a considerable range of heights over the reflecting surface. As a result, destructive interference sets in for the higher scattering elements at smaller depression angles than for the lower scattering elements. At times this can result in the breakdown of the area-extensive character of the clutter, when only isolated wave crests receive strong illumination. This is illustrated in the *A*-scope photographs shown in Figs. 4 and 5,[7] taken from the NRL Bermuda data. Fig. 4 was taken from a depression angle of 6°, while Fig. 5 was taken from a depression angle of 0.85°. In Fig. 4 the clutter gives an appearance resembling white noise, while in Fig. 5 the clutter appears to be concentrated at discrete ranges, giving a "spiky" appearance to the *A*-scope presentation. This "spiky" appearance occurs in spite of the fact that the pulse length ($\frac{1}{2}$ microsecond) was not short enough to resolve the individual waves.[8]

Thus, from the reflection mechanism discussed earlier, many of the previously reported characteristics of sea clutter are readily explainable. The so-called "critical angle" is the one which corresponds to the transition range. If due account is taken of the illumination of the scattering elements, then σ^0 is a slowly-varying function of frequency. The observed polarization properties apparently are completely explainable in terms of the reflection mechanism, so that it then follows that intrinsically the scattering is about the same for horizontal and vertical polarizations. Spikiness at very small depression angles takes place when destructive interference reduces the illumination of all except isolated wave crests.

The existence of the reflection mechanism has been deduced from the nature of the experimental results. The details of the reflection process, as related to the actual form of the sea surface, remain to be worked out, however. This will not be undertaken here.

Scattering Mechanism

Since σ^0 at small depression angles is a slowly-varying function of frequency, the problem of deducing a scattering mechanism which will fit the experimental data satisfactorily is greatly simplified. Since the order of magnitude of σ^0 for small depression angles is about

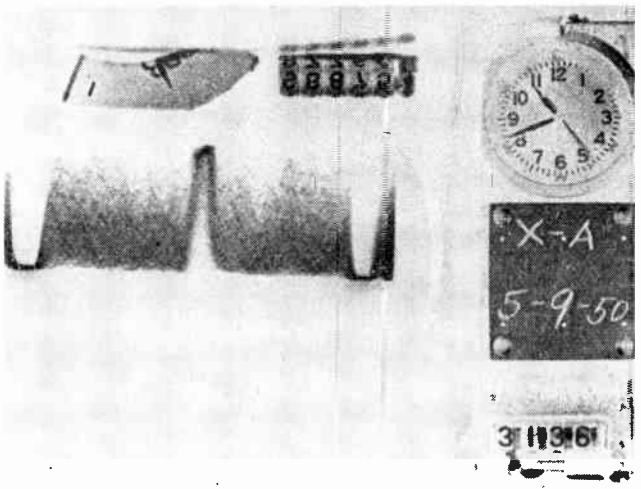

Fig. 4—Expanded *A*-scope photograph of sea clutter showing noise-like character of the clutter. The saturated echo in the center of the sweep is from a stationary ship. Blanking gates near both ends of the sweep define the base line. Wavelength 3.2 cm, altitude 5000 feet, range 16,000 yards.

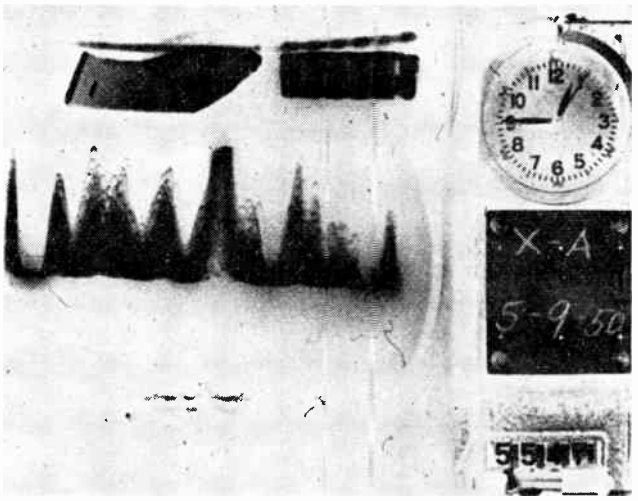

Fig. 5—Expanded A-scope photograph showing spiky clutter at 0.85 degrees depression angle. Wavelength 3.2 cm, altitude 200 feet, range 4500 yards.

10^{-4}, or less, for $\lambda = 10$ cm, a mechanism which is rather highly directive is required. This suggests that the scattering properties of inclined flat plates be investigated. Hence the following mechanism will be considered here: The basic scattering elements will be assumed to be the small facets which overlie the main large-scale wave pattern, or swell. The surface of the sea is considered to be the superposition of facets of various sizes, with orientations distributed about the mean sea contour. These facets are assumed to move randomly, so that their phases are independent. For small depression angles, the back scattering corresponds to angles far removed from the facet normals. Although this model has been proposed to explain the characteristics at small depression angles, it will be found that it gives a satisfactory explanation of most of the observed clutter characteristics over the entire range of depression angles.

[7] The saturated echo in the middle of the sweep is from the surface vessel used for oceanographic measurements, while blanking gates are provided at each end of the sweep to fix the baseline.

[8] A similar type of presentation was shown by Goldstein, *op. cit.*, p. 492, but this was taken with a short pulse which could resolve the individual waves.

Scattering From Flat Plates

As a first step, the scattering from flat plates will be considered. After a discussion of the basic principles involved, a quantitative treatment, taking into account a distribution of facet sizes and slopes, is given. The details are worked out in the Appendix, and will only be summarized here.

Scattering at Small Depression Angles: For a flat plate of area A whose dimensions are large relative to λ, the maximum back scattering occurs when the plate is parallel to the incident wave front, and is proportional to A/λ^2. If the plate is tilted in the plane of incidence, a progressive phase lag between the farther and nearer elements of the plate is introduced, whereupon the back scattering is reduced to, at most, that from a single Fresnel zone of length $\lambda/4$. The maximum back-scattered field is then independent of the length of the plate. Similarly, if the plate is given an additional tilt at right angles to the plane of incidence, so that the width elements are no longer excited in phase, the maximum back scattering then also becomes independent of the width, and hence completely independent of the size of the plate. Since the total field intercepted by the plate is proportional to $\sin\theta$, the maximum back-scattered power for inclined plates varies as $\sin^2\theta$, and thus increases as the angle of the plate to the wave normal is increased. If we consider the application of these principles to the sea surface, it becomes evident that, for plates large relative to λ, the important back scattering at low angles will come from the heads of the wave crests, where the slopes are steepest and face the observer.

For circular plates we find

$$\sigma \propto \lambda A^{1/2}, \qquad \sigma/A \propto (A/\lambda^2)^{-1/2}.$$

This is the same as the average of an ensemble of rectangular plates distributed over a range of azimuth angles. The quantity σ/A is important for assessing relative contributions to σ^0, since the number of plates of a given size which can be accommodated in a unit area of surface is inversely proportional to the plate area. From this relation, it is evident that for "large" plates, the larger the plate the smaller is its average contribution to σ^0.

For plates whose dimensions are small relative to λ, on the other hand, the scattering is not strongly dependent on angle, and is proportional to D^6/λ^4, so that

$$\sigma \propto A^3/\lambda^4, \qquad \sigma/A \propto (A/\lambda^2)^2.$$

Thus, for "small" plates, the contribution to σ^0 is larger the larger the plate.

From the relations for "large" and "small" plates given above, it is apparent that there must be some intermediate range of plate size (measured in terms of λ^2) which is most effective for small-angle back scattering. The quantitative relations in this intermediate range are not available in easily calculable form, so an approximation is used here which is based on extrapolation of the "small" and "large" size relations into the intermediate region until they meet.

For facets which are circular disks, the resulting behavior as a function of plate size for several values of facet tilt are shown in Fig. 6. From this it is found that the optimum diameter, D_1, is about $\lambda/(2\pi)$, or the circumference is about a half-wavelength. In effect, then, the operating frequency focuses attention on the facets whose dimensions are of the order of the wavelength ($2\pi D/\lambda \approx 1$). From this, one would expect that the frequency dependence of σ^0 would be linked to the size distribution of the facets. This will be borne out by the quantitative analysis to be discussed below.

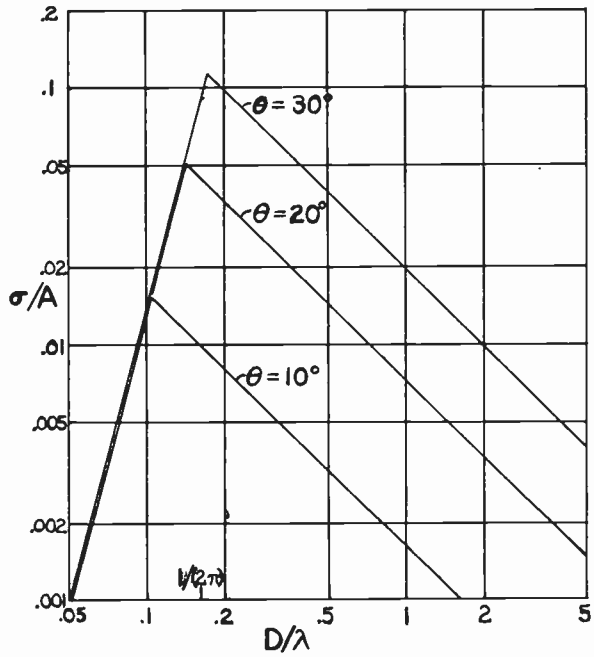

Fig. 6—σ/A for inclined circular disks.

It is evident that facets of various sizes and slopes have to be considered. In the absence of contrary information, it is assumed that the size and slope distributions are independent of each other. The distributions are assumed to be continuous, so that the value of σ^0 is found by integrating values of σ for all facets in a unit area of surface. The result, which is worked out in the Appendix, shows that the functional form of the size distribution determines the frequency dependence of σ^0 at small depression angles, and conversely. In general, if $\sigma^0 \propto \lambda^{-n}$, then the number of facets per unit area is

$$N = N_0 A^{-(n+4)/2} \tag{2}$$

where N_0 is a constant. This result stems from the fact that $N\sigma$ is a decreasing function both above and below A_1, where A_1 corresponds to the joint of the lines in Fig. 6, and that A_1 is proportional to λ^2. It follows readily from this that σ^0 is approximately proportional to the fraction of the total area which is "large" (see the Appendix).

As far as is known to the writer, no measurements of facet size distribution exist. Indeed, it appears that radar back-scatter measurements offer an attractive means of deducing such information, as well as of slope distribution of the facets.

Relatively few measurements of slope distributions of the facets of wind-generated waves have been made, notably those by Duntley,[9] who measured the electrical resistance between spaced vertical wires, by Schooley,[10] and by Cox and Munk,[11,12] who used optical methods. They find that the probability distribution is approximately Gaussian, but is more peaked, and is skewed in the upwind-downwind direction. Cox and Munk expressed their results in quantitative form as a two-dimensional Gram-Charlier series, whose coefficients they expressed in terms of wind speed. This representation makes it possible to integrate over the angular distribution of the facets, so it is convenient for use here.

The Cox and Munk slope distribution is given by (16) of the Appendix. Cross sections through the two-dimensional surface representing the probability density of slope are shown in Fig. 7, corresponding to the upwind-downwind and the crosswind directions. Curves are shown for wind speeds of 10 and 20 knots.

Evaluation of σ^0 by the procedure outlined above gives the λ^{-n}-dependence discussed above, as well as a dependence on wind speed, W. For the upwind-downwind directions, and a value of $n=1$, the result obtained in the Appendix is

$$\sigma^0 \approx 9\cdot 10^{-3} N_0 \lambda^{-1} W^{3/4}(1 \pm 2\cdot 10^{-3} W). \qquad (3)$$

For the upwind direction sign of W is taken as positive, and negative for the downwind direction. In accordance with this relation, σ^0 should increase approximately linearly with wind speed. The Bermuda measurements show good agreement with this dependence.

From (3), the ratio of σ^0 upwind to that downwind is given by the theory as

$$\frac{\sigma_u{}^0}{\sigma_d{}^0} = \frac{1 + 2\cdot 10^{-3} W}{1 - 2\cdot 10^{-3} W}.$$

For a wind speed of 20 knots, for example, this gives a ratio of 1.08, or 0.34 decibel. Experimentally, however, ratios of 5 to 10 decibels have been observed. Thus the present theory greatly underestimates the upwind-downwind ratio.[13]

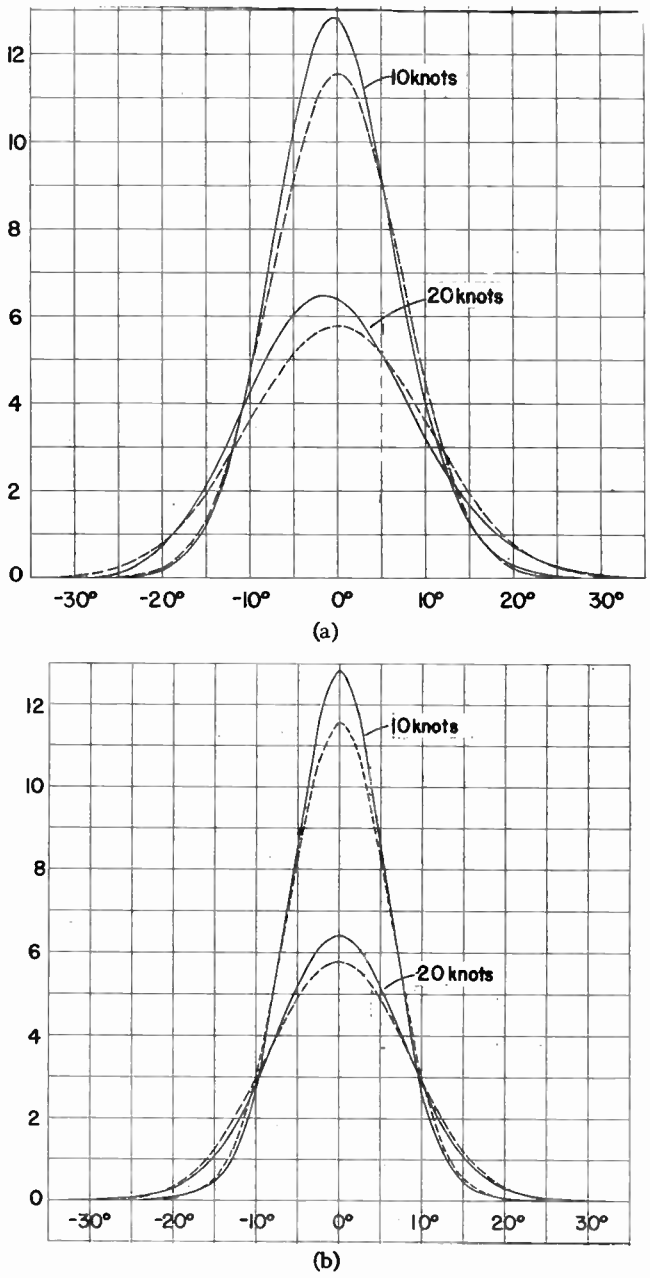

Fig. 7—Facet slope distributions according to Cox and Munk;[11,12] (a) shows the probability density vs inclination angle for the upwind-downwind direction, (b) for the crosswind direction. The dotted curves represent Gaussian distributions of the same mean-square slopes as the corresponding solid curves.

For a wind speed of 20 knots upwind, there is obtained from (3)

$$\sigma^0 = 8.85\cdot 10^{-2} N_0 \lambda^{-1}.$$

Inserting a measured value upwind (at Bermuda) of $8\cdot 10^{-4}$ at $\lambda = 3.2$ cm, and allowing for an illumination factor $\overline{F}$ of 4, this leads to

$$N_0 = 7.2\cdot 10^{-5}.$$

σ^0 was introduced to represent the radar area of unit area of sea surface. In a comparable way, we can introduce the numeric A^0, defined as the total area of facets per unit projected area of sea surface. Accordingly,

[9] S. Q. Duntley, "The visibility of submerged objects," Visibility Lab., Mass. Inst. Tech., Cambridge, Mass.; August 31, 1952.

[10] A. H. Schooley, "A simple optical method for measuring the statistical distribution of water surface slopes," *J. Opt. Soc. Amer.*, vol. 44, pp. 37–40; January, 1954.

[11] C. Cox and W. Munk, "Measurement of the roughness of the sea surface from photographs of the sun's glitter," *J. Opt. Soc. Amer.*, vol. 44, pp. 838–850; November, 1954.

[12] C. Cox and W. Munk, "Statistics of the sea surface derived from sun glitter," *J. Marine Res.*, vol. 13, pp. 198–227; November 1, 1954.

[13] If shadowing of the wave troughs by the preceding wave crests takes place (see Appendix and Fig. 9), then the upwind-downwind ratio will be increased greatly. Shadowing is neglected in this paper.

$$A^0 = \int_{A_0}^{A_2} N(A) A dA, \tag{4}$$

where A_0 and A_2 are the smallest and largest facet areas present, respectively. If the facets make up the entire sea surface, then A^0 should be about unity.

The value of A^0 depends mainly on A_0, the smallest facet area, since with the relation $\sigma^0 \propto \lambda^{-1}$ the density of the facets varies as $A^{-5/2}$, and the contribution to A^0 as $A^{-1/2}$. It follows from this that the relation $\sigma^0 \propto \lambda^{-1}$ cannot continue indefinitely to small values of λ, since this would require a corresponding decrease of $A_0^{1/2}$, and thus an increasingly large value of A^0.

The measured values of σ^0 may be used to estimate the smallest value to which the relation $\sigma^0 \propto \lambda^{-1}$ can be expected to continue. If we denote this by λ_0, and set $A_0^{1/2}$ equal to one-half the optimum dimension, we obtain from the value of N_0 computed above

$$\lambda_0 \approx 16 A_0^{-1/2} \approx 2 \cdot 10^{-3} \text{m} = 2 \text{ mm}.$$

It should be noted that this limiting value is based on the Cox and Munk slope measurements. Since they omitted whitecaps from their photometric measurements, it is quite possible that the above limit may not hold in practice.

The theory of low-angle back scattering by facets developed above thus yields the following characteristics: The facets which back scatter most effectively are those whose perimeter is about a half-wavelength. The back scattering increases approximately as the square of the facet slope, so that facets near the wave crest contribute most strongly. The frequency dependence of σ^0 is linked with the size distribution of the facets, σ^0 being proportional to the fraction of the total facet area which is "large." On the basis of the optical measurements of facet slopes by Cox and Munk (which omit whitecaps), σ^0 at small depression angles is approximately proportional to wind speed, and must ultimately decrease with increasing frequency. The facet mechanism accounts for scattering by the entire surface of the sea.

Scattering at Large Depression Angles: The facet mechanism allows the qualitative variation of σ^0 at large angles to be deduced quite readily.[14] At high angles some of the facets are viewed broadside, so that these give a preponderant echo, which will be proportionately stronger the larger the facet. In the main (broadside) back-scattering beam of a large facet, the radar area σ will depend on A^2/λ^2, but at the same time the average width of the beam will be proportional to $\lambda/A^{1/2}$. Thus, for a distribution of facet slopes, the overlapping of the beams of adjacent slopes will be less the larger the facet. For a two-dimensional slope distribution, the extra gain of a large facet is just counterbalanced by the reduction in the overlapping of adjacent beams due to the narrower beamwidth, so that the total back-scattered power in the main lobe is about equal to the power intercepted by the facet. Hence it follows that, insofar as scattering by the large facets is concerned, the back-scattered power will be proportional to the fraction of the surface which is "large."

A small facet (A/λ^2 small), on the other hand, will scatter rather isotropically in accordance with the relation A^3/λ^4, so that its total back-scattered power will be much less than the power intercepted. Hence high-angle back scatter will be due mainly to the large facets (A/λ^2 large).

It already has been assumed that the size distribution is independent of the slope distribution. This means that the relative number of facets in a given area range is the same at all angles. Then, since the fraction of the surface which is "large" determines σ^0 both at small and large depression angles, and in both regions this fraction is determined by $N(A)$, it follows that the frequency dependence of σ^0 at high angles is the same as at low angles, as long as $\sigma^0 \propto \lambda^{-n}$. However, if λ is reduced to the point where σ^0 at small depression angles starts leveling off, then the parallelism between the low-angle and high-angle frequency dependencies will cease. At high angles σ^0 then will remain sensibly constant with further decrease of λ, since all of the facets will have become "large."

It is easy to see that the angular dependence at high angles is determined by the slope distribution. In fact, to a first approximation, the angular variation of σ^0 is the complement of the slope distribution. This can be shown by the following argument:

The back-scattered power at a given angle of incidence comes mainly from the facets which are broadside, or nearly so (within their beamwidths) to the incident wave normal. The beamwidth of the back-scattering pattern of a facet determines the extent to which the power intercepted by the facet is "spread" over a range of adjacent angles. If all slopes were equally probable, then the degree of this "spreading" would be the same for all angles of incidence; that is, the contribution at a given angle of incidence from facets broadside to adjacent angles would be the same for all angles, since there would be the same number of facets at all angles. In the actual case, however, there are more facets which have very small slopes than large slopes, as shown by the slope distributions of Fig. 7. Then there will be more spreading from high angles to lower angles, so that the resulting angular distribution of σ^0 should be somewhat less steep than the slope distribution.

Finally, if the slope and size distributions are independent, it follows that the angular dependence of σ^0 is substantially independent of frequency.[15]

An estimate of the value of σ^0 at vertical incidence may be obtained if the "spreading" discussed above is

[14] A quantitative treatment will be given in a later paper.

[15] One should be careful *not* to conclude from this that the curve of received clutter power vs depression angle observed with a given radar set should be the same for radar sets of any frequency, or that such a curve represents the form of σ^c. Usually the radar antenna beamwidth will be large enough so that clutter power is received from a range of angles over which σ^0 varies appreciably. Also, the area of the surface which is illuminated, and the range, vary with depression angle.

neglected. σ^0 then may be written as the product of the Cox and Munk angular distribution and the fraction of the surface which is composed of "large" facets. Denoting the latter by ρ, we have approximately

$$\sigma^0 = 256\rho/W,$$

where W is the wind speed. Thus at vertical incidence σ^0 is inversely proportional to wind speed.

Since σ^0 at grazing angles has also been shown to be proportional to ρ, the above relation can be applied to obtain a first approximation for the ratio of σ^0 at vertical incidence to that at grazing incidence. The result is

$$\sigma_{90^\circ}{}^0/\sigma^0{}_{\theta\to 0} = 1.7\cdot 10^{-5}W^{-7/4}.$$

At a wind speed of 20 knots, for example, this gives a ratio of 29.6 db, while at 1 knot the ratio is 52.3 db.

Limitations of the Theory

Certain assumptions and approximations which were made in order to reduce the complexity of the analysis require further examination in a refinement of the theory aimed at the attainment of greater accuracy and wider applicability. In particular, the forward-reflection mechanism which results in the reduced illumination of the scattering elements at very small depression angles is in need of quantitative specification, so that the near- and far-zone regions may be calculated for various wave heights and frequencies. The shadowing due to adjoining wave crests, as mentioned in connection with Fig. 9, will need to be considered in this connection also. These effects will become less important as the depression angle increases, so that the transition from a high degree of coherence to incoherence between the direct and surface-reflected fields will require evaluation in a transition range of depression angles.

The transition from "small" to "large" facets has been effected by bold extrapolation into the region of intermediate size. Although the rigorous theory of diffraction by circular disks has been worked out[16,17] numerical evaluation is very cumbersome. Furthermore, it applies only to isolated discs for which the edge condition is applicable.[18,19] The effect of the interconnections between the edges of the facets on the sea surface is a problem which must be attacked by boundary-value methods. Since the intermediate sizes are the most effective for back scattering in the present theory, a more accurate evaluation for this size region is needed.

An explicit assumption introduced at the outset is that the scattered fields from the various facets are completely random. Although this assumption may be justifiable at microwave frequencies, at low frequencies the separation between adjacent facets becomes such a small fraction of a wavelength, that the phase variations between them may no longer be considered as random. A correlation analysis, such as has been employed by Davies,[3] then, may be required. It should be noted, however, that Davies' assumption that the correlation distance is small compared to the size of a facet prevents the realization of the frequency selectivity of facets, such as exhibited in Fig. 10.

Another assumption which has been introduced for simplicity is that the size and slope distributions of the facets are independent. A consequence of this has been shown to be that the shape of the curve of σ^0 vs angle in the region around vertical incidence should be substantially independent of frequency. Hence, simultaneous measurements at several frequencies in this angular region can serve as a check on this assumption, and thus indicate whether a more complicated relationship need be explored.

One of the deductions of the theory is that σ^0 at small depression angles ultimately should decrease with increasing frequency. This conclusion, however, is based on the Cox and Munk slope distribution, which omits whitecaps. The importance of whitecaps in radar back scattering thus needs to be determined.

The outstanding disagreement between the theory as developed in this paper and experiment lies in the upwind-downwind ratio. It was pointed out that this may be due to the neglect of shadowing.

Conclusion

The theory of sea clutter developed in this paper has been based on physical principles which were recognized from the results of experimental measurements. In particular, measurements show that the illumination of the scattering elements is a combination of direct and surface-reflected fields. Destructive interference between these field components sets in at small depression angles. This interference effect itself is dependent on frequency and wave height. It results in the so-called "critical angle," polarization dependence, and complicated frequency dependence. It also gives rise to "spikiness" at very small depression angles. When the interference effect is separated from the over-all phenomenon, the remaining characteristics show a regular and rather simple behavior.

Because measurements show that only a small amount of the intercepted power is back scattered at small depression angles, a rather directive scattering mechanism is indicated. The theory, therefore, has been based on plane facets as the basic scattering elements. It is found that facets having a perimeter of about a half-wavelength back scatter most effectively at small depression angles, and that the back scattering of a facet increases about as the square of its slope. Thus, facets near the wave crests contribute most strongly to the back scatter.

[16] J. Meixner and W. Andrejewski, "Strenge Theorie der Beugung ebener elektromagnetischer Wellen an der vollkommen leitenden Kreisscheibe und an der kreisförmigen Öffnung im vollkommen leitenden ebenen Schirm," *Ann. d. Phys.*, (6), vol. 7, pp. 157–168; 1950.

[17] C. J. Bouwkamp, "On the diffraction of electromagnetic waves by small circular disks and holes," *Philips Res. Rep.*, vol. 5, pp. 401–422; December, 1950.

[18] J. Meixner, "Die Kantenbedingung in der Theorie der Beugung elektromagnetischer Wellen an vollkommen leitenden ebenen Schirm," *Ann. d. Phys.*, vol. 6, pp. 1–9; 1949.

[19] C. J. Bouwkamp, "Review of Copson's paper," *Math. Rev.*, vol. 8, pp. 179–180; 1947.

The frequency dependence of the back-scattering parameter σ^0 then is determined by the size distribution of the facets.

At large depression angles, some of the facets are viewed at normal incidence, and thus back scatter strongly. The angular variation of σ^0 then is determined mainly by the slope distribution of the facets. On the basis of optical measurements of slope distribution, σ^0 at vertical incidence is inversely proportional to wind speed, but at grazing incidence it is approximately proportional to wind speed.

Appendix[20]

For a linearly-polarized wave, the radar area, σ, of a large circular disk of diameter D, at an angle θ_d from the plane of the disc, is given by[21]

$$\sigma/\sigma_{max} = [2 \sin \theta_d J_1(x)/x]^2, \tag{5}$$

where $\sigma_{max} = 4\pi(A/\lambda)^2$, and $x = 2\pi D \cos \theta_d/\lambda$. A disk is "large" if $2\pi D/\lambda \gg 1$. A plot of $[2J_1(x)/x]^2$ appears in Fig. 8. For angles outside the main lobe, the amplitude oscillates, and the average value over a cycle of the oscillations is approximately half the envelope shown by the dotted line in Fig. 8. If we denote this average value of σ by $\bar{\sigma}$, we obtain

$$\begin{aligned} \bar{\sigma} &= \lambda D \tan^2 \theta_d \sec \theta_d/(8\pi) \\ &= f_1(\theta_d)\lambda A^{1/2}, \end{aligned} \tag{6}$$

where $A = \pi D^2/4$ is the disc area, and

$$f_1(\theta_d) = (4\pi^{3/2})^{-1} \tan^2 \theta_d \sec \theta_d. \tag{7}$$

For small discs, *i.e.*, $2\pi D/\lambda \ll 1$, the radar area may be obtained from Bethe's paper on diffraction by small holes[22] by the application of Booker's generalization of Babinet's principle.[23,24] In this case the back scattering does depend on the polarization direction. Since our main interest is in the case of horizontal polarization, we may write for small discs,

$$\bar{\sigma} = f_2(\theta_d)A^3/\lambda^4, \tag{8}$$

where

$$f_2(\theta_d) = (4^5/9)(1 + \cos^2 \theta_d/2)^2. \tag{9}$$

(6) and (8) attain the same value at an area A_1 (diameter D_1), where

$$A_1/\lambda^2 = (f_1/f_2)^{2/5}. \tag{10}$$

The procedure which will be followed here is to use (6) for $D > D_1$, and (8) for $D < D_1$.

[20] M. Katzin, "Back scattering from the sea surface," 1955 IRE Convention Record, Part 1, pp. 72–77. In that preliminary report (2) and (3) are in error.

[21] Kerr, *op. cit.*, p. 458.

[22] H. A. Bethe, "Theory of diffraction by small holes," *Phys. Rev.*, vol. 66, pp. 163–182; October 1 and 15, 1944.

[23] H. G. Booker, "Slot aerials and their relation to complementary wire aerials (Babinet's principle)," *J.IEE*, vol. 93, part IIIA, pp. 620–626; 1946.

[24] E. T. Copson, "An integral-equation method of solving plane diffraction problems," *Proc. Roy. Soc.* (*A*), vol. 186, pp. 100–118; June 4, 1946.

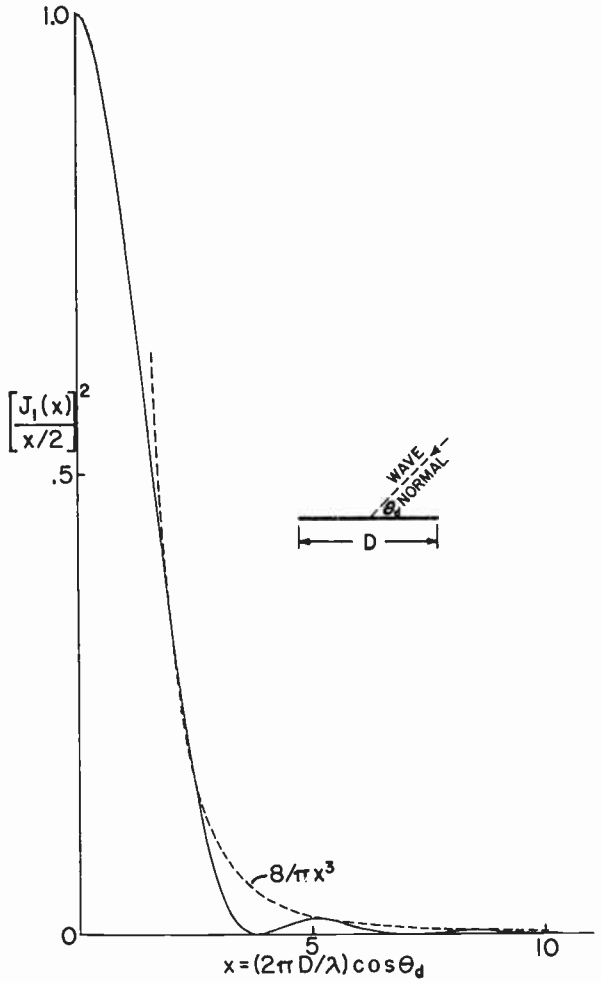

Fig. 8—Curve for radar area of a large circular disk.

Eqs. (6) and (8) apply for an assembly of isolated discs between which there is no interaction. Then the scattering diagram of a disc is symmetrical with respect to the plane of the disc, since it makes no difference which side of the disc is turned toward the observer. On the sea surface, however, the facets are not isolated; in particular, the "back" faces of the facets are not exposed to illumination when the angle which the wave normal makes to the disc normal exceeds 90 degrees. Furthermore the facets on the backs of the (sea) waves are shielded from direct illumination by the preceding wave crest (the region from A to B in Fig. 9). A complete treatment would have to include the effect of diffraction by the crest A on the illumination of the facets. Again in order to simplify the treatment, this complication is dodged here, and the back scattering for angles greater than 90 degrees is neglected. The uncertainty introduced by this assumption probably is less than a factor of 2.

Since $\bar{\sigma}$ depends on facet slope, as well as facet size, it is necessary to sum the contributions from facets of different slopes and sizes. Three assumptions are made at this point: 1) that the phases of the waves backscattered by the facets vary randomly, so that the back-

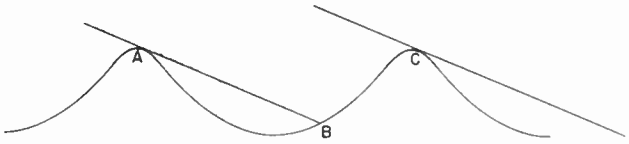

Fig. 9—Illustrating shadowing at small depression angles due to wave crests.

scattered powers are additive; 2) that the slope and size distributions are independent of each other; and 3) that each distribution embraces a continuous range. σ^0 is then found by integrating the values of $\bar{\sigma}$ for all facets in a unit area of sea. This may be formulated by introducing the slope and area distributions as follows:

Let $p(s)$ be the probability density of facet slope, and let $N(A)$ be the number density of facet size. Then

$$\sigma^0 = \int\int N(A)p(s)\bar{\sigma}(s, A)dA\,ds. \tag{11}$$

Since different functional forms are to be used for $\bar{\sigma}$ for A below and above A_1, the area integral correspondingly splits into two integrals. But A_1 depends on s (*i.e.*, on θ_d) in virtue of (10), so that the area integral should be evaluated first. With a view to the approximate form of the experimentally-determined dependence of σ^0 on λ, $N(A)$ is taken to be

$$N(A) = N_0A^{-m}, \tag{12}$$

where N_0 is a constant. The limits of the area integration are A_0 and A_2, the smallest and largest facet areas, respectively, in the distribution. If $N(A)$ decreases markedly towards these limits, we may, without appreciable error, put $A_0=0$, $A_2=\infty$ in (11). Then the result of the area integration in (11) may be written

$$\int N(A)\bar{\sigma}dA = N_0F(\theta_d)\lambda^{-n} \tag{13}$$

where $n=2m-4$, and

$$F(\theta_d) = [2.5/(n+1)(4-n)]f_1^{(4-n)/5}f_2^{(n+1)/5}, \tag{14}$$

f_1 and f_2 being given, respectively, by (7) and (9).

It can be seen from (13) and (11) that the size distribution of the facets determines the frequency dependence of σ^0.

In the limit of grazing incidence, $\tan\theta_d=s$, and since $\sec\theta_d$ in (7) may be replaced by unity for small values of θ_d, (7) becomes

$$f_1 \approx (4\pi^{3/2})^{-1}s^2 \equiv k_1s^2.$$

The angular dependence of f_2 is not great in the range of interest for low-angle scattering, so that the average value of the factor $(1+\cos^2\theta_d/2)^2$ in (9) may be taken to be about 2. Then (9) becomes

$$f_2 = 2^{11}/9 \equiv k_2. \tag{9a}$$

Eq. (11) then becomes

$$\sigma^0 = N_0\lambda^{-n}G(s) \tag{15}$$

in which

$$G(s) = \int p(s)F(s)ds.$$

Measurements of wave slope which have been made[9–12] show nearly a Gaussian distribution. The Cox and Munk representation[11,12] will be used, since it makes possible the evaluation of the function $G(s)$ in (15).

Fig. 10 defines the geometry. If m denotes the slope of a facet, then the crosswind component of slope z_x, and the upwind component of slope, z_y, are given respectively by

$$z_x = m\sin\alpha = \sin\alpha\tan\beta = \tan\gamma,$$
$$z_y = m\cos\alpha = \cos\alpha\tan\beta = \tan\delta.$$

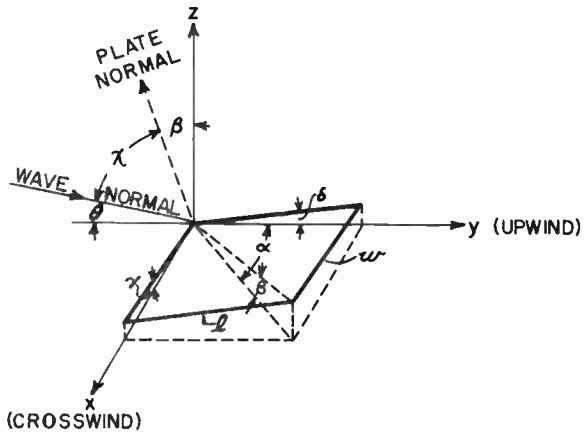

Fig. 10—Geometrical relationships for the facets in the Cox and Munk slope distribution.

The two-dimensional probability density distribution of z_x and z_y given by Cox and Munk is

$$p(z_x, z_y) = (2\pi\sigma_c\sigma_u)^{-1}e^{-1/2(\xi^2+\eta^2)} \cdot \{1 - \tfrac{1}{2}c_{21}(\xi^2-1)\eta - \tfrac{1}{6}c_{03}(\eta^3-3\eta) + \tfrac{1}{24}c_{40}(\xi^4-6\xi^2+3) + \tfrac{1}{4}c_{22}(\xi^2-1)(\eta^2-1) + \tfrac{1}{24}c_{04}(\eta^4-6\eta^2+3)\}, \tag{16}$$

in which σ_c, σ_u are the rms values of z_x and z_y, respectively, and ξ, η are the "standardized" slope components

$$\xi = z_x/\sigma_c, \qquad \eta = z_y/\sigma_u,$$

For a clean sea surface Cox and Munk give approximately:[25] $\sigma_c^2=1.15\cdot10^{-3}\ W$, $\sigma_u^2=1.65\cdot10^{-3}\ W$, $c_{21}=-0.0039\ W$, $c_{02}=-0.015W$, $c_{40}=0.40$, $c_{22}=0.12$, $c_{04}=0.23$, where W is the wind speed in knots.

It is readily found that the radar area of a "large" facet is given by

$$\sigma = 4\pi\left(\frac{A}{\lambda}\cos\chi\frac{\sin x}{x}\frac{\sin y}{y}\right)^2, \tag{17}$$

[25] Readjustments have been made in the values of σ_c, c_{21}, and c_{03} given by Cox and Munk in order to reduce them to zero for zero wind speed.

where

$$x = kl \cos(\theta + \delta),$$
$$y = kw \sin\theta \sin\gamma,$$
$$\cos\chi = \cos\beta \sin\theta + \sin\beta \cos\theta \cos\alpha$$
$$A = lw.$$

For grazing angles of the wave normal, we may put $\theta = 0$, whence $y = 0$, and replace $\sin^2 x$ in (17) by its average 1/2. Putting $w = l$, since the average of all rectangular shapes is the square, (17) becomes

$$\bar{\sigma} = [1/(2\pi)z_y^2(1 + z_y^2)/(1 + z_x^2 + z_y^2)]A = SA \quad (18)$$

For the small facets, we assume that (8) holds, and that f_2 may be approximated by (9a), so that

$$\bar{\sigma} = f_2 A^3/\lambda^4 \approx (2^{11}/9)A^3/\lambda^4 = k_2 A^3/\lambda^4. \quad (19)$$

We use (18) for $A > A_1$, and (19) for $A < A_1$, where

$$A_1/\lambda^2 = (s/k_2)^{1/2}. \quad (20)$$

With (12) and (16) we then obtain for σ^0 the same form of result as (15)

$$\sigma^0 = N_0 \lambda^{-n} G(W),$$

where now

$$G(W) = \frac{8k_2^{n/4}}{n(4-n)} \int_0^\infty \int_{-\infty}^\infty p S^{1-n/4} dz_x dz_y, \quad (21)$$

W being the wind speed which appears in the coefficients of (16). The double integral may be evaluated by expanding S from (18) in a power series, whereupon the resulting integrals represent the gamma functions. If we put $n = 1$, then

$$G(W) = (8k_2^{1/4}/3)(2\pi)^{-5/4}\sigma_u^{3/2} \sum_{m=0}^{\infty} 2^{(2m+1)/4} b_m \Gamma[(2m+5)/4],$$

from which there results for the upwind-downwind directions

$$\sigma^0 \approx 9 \cdot 10^{-3} N_0 \lambda^{-1} W^{3/4}(1 \pm 2 \cdot 10^{-3} W). \quad (22)$$

For the upwind direction, the sign of W is taken as positive, and negative for the downwind direction.

The ratio of σ^0 upwind to that downwind thus is

$$\frac{\sigma_u^0}{\sigma_d^0} = \frac{1 + 2 \cdot 10^{-3} W}{1 - 2 \cdot 10^{-3} W}. \quad (23)$$

In like manner to the numeric σ^0, we may introduce a numeric A^0, the total area of facets per unit (projected) area of sea, which is defined by

$$A^0 = \int_{A_0}^{A_2} N(A) A dA.$$

With $N(A)$ given by (12), we have

$$A_0 = \int_{A_0}^{A_2} N_0 A^{1-m} dA = 2(N_0/n)(A_0^{-n/2} - A_2^{-n/2})$$
$$\approx 2(N_0/n) A_0^{-n/2}, \quad (24)$$

since $A_0 \ll A_2$. If we use (15) to determine N_0, then

$$A^0 = 2\sigma^0 \lambda^n / (nG(s) A_0^{n/2}). \quad (25)$$

A general consequence of the splitting of the area integration in (11) into two integrals, corresponding to the different dependence on A for small and large facets, is that, in the frequency range for which $\sigma^0 \propto \lambda^{-n}$, σ^0 is proportional to the fraction of the total facet area which is "large." This fraction, ρ, may be defined as

$$\rho = \int_{A_1}^{A_2} N(A) A dA \Big/ \int_{A_0}^{A_2} N(A) A dA$$
$$\approx (2/n) N_0 (A_1^{-n/2} - A_2^{-n/2}) \approx (2/n) N_0 A^{-n/2} \quad (26)$$

if $\int_{A_0}^{A_2} N(A) A dA \approx 1$. Since $A_1 \propto \lambda^2$, it follows from (26) that $\rho \propto \lambda^{-n}$, so that $\sigma^0 \propto \rho$.

For high depression angles, the value of σ^0, in first approximation, is the product of ρ and the slope distribution, where ρ may differ from that at grazing angles. The appropriate value of ρ for high depression angles may be determined as follows: For large plates at normal incidence

$$\sigma_l/A = 4\pi(A/\lambda^2), \quad (27)$$

while for small plates, from (A4) and (A5),

$$\sigma_s/A = (2^{10}/9)(A/\lambda^2)^2, \quad (28)$$

(27) and (28) give the same value at $A = A_1'$, where

$$A_1'/\lambda^2 = 0.1104.$$

From (26), then

$$\rho = 5.98 N_0 \lambda^{-n}.$$

Thus at vertical incidence, if we use the Cox and Munk slope distribution given in (16), and affix a factor 2 to take account of the fact that the incident power is scattered into only a hemisphere, we have as a first approximation, with $n = 1$,

$$\sigma_{90^\circ}^0 \approx 2\rho p(0, 0) = 256\rho/W = 1.53 \cdot 10^3 N_0/(\lambda W). \quad (29)$$

The ratio of σ^0 at vertical incidence to that at grazing incidence then is, from (29) and (24)

$$\sigma_{90^\circ}^0/\sigma_{\theta \to 0}^0 \approx 1.7 \cdot 10^5 W^{-7/4}. \quad (30)$$

Acknowledgment

The experimental results on which this paper is based were obtained by the Wave Propagation Branch of the Naval Research Laboratory, and involved the cooperative efforts of many individuals. In particular, D. L. Ringwalt was responsible for the development of the measuring equipment and was in charge of the experimental program. The analysis of the extensive data taken was under the direction of W. S. Ament. The recognition of consistent spikiness in the low-angle data was due to F. C. Macdonald, and its explanation in terms of the destructive interference mechanism previously recognized was supplied by W. S. Ament. The assistance and contributions of these individuals and the other members of the Wave Propagation Branch is gratefully acknowledged.

Measured Statistical Characteristics of VLF Atmospheric Radio Noise*

A. D. WATT†, SENIOR MEMBER, IRE, AND E. L. MAXWELL†

Summary—Instrumentation for measuring the cumulative distribution of the amplitudes and spacings of pulses in the instantaneous envelope of the atmospheric noise field strength is described. In general, the vlf atmospheric noise observed at 22 kc in a 1-kc band during the fall of 1955 from 9°N to 71°N latitude was found to have a maximum variation in average power level, including the effects of both time and geographic location, of about 46 db. The dynamic range of the instantaneous noise envelope, measured during a 20- to 30-minute period of time, is defined to be the ratio of the field strength exceeded 0.0001 per cent of the time to that exceeded 90 per cent of such periods of time. This dynamic range in a 1-kc band, for the 66 periods measured, varied from 59 to 102 db. The average dynamic range in the Arctic was 68 db and in the tropics 81 db. The noise envelope at the low amplitude levels is found to be Rayleigh distributed, while that at the higher levels approaches a distribution having a much greater change in level for a given change in probability. In general, at higher levels, the spacing between pulses does not appear to be random at temperate and arctic locations, but the noise pulses observed in the tropics appear to be more randomly spaced. When the bandwidth of the receiver is reduced, the dynamic range approaches 21.18 db, the value expected for the Rayleigh distributed envelope resulting from a thermal noise input. The bandwidth at which this occurs will depend on the character of the atmospheric noise at the time of observation, but appears from our measurements at 22 kc to be approximately 0.2 cycle per second.

INTRODUCTION

IT IS a well-known fact that the carrier-to-noise ratio required for a specified grade of service in a given radio system is dependent upon the characteristics of the noise as well as those of the modulation employed at the transmitter and the demodulation employed at the receiver. Because of the importance of knowing the character of the noise as well as its level when evaluating or predicting radio system performance, the need for a detailed investigation of the statistical characteristics of atmospheric noise is readily apparent.[1]

Atmospheric noise rather than thermal or man-made impulse noise is the limiting noise factor for a greater percentage of the time in the vlf range than in the other frequency ranges. For this reason we have chosen this area of the frequency spectrum for the initial phases of a detailed study of the statistical characteristics of atmospheric noise.

The atmospheric radio noise field results from the combination of a large number of essentially independent events, and this makes it readily amenable to statistical treatment. Although the lightning discharges—which are the primary source of atmospheric noise—are essentially independent events, the variations in noise field at the receiver do not occur entirely at random. This departure from a random time distribution is caused by the time correlation introduced by multiple propagation paths with their various characteristic propagation delays, and the fact that individual lightning discharges usually[2] contain multiple strokes.

A precise specification of the noise field in the statistical sense can be very complex and requires the accumulation of large amounts of data. Discussions of these problems are given by Hoff and Sullivan,[3] Horner,[4] and Hoff and Johnson.[5] It is possible, however, to obtain most of the pertinent information about the envelope of the atmospheric noise field by measuring its amplitude distribution and the pulse-spacing distribution. These two distributions give information which is very useful in predicting the performance of radio systems operating in the presence of such noise. The type of data obtained is best explained by examining the equipment employed in making the measurements. It should be mentioned that, although the results presented here are only for the vlf frequency band, a limited number of similar measurements have been made with this equipment at higher frequencies. To date the higher frequencies appear to have smaller dynamic ranges, but further investigation of this and other characteristics of high frequency noise is planned.

PARAMETERS MEASURED AND EQUIPMENT EMPLOYED

Cumulative distributions of the instantaneous amplitude of the envelope of radio noise fields were obtained with the equipment shown in Fig. 1. The antenna employed for all of the measurements reported here was a 6-foot-square, 15-turn, shielded loop. Some early measurements were made with a vertical whip; however, it was found in many locations that the shielded loop provided a substantial reduction in locally-generated noise. Another reason for the choice of the loop was that arctic region measurements were to be taken, and whips operating in this area are frequently subjected to a high amount of precipitation-type static. Loop antennas are

* Original manuscript received by the IRE, June 27, 1956.

† National Bureau of Standards, Boulder, Colo.

[1] Much of the work in this field of Terrestrial Atmospherics has been reported to Commission IV of the International Scientific Radio Union (URSI). Of particular interest are the Commission IV papers published in the *Proceedings* of the 9th, 10th, and 11th General Assemblies.

[2] J. H. Hagenguth, "Photographic study of lightning," *Trans. Amer. Inst. Elec. Engrs.*, vol. 66, pp. 577–585; 1947.

[3] R. S. Hoff and A. W. Sullivan, "A survey of the atmospheric noise problem," *Proc. URSI X General Assembly*, vol. 8, p. 297; September, 1950.

[4] F. Horner, "Notes on the significant characteristics of atmospheric noise," *Proc. URSI XI General Assembly*, vol. 10, p. 32; September, 1954.

[5] R. S. Hoff and R. C. Johnson, "A statistical approach to the measurement of atmospheric noise," PROC. IRE, pp. 185–187; February, 1952.

frequently employed at vlf receiving sites, and the use of a loop provides equivalent noise fields which are the same as those which would actually be encountered in practice. The directional characteristics of the loop also permit examination of the change in character of the noise arriving from different directions. The receiver was calibrated in terms of an equivalent electric field, in microvolts per meter, for a signal in the plane of the loop, and the equivalent noise field measured is the integral over all directions of arrival, modified by the directional characteristics of the loop. The relatively large loop was employed because it has a low equivalent thermal noise field of approximately 0.4 $\mu v/m$ in a 1000 c bandwidth[6] at 20 kc. This provides negligible contamination of the atmospheric noise field at 2 μv/m, the lowest fields measured with this bandwidth.

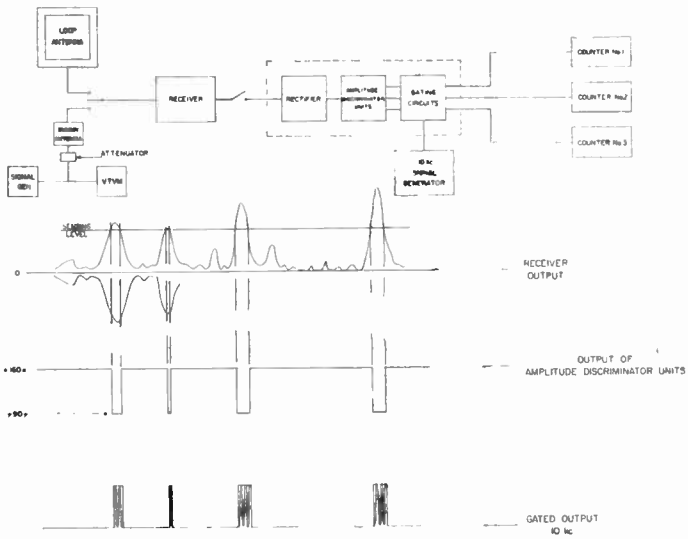

Fig. 1—Equipment for measuring cumulative distributions of envelope amplitudes.

The receiver unit shown in the block diagram, Fig. 1, has a built-in attenuator which permits the effective sensing levels of the amplitude discriminator units to be varied from 2 μv/m to 0.5 v/m. The low pass filter in the rectifier unit was carefully chosen to provide sufficient attenuation at the center or carrier frequency and yet to have negligible attenuation at the frequencies contained in the noise envelope. This is essential if the high probability densities are to be accurately represented. The amplitude discriminator and gating circuits will operate at frequencies in excess of 100 kc, so they are well able to follow all variations in the envelope voltage. The amplitude discriminators and gating circuit have a hysteresis of approximately 0.2 volt at the sensing level, while the threshold levels for the three amplitude discriminators are 2, 5, and 10 volts respectively.

[6] Six-db bandwidths are employed throughout with the exception that the 3-db bandwidth is employed in Fig. 14.

Cumulative distributions are obtained by gating at 10-kc signal on for the period of time during which readings are to be obtained, and counting the number of cycles during which the threshold voltage of the amplitude discriminator is exceeded. Various time bases are required to obtain statistically constant data; in general, 100 seconds are used for values of 5 per cent[7] and greater, 200 seconds for values in the range of 0.0005 to 5 per cent, and 300 to 1000 seconds for values less than 0.0005 per cent. In general, a total of about 10 minutes is required to obtain all but the last three low-percentage readings, which themselves may take 10 to 20 minutes in order to obtain statistically constant data. The total time required is a function of the type of noise being measured, with longer times required for noise with a large dynamic range.

Time distributions were obtained with the equipment indicated in Fig. 2. Essentially the same circuitry as

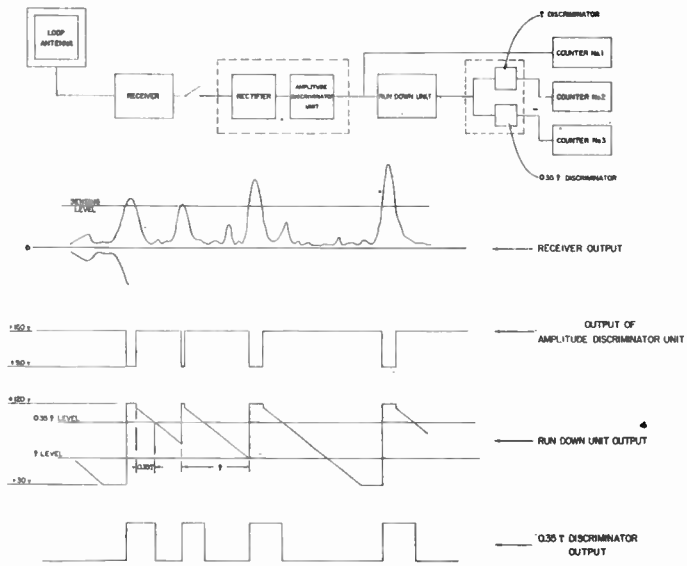

Fig. 2—Equipment for measuring cumulative distributions of envelope pulse widths and spacings.

shown in Fig. 1 is used up to the input of the run-down or phantastron unit. Phantastron-type circuits are described in detail by Chance *et al.*[8] This unit, operating at a specific sensing level, translates the time spacings between pulses into amplitude variations.[9] Two additional amplitude discriminator units designated as T discriminator and 0.35 T discriminator are arranged to record a count on the appropriate counter when the spacing between pulses exceeds the value shown. The actual value of T is selected by a switch which changes

[7] That is, field strengths which are exceeded for 5 per cent of the time base, or measuring period.

[8] B. Chance, V. Hughes, E. F. MacNichol, D. Sayre, and F. C. Williams, "Waveforms," M.I.T. Radiation Lab. Ser., McGraw-Hill Publishing Co. Inc., New York, N. Y., vol. 19, pp. 195–204; 1949.

[9] The use of a run-down circuit at this point, in place of a more complex counting technique, was suggested to one of the authors by F. Horner, D.S.I.R., Radio Res. Sta., Slough, Eng.

the run-down slope in this unit. The available values of T range from 0.1 millisecond to 10 seconds. The actual percentages of time that the spacing between pulses exceeds the values of T and 0.35 T are obtained by dividing the readings of counters 2 and 3 by the reading on counter 1, which records the total number of discharges exceeding the given level. The actual time required to obtain statistically constant percentages varies with level in a similar manner to that described for the amplitude distributions.

Information on pulse width distribution can readily be obtained by reversing the polarity of the first amplitude discriminator, but such distributions are not given in this paper.

Measured Amplitude and Time Distributions

Statistical measurements of atmospheric noise have been made with the equipment described in the preceding section at Point Barrow, Alaska (71.2°N, 156.8°W); Kenai, Alaska (60.4°N, 150.3°W); Boulder, Colo. (40°N, 005.3°W); and Balboa, Canal Zone (9°N, 80°W). Similar measurements of atmospheric noise amplitude distributions have been made by others with considerably different instrumentation at Slough, England,[10] and Gainesville, Fla.

A number of interesting properties of atmospheric noise can be ascertained by observing specific samples of the distributions measured. It should be emphasized that, although well over one hundred distributions have been measured during this period of several months, more data must be obtained over a greater period of time and at more geographic locations before sufficiently precise specifications of the expected noise-field distributions can be made. It is felt, however, that the data do form the basis for a good first approximation to the statistical character of the vlf noise field and the factors which affect this character.

The approximate range of variations in level which can be expected for the noise field can be seen in Fig. 3, where the distributions with the highest and lowest observed average power levels are shown. The high-level curve was obtained at Boulder, Colo., on a day with a large number of local afternoon mountain thunder storms. The low-level curve was obtained at Point Barrow, Alaska, during the morning of a relatively quiet day. These variations in noise level as a function of time, location, and direction are well known.[11] Very little, however, is known about the variations in statistical character as a function of these various parameters. Fig. 4(a) and 4(b) contain distributions which were

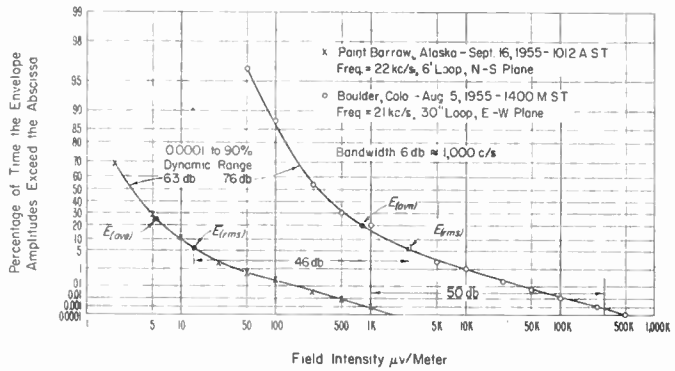

Fig. 3—Amplitude distributions of atmospheric noise envelopes showing maximum range of amplitude level observed at all five stations.

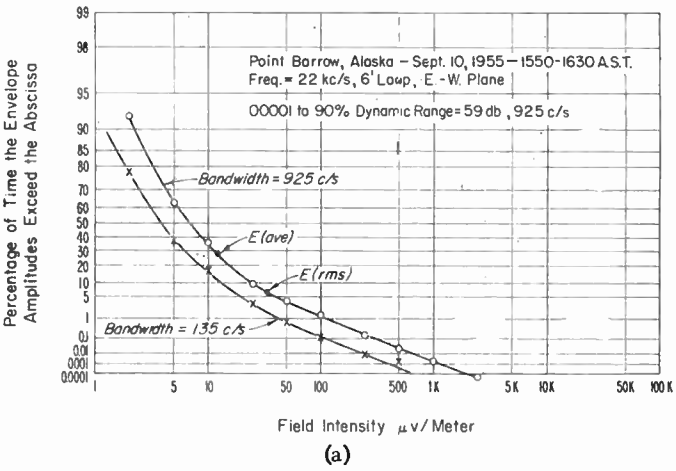

Fig. 4—(a) Amplitude distributions of atmospheric noise envelopes. (b) Amplitude distributions of atmospheric noise envelopes.

taken one immediately following the other but with different antenna orientations. The observed change in dynamic range from 59 db to 67.4 db is typical of the changes in noise character due either to change in antenna orientation or to change in time. The 59-db dynamic range from the 0.0001 per cent to 90 per cent values is the smallest dynamic range observed during

[10] F. Horner and J. Harwood, "An investigation of atmospheric radio noise at very low frequencies," to be published in *Proc. I.E.E.*

[11] W. Q. Crichlow, D. F. Smith, R. N. Morton, and W. R. Corliss, "Worldwide Radio Noise Levels Expected in the Frequency Band 10 Kilocycles to 100 Megacycles," NBS Circular 557, Boulder, Colo.; August 25, 1955.

these tests in a one kc band at 22 kc. Some idea of the observed dynamic ranges can be obtained from Table I.

TABLE I

OBSERVED ATMOSPHERIC NOISE ENVELOPE DYNAMIC RANGES (DB) 0.001 TO 90 PER CENT VALUES 22-KC, 1200 C/S BANDWIDTH AUGUST–NOVEMBER, 1955

Place	Average	Maximum	Minimum
Point Barrow, Alaska	68	84	59
Kenai, Alaska	73	84	65
Boulder, Colo.	71	80	63
Balboa, Canal Zone	81	102	66

A typical Canal Zone noise envelope amplitude distribution is shown in Fig. 5(a) with a dynamic range of 80 db, and the distribution with the smallest dynamic range observed at the Canal Zone is shown in Fig. 5(b).

Plotting the log-log of probability vs log of field strength reveals several interesting facts about the distributions. In all measurements where uncontaminated atmospheric noise was observed, the low field strength values approach or form a straight line with a slope [m of (1)] of -2. The high field strength region frequently approaches a straight line with values of slope which range from -0.1 to -0.4. On some occasions the high amplitude ends of the distribution curves turn downward rather rapidly in the region of 0.0001 per cent. This last phenomenon indicates that there are no thunderstorms close enough to produce fields exceeding a given level.

The log log-vs-log graph paper employed for plotting of the data has the interesting property of yielding a straight line with a negative slope of m for any distribution having the form

$$P = 100 \exp - x^m. \qquad (1)$$

When $m = -2$, the Rayleigh distribution is obtained, which is the distribution expected for the envelope of narrow-band thermal noise.[12,13] Because of this fact, it is very easy to see what part of the atmospheric noise behaves the same as thermal noise.

The variations in dynamic range agree with expectations based on the distribution of distances to thunderstorms where it is apparent, in the frequency range considered, that small dynamic ranges will result if the range of distances to the effective thunderstorms is small.

It should also be mentioned that many of the amplitude distributions obtained were plotted on log-normal grids to see if the instantaneous noise-field envelope is log-normally distributed. All of the measurements have

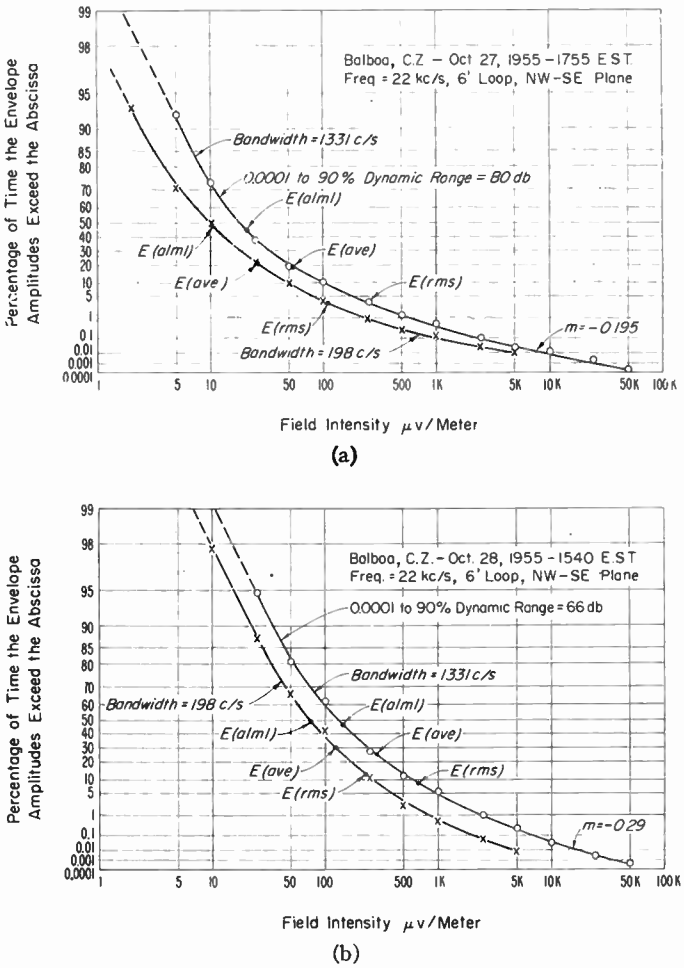

Fig. 5—(a) Amplitude distributions of atmospheric noise envelopes. (b) Amplitude distribution of atmospheric noise envelope.

shown that the instantaneous amplitude does not closely follow a log-normal distribution over the total range of probabilities measured, although many of the distributions approached the log-normal over narrower, intermediate, dynamic ranges.

In the low field intensity region of the atmospheric noise distribution, the total field is the resultant of a large number of essentially independent overlapping events. It is a well-known fact that a normal distribution results from the combination of a large number of independent overlapping events, and that the envelope of a normally distributed function is Rayleigh distributed. Since the Rayleigh distribution density function approaches the origin with a positive slope, it is readily apparent that the log-normal distribution cannot provide a good fit for atmospheric noise in this region. This is due to the fact that the density function of any log-normally distributed variable approaches the origin tangential to the x axis.

The principal effect of a predetection bandwidth reduction on the amplitude distributions is, as shown in Fig. 6, simply a reduction in dynamic range. Other

[12] V. D. Landon, "The distribution of amplitude with time in fluctuation noise," PROC. IRE, vol. 30, pp. 425–429; September, 1942.

[13] S. O. Rice, "Properties of a sine wave plus random noise," *Bell Sys. Tech. J.*, vol. 27, pp. 109–157; January, 1948.

measurements in a two-tenths (0.2) of a cycle band yielded a Rayleigh distribution over the entire range measured.

Fig. 7 shows the manner in which the various noise moments vary as a function of bandwidth. These moments[14] are defined by the following equations:

$$E_{\text{rms}} = \sqrt{\frac{1}{T}\int_0^T e^2 dt} \tag{2}$$

$$E_{\text{ave}} = \frac{1}{T}\int_0^T e\,dt \tag{3}$$

$$E_{\text{alml}} = \text{anti log}\,\frac{1}{T}\int_0^T \log e\,dt. \tag{4}$$

E_{rms}, E_{ave}, and E_{alml} are, respectively, the root mean square, average, and antilog of the mean log voltages acting over the time interval T, and e is the instantaneous envelope amplitude voltage. The dashed lines are included to show the results which would be obtained with thermal noise whose power level per unit bandwidth is the same as this particular sample of atmospheric noise. It is interesting to note that the atmospheric noise moments approach those for thermal noise as the observing bandwidth is reduced. Norton[15] has listed the four requirements necessary to produce a function which has Rayleigh distributed envelope, and it is interesting to note, that in a large observing bandwidth, the first requirement of a constant input energy, and the second requirement that the energy in any one component must be small compared to the total received energy, are the ones which are not met by atmospheric noise. When the observing bandwidth is reduced, the energy from all the received impulses is spread out over a greater period of time, and, as a result, this criterion of constant energy is more nearly approached. In addition, the energy received from any one impulse becomes a smaller fraction of the total as more impulses are contributing at a given time, with the result that the atmospheric noise envelope approaches the Rayleigh distribution as was seen in Figs. 6 and 7.

Up to this point, we have considered only the measured statistical properties of the variations in amplitude of the noise envelope. When consideration is given to the various ways that a given amplitude distribution can be generated, it is readily apparent that the amplitude distribution does not uniquely define the component of the noise field that is being observed. It has been shown by Rice[13] that the statistical properties of the envelope

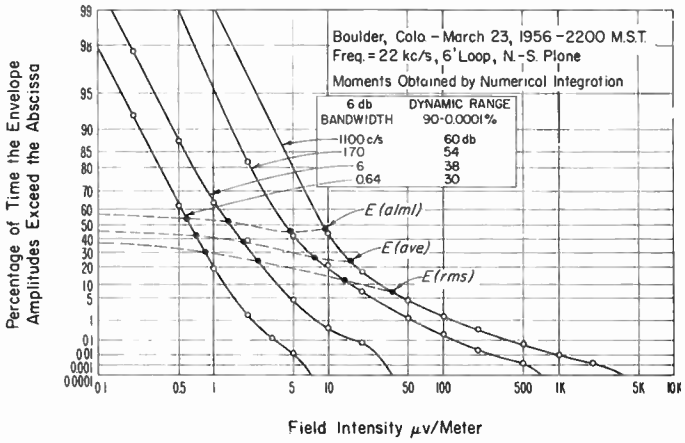

Fig. 6—Amplitude distributions of atmospheric noise envelopes.

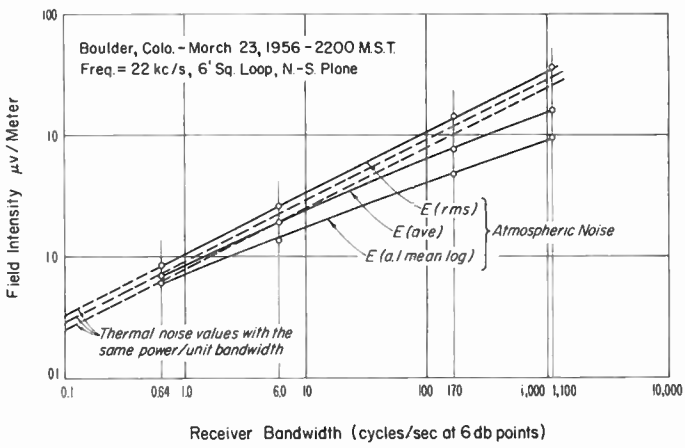

Fig. 7—Atmospheric noise moments as a function of receiving bandwidth.

variations of random noise from a band-pass system, whose bandwidth is small compared to the center frequency, are uniquely defined by the rms value of the noise and the band-pass characteristics of the filter.

In particular, Rice[13] has shown that the expected number of positive crossings of a given voltage level of the envelope of random noise or of random noise plus a carrier is equal to a bandwidth factor times the probability density of the envelope amplitudes. This relationship does not hold for atmospheric noise as can readily be seen from the curves of Fig. 8, where the measured probability density function times an appropriate constant is plotted along with two measured noise envelope crossing curves. The departure in the direction of smaller probability densities at the high field strength values is probably due to the fact that the atmospheric noise voltages are not normally distributed at high amplitudes, as is evidenced by the fact that the envelopes are not Rayleigh distributed.

The average crossing rate does not give any indication of expected departures from a random time distribution for the received noise impulses. This type of information

[14] K. G. Jansky, "An experimental investigation of the characteristics of certain types of noise," PROC. IRE, vol. 27, pp. 763–768; December, 1939.

[15] K. A. Norton, L. E. Vogler, W. V. Mansfield, and P. J. Short, "The probability distribution of the amplitude of a constant vector plus a Rayleigh-distributed vector," PROC. IRE, vol. 43, pp. 1354–1361; October, 1955.

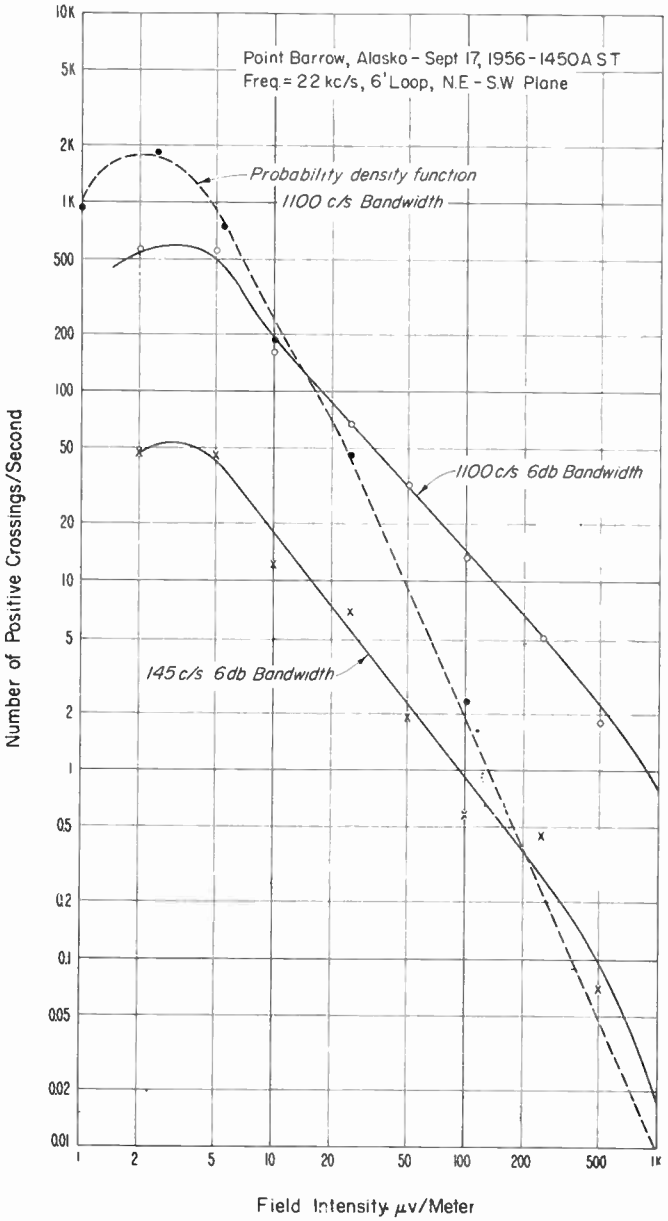

Fig. 8—Crossing rate of noise envelopes.

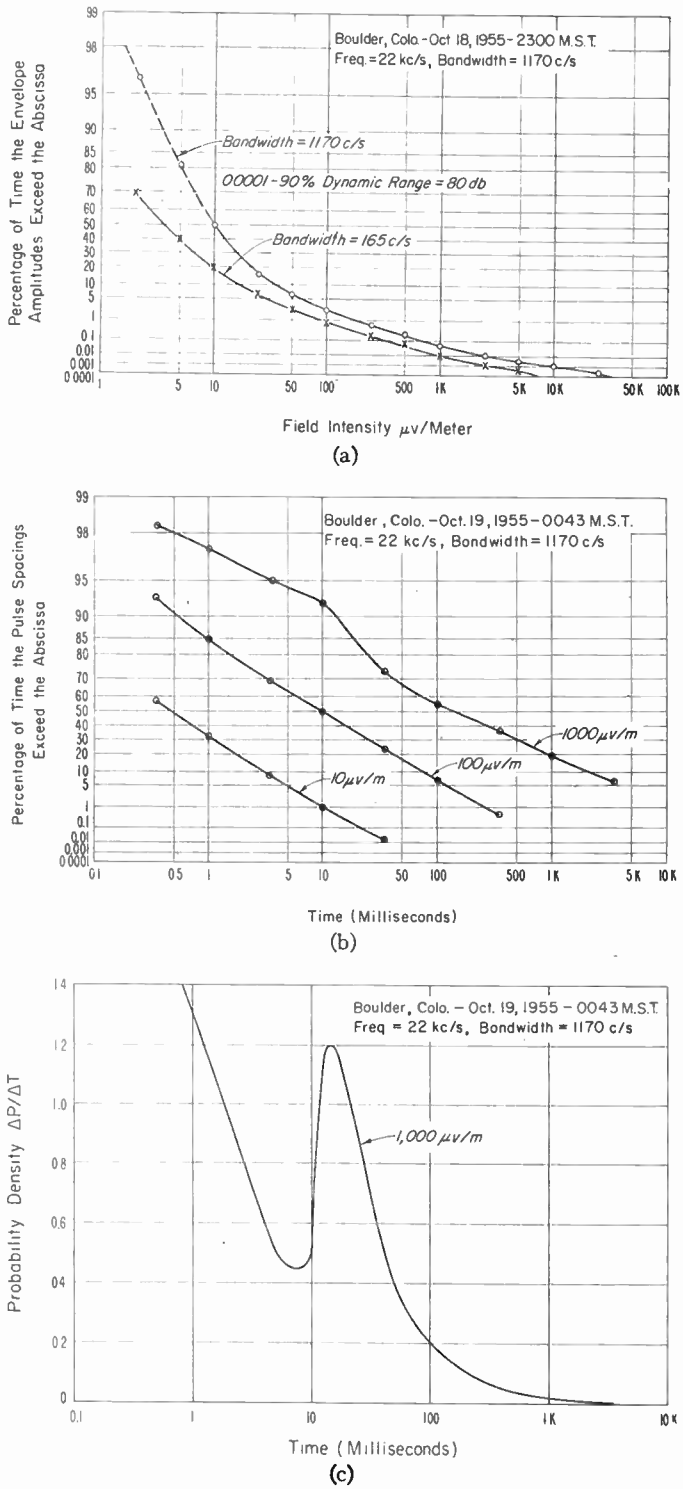

Fig. 9—(a) Amplitude distributions of atmospheric noise envelopes. (b) Distribution of the time between pulses of the atmospheric noise envelope. (c) Probability density of the time between pulses of the atmospheric noise envelope.

can, however, readily be obtained with the aid of the time-distribution measuring equipment described earlier. Fig. 9(a), (b), and (c) present typical amplitude and time distributions taken consecutively at Boulder, Colo. If the occurrence of the observed pulses were purely random, the time T in seconds between leading edges would be expected to follow the law $P(T \geqq T_1) = \exp(-NT_1)$, where N is the average number of pulses per second.[16] The time spacing actually measured is that between pulses; however, as long as the intervals considered are long compared to the impulse response time of the receiver band-pass filter, the values obtained should, if the spacing is random, form a straight line with a slope of (-1) on the log log-vs-log paper employed. Actual measurements with thermal noise yield this straight line with a slope of (-1) down to spacings

[16] W. Feller, "An Introduction to Probability Theory and Its Applications," John Wiley and Sons, New York, N. Y., vol. 1, pp. 218–221; 1950.

of 5 milliseconds. The fact that the curves shown in Fig. 9(b) have a slope of less than one indicates, as was expected, that some received pulses are dependent on preceding ones.

The cumulative time distributions described here contain only the information about the time variations of the atmospheric noise field as observed in a narrow bandwidth. The fine structure such as that caused by the discharge mechanism or the multiple propagation paths or modes is not in general observable. Measurements with these narrow bandwidths, chosen because they approximate typical communication receiver bandwidths and also because they permit observation of the low atmospheric noise fields without signal interference, do, however, yield statistical information about the observed noise envelope which is useful in determining communication system performance.

At the higher field-strength levels the correlation between pulses in the envelope becomes apparent, and the probability density function of Fig. 9(c) shows that on this particular night there was an unusually large number of pulses spaced by 10 to 100 milliseconds. This increase in density is in very good agreement with measurements made by electric power companies in cloud-to-ground discharges where individual lightning discharges are observed to contain several multiple current strokes. Typical data of this type, adapted from Hagenguth,[2] are shown in Fig. 10, where the 10 to 100 millisecond spacing

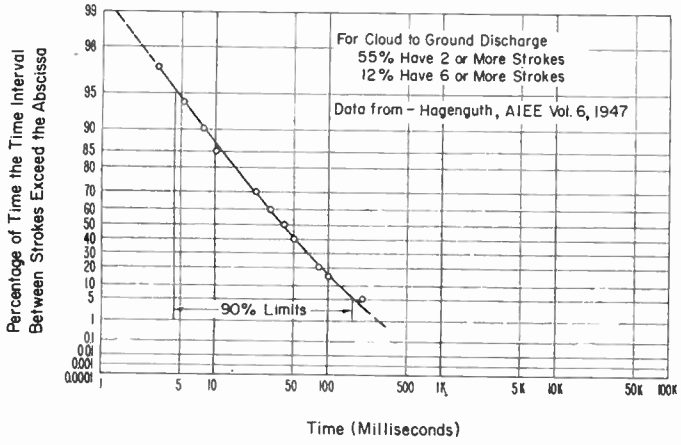

Fig. 10—Time interval between successive current peaks (strokes) of a complete lightning discharge.

is seen to include the majority of the multiple strokes.

Another set of amplitude and time distributions, taken at Kenai, Alaska, is shown in Fig. 11(a) and (b). The time distributions in this case also show evidence of correlation; however, as the level of observation is decreased, it is apparent that the slopes are increasing. This indicates that the low level values are becoming more random in nature due to the increased probability of pulse overlapping.

The effect of geographic location on the time distributions for the month of October can be seen by comparing

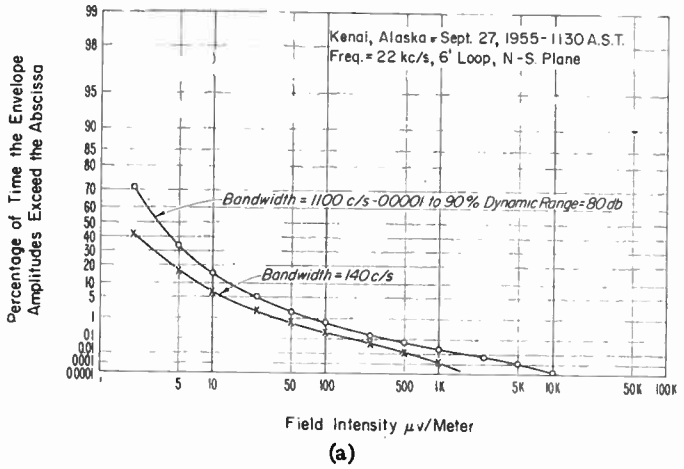

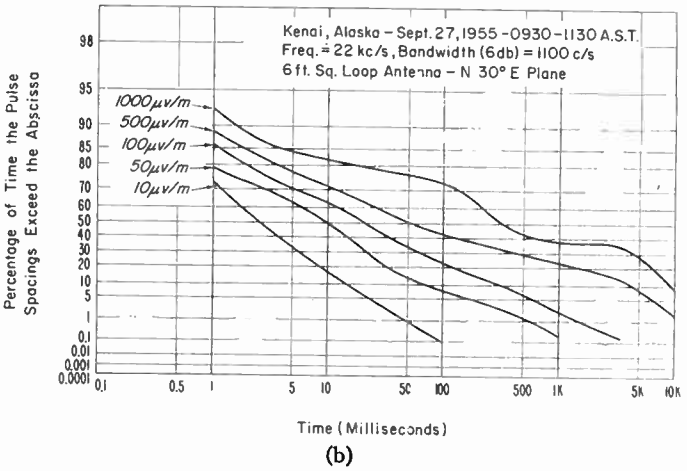

Fig. 11—(a) Amplitude distributions of atmospheric noise envelopes. (b) Cumulative pulse spacing distribution vlf atmospheric noise.

Figs. 12 and 13, where the amount of time correlation is found to be less in the Canal Zone data than in the Colorado data. This is evidenced by the reduction of appreciable slope changes in the Canal Zone data and also by the fact that these curves are steeper than the Boulder curves. A possible explanation of this result may be the fact that tropical storms rarely contain multiple strokes while the frontal type of storm frequently observed in the temperate zone usually contains multiple strokes.[17]

An additional interesting observation which can be made from the upper curves in Figs. 11(b) and 12 is the apparent increase in pulse spacing in the five-second region, a phenomenon which is even more evident in a few of the other Alaskan time distributions. These large delay times are in agreement with delays observed at this frequency for the whistler mode of propagation, and it may be that this mode of propagation contributes on occasions to the total noise field.

Figs. 14 and 15 are included to show the amplitude

[17] H. R. Byers, "Thunderstorm Electricity," Univ. of Chicago Press, Chicago, Ill., pp. 267–275; 1956. (See R. E. Holzer, ch. 13.)

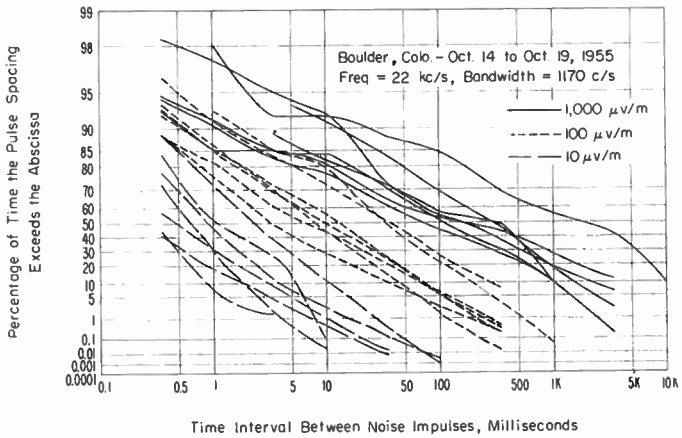

Fig. 12. Distribution of the time between pulses of the atmospheric noise envelope.

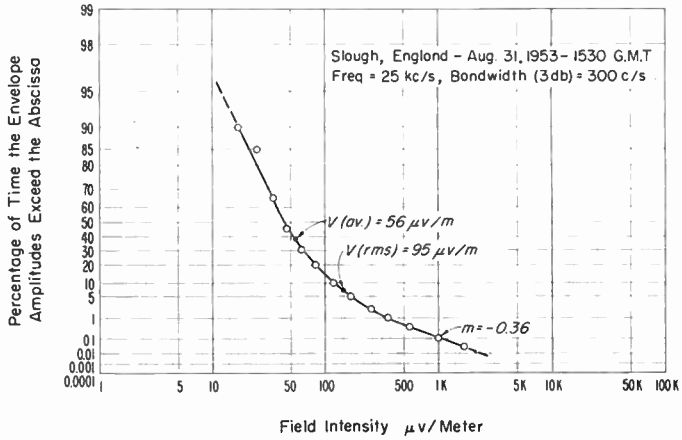

Fig. 14—Amplitude distribution of atmospheric noise envelope.

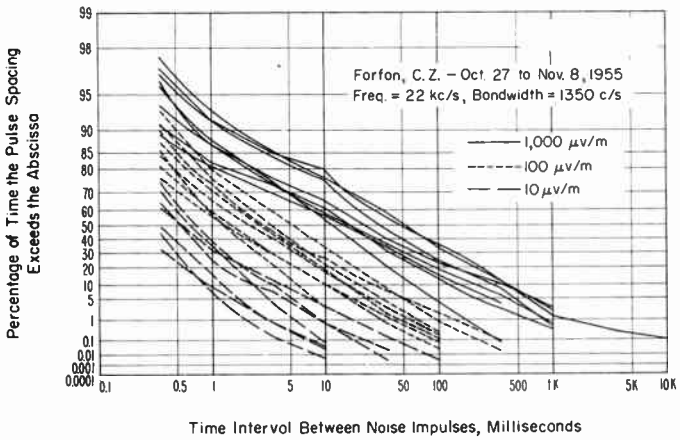

Fig. 13—Distribution of the time between pulses of the atmospheric noise envelope.

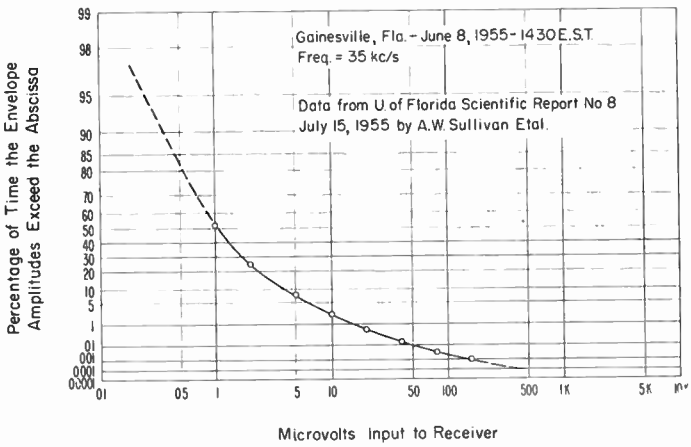

Fig. 15—Amplitude distribution of atmospheric noise envelope.

distributions obtained at two additional geographic points. Although very different instrumentation was employed, the characteristics are very similar to those which we have obtained. The data for Fig. 14 were obtained by private communication from Frederick Horner, and those for Fig. 15 from a report by Sullivan *et al.*[18]

[18] A. W. Sullivan, S. P. Hersperger, R. F. Brown, and J. D. Wells, "Investigation of Atmospheric Radio Noise," Scientific Rep. No. 8, Florida State Univ., Tallahassee, Fla.; June 30, 1955.

Acknowledgment

The authors are indebted to R. M. Coon and V. J. Zurick for obtaining all of our Canal Zone data, and for their assistance in many other ways; to S. S. Barnes and D. M. Waters for their assistance in obtaining suitable facilities and sites for our measurements in Alaska; to W. Q. Crichlow and F. F. Fulton, Jr. for suggested circuitry and methods of presentation; to L. P. Benedict for performing the numerical integrations; and to T. C. Baird for his assistance in construction of equipment.

IRE Standards on Electron Tubes: Physical Electronics Definitions, 1957*

(57 IRE 7. S1)

COMMITTEE PERSONNEL

Subcommittee on Physical Electronics
1955–1956

R. M. MATHESON, *Chairman*

R. W. Atkinson
J. G. Buck
L. Cronin
H. B. Frost
C. T. Goddard
P. N. Hamblenton
J. M. Lafferty
J. E. White

Committee on Electron Tubes
1956

P. A. REDHEAD, *Chairman*
G. A. ESPERSEN, *Vice-Chairman*

J. R. Adams
E. M. Boone
A. W. Coolidge
P. A. Fleming
K. Garoff
T. J. Henry
E. O. Johnson
W. J. Kleen
P. M. Lapostolle
R. M. Matheson
L. S. Nergaard
G. D. O'Neill
H. J. Reich
A. C. Rockwood
H. Rothe
W. G. Shepherd
R. W. Slinkman
R. G. Stoudenheimer
B. H. Vine
R. R. Warnecke

Standards Committee
1956

M. W. BALDWIN, JR., *Chairman*
C. H. PAGE, *Vice-Chairman*
R. F. SHEA, *Vice-Chairman*
L. G. CUMMING, *Vice-Chairman*

W. R. Bennett
J. G. Brainerd
P. S. Carter
P. S. Christaldi
A. G. Clavier
J. E. Eiselein
H. Goldberg
V. M. Graham
R. A. Hackbusch
H. C. Hardy
D. E. Harnett
Hans Jaffe
Henry Jasik
A. G. Jensen
J. L. Jones
I. M. Kerney
J. G. Kreer, Jr.
E. A. Laport
W. A. Lynch
A. A. MacDonald
Wayne Mason
D. E. Maxwell
K. R. McConnell
H. R. Mimno
M. G. Morgan
G. A. Morton
H. L. Owens
P. A. Redhead
R. Serrell
R. M. Showers
H. R. Terhune
W. E. Tolles
J. E. Ward
E. Weber
W. T. Wintringham

Definitions Coordinator
1956

C. H. PAGE

* Approved by the IRE Standards Committee, October, 1956. Reprints of this Standard, 57 IRE 7. S1, may be purchased while available from the Institute of Radio Engineers, 1 East 79th Street, New York, N. Y., at $0.50 per copy. A 20 per cent discount will be allowed for 100 or more copies mailed to one address.

Cathode Coating Impedance. The impedance, excluding the *Cathode Interface (Layer) Impedance*, between the base metal and the emitting surface of a coated cathode.

Cathode Interface (Layer) Impedance. An impedance between the cathode base and coating.

Note: This impedance may be the result of a layer of high resistivity or a poor mechanical bond between the cathode base and coating.

Cathode Interface (Layer) Resistance. The low frequency limit of *Cathode Interface Impedance.*

Cathode Interface (Layer) Capacitance. A capacitance which, in parallel with a suitable resistance, forms an impedance approximating the *Cathode Interface Impedance.*

Note: Because the *cathode interface impedance* cannot be represented accurately by the two-element RC circuit, this value of capacitance is not unique.

Contact Potential Difference. The difference between the *Work Functions* of two materials, divided by the electronic charge.

Cyclotron Frequency. The frequency at which a charged particle traverses an orbit in a steady, uniform, magnetic field, and zero electric field.

Electrode Current (of an Electron Tube). The net current from an electrode into the interelectrode space.

Note: The terms cathode current, grid current, anode current, plate current, and so forth, are used to designate electrode currents for these specific electrodes. Unless otherwise stated, an electrode current is measured at the available terminal.

Electron Device. A device in which conduction is principally by electrons moving through a vacuum, gas, or semiconductor.

Electron Emission. The liberation of electrons from an electrode into the surrounding space.

Electron Tube. An *Electron Device* in which conduction takes place by electrons moving through a vacuum or gaseous medium within a gas-tight envelope.

Electronic. Of or pertaining to devices, circuits, or systems utilizing *electron devices.* Examples: Electronic control, electronic equipment, electronic instrument, and electronic circuit.

Electronics. That field of science and engineering which deals with *Electron Devices* and their utilization.

Electronics. (Used as an adjective) signifies of or pertaining to the field of electronics. Examples: Electronics engineer, electronics course, electronics laboratory, and electronics committee.

Emission Characteristic. The relation between the emission and a factor controlling the emission such as temperature, voltage, or current of the filament or heater.

Field Emission. The liberation of electrons from a solid or liquid by a strong electric field at the surface.

Field-Enhanced Photoelectric Emission. The increased *Photoelectric Emission* resulting from the action of a strong electric field on the emitter.

Field-Enhanced Secondary Emission. The increased *Secondary Emission* resulting from the action of a strong electric field on the emitter.

Field-Free Emission Current (of a Cathode). The electron current emitted by a cathode when the electric field at the surface of the cathode is zero.

Flection-Point Emission Current. That value of current on the diode characteristic for which the second derivative of the current with respect to the voltage has its maximum negative value. This current corresponds to the upper flection point of the diode characteristic.

Gas (Ionization) Current (in a Vacuum Tube). A positive ion current produced by collisions between electrons and residual gas molecules.

Gas Ratio. The ratio of the ion current in a tube to the electron current that produces it.

Hot Cathode (Thermionic Cathode). A cathode that functions primarily by the process of *Thermionic Emission.*

Hot Cathode Tube. An electron tube containing a *Hot Cathode.*

Inflection-Point Emission Current. That value of current on the diode characteristic for which the second derivative of the current with respect to the voltage is zero.

Note: This current corresponds to the inflection point of the diode characteristic and is, under suitable conditions, an approximate measure of the maximum space-charge-limited emission current.

Photoelectric Emission. The ejection of electrons from a solid or liquid by electromagnetic radiation.

Radiation (Nuclear). In nuclear work, the usual meaning of radiation is extended to include moving nuclear particles, charged or uncharged.

Schottky Emission. The increased *Thermionic Emission* resulting from an electric field at the surface of the cathode.

Secondary Emission. The ejection of electrons from a solid or liquid as a result of charged-particle impact.

Secondary Emission Ratio (Electrons). The average number of electrons emitted from a surface per incident primary electron.

Note: The result of a sufficiently large number of events should be averaged to ensure that statistical fluctuations are negligible.

Space Charge. The net electric charge within a given volume.

Space-Charge Density. The net electric charge per unit volume.

Space-Charge-Limited Current (of a Vacuum Tube). The current passing through an interelectrode space when a *Virtual Cathode* exists therein.

Thermionic Emission. The liberation of electrons or ions from a solid or liquid as a result of its thermal energy.

Thermionic Tube. An *Electron Tube* in which the heating of one or more of the electrodes is for the purpose of causing electron or ion emission.

Vacuum Tube. An *Electron Tube* evacuated to such a degree that its electrical characteristics are essentially unaffected by the presence of residual gas or vapor.

Virtual Cathode. The locus of such a space-charge-potential minimum that only a portion of the electrons approaching it is transmitted, the remainder being reflected.

Work Function. The minimum energy required to remove an electron from the Fermi level of a material into field-free space.

Note: Work function is commonly expressed in electron volts.

CORRECTION

Amos Nathan, author of "A Note on Bandwidth," which appeared on pages 788–790 of the June, 1956 issue of PROCEEDINGS OF THE IRE, has brought the following corrections to the attention of the editors.

1) In (5) the denominators should read

$$\int_{-\infty}^{\infty} e_{N_0}^2(t)dt \quad \text{and} \quad \int_{-\infty}^{\infty} |\overline{H}_N|^2 d\omega \quad \text{respectively.}$$

The denominators of (7) and (9) should read

$$\int |\overline{H}_I|^2 d\omega \int |\overline{H}_N|^2 d\omega \quad \text{and}$$

$$\int_0^{\infty} W_I^2(t)dt \int_0^{\infty} W_N^2(t)dt.$$

2) Footnote 1 should be deleted.

3) On page 790, first column:

7th row should read

$$\frac{1}{1+(\omega T)^2},$$

last integral should read

$$d\omega T \quad \text{for} \quad d\omega,$$

last equation should read

$$\omega_1 T \cong 1/\sqrt{3}\,\varepsilon = 1/1.73\,\varepsilon.$$

4) On page 790, second column:

4th row should read

$$E^{-t/T}1(t),$$

6th row should read

$$T_c \ll T,$$

9th row should read

$$\cong T_c\left[1 - \frac{T_c}{T} + \frac{2}{3}\left(\frac{T_c}{T}\right)^2\right].$$

11th row should read

$$\cong T_c[\,\cdots\,].$$

The last two equations should be

$$\varepsilon_\infty^2 = \frac{1}{12}\left(\frac{T_c}{T}\right)^2$$

$$T_c/T \cong \sqrt{12}\,\varepsilon_\infty = 3.46\,\varepsilon_\infty.$$

The corrections do in no way alter the essence of the paper. In particular, (7) and (9) as printed are valid approximations for the case of small errors and their correction does not affect the examples.

Mr. Nathan is indebted to J. Sklansky of RCA for pointing out the errors in (5) and (7).

Confined Electron Flow in Periodic Electrostatic Fields of Very Short Periods*

KERN K. N. CHANG†

Summary—By utilizing the centrifugal force of an electron, resulting from a magnetic field in the cathode plane as a restoring force, an electrostatically-confined beam flow can be obtained through the strong focusing of a periodic electric field. Because of the extremely steep nature of the potential valley derived from its particular force field, the focusing scheme is far more stable than any previous ones.

A uniform magnetic field threading the cathode is employed when a very thin, hollow beam is to be focused. By using a radially varying magnetic field, the focusing scheme can be applied to thick hollow beams, of low as well as of high perveance. Experimental results indicate that the focusing performance obtained is much less critical than that obtained with a periodic magnetic field which has been recently tested extensively.

Introduction

PERIODIC electrostatic fields for beam focusing were first used on velocity modulated tubes in 1939.[1] In the following year Smith and Hartman[2] attempted to obtain a periodic focusing field by means of helical grid. In 1948, R. W. Peter[3] in this laboratory, proposed the formation of a focusing field by the use of a pair of bifilar helices at different potentials. During the last two years, both theoretical and experimental studies have been made on beam focusing with electrostatic fields of comparatively long periods.[4–6] The only significant work on electrostatic focusing with short-period periodic fields was done by P. K. Tien.[7] A 78 per cent current transmission was observed on his bifilar-helix traveling-wave tube. It was, however, concluded by Tien that a specific radial distribution on the space charge density is required to obtain a well-focused beam.

The practical difficulty of realizing an electron beam with nonuniform current distribution has discouraged many workers from using the periodic electrostatic field as a focusing device. Instead, a periodic magnetic field[8,9] has been preferred. However, in spite of its advantages over uniform magnetic-field focusing, beam focusing with periodic magnetic field has its own drawbacks. For example, even a small amount of asymmetry in the transverse field, which is difficult to avoid completely in a practical magnet assembly, will degrade the focusing performance. Secondly, it is by no means easy to control or vary the periodic field which is produced by a permanent magnet.

The attractiveness of using the periodic electrostatic field as a focusing device lies mainly in the noncriticalness of its field. There need be no worry about any unsymmetrical field which might be serious enough to change focusing appreciably. If something could be done to remove the requirement of nonuniform current density in the electron beam, the periodic electrostatic field would become a potential focusing device superior to any existing one.

The following presentation will describe a new method for focusing an electron beam of *uniform* space charge density with an electrostatic field. The method involves the use of a rotation resulting from a net magnetic flux threading through the cathode plane. The centrifugal force due to this rotation is used as the restoring force to the focusing force produced by the electrostatic field, instead of the space charge force as employed in previous electrostatic focusing schemes. The rotation produces such a strong centrifugal defocusing force that, in most of the practical cases, the defocusing force due to space charge can be ignored.

As will be shown, a uniform magnetic field can be used in the cathode plane if a very thin hollow beam is to be focused. By radially shaping the magnetic field, this focusing scheme can be applied also to thick hollow beams or even to solid beams. It is a simpler matter to shape a magnetic field than it is to shape the current density as required in previous schemes.

Initial Magnetic Field

Any amount of net initial magnetic flux lines threading through the electron emitter will give rise to a rotation of the electrons around the beam axis. The effect can be demonstrated by the well known equation of

* Original manuscript received by the IRE, October 5, 1956. This paper was presented at the IRE Electron Tube Research Conference, University of Colorado, Boulder, Colo.; June, 1956.

† RCA Labs., Princeton, N. J.

[1] W. C. Hahn and G. F. Metcalf, "Velocity-modulated tubes," PROC. IRE, vol. 27, pp. 106–116; February, 1939.

[2] L. P. Smith and P. L. Hartman, "The formation and maintenance of electron and ion beams," *J. Appl. Phys.*, vol. 2, pp. 220–229; March, 1940.

[3] Unpublished theoretical study, RCA Laboratories.

[4] J. R. Pierce, "Theory and Design of Electron Beams," D. Van Nostrand Co. Inc., New York, N. Y., p. 210; 1954.

[5] A. M. Clogston and H. Heffner, "Focusing of an electron beam by periodic fields," *J. Appl. Phys.*, vol. 25, p. 436; April, 1954.

[6] K. K. N. Chang, "Beam focusing by periodic and complementary fields," PROC. IRE, vol. 43, pp. 62–71; January, 1955.

[7] P. K. Tien, "Focusing of a long cylindrical electron stream by means of periodic electrostatic fields," *J. Appl. Phys.*, vol. 25, pp. 1281–1288; October, 1954.

[8] J. T. Mendel, C. F. Quate, and W. H. Yocom, "Electron beam focusing with periodic permanent magnet fields," PROC. IRE, vol. 42, pp. 800–810; May, 1954.

[9] K. K. N. Chang, "Periodic magnetic field focusing for low-noise traveling-wave tubes," *RCA Rev.*, vol. 16, pp. 423–431; September, 1955.

angular motion[10] in axially symmetrical fields

$$\frac{d}{dt}\left(r^2\dot{\phi} + \frac{\eta}{2\pi}\psi\right) = 0 \tag{1}$$

cylindrical coordinates (r, ϕ, z) being used. Here $\dot{\phi}$ is the angular velocity, η is the ratio of electron charge to mass, and ψ is the total flux through a concentric circle of radius r

$$\psi = \int^{r} B(r) 2\pi r dr. \tag{1a}$$

Eqs. (1) and (1a) give precisely the relationship between the angular velocity of electrons and the position (radius r) of the electron if the radial magnetic field distribution $B(r)$ is known.

Suppose now that the axial magnetic field has a distribution in the gun as shown by Fig. 1. The field assumes a value of B_c in the cathode plane and then reduces to zero at and beyond the plane Z_1. Since the magnetic field lines are continuous, they become gradually transverse as the axial field intensity is reduced, and therefore, electrons must cross the full amount of flux ψ_c which had threaded the cathode at the plane Z_1. Consequently, by (1) and (1a) the electrons beyond the plane Z_1 will have the angular velocity $\dot{\phi}$ given by

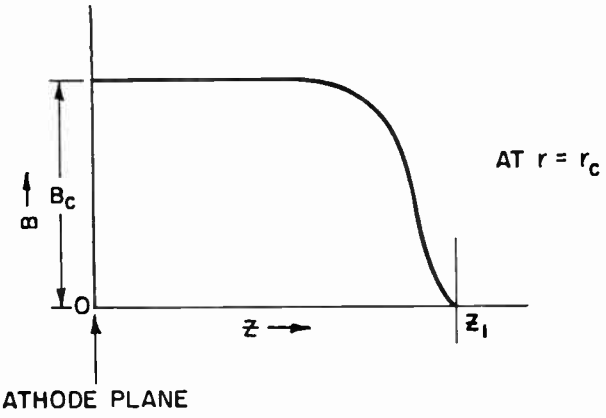

Fig. 1—Axial magnetic field distribution in the electron gun.

$$\dot{\phi} = -\frac{\eta}{2\pi r^2}\psi_c = -\frac{\eta}{r^2}\int_0^{r_c} B_c(r) r dr \tag{2}$$

where r_c is the cathode radius. The rotation of electrons with angular velocity $\dot{\phi}$ will be used to produce the restoring force in the focusing scheme to be discussed in the next section.

Electron Motions in Periodic Electrostatic Field

The electron motions in an electrostatic field in three coordinates (r, ϕ, z) are

[10] Pierce, *op. cit.*, p. 36.

$$\ddot{r} - r\dot{\phi}^2 - \eta\frac{\partial V}{\partial r} = \frac{\eta^2}{4} B_b^2 \frac{r_c^2}{r} \tag{3}$$

$$r\ddot{\phi} + 2\dot{\phi}\dot{r} = \frac{1}{r}\eta\frac{\partial V}{\partial \phi} \tag{4}$$

$$\ddot{z} = \eta\frac{\partial V}{\partial z}. \tag{5}$$

Here dots denote the derivatives with respect to time, V is the electrostatic potential, and B_b is the equivalent Brillouin field which represents the space charge effect. In mks units[6]

$$B_b^2 = \frac{\sqrt{2}I}{\pi\epsilon_0\eta^{3/2}V^{1/2}r_c^2} = 0.69 \times 10^{-6}\frac{I}{V^{1/2}r_c^2}. \tag{6}$$

The potential V in a periodic cylindrical structure with dc potential V_1 and V_2 (Fig. 2) can be expressed as

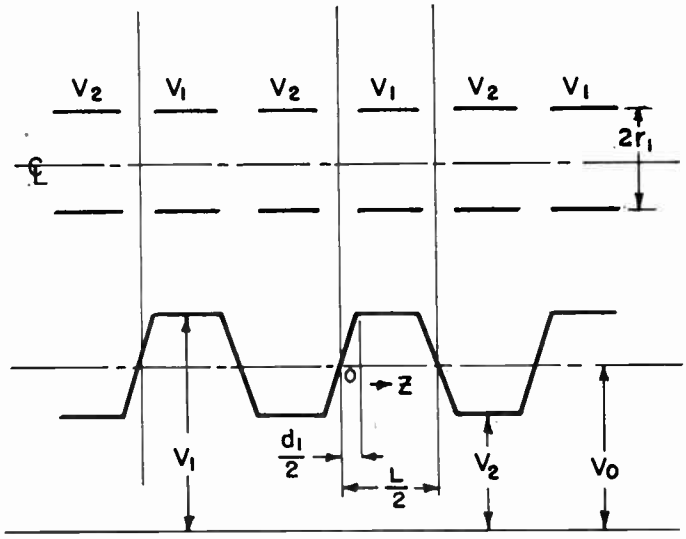

Fig. 2—Potential distribution on the boundary of a periodic structure.

$$V = V_0 + \hat{V}(r)\cos\left(\frac{2\pi}{L}z - \phi\right), \quad V_0 \gg \hat{V}(r) \tag{7}$$

where V_0 is the average dc beam potential and $\hat{V}(r)$ is the superimposed alternating potential.[7]

$$\hat{V}(r) = 2(V_1 - V_2)\frac{\sin\sigma_1\pi}{\sigma_1\pi^2}\frac{I_n\left(\frac{2\pi}{L}r\right)}{I_n\left(\frac{2\pi}{L}r_1\right)}. \tag{8}$$

Here σ_1 is the ratio of the distance d_1 between adjacent boundaries of the periodic structure to the period L (see Fig. 2). The periodic structure has an inner radius r_1 as shown by Fig. 2. I_n is the modified Bessel's function. For circularly symmetrical rings, n is zero; for bifilar helices, n is 1. The phase angle ϕ in (7) is a constant for

rings. In the case of bifilar helices, however, the potential is also dependent on ϕ because of the winding pitch.

The equations of electron motion (3)–(5) can be solved approximately in the appendix by assuming that the beam is perturbed to a very small radius $\hat{r}$ around an average radius r_0. The angular velocity $\dot{\phi}$ has an initial value given by (2). By substituting the approximate first order solution into these equations, one can arrive at a very important relation among the magnetic field at the cathode, the voltage variations on the periodic structure, the space charge effect, and the geometry of the structure, at a focused beam radius r_0. This relation is

$$\left[\left(\frac{L}{2\pi}\right)^2\hat{V}'' + \hat{V} + \left(\frac{L}{2\pi r_0}\right)^2\hat{V}\right]\frac{\hat{V}'}{V_0} = \frac{1}{r_0}\left(\frac{L}{2\pi r_0}\right)^2\frac{\hat{V}^2}{V_0} + 4r_0\left(\frac{2\pi}{L}\right)^2 V_0 \cdot\left[\left(\frac{L}{\lambda_b}\right)^2\left(\frac{r_c}{r_0}\right)^2 + \left(\frac{L}{\lambda_c}\right)^2\left(\frac{r_c}{r_0}\right)^4\left(\frac{\psi_c}{\psi_c}\right)^2\right]. \quad (9)$$

Primes indicate derivatives with respect to r. The value of $\bar{\psi}_c$ is set equal to ψ_c at $r=r_0$ [see definition (1a)]. λ_b and λ_c carry respectively the physical meanings of the plasma wave length and the scalloping wave length of a beam in a uniform magnetic field; they are in mks units

$$\lambda_b = \frac{4\pi\sqrt{V_0}}{\sqrt{\eta}B_b} \quad (10)$$

$$\lambda_c = \frac{4\pi\sqrt{V_0}}{\sqrt{\eta}B_c(r_0)}. \quad (11)$$

Eq. (9) gives the force balance on the electron beam. The terms on the left-hand side represent respectively the focusing forces contributed by the radial, the axial, and the angular fields. The defocusing force, or the restoring force, on the right-hand side, consists of the rotation due to the angular field and the initial magnetic field and the spreading of the space charge. Eq. (9) has almost the same form as that given by Tien except the last term. This is the term, which, produced by the magnetic field in the cathode, is used basically as the restoring force to the focusing effect. This term can be made large enough, in some instances, so that the second term on the right-hand side of (9) which accounts for the space charge force may well be neglected. This corresponds to a type of electron flow which we call "electrostatically confined flow," where the focusing and defocusing forces are very strong compared to the space charge force.

Force Equilibrium

The requirement for a stable focusing system is that a potential valley exist along the path where the beam is to be focused. The steeper the valley is, the stiffer is the beam and the more stable is the focusing. This potential valley is usually derived from a resultant of two different kinds of radial forces balancing each other on the beam, one focusing and the other defocusing. In Fig. 3 a plot of force balance is shown for different kinds

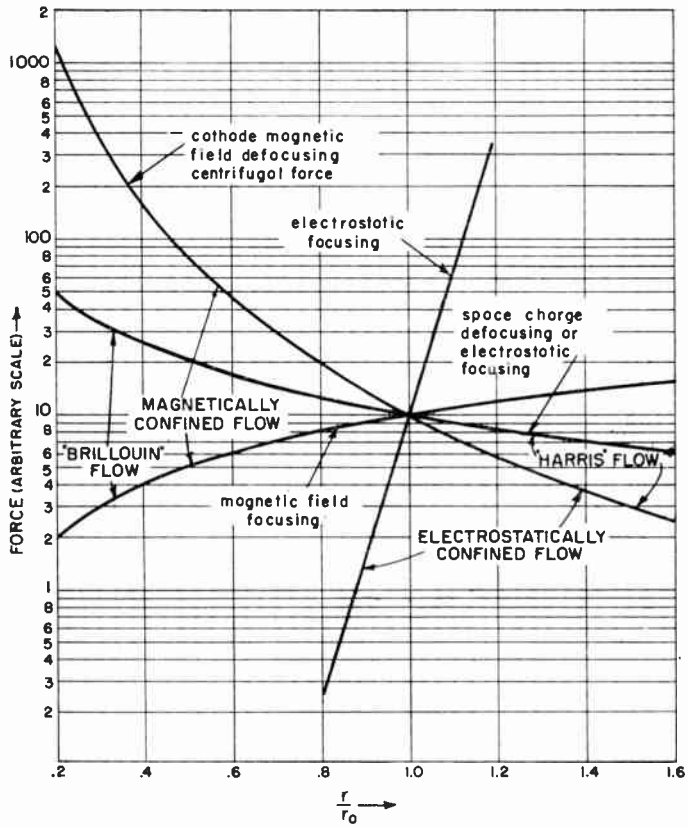

Fig. 3—Force balance of different focusing systems.

of beam flow produced by different focusing systems. For comparison, all the focusing systems have been assumed to focus the beam at the same equilibrium radius. With a beam of a given size and perveance, the defocusing force due to space charge would be fixed. For confined-flow systems employing cathode field, the defocusing forces are usually much higher than space-charge forces. It is, therefore, quite fair to compare the stability of all the focusing systems with the same defocusing force (which is the space-charge force in "Brillouin" flow case) at the equilibrium radius r_0, as indicated by Fig. 3. "Brillouin" flow is formed usually by a magnetic force which is proportional to the radius r and a space charge force proportional to $1/r$. The magnetic field is either a uniform one or a periodic one, with no field in the cathode. If a magnetic field is introduced in the cathode, at about the same magnitude as that in the drift region, the electron flow is magnetically confined,[11]

[11] Pierce, *op. cit.*, p. 161.

when the magnetic field is high enough. The force balance in this case takes place essentially between the magnetic focusing force proportional to r and the centrifugal force proportional to $1/r^3$. If the centrifugal force balances an electrostatic field of type $1/r$, "Harris flow" results.[12,13] Beam focusing with an electrostatic field of long periods produces a beam flow similar to Brillouin flow, since the focusing field is again proportional to the radius r.

The new focusing system described here is actually electrostatically confined rather than magnetically confined. It utilizes the centrifugal force (which is produced by the rotation due to the magnetic field in the cathode) to counteract a strongly varying electrostatic focusing force. The focusing force, which is formed by the periodic electrostatic field of very short periods, varies as a modified Bessel function given by (9) with respect to the beam radius. The modified Bessel function has approximately exponential variation over a narrow region. In a logarithmic scale, the focusing force should vary linearly in the neighborhood of r_0. This linearity is shown in Fig. 3.

The net forces acting on the beam in different focusing systems are replotted in Fig. 4. The strongest restoring

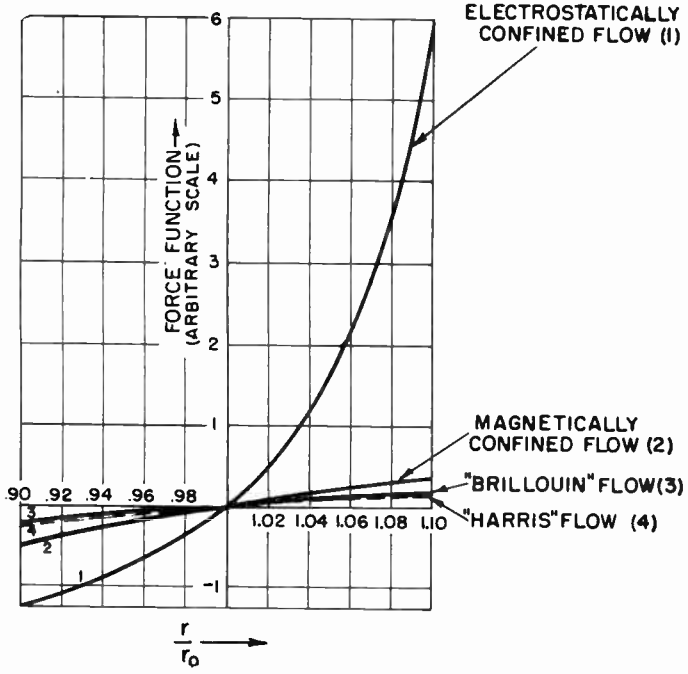

Fig. 4—Force functions near the equilibrium radius.

force in the vicinity of the equilibrium radius r_0 is found for electrostatically confined flow.

The degree of stability in different types of electron flow is determined by their potential functions, which are indicated by Fig. 5. The potential functions are derived from the net force shown in Fig. 4. It is seen clearly that electrostatically confined flow is the most stable flow due to its exponentially varying force, which leads to the steepest potential valley.

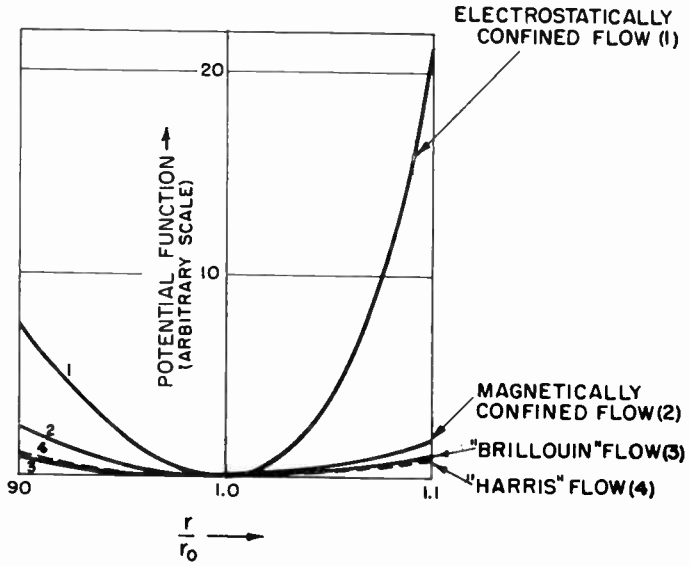

Fig. 5—Potential valley near the equilibrium radius.

Numerical Results

As described above, the electron beam is focused in electrostatically confined flow according to (9). The variations in the initial magnetic field and in the space charge force, which are represented by the last two terms of the right-hand side of (9), are plotted in Fig. 6 as a function of the ratio of the beam radius to the period of the electrostatic field, produced by bifilar helices, at a fixed ratio of the beam radius to the helix radius ($r_0/r_1=0.8$), on a very thin hollow beam of an arbitrary radius r_0. The focusing forces are computed for voltage variations ($\hat{V}/V_0$) in the beam region of 5 per cent and 10 per cent. A uniform magnetic field is used in the cathode plane for the thin hollow beam. The ratio of cathode to beam radius (r_c/r_0) being a function of the ordinate in Fig. 6, determines whether the beam has to start from a convergent $[(r_c/r_0)>1]$, a parallel $(r_c/r_0=1)$, or a divergent $[(r_c/r_0)<1]$ gun. It is noted from Fig. 6 that with a fixed ratio of r_0/r_1 a beam of smaller radius encounters a stronger focusing effect, which is as it should be. The actual voltage variations on the bifilar helices versus the ratio of the beam radius to the period for two given voltage variations on the beam (5 per cent and 10 per cent) are shown by Fig. 7.

As also revealed by (9), the focusing condition is only correctly satisfied by the electrons for one radius in the beam, if the magnetic field remains radially constant in the cathode plane. For applications to thick hollow beams or solid beams, it is necessary to shape the mag-

[12] L. A. Harris, "Axially symmetrical electron beam and magnetic-field systems," PROC. IRE, vol. 40, pp. 700–708; June, 1952.
[13] Pierce, *op. cit.*, p. 170.

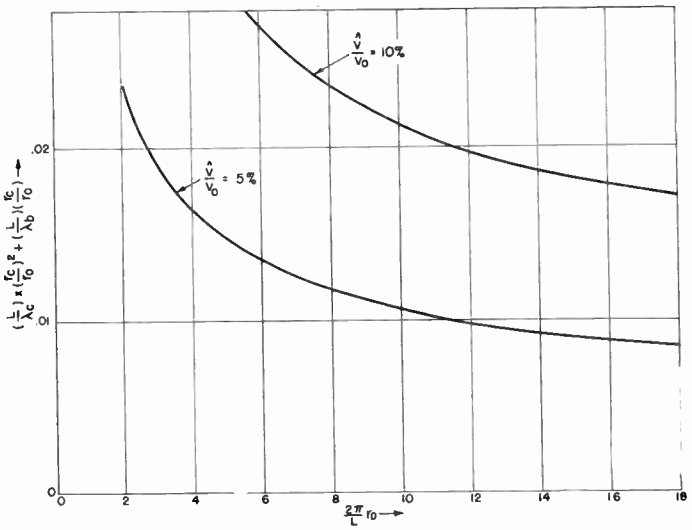

Fig. 6—Variations of initial magnetic field and space charges effect as a function of the ratio of the beam radius to the period.

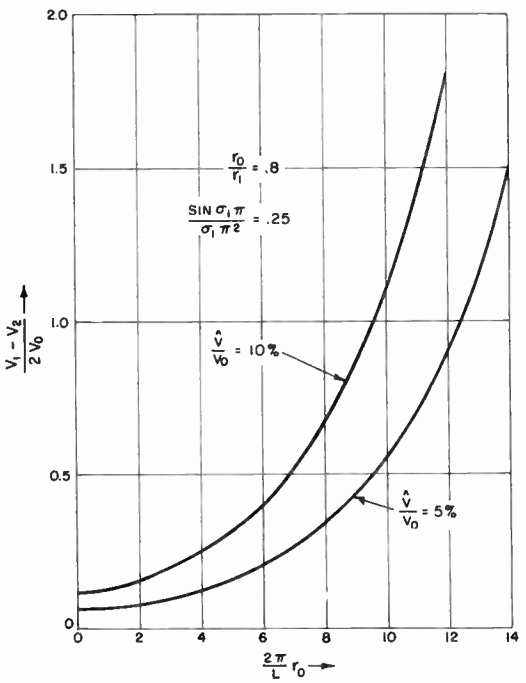

Fig. 7—Voltage difference on bifiler helices as a function of the ratio of the beam radius to the period, and the voltage variations on the beam.

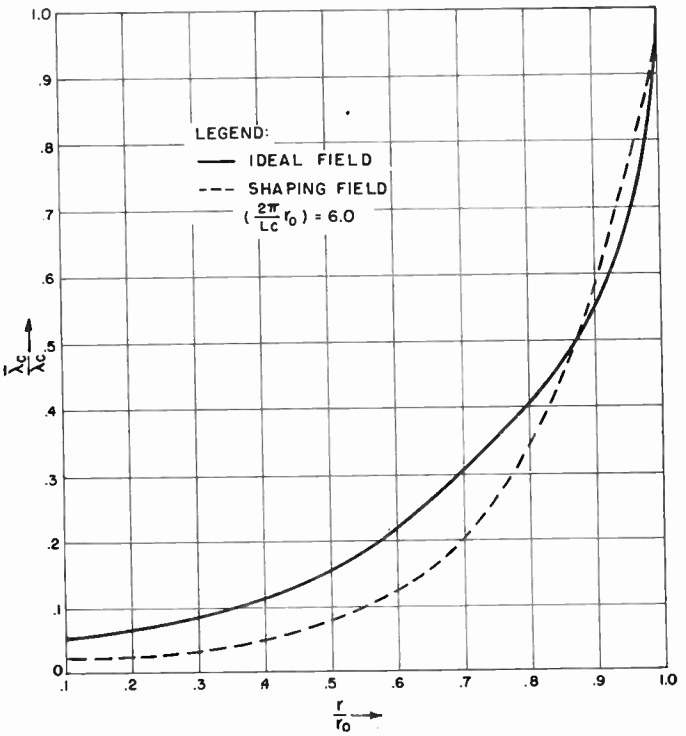

Fig. 8—Magnetic field distribution across a hollow beam.

perfect focusing if the space charge can be ignored, while the dotted one is the field produced by a periodic magnet of period L_c near the cathode. The periodic magnet, which has been previously referred to[14], is employed here to illustrate one of the possible ways to produce a radially varying magnetic field in the cathode plane. The cathode is placed where the periodic magnetic field reaches its peak value in the axial direction. The peak field can be shown to vary in the r direction as a Bessel function (I_0). The maximum value of the argument of the Bessel function $I_0[(2\pi/L_c)r_0]$ in the specific example shown by Fig. 8 is equal to 6.

The second example, plotted in Fig. 9, opposite, illustrates the magnetic field distributions for a thick hollow beam if the space-charge force cannot be neglected. For instance, in the parallel flow gun case ($r_c = r_0$), $(\lambda_f/\lambda_b)^2 = \frac{1}{4}$, where λ_f physically has the meaning of the scalloping wave length in the beam acted on by the electrostatic field; in dimensionless units.

$$\frac{\lambda_f^2}{L^2} = \frac{16\pi^2 r_0 V_0^2/L^2}{\left[\hat{V} + \left(\frac{L}{2\pi}\right)^2 \hat{V}'' + \left(\frac{L}{2\pi r_0}\right)^2 \hat{V}\right]\hat{V}' - \frac{1}{r_0}\left(\frac{L}{2\pi r_0}\right)^2 \hat{V}^2} \tag{12}$$

netic field. Using (9), two examples of shaping the field are given. In Fig. 8 two radial distributions of magnetic field at the cathode are shown. The ordinate $1/\lambda_c$ which relates to the magnetic field according to (11) is normalized by $1/\bar{\lambda}_c$, the corresponding value at the outermost beam radius r_0. The solid curve is the desired field for

and

$$\frac{L^2}{\lambda_f^2} = \frac{L^2}{\lambda_c^2}\left(\frac{r_c}{r_0}\right)^4 \left(\frac{\psi_c}{\bar{\psi}_c}\right)^2 + \frac{L^2}{\lambda_b^2}\left(\frac{r_c}{r_0}\right)^2. \tag{13}$$

[14] K. K. N. Chang, "Optimum design of periodic magnet structures for electron beam focusing," *RCA Rev.*, vol. 16, pp. 65–81; March, 1955.

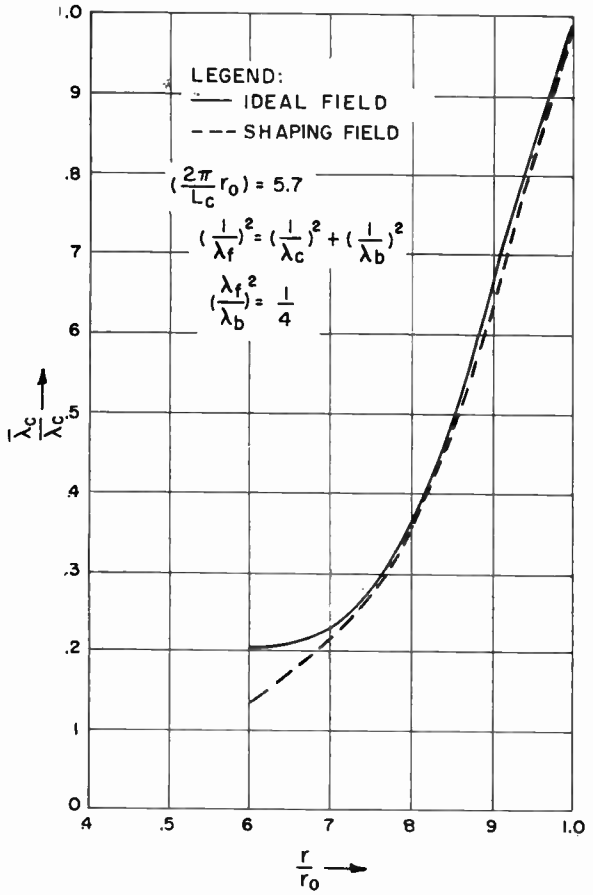

Fig. 9—Magnetic field distribution across a hollow beam.

Again the solid curve represents the ideal field for perfect focusing. The dotted one is the field produced by a periodic magnet with a Bessel argument value of 5.7. The close agreement between the ideal field and the shaping field, as shown by Fig. 9, is just coincident. Nevertheless, it is evident that a close approximation of a desired magnetic field is quite feasible, especially if the pole pieces of the magnets which produce the cathode field are shaped properly.

To demonstrate the application of the proposed focusing scheme, design data of three typical beam-type microwave tubes has been calculated and listed in Table I, for a low-noise tube, a power tube, and a backward-wave tube. The low-noise tube and the backward-wave tube are designed to use a thin hollow beam, since the beam perveances employed are relatively small. The power tube, on the other hand, uses a thick hollow beam, with a magnetic field in the cathode shaped according to Fig. 9. The table indicates that in both the low-noise tube and the backward-wave tube, the Brillouin field B_b—equivalent to the space-charge effect—is practically negligible with respect to the cathode field B_c. A magnetic field of a maximum value of 1050 Gauss at the outer radius of the hollow beam is required for the power tube.

It should be noted by (13) that in order to have room for the cathode field ($\propto 1/\lambda_c$) shaped up to satisfy the equation for all electrons in the beam, the focusing field ($\propto 1/\lambda_f$) must be considerably greater than the Brillouin field ($\propto 1/\lambda_b$). A high focusing field requires a large percentage variation of the voltage on the beam. The maximum tolerable voltage variation thus determines the maximum value of beam perveance which can be focused.

TABLE I

	Low Noise Tube (Very Thin Hollow Beam)	Power Tube (60 Per Cent Hollow Beam)	Backward Wave Tube (Very Thin Hollow Beam)
V_0	650 v	3600 v	400 v–2800 v
I_0	0.3 ma	250 ma	1 ma
$0.8 \times \cot \psi$	10.7	5.0	8
B_b	32 G	210 G	35.5 G–24.6 G
B_c	300 G	max. 1050 G	126 G–126 G
$\frac{V_1 - V_2}{2V_0}$	1.1	0.35	0.65–0.2
$\frac{\hat{V}}{V_0}$	10 per cent	10 per cent	10 per cent–3.78 per cent

Experimental Results

An experimental tube for testing the focusing performance was built and is shown in Fig. 10. The tube uses a thin hollow beam and a bifilar-helix circuit. Its data are as follows:

Hollow cathode: od = 0.074 inch
id = 0.070 inch
Bifilar helices: tpi = 48
od = 0.100 inch
id = 0.090 inch
Helix length: = 6 inches

The experimental setup is shown by Fig. 11. An undirectional magnetic field B_c is used in the gun and shielded from the bifilar helices by a μ-metal plate. The beam was properly adjusted before its entrance to the periodic electric field region by either varying the electrode potential in the gun, or partially changing the magnetic field near the entrance by an additional small coil.

Fig. 12 shows the results of percentage current transmission vs the beam current with a cathode field of 300 Gauss. Percentage current transmission vs the mag netic field in the cathode at a beam current of 0.350 ma is plotted in Fig. 13. The current transmission reaches a peak of 97 per cent and is above 90 per cent for a large range of reasonable values of magnetic field at the cathode. The average voltage used is about 650 v. The voltage difference between the bifilar helices is 700 v, while the percentage voltage variation in the beam is only 10 per cent.

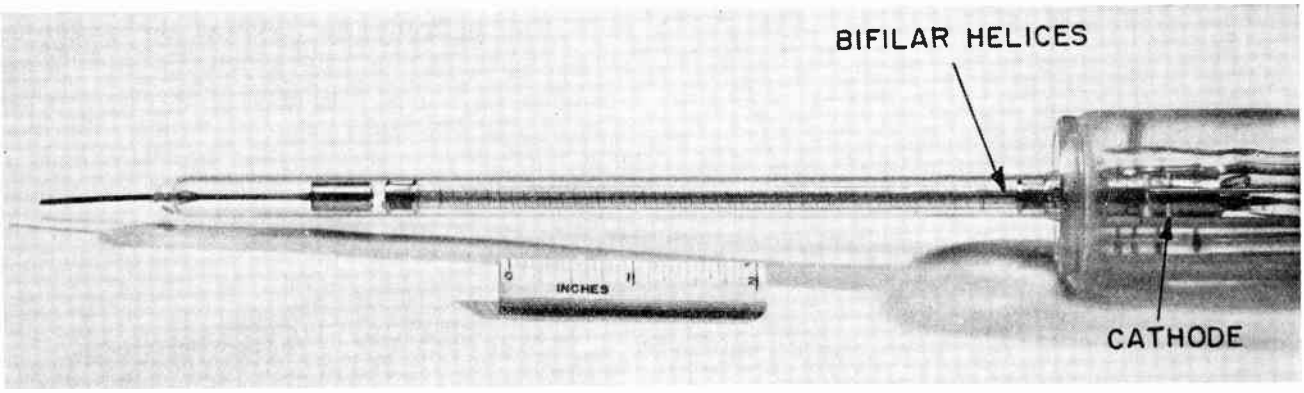

Fig. 10—Experimental tube.

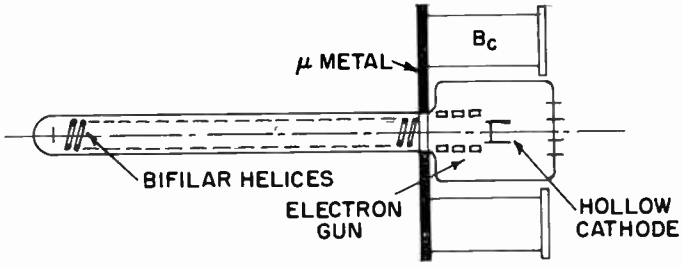

Fig. 11—Focusing test of an experimental traveling-wave tube.

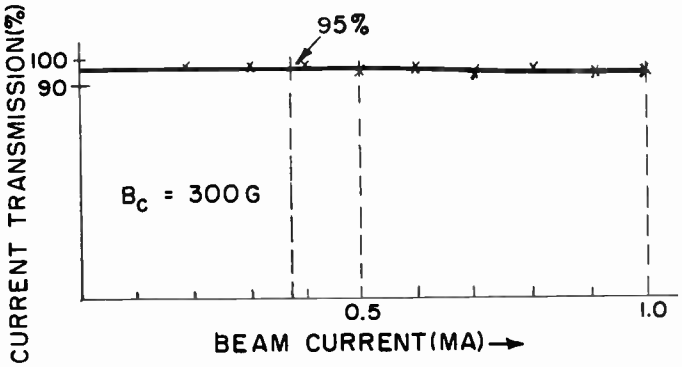

Fig. 12—Current transmission as a function of beam current.

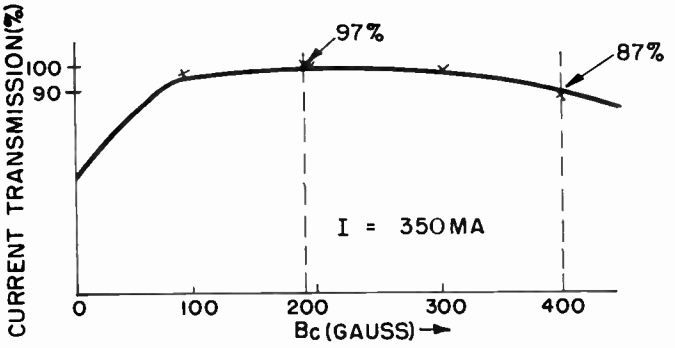

Fig. 13—Current transmission as a function of magnetic field.

The tube was not built in a precise fashion. The crude gun structure used did not allow adjustment of the beam properly for correct initial slope and radius. These factors account for the somewhat lower current transmission at high magnetic fields and high beam current. Experiments show that at high fields and high beam currents the focusing should be accomplished more precisely.

Conclusion

By utilizing the centrifugal force of rotating electrons, as a restoring force to balance the strong focusing force due to a periodic electrostatic field of very short period, an electrostatically confined beam flow can be obtained. Because of the extremely steep nature of the potential valley derived from the force balance, the new focusing scheme is far more stable than any previous one.

A uniform magnetic field is employed in the cathode when a very thin hollow beam is to be focused. By the use of a radially varying field, the focusing scheme can be applied to thick hollow beams and to solid beams. The limitation on the maximum perveance is given by the maximum tolerable voltage variation along the beam. Experimental results indicate that the focusing performance of the new scheme is much less critical than that of the one utilizing periodic magnetic fields, which has been recently tested extensively. The noncriticalness is due to its steep potential valley and also to the absence of any major undesirable transverse fields, which are difficult to avoid in practical focusing magnets.

Appendix

Confined Electron Flow in Periodic Electrostatic Fields——First-Order Solution

Suppose the first-order solutions of (3)–(5) are

$$r = r_0 + \hat{r}_0 \cos\left(\frac{2\pi}{L} z - \phi\right), \quad r_0 \gg \hat{r}_0 \tag{14}$$

$$\dot{\phi} = \dot{\phi}_0 + \hat{\dot{\phi}}_0 \cos\left(\frac{2\pi}{L} z - \phi\right), \quad \dot{\phi}_0 \gg \hat{\dot{\phi}}_0 \tag{15}$$

where $\dot{\phi}_0$ is the initial angular velocity given by (2) at the average beam radius r_0. By differentiating (14) and (15) with respect to time, it follows that

$$\dot{r} = \hat{r}_0 \left[\dot{\phi} - \frac{2\pi}{L}\dot{z}\right] \sin\left(\frac{2\pi}{L} z - \phi\right) \tag{16}$$

$$\ddot{\phi} = \hat{\dot{\phi}}_0 \left[\dot{\phi} - \frac{2\pi}{L}\dot{z}\right] \sin\left(\frac{2\pi}{L} z - \phi\right) \tag{17}$$

where

$$\dot{z} = \sqrt{2\eta V} \cong \sqrt{2\eta V_0}\left[1 + \frac{\hat{V}(r)}{2V_0}\cos\left(\frac{2\pi}{L}z - \phi\right)\right]$$

$$= \dot{z}_0\left[1 + \frac{\hat{V}(r)}{2V_0}\cos\left(\frac{2\pi}{L}z - \phi\right)\right], \quad V_0 \gg \hat{V}(r). \tag{18}$$

Using the relation

$$\ddot{r} = \frac{\partial^2 r}{\partial z^2}\dot{z}^2 + \frac{\partial^2 r}{\partial \phi^2}\dot{\phi}^2 + 2\dot{\phi}\dot{z}\frac{\partial^2 r}{\partial \phi \partial z} + \ddot{z}\frac{\partial r}{\partial z} + \ddot{\phi}\frac{\partial r}{\partial \phi} \tag{19}$$

and expanding $\hat{V}(r)$ and $\hat{V}'(r)$ and dropping high order terms

$$\hat{V}(r) = \hat{V}(r_0) + \hat{V}'(r_0)\hat{r}_0\cos\left(\frac{2\pi}{L}z - \phi\right) \tag{20}$$

$$\hat{V}'(r) = \hat{V}'(r_0) + V''(r_0)\hat{r}_0\cos\left(\frac{2\pi}{L}z - \phi\right) \tag{21}$$

then substituting (5), (14)–(21) in (3) and (4), equating the constant terms and the coefficients of the cosine terms of (3) and (4), and remembering that $\hat{r}_0$ and $\hat{\phi}_0$ are small compared to r_0 and $\dot{\phi}_0$, we have

$$\hat{r}_0 = -\left(\frac{L}{2\pi}\right)^2 \frac{V'(r_0)}{2V_0}\left\{\left(1 - \frac{\dot{\phi}_0}{\dot{z}_0}\frac{L}{2\pi}\right)^2 + \frac{\dot{\phi}_0^2}{\ddot{z}_0^2}\left(\frac{L}{2\pi}\right)^2\right\}^{-1} \tag{22}$$

$$\hat{\phi}_0 = -\left(\frac{L}{2\pi}\right)\frac{\dot{z}_0}{r_0^2}\frac{\hat{V}(r_0)}{2V_0}\left\{\frac{1}{\left(1 - \frac{\dot{\phi}_0}{\dot{z}_0}\frac{L}{2\pi}\right)} - \frac{\hat{V}'(r_0)}{\hat{V}(r_0)}r_0\left(\frac{L}{2\pi}\right)\frac{\dot{\phi}_0}{\dot{z}_0}\left[\left(1 - \frac{L}{2\pi}\frac{\dot{\phi}_0}{\dot{z}_0}\right) + \frac{\dot{\phi}_0^2}{\dot{z}_0^2}\left(\frac{L}{2\pi}\right)^2\right]^{-1}\right\} \tag{23}$$

and

$$\left[\left[\frac{L}{2\pi}\right]^2 \hat{V}''(r_0) + \hat{V}(r_0) + \left(\frac{L}{2\pi r_0}\right)^2 \hat{V}(r_0)\left[\frac{\dot{z}_0\frac{2\pi}{L}}{\dot{\phi}_0 - \frac{2\pi}{L}\dot{z}_0}\right]\right]\frac{\hat{V}'(r_0)}{V_0}$$

$$= \left\{\frac{1}{r_0}\left(\frac{L}{2\pi r_0}\right)^2\frac{\hat{V}^2(r_0)}{V_0} + 4r_0\left(\frac{2\pi}{L}\right)^2 V_0\left[\left(\frac{L}{\lambda_b}\right)^2\left(\frac{r_c}{r_0}\right)^2 + \left(\frac{L}{\lambda_c}\right)^2\left(\frac{r_c}{r_0}\right)^4\left(\frac{\psi_c}{x_c}\right)^2\right]\right\}\left\{\left(1 - \frac{\dot{\phi}_0}{\dot{z}_0}\frac{L}{2\pi}\right)^2 + \frac{\dot{\phi}_0^2}{\dot{z}_0^2}\left(\frac{L}{2\pi}\right)^2\right\} \tag{24}$$

where

$$\lambda_b = \frac{4\pi\sqrt{V_0}}{\sqrt{\eta}B_b} \tag{25}$$

$$\lambda_c = \frac{4\pi\sqrt{V_0}}{\sqrt{\eta}B_c(r_0)} \tag{26}$$

$$\psi_c = 2\pi\int_0^{r_c} B_c(r)rdr \tag{27}$$

$$\bar{\psi}_c = \pi[B_c(r_0)]r_0^2. \tag{28}$$

In most of the practical cases, however, in which periodic focusing fields of very short periods are used, $(2\pi/L)\dot{z}_0$ is much greater than $\dot{\phi}_0$. Then (24) reduces to

$$\left[\left(\frac{L}{2\pi}\right)^2 V'' + V + \left(\frac{L}{2\pi r_0}\right)^2 \hat{V}\right]\frac{\hat{V}'}{V_0}$$

$$= \frac{1}{r_0}\left(\frac{L}{2\pi r_0}\right)^2\frac{\hat{V}^2}{V_0} + 4r_0\left(\frac{2\pi}{L}\right)^2 V_0$$

$$\cdot\left[\left(\frac{L}{\lambda_b}\right)^2\left(\frac{r_c}{r_0}\right)^2 + \left(\frac{L}{\lambda_c}\right)^2\left(\frac{r_c}{r_0}\right)^4\left(\frac{\psi_c}{\bar{\psi}_c}\right)^2\right]. \tag{29}$$

which is (9) of the text.

Signal-Flow Graphs and Random Signals*

WILLIAM H. HUGGINS†, FELLOW, IRE

Summary—A compact and meaningful description of a signal is offered by the *flow-graph representation* of the signal *generator*. A large class of important signal generators may be represented by a "trigger generator" which delivers a sequence of one or more impulses to various waveform generators. By describing the "trigger generator" by a Markoff process, by identifying the transition probability-densities between states of the Markoff process with impulse responses, and by interpreting the final response as an expectation-density (or average over the ensemble of possible signals), it is possible to obtain, by methods which are very similar to those used in computing the transfer function of an ordinary circuit, expressions for the power spectrum and correlation functions of signals produced by such sources.

The important relationships between stochastic processes and familiar circuit concepts are first illustrated by calculating the probabilities associated with four different coin-tossing experiments of increasing complexity. As a fifth example, these relations are used to develop the well-known Poisson distribution and to introduce the expectation-density of occurrence of a recurrent event.

General formulas for the correlation functions and power spectra of signals produced by Markoffian sources are then obtained for: a random telegraph message; a series of identical pulses having time jitter, both for the free-running and clock-synchronized cases; and, finally, a series of identical pulses of alternating polarity but with random spacing.

Introduction

THIS PAPER discusses the application of some of the mathematical representations, used extensively in network theory, to the solution of certain problems arising in the theory of probability and statistical communication theory. Most of the results are not new if considered as a contribution to statistical theory. However, it is believed that many circuit theorists are not aware that the familiar techniques that they use in solving linear systems may also be used to determine some of the statistics associated with complicated Markoff processes and to determine analytical expressions for the correlation functions and power spectra of signals arising from such processes. It is to these persons that this paper is addressed. (Other papers, discussing the application of circuit-theory representations to the study of signals, are those by Sittler and Widrow.[1])

The mathematical representations which are of most interest are: the Laplace transform; the z (or x) transform; and linear-directed (signal-flow) graphs. The Laplace transform is well known and need not be discussed here. The z (or x) transform is being used increasingly in the analysis of sampled-data systems and for the numerical manipulation of signal waveforms.[1,2] It is derived from the Laplace transform by the simple change of variable $z=\exp(sT)$ or $x=\exp(-sT)$ where T is the sampling interval. A selected bibliography and examples of applications of the method may be found in footnote 2. Linear graphs, which have been used by Mason in analyzing the flow of signals in feedback systems,[3] have an extensive mathematical literature,[4,5] but the published references on engineering applications are rather meager and not commensurate with the potential importance of the linear graph as a tool in the systematic analysis of complex physical systems.[1,2,6] For this reason, a brief description of the signal-flow graph will first be given.

Signal-Flow Graphs

The signal-flow graph consists of a collection of nodes which are connected by directed branches—branch jk originating at node j and terminating at node k. A simple graph having four nodes is shown in Fig. 1.

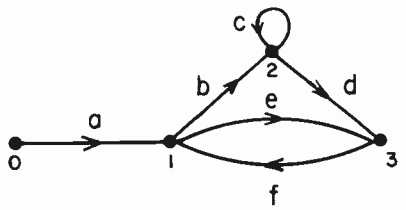

Fig. 1—Simple flow graph.

For use in the analysis of physical systems, each node is identified with some signal (*i.e.*, observable) of the system, and each branch represents a functional relationship between the pair of signal nodes that it joins. Because of the directed property, branch jk indicates that signal k depends in some manner upon signal j but it carries no implication concerning the reverse, direct dependence of j upon k. Because of this directed prop-

* Original manuscript received by the IRE, July 12, 1956. Presented at Session 32, WESCON, San Francisco, Calif; August 26, 1955. Also given before the Long Island Section of the IRE, December 13, 1955.

† Johns Hopkins University, Baltimore 18, Md.

[1] R. W. Sittler, "Systems analysis of discrete Markov processes," IRE TRANS., vol. CT-3, December, 1956.
B. Widrow, "A study of rough amplitude quantization by means of Nyquist sampling theory," IRE TRANS., vol. CT-3; December, 1956.

[2] J. G. Truxal, "Automatic Feedback Control System Synthesis," McGraw-Hill Book Co., Inc., New York, N. Y.; 1955.
J. G. Truxal, "Numerical analysis for network design," IRE TRANS., vol. CT-1, pp. 49–60; September, 1954.

[3] S. J. Mason, "Feedback theory: some properties of signal flow graphs," PROC. IRE, vol. 41, pp. 1144–1156; September, 1953.
S. J. Mason, "Feedback theory—further properties of signal-flow graphs," PROC. IRE, vol. 44, pp. 920–926; July, 1956.

[4] J. K. Percus, "Matrix analysis of oriented graphs with irreducible feedback loops," IRE TRANS., vol. CT-2, pp. 117–127; June, 1955.

[5] D. Konig, "Theorie der Endlichen und Unendlichen Graphen," Chelsea Publishing Co., New York, N. Y.; 1950.

[6] H. M. Trent, "Isomorphisms between oriented linear graphs and lumped physical systems," *J. Acoust. Soc. Amer.*, vol. 27, pp. 500–527; May, 1955.

erty, the topology of signal-flow graphs differs from that of ordinary bilateral networks. This property is a real advantage—whereas ordinary networks must contain equivalent current or voltage generators to represent such unilateral devices as a vacuum tube, no such complication arises when representing a vacuum tube by means of a signal-flow graph. Indeed, since each branch acts like a unilateral amplifier which delivers to its output node a signal component which is related to the signal at its input node, the signal-flow graph is particularly suited for representing active as well as passive systems. Furthermore, Trent has shown in a recent paper[6] that the linear graph preserves the underlying fundamental relationships between the discrete observables of a linear physical system and that it, rather than some equivalent *electrical* circuit, offers the simplest and most direct method of establishing analogies between acoustical, electrical, mechanical, etc., systems.

When the observables represented by the various nodes of the signal-flow graph are related to one another by time-invariant linear operators, the algebraic properties of these operators allow the graph to be transformed into simpler reduced forms. By first taking the Laplace (or z) transform of all observables, one can reduce the integro-differential relationships between the signals in the time domain to simple algebraic relationships in the frequency domain.

To illustrate, Fig. 1 shows the linear graph associated with the set of linear algebraic equations

$$\begin{aligned} x_0 &= x_0 \\ x_1 &= ax_0 + fx_3. \\ x_2 &= bx_1 + cx_2 \\ x_3 &= ex_1 + dx_2. \end{aligned} \tag{1}$$

It is helpful to think of each branch as an amplifier, having the transmittance or amplification specified thereon, and each node as a summation point having a signal value equal to the total flow into that node.

Some of the elementary transformations that may be used to reduce the complexity of a signal-flow graph are illustrated in Fig. 2. The first three transformations follow easily from the fact that the over-all amplification of several amplifiers in cascade is given by the product of the amplifications of the individual amplifiers, and by application of the principle of superposition. The fourth transformation is of fundamental importance to feedback theory. Considering the original graph on the left, we seen that there are an infinite number of transmission paths corresponding to repeated circulations around the closed loop so that the total transmittance is $(1+f+f^2+f^3+\cdots)=1/(1-f)$ times what it would be without the self loop. The transformations are illustrated in Fig. 3 which shows the steps in the reduction of the graph of Fig. 1 to a single branch (characterized by a transmittance which is a rational algebraic function of the original branch transmittances).

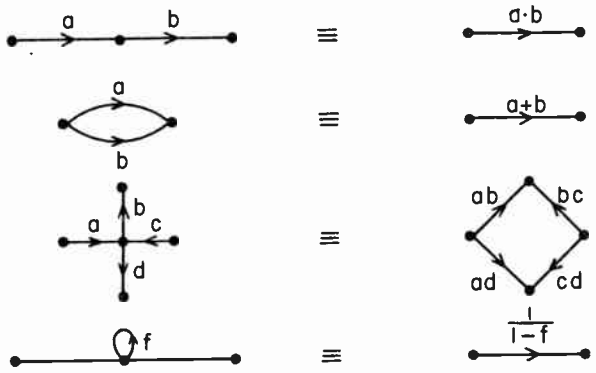

Fig. 2—Elementary transformations.

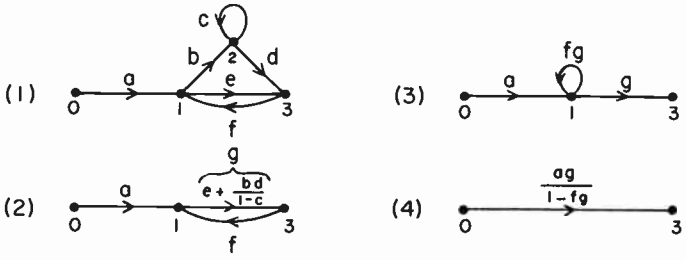

Fig. 3—Steps in the reduction of the flow graph of Fig. 1 to express x_3 in terms of x_0.

Random Signal Generators

We next describe the type of random signal to be considered in the rest of this paper. It is assumed that the signal (or message) is composed of a discrete set of component functions (*i.e.*, waveforms) such as, for example, the dot and the dash of a telegraph message. These component functions are selected according to the various outcomes of an on-going random process. Our task is to relate the statistical specifications of the various events associated with the random process to some of the properties of the message which results.

With reference to Fig. 4, we may consider the component-function generators to be a group of linear circuits each having a unit-impulse response which is identical to the waveform associated with that component. The random process then becomes in effect the equivalent of a trigger generator which, at the instant of occurrence of the event $\mathcal{E}_k$ delivers a unit impulse to the appropriate component function generator $\Delta_k(\tau)$.

The random process is considered to be Markoffian, that is, a mechanism completely characterized by a number of discrete states in which the conditional probability p_{jk} of a transition from any state j to another state k is independent of the history of the system prior to reaching state j. *However, the probability p_{jk} of transition from any state j to another state k is not necessarily a constant in time but may vary with the length of time τ that the system has been in state j.* That is, the probability of transition during the time interval $(\tau, \tau+d\tau)$ may be written in density form as $p_{jk}(\tau)d\tau$. We consider only the simplest case where $p_{jk}(\tau)$ is independent of the absolute

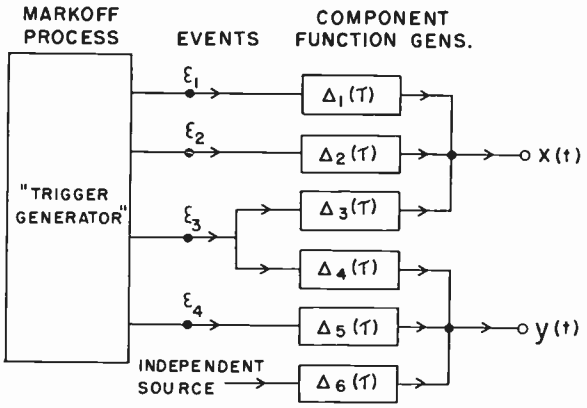

Fig. 4—Random signal generator.

time at which the system entered state j so that the conditional probabilities are *time invariant* even though functions of the *state age* τ. It is apparent that quite complex probability patterns relating the occurrences of the successive events in time are obtainable even with this simplest probabilistic model.

Fig. 4 also indicates how two (or more) separate messages $x(t)$ and $y(t)$ may be generated by the same random process. This multiple-signal problem will, however, not be treated extensively in this paper, although some of the general formulas will be derived.

First Occurrences of Random Processes

We have already defined $p_{jk}(\tau)$ as the probability density of *first* transition out of state j into state k when the system has been in state j for a time τ. Let us now examine the probabilities associated with two or more successive transitions, such as the transition from state *0* thru *1* to *2* as indicated in Fig. 5(a).

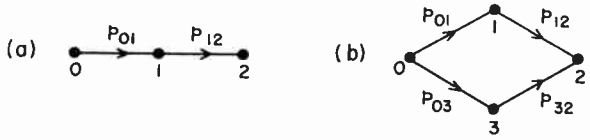

Fig. 5—Pertaining to first transitions from states *0* to *2*.

Assuming that the system entered state *0* at $\tau=0$, the probability density of it reaching state *2*, *via* state *1*, at some subsequent time τ is

$$p_{02}(\tau) = \int p_{01}(\tau_1)p_{12}(\tau - \tau_1)d\tau_1 \qquad (2)$$

$$= p_{01} * p_{12}$$

which is the probability density associated with the *sum* of the two independent, randomly-distributed transition times.

If the system can reach state *2* from state *0 via* two (or more) mutually exclusive paths, as in Fig. 5(b), the resulting probability density is the sum of the probability densities associated with each path, *viz.*:

$$p_{02}(\tau) = (p_{01} * p_{12}) + (p_{03} * p_{32})$$

$$= p_{02,\bar{3}} + p_{02,\bar{1}}. \qquad (3)$$

The relations (2) and (3) require convolution of the probability densities. Since these densities must all vanish for negative time (*i.e.*, for $\tau<0$), their Laplace transform

$$\mathfrak{L}[p_{jk}(\tau)] \triangleq P_{jk}(s) \qquad (4)$$

exists and may be introduced to replace the operation of convolution by that of simple multiplication, *viz.*:

$$P_{02}(s) = P_{01}(s)\cdot P_{12}(s) \qquad (2a)$$

or

$$P_{02}(s) = P_{01}(s)P_{12}(s) + P_{03}(s)P_{32}(s). \qquad (3a)$$

In statistical theory, $P_{jk}(-j\omega)$ is called the *characteristic function* of $p_{jk}(\tau)$. However, following the common practice of treating time and frequency domain representations as equivalent, we shall refer to *either* $p_{jk}(\tau)$ or $P_{jk}(s)$ as "the transitional probability from state j to k" since the domain of the representation will ordinarily be clear from the usage and no ambiguity will result.

The Laplace-transform representation $P(s)$ of a probability density $p(\tau)$ may be expanded in a power series about $s=0$ to yield the well-known relations between the *time moments* of $p(\tau)$ and the coefficients of the power series

$$P(s) = a_0 + a_1 s + a_2 s^2 + \cdots$$

where

$$a_0 = \int p(\tau)d\tau = P(0)$$

$$a_1 = \int -\tau p(\tau)d\tau = P'(0)$$

$$2a_2 = \int \tau^2 p(\tau)d\tau = P''(0) \qquad (5)$$

etc.

Hence,

a_0 is the probability of transition at any time;

$-a_1/a_0$ is the mean (average) time delay before transition;

$\dfrac{2a_2}{a_0} - \left(\dfrac{a_1}{a_0}\right)^2$ is the variance (or mean-square fluctuation about the mean delay) of the transition time.

First Example

To illustrate the above formulation with a very simple random process, let us consider the random event

$\mathcal{E}_1$: *Obtaining a head (H) for the first time on the* n*'th toss of a coin.*

Assume that the coin is unbiased and is tossed every T seconds. This process has two states, T and H. The transition probabilities, $p_{TT}(\tau)=\frac{1}{2}\delta(\tau-T)=p_{TH}(\tau)$ are represented in the transform domain by

$$P_{TH} = P_{TT} = \tfrac{1}{2}e^{-sT} = x/2 \tag{6}$$

where $x=\exp(-sT)$.

The linear graph of this process is shown in Fig. 6 (a). It consists of the two "state" nodes T and H and a "start" node to which a unit impulse is assumed to be applied at $t=0$. The transmittances from this "start" node to each of the "state" nodes represent the initial probability densities of the first occurrence of each state subsequent to the beginning epoch at $t=0$. These probabilities may be equal, as in the present example, or may be assigned different values both in *magnitude* and in *time* of first occurrence. When many of the transitional probabilities are alike it is sometimes possible to reduce immediately the graph by combining the "start" node with one of the "state" nodes. Thus, insofar as the occurrence of the event $\mathcal{E}_1$ is concerned, the occurrence of a tail is equivalent to starting anew, and the graph of Fig. 6 (a) may be replaced with the simpler graph of Fig. 6 (b). Although this simplification will be used whenever applicable in the examples given subsequently, the most general formulation should incorporate a "start" node that is distinct from the other state nodes of the graph in order to accommodate any arbitrary distribution of initial-state probabilities. This general graph may always be reduced and superfluous nodes eliminated by the usual flow-graph reduction techniques.[3]

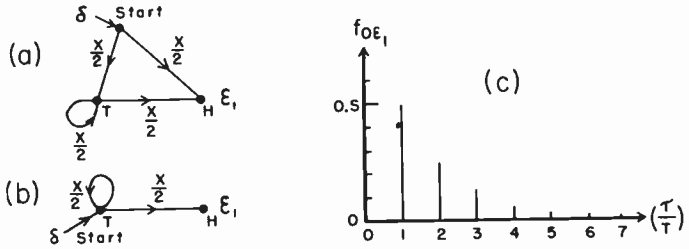

Fig. 6—(a) Flow-graph for the probability of obtaining a head H for the first time on the n'th toss of a coin. (b) Simplified graph, equivalent to (a) in its response at $\mathcal{E}_1$. (c) Probability distribution of this event.

In a private communication, L. A. Zadeh has remarked that it may be helpful in setting up the graph to note that a path from the starting node to any node in the graph corresponds to a sequence of events identified with the nodes through which the path passes. If all transmittances are equal to, say, g, then the probability of the occurrence of the event associated with the sink on the n'th trial is equal to g^n times the number of paths of length n. Every path from the starting node to the sink should correspond to an event which implies the event associated with the sink (*i.e.*, $\mathcal{E}_1$, say). The necessary and sufficient condition for the validity of a graph is that the totality of all simple events which imply the event of interest should correspond to the totality of all paths from the starting node to the sink.

Now, the actual random process results in a series of discrete random events. However, if we are only interested in *what will happen on the average over a great many similar trials*, we may consider that at time T an impulse of value $\frac{1}{2}$ is delivered to node H, and a similar impulse is delivered to node T. It is clear that this assumption will lead to the same average value (or expectation) as obtained with the actual random process. That is, to calculate the probability of a compound event, composed of statistically independent atomic events, we may replace the random atomic events by their probabilities (or expectations). Thus, we may write directly the probability of the first occurrence of $\mathcal{E}_1$

$$F_{0\mathcal{E}_1}(s) = \frac{x/2}{1-x/2} = \frac{x}{2-x} \tag{6a}$$

$$= \frac{1}{2}x + \frac{1}{4}x^2 + \frac{1}{8}x^3 + \cdots \tag{6b}$$

where (6b) is obtained by long-division of the middle expression of (6a). Upon transforming this back into the time domain, we see that the probability of a head occurring on the first toss is $\frac{1}{2}$ and on the n'th toss is $\frac{1}{2}^n$. Thus, the coefficients of the power series expansion (6b) give us directly the desired probabilities of the occurrence of the event $\mathcal{E}_1$ as a series of discrete impulses whose values are plotted in Fig. 6(b).

With reference to (5) *et sequens*, we note that $s=0$ corresponds to $x=1$; hence, the total probability of first occurrence at *any* time is

$$F_{0\mathcal{E}_1}(0) = 1 \tag{6c}$$

and we may conclude that *the event* $\mathcal{E}_1$ *is certain.*[7] To estimate the mean occurrence time, we substitute the power-series expansion,

$$x = \exp(-sT)$$
$$= 1 - sT + (sT)^2/2! + (sT)^3/3! + \cdots,$$

in

$$\frac{x}{2-x} = \frac{1 - sT + (sT)^2/2! + \cdots}{1 + sT - (sT)^2/2! - \cdots}$$
$$= 1 - 2Ts + 3T^2s^2 - \cdots \tag{6d}$$

and find that

mean occurrence time, $(-a_1/a_0)$, is $\cdots 2T$,

variance, $(6T^2 - 4T^2)$, is $\cdots 2T^2$.

For an excellent, readable, and thorough discussion of generating functions and discrete Markoff processes, the reader is referred to the reference given in footnote 7 which also discusses in detail, but without the aid of

[7] W. Feller, "An Introduction to Probability Theory and its Applications," John Wiley and Sons, Inc., New York, N. Y.; 1950; chs. 11, 12, and 13, particularly.

linear graphs, this and several of the other examples to be given subsequently. A comparison of the derivation of the results of examples three and four, particularly, will show the usefulness of the linear graph in formulating the correct generating expressions for the desired probability distributions.

Second Example

Let us consider next the event

$\mathcal{E}_2$: *Obtaining the third head on the* n*'th toss of a coin.*

The event $\mathcal{E}_2$ results when three successive events $\mathcal{E}_1$ have occurred. Thus, the process may be represented by three graphs, all identical to that shown in Fig. 6, connected in cascade so that the output of one (*i.e.*, the occurrence of $\mathcal{E}_1$) serves as the input of the next (*i.e.*, initiates the *next* occurrence of $\mathcal{E}_1$), as illustrated in Fig. 7. It should be noted that each possible path from the first node to the sink $\mathcal{E}_2$ corresponds to some possible sequence of tails and heads culminating in the final occurrence of three heads.

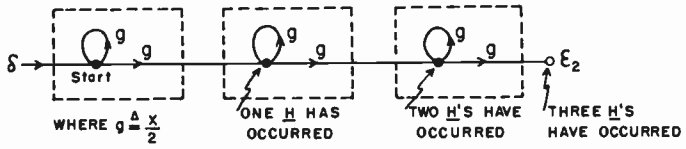

Fig. 7—Flow graph for the probability of obtaining the third head on the *n*'th toss of a coin.

The probability of first occurrence of $\mathcal{E}_2$ is, therefore,

$$F_{0\epsilon_2} = \left[\frac{x}{2-x}\right]^3 \tag{7}$$

$$= \frac{x^3}{8 - 12x + 6x^2 - x^3} \tag{7a}$$

$$= \left\{\underline{0}, 0, 0, \frac{1}{8}, \frac{3}{16}, \frac{3}{16}, \frac{5}{32}, \frac{15}{128}, \cdots\right\} \tag{7b}$$

where we have followed, in writing (7b), the time-series convention of indicating only the coefficients of the power series development of x (the coefficient of x^0 is underlined).[8,9]

The n'th coefficient ($n>2$), in this expansion for the probability distribution of the occurrence of the event $\mathcal{E}_2$, is found to be

$$p_n = (n-1)(n-2)(1/2)^{n+1}. \tag{7c}$$

By substitution of $x = 1 - sT + (sT)^2/2 - \cdots$ into (7a) one obtains a power series in s and finds that

$$F_{0\epsilon_2} = 1 - 6Ts + 21T^2s^2 - \cdots \tag{7d}$$

from which we may conclude that

$\mathcal{E}_2$ is a "certain" event,

mean occurrence time is $\cdots\cdots\cdots 6T$,

variance of the occurrence time is $\cdots 6T^2$.

Third Example

It is instructive to compare the event $\mathcal{E}_2$ just considered with the event

$\mathcal{E}_3$: *Obtaining the run HHH for the first time on the* n*'th toss.*

Here, the system is either on its way toward achieving the run or it is just starting, as it must following the occurrence of a *tail*. Hence, the "start" state and the "tail" state are identical, and the signal-flow graph appears as shown in Fig. 8.

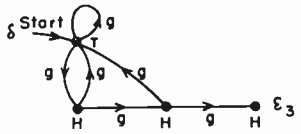

Fig. 8—Flow graph for the probability of obtaining the run *HHH* for the first time on the *n*'th toss.

The transmittance from the start node to the output node $\mathcal{E}_3$ is found by routine reduction of the graph to be

$$F_0\mathcal{E}_3 = \frac{x^3}{8 - 4x - 2x^2 - x^3} \tag{8}$$

$$= \frac{1 - 3sT - 9(sT)^2/2 + \cdots}{1 + 11sT - 33(sT)^2/4 + \cdots} \tag{8a}$$

$$= 1 - 14sT + \frac{667}{4}(sT)^2 + \cdots \tag{8b}$$

from which we conclude that

$\mathcal{E}_3$ is a certain event,

mean occurrence time, $\cdots\cdots\cdots 14T$,

variance of occurrence time $\cdots (11.9T)^2$.

To obtain the actual probabilities, we divide numerator by denominator of (8) to obtain a power series in x whose coefficients are the probabilities

$$p_n = \frac{1}{8}\left[\underline{0}, 0, 0, 1, \frac{1}{2}, \frac{1}{2}, \frac{1}{2}, \frac{7}{16}, \cdots,\right]. \tag{8c}$$

The probabilities for large n may be found most readily by making a partial-fraction expansion of (8) and evaluating only the transient term which decays most slowly (that is, the term whose singularity is nearest to the unit circle in the complex-x plane, or nearest the $j\omega$ axis in the complex-s plane). The denominator of (8) has a single real zero at $x_1 = 1.087$ and pair a of complex roots whose moduli are larger, $|x_{2,3}| = 2.71$. Hence, the contribution to p_n for large n will arise almost entirely from the first term of the partial-fraction expansion

[8] W. E. Thomson, "A theory of time series for waveform-transmission systems," *Proc. IEE*, vol. 99, part IV, pp. 397–409; December, 1952.

[9] N. W. Lewis, "Waveform computations by time-series method," *Proc. IEE*, vol. 99, part III, pp. 294–306; September, 1952.

$$\frac{x^3}{8 - 4x - 2x^2 - x^3} = \frac{0.108}{1.087 - x} + \frac{N(x)}{7.36 + 3.087x + x^2}$$

so that

$$p_n \doteq 0.108\left[\frac{1}{1.087}\right]^{n+1}. \tag{8d}$$

This approximation is surprisingly good—the value of p_n for $n=7$ is found from (8c) to be $\frac{1}{8}[\frac{7}{8}]=0.0546$, whereas (8d) gives $p_7=0.055$. Thus, the familiar procedure in transient analysis of ignoring the short-lived transients in finding the long-time behavior is useful here in estimating the ultimate decay-to-zero of a probability distribution.

Fourth Example: Mutually Exclusive Events

The method may also be applied to find the probability that a given event will occur for the first time before a second specified event has occurred. As an example, consider

$\mathcal{E}_{3,\bar{4}}$: *Obtaining the run HHH for the first time before the run HTH has occurred.*

The flow graph for this event is shown in Fig. 9. The events $\mathcal{E}_{3,\bar{4}}$ (*i.e.*, *HHH* before *HTH*) and $\mathcal{E}_{4,\bar{3}}$ (*i.e.*, *HTH* before *HHH*) are mutually exclusively, since the two states representing these events are both sinks (*i.e.*, the process terminates with the occurrence of either event), and the "probability flow" into one event is "absorbed" and kept from reaching the other. (It follows that any number of mutually exclusive events may be represented in a similar manner.)

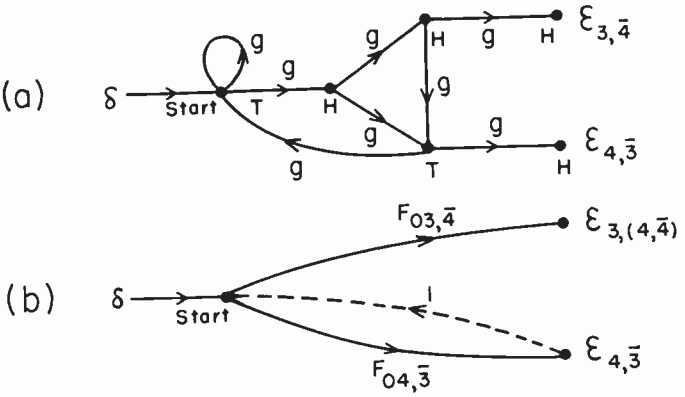

Fig. 9—(a) Flow graph for the probability of obtaining the run *HHH* before the run *HTH* has occurred, (b) of obtaining the run *HHH* for the first time with all *H*'s belonging to any sequence *HTH* discounted.

The probabilities of first occurrence of these two events are found by evaluating the transmittances from the start node to the two output nodes, again using standard signal-flow graph reduction operations

$$F_{03,\bar{4}} = \frac{2x^3}{16 - 8x - 2x^3 - x^4} \tag{9a}$$

$$F_{04,\bar{3}} = \frac{2x^3 + x^4}{16 - 8x - 2x^3 - x^4}. \tag{9b}$$

Since $F_{03,\bar{4}}(0)=2/5$ and $F_{04,\bar{3}}(0)=3/5$, we see that neither event is certain, although the occurrence of one *or* the other is certain.

Starting with the probability expressions (9a) and (9b) we may derive other probability distributions which are of interest. For instance, the probability of the first occurrence of *either HHH* or *HTH* is

$$F_{03,\bar{4}} + F_{04,\bar{3}} = \frac{4x^3 + x^4}{16 - 8x - 2x^3 - x^4} \tag{9c}$$

and is a "certain" event, as already noted.

Also, we may find the probability of first occurrence of one event with the condition that the second event may have occurred one or more times already. That is, let us find the probability of first occurrence of $\mathcal{E}_{3,(\bar{4},\bar{4})}$ (*i.e.*, *HHH*) under the condition that the event $\epsilon_{4,\bar{3}}$ (*i.e. HTH* before *HHH*) may have occurred one or more times. The flow diagram for this event is obtained by connecting the output node $\mathcal{E}_{4,\bar{3}}$ of Fig. 9(a) to the start node as shown in Fig. 9(b). The resulting probability expression is thus found to be

$$F_{03,(\bar{4},\bar{4})} = \frac{F_{03,\bar{4}}}{1 - F_{04,\bar{3}}} = \frac{x^3}{8 - 4x - 2x^3 - x^4}. \tag{9d}$$

At first glance, this expression may be mistaken for the probability of occurrence of the event $\mathcal{E}_3$ (*i.e.*, *HHH*) given by (8). However, careful examination will show that the denominators of the two expressions are different. The reason that the two probabilities are different is that, by convention, *a given state arising in a particular sequence can only be associated with one event at a time.* For instance, with the occurrence of the event *HTH*, the last head must be associated with the event $\mathcal{E}_{4,\bar{3}}$ and cannot be used again in a subsequent occurrence of the event $\epsilon_{3,(\bar{4},\bar{4})}$. Thus, the sequence *HTHHH* contains the event $\mathcal{E}_{4,\bar{3}}$ but not the event $\mathcal{E}_{3,(\bar{4},\bar{4})}$—whereas the sequence *HTHHHH* contains both events.[10]

Recurrent Events

In the previous section, we have illustrated the use of the flow graph for obtaining expressions for the probability of first occurrences of some specified event. This probability was represented in the frequency domain by the function $F(s)$. We now consider the representation of recurrent events in which, with each occurrence, the process may be regarded as starting anew.

To represent a recurrent event, the graph for the first occurrence is modified simply by connecting the "event"

[10] In order to obtain (8) from the diagram of Fig. 9(a), the event node $\mathcal{E}_{4,\bar{3}}$ should be connected to the first *H* node following the start node, rather than to the start node itself.

node to the "start" node, as shown in Fig. 10.

Fig. 10—Closing the feedback loop produces a recurrent process from the single-event diagram.

The "response" at the node $\mathcal{E}$ representing the recurrent event is then

$$U(s) = \frac{1}{1 - F(s)} = 1 + F(s) + F^2(s) + F^3(s) + \cdots \qquad (10)$$

and the terms in the power-series expression indicate that the event certainly occurred at $t=0$ (by hypothesis, a unit impulse of "probability" was applied at that time); the term $F(s)$ gives the probability of the first occurrence of the event at any subsequent time; $F^2(s)$ gives the probability of the second occurrence of the event at any subsequent time; $F^3(s)$, the probability of third occurrence, etc. The quantity $U(s)$, however, is not a probability density since $U(0)$ no longer has an upper bound of 1, and is, in fact, infinite for a "certain" first occurrence. There appears to be no standard name for a quantity such as $u(t)$ which is the sum of an infinite number of probability densities. In order to avoid confusion with proper probability densities, we shall refer to $U(s)$ and its corresponding time representation $u(t) = \mathcal{L}^{-1}[U(s)]$ as an *expectation-density* of occurrence since:

> The expected number of occurrences of the event within the time interval $(\tau, \tau+d\tau)$ following a known occurrence at $\tau=0$, is given by $u(\tau)d\tau$.[11]

For ergodic processes, which are stationary under translation in time, it is necessary that $u(\tau)$ approach a constant as $\tau \to \infty$. This constant is the *steady-state expectation of occurrence* of the recurrent event. It has the dimensions of (events per unit time) and its numerical value may be found by evaluating the dc component in inverse transform of $U(s)$

$$p_\epsilon = \text{Res. } U(s)\Big|_{s=0} = \frac{1}{-F'(0)}. \qquad (10a)$$

In the case of a periodic process, such as that associated with a sampled-data system, $u(\tau)$ approaches a sequence of impulses of constant magnitude. The magnitude of these impulses in the limit is usually referred to as the *steady-state probability* of the recurrent event.

[11] The integral $\int_a^b u(\tau)d\tau$ apparently has the following significance: Let us conduct N experiments, each of which consists of starting the recurrent process at $\tau=0$ and observing the epochs of first, second, third, etc., subsequent occurrences. The expected number of events observed in the interval $a<\tau<b$ for N experiments would then be $N\int_a^b u(\tau)d\tau$. Hence, $u(\tau)$ is the expectation-density of occurrence at time τ per occurrence at $\tau=0$.

For an ergodic process, $U(s)$ will always have a simple pole at $s=0$, and the steady-state expectation of occurrence is the residue at that pole. Periodic processes will, in general, have other poles along the $j\omega$ axis in the s plane (or upon the unit circle in the x plane), and these give rise to line spectra, as we shall see later. It may be noted that a pole at $s=0$ implies that $F(0)=1$, so the first occurrence of the event is always certain.

More generally, consider a complicated Markoff process having many states, some of which are shown in Fig. 11(a). We are concerned here with the relationship between two particular states j and k. By the usual reduction methods, all other nodes may be eliminated to obtain the graph of Fig. 11(b), for which $F_{jk}(s)$ is the probability of first occurrence of k, state j having just occurred at $\tau=0$, and is found by making node k into a *sink* and applying a unit impulse to node j at $\tau=0$. Similarly, F_{kk} is the self-return to node k and is found in a similar manner. In terms of these two probabilities of *first* occurrence, the *expectation* of an occurrence of state k following a known occurrence of state j at $\tau=0$ is simply

$$U_{jk} = \frac{F_{jk}}{1 - F_{kk}} + \delta_{jk} \qquad (10b)$$

where δ_{jk} is kronecker's delta and represents the certain occurrence at $\tau=0$ when $j=k$.

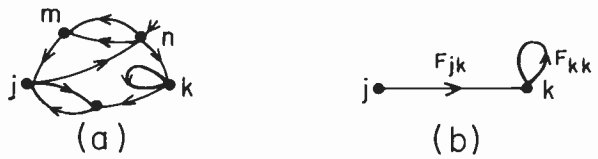

Fig. 11—(a) Illustrating the determination of the expectation of state k, subsequent to an occurrence of stage j, (b) reduced graph showing probabilities of first occurrence, and of first *re*currence, of state k.

It is seen that U_{jk} is simply the "response" at the k'th node to a unit impulse "applied" at $\tau=0$ to the j'th node. In other words, *expectations behave just like signals and may be computed in exactly the same way.*

Fifth Example—Poisson's Process

As a very simple application of (10b), let us consider the inverse problem of finding the probability of first occurrence, given the expectation. Suppose that we have a process in which the expectation of the event in question is a constant λ independent of τ for $\tau \neq 0$, *viz.*,

$$u(\tau) = \lambda + \delta(\tau). \qquad (11)$$

What is the probability of the first recurrence of the event after a known occurrence at $\tau=0$?

Here

$$U(s) = \frac{\lambda}{s} + 1 = \frac{s+\lambda}{s}. \qquad (11a)$$

But from (10),

$$F(s) = 1 - \frac{1}{U(s)} \tag{12}$$

$$= 1 - \frac{s}{s+\lambda} = \frac{\lambda}{s+\lambda} \tag{13}$$

and the probability density of the time intervals between successive occurrences of the event is

$$f(\tau) = \mathcal{L}^{-1}[F(s)]$$
$$= \lambda e^{-\lambda\tau}. \tag{14a}$$

Similarly, the probability density for the distribution of the time intervals between two successive (*i.e.*, alternate) occurrences is, by analogy, with the second example,

$$\mathcal{L}^{-1}\left[\frac{\lambda}{s+\lambda}\right]^2 = \lambda(\lambda\tau)e^{\lambda\tau} \tag{14b}$$

and the probability density of the random time intervals for exactly K occurrences is

$$\mathcal{L}^{-1}\left[\frac{\lambda}{s+\lambda}\right]^K = \lambda\frac{(\lambda\tau)^{K-1}}{(K-1)!}e^{-\lambda\tau}. \tag{14c}$$

This is one form of the well-known Poisson distribution. [The extra λ enters because this is the probability density of the occurrence of the K'th event which is equal to the probability of exactly $K-1$ events, occurring in the interval 0 to τ, multiplied by the probability $\lambda d\tau$ of another occurrence (*i.e.*, the K'th occurrence), in the interval $(\tau, \tau+d\tau)$.]

Before closing this section, it should be remarked that more complicated events may be formulated in a manner analogous to the examples of first-occurrences already given. For example, with reference to the process indicated by Fig. 11, the expectation for the recurrence of state k following a known occurrence of state j at $\tau=0$ *with the additional condition that states m and n have not yet occurred*, would be given by

$$U_{jk,\overline{mn}} = \frac{F_{jk,\overline{mn}}}{1 - F_{kk,\overline{mn}}} + \delta_{jk} \tag{10c}$$

and $F_{jk,\overline{mn}}$ and $F_{kk,\overline{mn}}$ would be found from the graph of Fig. 11(a), by first "killing" all flow thru the states m and n (*i.e.*, m and n are made into sinks, thus removing any probability of their occurrence before the recurrence of state k).

Correlation Functions and Power Spectra

Here, we use the methods elaborated above as a systematic procedure for determining the correlation functions and power spectra associated with the signals arising from a random process of the type by Fig. 4.

The correlation function between two random signals $x(t)$ and $y(t)$ may be defined as an ensemble average, which for ergodic signals is the same as the time average, of the displaced product

$$\phi_{xy}(\tau) = \overline{x(t)y(t+\tau)}$$
$$= \int\int xyW(x, y; \tau)dxdy. \tag{15}$$

It is convenient to replace the joint probability $W(x, y; \tau)$ by the product $p(x)\cdot W_x(y; \tau)$, where $W_x(y; \tau)$ is the conditional probability of y at time τ, given x at time $\tau=0$. Then

$$\phi_{xy}(\tau) = \int p(x)x\bar{y}_x(\tau)dx, \tag{16}$$

where

$$\bar{y}_x(\tau) = \int yW_x(y; \tau)dy$$

is the conditional expectation of y at time τ, given x at time zero. That is, the correlation function may be decomposed into a (perhaps, infinitesimal) contribution associated with each value of x, *e.g.*, $xdx\bar{y}_x(\tau)$. Addition of contributions from all x, in proportion to the probability density $p(x)$ of x, yields the correlation function (16).

Instead of regarding x as a particular *value* of the first signal, we may consider x to be one of the particular *component* functions $x_j(\tau)=\Delta_j(\tau)$ which comprise the first signal. The contribution of this j'th component to the correlation function would then be

$$p_j\int x_j(t)\bar{y}_j(t+\tau)d\tau \tag{17}$$

where $\bar{y}_j(t)$ is the expectation, or average, over-all possible signals y that may follow a given $x_j(t)$, and p_j is the steady-state probability of occurrence of $x_j(t)$. To show that this is so, we start with the representation of $x(t)$ in terms of its components,

$$x(t) = \sum_j \sum_k \Delta_j(t - t_{j,k})$$

where the $t_{j,k}$ is the epoch of the k'th occurrence of the j'th component. Then, the correlation between $x(t)$ and the signal $y(t)$ may be written as

$$\phi_{xy}(\tau) = \lim_{T\to\infty}\frac{1}{T}\int_0^T x(t)y(t+\tau)dt$$
$$= \lim_{T\to\infty}\frac{1}{T}\int_0^\Delta \sum_j \Delta_j(t)\sum_{0\leq t_k\leq T} y(t + t_{j,k} + \tau)dt$$
$$= \sum_j \int_{-\infty}^{\infty}\Delta_j(t)\lim_{T\to\infty}\frac{1}{T}\sum_{t_k=0}^{t_k\leq T} y(t + t_{j,k} + \tau)dt.$$

where in the last expression the integration over the finite duration, 0 to Δ, of each component function has been written with infinite limits. As $T\to\infty$, new $t_{j,k}$'s are added at an *average* rate of p_j components per second (this is the steady-state expectation of the occurrence of the event j previously described), and hence the limit may be written

$$\lim_{T\to\infty}\frac{1}{T}\sum_{t_k=0}^{t_k\leq T} y(t+t_{j,k}+\tau)=p_j\bar{y}_j(t+\tau)$$

thus defining $\bar{y}_j(t)$ as the expectation of y, t seconds after the occurrence of $\Delta_j(t)$. In terms of this average message, the correlation function may be written as

$$\phi_{xy}(\tau)=\sum_j p_j\int_{-\infty}^{\infty}\Delta_j(t)\bar{y}_j(t+\tau)dt \tag{17a}$$

which confirms (17).

The above relations may be expressed more simply in the frequency domain, where the correlation of two real time functions (which vanish for negative time) may be written as the product of their transforms, provided the sign of s is changed in the first, *viz.*

If

$$\phi_{12}(\tau)=\int_{-\infty}^{\infty}f_1(t)f_2(t+\tau)dt$$

then

$$\Phi_{12}(s)=F_1(-s)F_2(s). \tag{18}$$

Since $x_j(\tau)$ and $\bar{y}_j(\tau)$ both vanish for negative τ, we have as the equivalent of (17) for the frequency domain

$$p_jX_j(-s)\overline{Y}_j(s) \tag{19}$$

and the transform of the correlation function for $\tau>0$[12] will be

$$\Phi_{xy}(s)=\sum_j p_jX_j(-s)\overline{Y}_j(s). \tag{20}$$

In order to obtain an expression for the correlation function over the domain of $\tau<0$, we note that

$$\phi_{xy}(\tau)=\phi_{xy}(-\tau). \tag{21}$$

Hence, *by reversing the roles of x and y in the above equations, we may obtain the other half of the correlation function.* That is, we consider each component $\Delta_k(\tau)=y_k(\tau)$ comprising the $y(t)$ signal, and correlate each component with the average or expected value $\bar{x}_k(\tau)$ following the occurrence of each $y_k(\tau)$ symbol. This gives instead of (20)

$$\Phi_{yx}(s)=\sum_k p_kY_k(-s)\,\overline{X}_k(s). \tag{22}$$

Eqs. (20), (21), and (22) describe the correlation function for *all* τ.

We must now develop a systematic method of finding the average or expected message $\overline{Y}_k(s)$ that follows the occurrence of a symbol $X_k(s)=\Delta_k(s)$. Each of these symbols is associated with a particular state of a Markoff process shown in Fig. 4. We have already obtained in (10) a representation for the expected occurrence of the k'th state on the condition that the j'th state occurred at $\tau=0$. The expected signal following the occurrence of the j'th symbol is, therefore,

$$\overline{Y}_j(s)=\sum_k U_{jk}(s)\Delta_k(s) \tag{23a}$$

where the index k ranges over all symbols appearing in $y(t)$, and the index j ranges over all symbols appearing in $x(t)$. Similarly,

$$\overline{X}_k(s)=\sum_j U_{kj}(s)\Delta_j(s). \tag{23b}$$

These formal expressions state a very simple relationship when interpreted in terms of the signal-flow graph:

The expected (i.e., averaged) messages $\bar{x}(t)$ and $\bar{y}(t)$ following the occurrence of a particular symbol, say $\Delta_1(\tau)$, are simply the responses of the total graph of Fig. 4 (Markoff process plus component-function generators) at the terminals marked X and Y, respectively, when a unit impulse is applied to state node $\mathcal{E}_1$.

Thus, the expressions for $\overline{Y}_j(s)$ and $\overline{X}_k(s)$ may be obtained directly from the signal-flow graph without the necessity for the explicit adding up of the contributions of the various symbols, as is done in (23).

We have thus found two closed expressions, the first (20) representing the correlation function $\phi_{xy}(\tau)$ over the range $\tau>0$, and the second (22), representing the function $\phi_{yx}(\tau)$ over the *same* range $\tau>0$. If the correlation function does not contain periodic components and belongs to class L_2 these two solutions may be pieced together to form a single Fourier transform $\Psi_{xy}(j\omega)$ of $\phi_{xy}(\tau)$ valid over the entire domain $-j\infty<j\omega<j\infty$. Some tailoring is ordinarily required in piecing the two functions together because, in general, the inverse transform of $\Phi_{xy}(s)$, which yields the exact value of $\phi_{xy}(\tau)$ for τ positive, will *not* vanish *nor* be equal to $\phi_{xy}(\tau)$ for all *negative* τ.

The reason that the inverse transform of $\Phi_{xy}(s)$ does not vanish for small negative τ is that the component function $\Delta(-\tau)$ (or, $\Delta(-s)$ in the frequency domain), which is associated with the factor $F_1(-s)$ in (18), extends slightly into the negative time region. A separate computation is usually required to determine the correlation function for $\tau<0$ because we have considered only transitions in the forward-time direction. This complication would not have arisen had we been able to find the expected $\bar{y}(\tau)$ that both *precedes* and *follows* the occurrence of a given x_j symbol. Instead, we treat the *backward* process as a separate problem by finding $\phi_{yx}(\tau)$ for positive τ and then join together these two solutions, taking care to eliminate the negative-τ artifact which will usually be associated with each solution. We summarize the steps in finding the Fourier Spectra as follows:

Let the Laplace transform of the negative-τ artifact be designated by $\Phi_{xy}^{-}(s)$ so that

$$\Phi_{xy}^{+}(s)=\Phi_{xy}(s)-\Phi_{xy}^{-}(s)$$

[12] The correlation function is defined by this expression only for $\tau>0$ because of the restrictions placed on $F_2(s)$ by (18) and the fact that only *forward* expectations and transition probabilities in time are used.

is the Laplace transform of a time function which is identical to $\phi_{xy}(\tau)$ for $\tau>0$ and which *vanishes* for all $\tau<0$. Define $\Phi_{yx}^{+}(s)$ in the same way. Then, the Fourier transform of the entire random part of the correlation function $\phi_{xy}(\tau)$, for $-\infty<\tau<\infty$, will be given by

$$\Psi_{xy}(j\omega) = \Phi_{xy}^{+}(s) + \Phi_{yx}^{+}(-s), \quad s = j\omega. \tag{24}$$

This Fourier transform is known as the *cross-spectrum.* It is of interest that any periodic components which may be present in $\phi_{xy}(\tau)$ and $\phi_{yx}(\tau)$ are suppressed in evaluating equation (24) so that it gives only the *continuous part* of the spectrum. The *discrete part* of the spectrum may be found by direct evaluation of the residues of $\Phi_{xy}(s)$ [or $\Phi_{yx}(s)$] at the associated singularities along the $j\omega$ axis, since, if the component is periodic, specification of the component in the interval $\tau>0$ will suffice to specify the component in the interval $\tau<0$.

The above relationships for finding cross-correlations simplify slightly for finding the autocorrelation function of a signal with itself. We let $y(t)=x(t)$ and combine (20) and (23) to obtain

$$\Phi_{xx}(s) = \sum p_j\Delta_j(-s)\overline{X}_j(s) \tag{25}$$

where

$$\overline{X}_j(s) = \sum_k U_{jk}(s)\Delta_k(s) \tag{25a}$$

and the summations range over all component functions. The power spectrum is then, simply,

$$\Psi_{xx}(j\omega) = \Phi_{xx}^{+}(s) + \Phi_{xx}^{+}(-s) \tag{26a}$$

$$= \Phi_{xx}(s) + \Phi_{xx}(-s) - \Phi_{xx}^{-}(s) - \Phi_{xx}^{-}(-s), \tag{26b}$$

the second form being often the most convenient, provided the artifact corrections can be identified in the original expression.

Sixth Example—Random Telegraph Message

We illustrate the use of the above equations by finding the power spectrum associated with a random telegraph message that consists entirely of dots and dashes which occur with equal frequency on the average. Each occurrence is assumed to be statistically independent of previous occurrences. Each dot has a unit amplitude for a duration of T seconds and is followed by a space of duration $2T$. Each dash has a unit amplitude for a duration of $2T$ seconds and is also followed by a space of duration $2T$.

The flow-graph representation for this telegraph message is shown in Fig. 12. Node *1* corresponds to the dot "trigger" and note *2* to the dash "trigger." From the specification of the message given above, it follows that the occurrence of a dot at $\tau=0$ will be followed with a probability 1/2 by either a dot or a dash, beginning $3T$ seconds later, hence, the two transmittances $x^3/2$ emitting from node *1*. Similarly, with the occurrence of a dash, the next dot or dash will occur $4T$ seconds later,

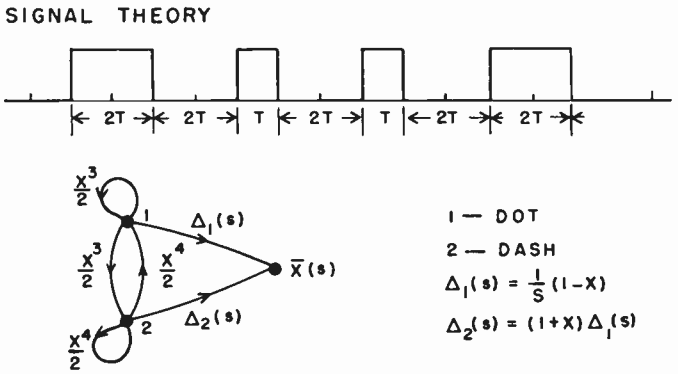

Fig. 12—Flow graph for a random telegraph message.

as represented by the transmittances $x^4/2$ emitting from node *2*. The shaping functions, which convert the impulses appearing at the nodes *1* and *2* into symbol waveforms at the message terminal $\overline{X}(s)$, are simply the Laplace transforms of the dot and dash, or

$$\Delta_1(s) = \frac{1}{s}(1-x)$$

$$\Delta_2(s) = (1+x)\Delta_1(s). \tag{27}$$

The expectations of the occurrence of a dot or a dash following the occurrence of a dot or a dash at $\tau=0$ are given by the expressions

$$U_{11} = \frac{2-x^4}{2-x^3-x^4}, \qquad U_{12} = \frac{x^3}{2-x^3-x^4}$$

$$U_{21} = \frac{x^4}{2-x^3-x^4}, \qquad U_{22} = \frac{2-x^3}{2-x^3-x^4} \tag{28}$$

where, it will be recalled from (10b), U_{jk} is simply the response at node k to an impulse applied at node j.

The steady-state expectations of the occurrence of a dot or a dash are found by evaluating the residues of (28) for the pole at $s=0$ (or $x=1$). These residues are found to be *all* equal to $1/7T$. That is, one dot (or one dash) will occur every $7T$ seconds, on the average. As is characteristic of Markoff processes, these probabilities are independent of which state initiated the message.

The average message following the occurrence of a dot is represented by the response at the message node when a unit impulse is applied to the dot node at $\tau=0$, *viz.*,

$$\overline{X}_1(s) = U_{11}\Delta_1 + U_{12}\Delta_2$$

$$= \Delta_1\left[\frac{2+x^3}{2-x^3-x^4}\right]. \tag{29a}$$

Similarly, the average message following the occurrence of a dash is

$$\overline{X}_2(s) = U_{21}\Delta_1 + U_{22}\Delta_2$$

$$= \Delta_1\left[\frac{2+2x-x^3}{2-x^3-x^4}\right]. \tag{29b}$$

From (29a) we may obtain by simple long division the actual average message following a dot, as shown in Fig. 13.

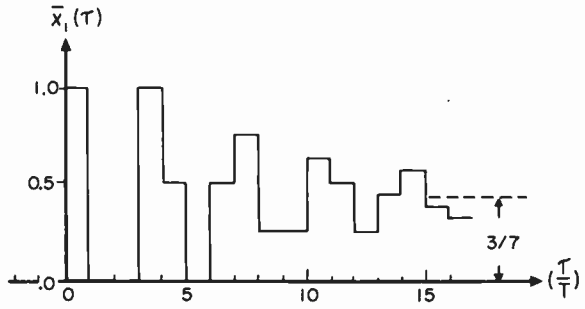

Fig. 13—Expected message following the occurrence of a dot.

$$\bar{X}_1(s) = \Delta_1\left[\underline{1}, 0, 0, 1, \frac{1}{2}, 0, \frac{1}{2}, \frac{3}{4}, \frac{1}{4}, \frac{1}{4}, \frac{5}{8}, \frac{1}{2}, \frac{1}{4}, \frac{7}{16}, \frac{9}{16}, \frac{3}{8}, \frac{11}{32}, \cdots\right].$$

By (25), the autocorrelation function of this telegraph message may be found from the transform

$$\Phi_{xx}(s) = p_1\Delta_1(-s)\bar{X}_1(s) + p_2\Delta_2(-s)\bar{X}_2(s) = \frac{1}{7T}\Delta_1(-s)\Delta_1(s)\left[\frac{2x^{-1} + 6 + 2x - x^2}{2 - x^3 - x^4}\right]. \quad (30)$$

The factor $\Delta_1(-s)\Delta_1(s)$ is recognized as the transform of the autocorrelation function of the dot, which is an isosceles triangle of altitude T and base width $2T$. The bracketed term, when expanded by simple long division, gives directly the amplitudes and delays of these triangular constituents of $\phi_{xx}(\tau)$ as shown in Fig. 14.

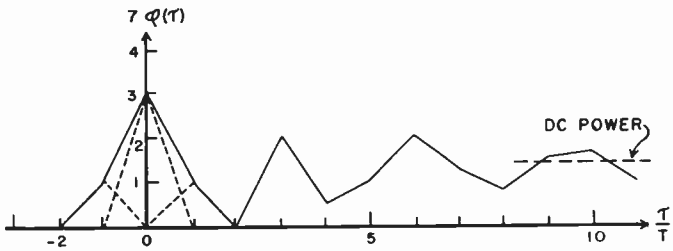

Fig. 14—A plot of the inverse transform of $\Phi_{xx}(s)$ (30) showing the triangular constituents and the negative-τ artifact.

Examination of Fig. 14 shows that in the interval $-2<\tau<0$, the function has nonzero values. This is the artifact which must be removed (or at least, accounted for) in completing the representation of the correlation function for negative τ. The transform of this artifact is

$$7T\Phi_{xx}^{-}(s) = \frac{1}{s^2}\left[x^{-2} + 2x^{-1} - 3\right] - \frac{3}{s}. \quad (31)$$

But, by symmetry, we may also write

$$\Phi_{xx}^{-}(s) + \Phi_{xx}^{-}(-s) = \frac{1}{7T}\Delta_1(-s)\Delta_1(s)\left[x^{-1} + 3 + x\right]. \quad (32)$$

Substitution of (30) and (32) in (26b) yields for the power spectrum

$$\Psi_{xx}(j\omega) = \frac{2}{7\omega^2 T}\left[\frac{1 - \cos 2\omega}{7 + 10\cos\omega + 6\cos 2\omega + 2\cos 3\omega}\right]. \quad (33)$$

As previously noted, (33) gives only the continuous part of the spectrum—the single discrete component at $s=0$, arising from the nonzero average value of the signal, has been suppressed. Its value may be found by evaluation of the residue of (30) at the single pole, $s=0$,

$$\text{dc power} = \frac{9}{49T^2} = (3/7T)^2 \quad (34)$$

which is the square of the average value of the telegraph message, as it should be.

Seventh Example—Power Spectrum of a Series of Identical Pulses Having Time Jitter

The previous example has illustrated the treatment of a random message of a discrete type which was synchronized to an underlying period T and, hence, could be expressed most readily in terms of X transforms. Lest this imply that the formulation developed thus far cannot be applied to continuous variations in the message parameters, we consider as our next example the power spectrum of a succession of identical pulses in which the interval between two successive pulses is a random variable which is statistically independent of the time interval between any other pair of pulses and which may be described by the probability density $f(\tau)$. Obviously, $f(\tau)$ is the probability density of *first occurrence* needed in our theory, and we may therefore represent the recurrent process by Fig. 15 and write:

For the steady-state expectation of a pulse

$$p_1 = \frac{1}{-F'(0)} = \frac{1}{T_0} \quad (35)$$

where T_0 is the "mean recurrence time".

For the average signal following a pulse

$$\bar{X}(s) = \frac{\Delta(s)}{1 - F(s)}; \quad (36a)$$

for the autocorrelation function

$$\Phi_{xx}(s) = p_1\Delta_1(-s)\bar{X}_1(s) = \frac{\Delta(-s)\Delta(s)}{T_0}\left[\frac{1}{1 - F(s)}\right]; \quad (36b)$$

for the power spectrum (continuous portion)

$$\Psi_{xx}(j\omega)=\frac{|\Delta(j\omega)|^2}{T_0}\left[1+\frac{F(s)}{1-F(s)}+\frac{F(-s)}{1-F(-s)}\right]_{s=j\omega} \quad (36c)$$

$$=\frac{|\Delta(j\omega)|^2}{T_0}\left[\frac{1-F(s)F(-s)}{1+F(s)F(-s)-F(s)-F(-s)}\right]_{s=j\omega}. \quad (36d)$$

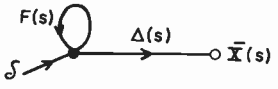

Fig. 15—Flow graph for a "free-running" pulser.

These equations may be evaluated for any particular distribution of jitter that is desired, the only limitation being that $f(t)$ must vanish for negative t to correspond to physical *causality*. For example, if the pulses were unit impulses and the interval between successive pulses was a random variable with a Poisson distribution (13), then $\Delta(s)=1$, $F(s)=\lambda/(s+\lambda)$, and $T_0=1/\lambda$. The power spectrum in this case reduces to a constant

$$\Psi(j\omega)=\lambda. \quad (37)$$

Thus, the spectrum is "white" except for a dc "discrete" component which is found by evaluating the residue of (36b) at $s=0$ to be λ^2.

Eq. (36) may also be used to determine the power spectrum of an almost-periodic signal such as that produced by, say, a free-running blocking oscillator having a noisy jitter. A reasonable assumption here is that the interval between successive pulses is normally distributed about a mean period T_0 with a standard deviation σ. Thus, we substitute

$$F(s)=\exp\left[-sT_0+\frac{\sigma^2}{2}s^2\right]$$

in (36d) and find that the power spectrum is

$$\Phi(j\omega)=\frac{|\Delta(j\omega)|^2}{T_0}\left[\frac{1-e^{-(\sigma\omega)}}{1-2(\cos\omega T_0)e^{-(\sigma\omega)^2/2}+e^{-(\sigma\omega)^2}}\right] \quad 38$$

where $|\Delta(j\omega)|^2$ is the energy spectrum of a single pulse.

The bracketed term produces peaks in the spectrum at frequencies which are a integral multiple of $\omega_0=2\pi/T_0$. For no jitter, these peaks become the periodic line spectrum. With jitter, these spectral lines broaden, their width increasing roughly as the square of the order of the harmonic. By further examination of the denominator of (38), it is found that the width of the n'th harmonic is given approximately by

$$\Delta\omega_n=\frac{1}{T_0}\left[\frac{2\pi\sigma n}{T_0}\right]^2. \quad (39)$$

Another important type of time jitter arises when there is an underlying, truly periodic series of "clock markers" about which the pulses are perturbed randomly in time.[13] Here, the time of occurrence of the n'th pulse will be given by

$$\tau_n=nT+\epsilon_n \quad (40)$$

where ϵ_n represents the jitter of the n'th pulse.

To set up a signal-flow graph for this process, we may first limit the random jitter ϵ_k to a finite number of discrete values (later, we shall let this number become infinite and replace the finite sums by integrals). As before, selection of each of these values of jitter is associated with a Markoff process and a set of transition probabilities (any particular jitter value ϵ_j will be followed by some value ϵ_k) are assumed to be known. We shall investigate here only the simplest case where one pulse's jitter is statistically independent of the jitter of any other. The signal-flow graph for the process then takes the elementary form in Fig. 16. Here, the self-return loop, x, generates the periodic clock markers, and the Markoff process consists of a simple distribution of these markers to various event nodes, each transmittance being a simple, scalar multiplier whose value is equal to the probability of the particular jitter. The "component-function generator" associated with the j'th event involves a delay $e^{-\epsilon_j s}$ and a waveform generator $\Delta(s)$. (In this simple case, the waveform is the same for all delay values. But, it obviously need not be, since different waveform generators could be associated with each delay operator, exactly as in example 6.)

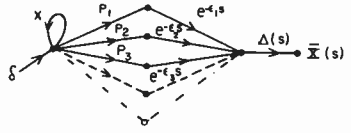

Fig. 16—Flow graph for a "clock-synchronized" pulser.

The *average* signal following the occurrence of a pulse having the jitter value ϵ_j is thus

$$X(s)=\Delta(s)\left[e^{-\epsilon_j s}+\frac{x}{1-x}\sum_k p_k e^{-\epsilon_k s}\right]. \quad (41)$$

If we now let the number of discrete values of ϵ_k become infinite we note that

$$\chi(s)\triangleq\sum_k p_k e^{-\epsilon_k s}\rightarrow\int p(\epsilon)e^{-\epsilon s}d\epsilon \quad (42)$$

which is simply the two-sided Laplace transform of the probability density of the jitter and is related to the probability of first occurrence of a pulse following the *previous* clock marker (at time $T+\epsilon$ earlier) by

$$F(s)=x\chi(s)$$

Hence, for the expected signal following a pulse of jitter ϵ_j

[13] R. M. Fortet, "Average spectrum of a periodic series of identical pulses randomly displaced and distorted," *Elec. Commun.*, vol. 31, pp. 283–287; December, 1954.

$$\overline{X}_j(s) = \Delta(s)\left[e^{-\epsilon_j s} + \frac{F(s)}{1-x}\right]. \tag{43}$$

The contribution to the correlation function of the pulses, having this particular value of jitter, is, by (25)

$$\frac{1}{T}\, p(\epsilon_j)\Delta(-s)e^{\epsilon_j s}\overline{X}_j(s) \tag{44}$$

and the average over-all jitter values, using (42), yields

$$\Phi_{xx}(s) = \frac{\Delta(-s)\Delta(s)}{T}\int\left[p(\epsilon_j) + p(\epsilon_j)e^{\epsilon_j s}\frac{F(s)}{1-x}\right]d\epsilon_j \tag{45}$$

$$= \frac{\Delta(-s)\Delta(s)}{T}\left[1 + F(-s)F(s)\,\frac{x}{1-x}\right], \tag{45a}$$

By application of (26b), we find that the continuous part of the power spectrum is given by

$$\Psi_{xx}(j\omega) = \frac{\Delta(-s)\Delta(s)}{T}\,[1 - F(-s)F(s)]_{s=j\omega} \tag{45b}$$

and the line spectrum of the periodic components is found from the residues of the singularities along the $j\omega$ axis of the second term within the brackets of (45a).

It is instructive to compare these results with the power-spectrum of the "free-running" oscillator given by (36), where only a continuous spectrum resulted (with the exception of the dc component) because the jitter of each pulse caused a displacement of *all successive pulses*, thus eliminating any true periodicities. This fundamental distinction between the two types of jitter associated with "synchronized" or "free-running" systems has sometimes been overlooked. For example, Tsien[14] describes the "free-running" situation, yet his analysis leading to his (9.43) [which is our 45b)] is appropriate to the synchronized case, rather than to the free-running case that he claims to be analyzing. (See also footnote 13.)

Eighth Example—Power Spectrum of a Series of Identical Pulses of Alternating Polarity and Random Spacing

Fig. 17 shows the signal-flow diagram for this random process, which is similar to that of Fig. 15, except that there are two polarity states with *certain* transition from one to the other. The steady-state expectation of either state is, by (10a),

$$\text{residue}\left[\frac{1}{1-F^2(s)}\right]_{s=0} = \frac{1}{2T_0} \tag{46}$$

where $T_0 = -F'(0)$ is mean recurrence time of the pulse train. The average signal following a positive pulse is

$$\overline{X}_1(s) = \Delta(s)\left[\frac{1-F(s)}{1-F^2(s)}\right]$$

$$= \Delta(s)\left[\frac{1}{1+F(s)}\right]. \tag{47}$$

[14] H. S. Tsien, "Engineering Cybernetics," McGraw-Hill Book Co., Inc., New York, N. Y.; 1954. (See Fig. 9.3.)

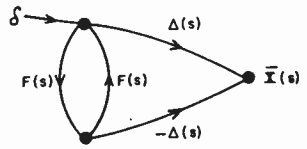

Fig. 17—Flow graph for a flip-flop.

A similar expression, but having opposite sign, is found for $\overline{X}_2(s)$. By (22), the correlation function is represented by

$$\Phi_{xx}(s) = \frac{1}{T_0}\,\Delta(-s)\Delta(s)\left[\frac{1}{1+F(s)}\right] \tag{48}$$

and the power spectrum by

$$\Psi_{xx}(j\omega) = \frac{1}{T_0}\,|\,\Delta(j\omega)\,|^2\left[1 - \frac{F(s)}{1+F(s)} - \frac{F(-s)}{1+F(-s)}\right]$$

$$= \frac{1}{T_0}\,|\,\Delta(j\omega)\,|^2\left[\frac{1-F(s)F(-s)}{1+F(s)+F(-s)+F(s)F(-s)}\right]_{s=j\omega}. \tag{49}$$

To illustrate, we may find the power spectrum of a flip-flop, which is triggered by Poisson-distributed impulses, by setting $\Delta(s) = 1/s$ (corresponding to the step-function components in the output voltage of a flip-flop), and $F(s) = \lambda/(s+\lambda)$ [for the Poisson distribution of first occurrences found in (13)]. Noting that $\lambda = 1/T_0$, we have after some reduction

$$\Psi(j\omega) = \frac{\lambda}{\omega^2 + (2\lambda)^2}. \tag{50}$$

Conclusion

We have attempted to show that the notation and techniques that have become highly developed by network and control-system theorists for finding the signal flow through linear systems of considerable complexity, may be applied directly to the problem of finding the "response" of Markoff processes of corresponding complexity and of determining analytical expressions for the power spectra and correlation functions associated with signals arising from such processes. Although the statistical results obtained in the eight examples are not new, it is hoped that their formulation in the language of circuit theory may suggest straight-forward computational procedures for analyzing statistical problems that might be difficult to set up and solve using the conventional methods of difference equations, etc.[15–17]

[15] W. H. Huggins, "Linear Systems and Group Dynamics," unpublished memorandum, Group Networks Lab., Res. Lab. Elec. M.I.T., Cambridge, Mass.; 1949. This memo presents some of the essential ideas of this paper, including example 6 giving the power spectrum of the telegraph message.

[16] R. W. Sittler, "Analysis and Design of Simple Nonlinear Noise Filters," Ph.D. Dissertation, M.I.T., September, 1954. This is an important treatment in which the analogy between discrete Markoff graphs and linear sampled-data systems is exploited and applied to the design of optimal noise filters.

[17] C. S. Lorens, "Theory and Application of Flow Graphs," Ph.D. dissertation, M.I.T.; July, 1956. Further work on the basic theory of flow graphs and their application to electrical networks also treats their relation to discrete statistical systems.

Correspondence

The Backward-Traveling Power in the High Power Traveling-Wave Amplifiers*

In a recent letter, Rowe and Hok[1] question the physical concept of the backward wave[2,3] and particularly doubt its useful function in the large-signal calculations.[3] To explain this, we shall consider two related problems, namely, the output power available from the circuit and the backward traveling power. It was in these studies that we found the concept of the forward and backward waves to be particularly useful.

In the large signal calculation, we are primarily concerned with the actual power output of the tube. The helix of a practical tube is matched to the output circuit but is decoupled from the beam at the output end ($z=D$). We may thus calculate the output power there, by assuming that the electron beam starts at $z=0$ and ends at $z=D$ and that the circuit is matched to the output circuit by cold measurements (Fig. 1). It may be seen that so far as the power flows in the circuit are considered, these assumptions are justified.

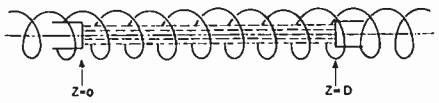

Fig. 1—The electron beam starts from $z=0$ and ends at $z=D$, and the circuit is matched to the output circuit.

Waves on the circuit must satisfy the circuit equation.[4] The solution of the circuit equation with the output conditions described above is[2,3]

$$V(z,t) = V_{\text{input}} e^{j\omega t-\Gamma_0 z} + \frac{\Gamma_0 \nu_0 Z_0}{2} e^{j\omega t-\Gamma_0 z}\int_0^z e^{\Gamma_0 z}\rho_\omega(z)dz + \frac{\Gamma_0 \nu_0 Z_0}{2} e^{j\omega t+\Gamma_0 z}\int_z^D e^{-\Gamma_0 z}\rho_\omega(z)dz. \quad (1)$$

Here V is the total voltage of the waves. ν_0 and Z_0 are respectively the phase velocity and the impedance of the cold circuit. z is the distance along the tube and t is the time. ρ_ω is the fundamental component of the linear electron charge density. $\Gamma_0=j(\omega/\nu_0)$ where $j=(-1)^{1/2}$ and ω is the angular frequency. We call the sum of the first two terms in (1) the *forward wave* or $F(z,t)$ for the following reasons: the first term is the voltage induced by the input signal, and it propagates forward as though the beam were not present. The second term is the voltage at z contributed by the charges between $z=0$ and $z=z$. It is the sum of the forward-traveling waves excited by the beam at the left of the point z. Similarly we call the third term in (1) the *backward wave* or $B(z,t)$. It is the voltage contributed by the charges between $z=z$ and $z=D$ and is the sum of the backward-traveling waves excited by the beam at the right of the point z.

Beyond the point D, the integral

$$\int_0^z e^{\Gamma_0 z}\rho_\omega(z)dz$$

of the forward wave becomes a constant and the integral

$$\int_z^D e^{-\Gamma_0 z}\rho_\omega(z)dz$$

of the backward wave vanishes. The forward wave is therefore a constant-amplitude forward-traveling wave with a propagation constant equal to that of the cold circuit for $z \geqq D$. It is the wave which travels through the point D without reflection and carries power along with it to the output circuit, whereas the backward wave vanishes there. The output power is therefore simply

$$\left(\frac{F^2(D,t)}{Z_0}\right)_{\text{ave.}} \quad (2)$$

It is seen that the forward and backward waves do have their physical interpretations distinct from each other at the output end of the tube. These concepts also greatly simplify the calculation of the output power.

Next we shall calculate the backward power flow and further illustrate the physical meaning of the backward wave. The backward wave for large signal has been calculated by Tien.[3] For small signal and assuming that ρ_ω varies as

$$\rho_\omega(z,t) = \rho_\omega(0)e^{j\omega t-\gamma z}$$

we have

$$B(z,t) = \frac{\Gamma_0 \nu_0 Z_0}{2}\frac{\rho_\omega(0)e^{j\omega t-\gamma z}}{\Gamma_0+\gamma} - \frac{\Gamma_0 \nu_0 Z_0}{2}\frac{\rho_\omega(0)e^{-(\gamma+\Gamma_0)D}}{\Gamma_0+\gamma}e^{j\omega t+\Gamma_0 z}. \quad (3)$$

The fact that the first term contains a forward propagation constant does not mean that the sum of the two terms in (4) is not the voltage contributed by the backward-traveling waves. As a matter of fact, we can easily show that $B(z,t)$ does carry backward-traveling power and (3) is just in the form which we should expect for the backward wave, Fig. 2(a) and 2(b) shows respectively the forward and backward power flows corresponding to the first and second terms in (3). Among them the backward power flow is always larger if the charge modulation along the beam is a growing wave. The net power flow corresponding to the sum of the two terms, or $B(z,t)$, therefore always travels backward [Fig. 2(c)]. Furthermore, the backward power flow shown in Fig. 2(c) is zero at the output end and is maximum at the input end. This should be so because at the output end the beam ends, and at the input end the backward wave is excited by the whole beam.

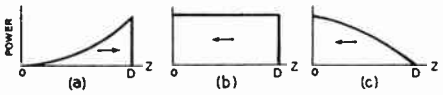

Fig. 2—The power flows corresponding to (a) the first term, (b) the second term, and (c) the sum of the two terms in (3). The arrows indicate the directions of the power flows.

At $z=0$, the second term is large compared with the first term in (3). We therefore should observe at the input end a backward wave traveling with a propagation constant equal to that of the cold circuit even though the circuit is matched by cold measurements. This wave may not be small compared with the input signal and might cause regenerative oscillation. Fortunately it can be eliminated by properly adjusting the output impedance. We shall not go into details here.

In Rowe's computation,[5] instead of dividing $V(z,t)$ into $F(z,t)$ and $B(z,t)$ components, it is solved directly from the circuit equation. Using $V(z,t)$ or $F(z,t)$ for numerical integration is only a matter of choice. However, if the power is computed by

$$P = 2CI_0V_0A^2(y)$$

as given in Rowe's paper,[5] the effect of the backward wave is ignored in view of (2). If the power is computed by

$$P = \tfrac{1}{2}\,\text{Re}\,[V*I]$$

as shown in Rowe and Hok's letter[1] the result is certainly not (2). However, the power actually obtained at the output of the tube depends on both the load impedance and the manner in which the beam is collected. It should be emphasized here that the effect of the backward wave is generally small and only amounts to few per cent of the output power. It is only significant when C is large.

PING K. TIEN
Bell Telephone Labs., Inc.
Murray Hill, N. J.

Letter from Mr. Rowe[6]

I have read Dr. Tien's letter on this disputed point with interest, but I am afraid that he has not understood the nature of the criticism outlined previously by Rowe and Hok[7] of his method of including the effect of the backward wave in the large-signal traveling-wave amplifier. Rowe and Hok intended to point out that the Poulter-Tien analysis, in terms of both forward and backward waves, is undesirable because it is necessarily complex and leads to some intuitive difficulties, whereas the Nordsieck-Rowe approach is a straightforward approach to the solution of a nonlinear problem.

* Received by the IRE, September 19, 1956.
[1] J. E. Rowe and G. Hok, "When is a backward wave not a backward wave?," PROC. IRE, vol. 44, pp. 1060–1061; August, 1956.
[2] H. C. Poulter "Large Signal Theory of the Traveling-Wave Tube," Tech. Rep. No. 73, Tech. Res. Lab., Stanford Univ., Stanford, Calif.; January, 1954.
[3] P. K. Tien, "A large signal theory of traveling-wave amplifiers," *Bell Syst. Tech. J.*, vol. 35, pp. 349–374; March, 1956.
[4] *Ibid.*, (4).
[5] J. E. Rowe, "A large signal analysis of the traveling-wave amplifier; theory and general results," IRE TRANS, vol. ED-3, pp. 39–57; January, 1956.
[6] Received by the IRE, October 15, 1956.
[7] Rowe and Hok, *loc. cit.*

Tien's foregoing discussion of the backward-traveling component of power is essentially that contained in his article[8] and adds no new evidence to the case. The accuracy of the expression $P=2CI_0V_0A^2(y)$ for the calculation of the forward component of power on the helix was discussed completely in my last communication[7] and the method was shown to be accurate to within a few per cent. Tien's implication that $P=\frac{1}{2}\mathrm{Re}\,(V^*I)$ does not give the forward power is obviously incorrect. Furthermore, it should be noted that if Tien's expression for calculating the forward-traveling power is correct then it should give the same answer as that obtained using the above expression.

I have also shown that Tien's equations[8] can be transformed into Rowe's equations after some purely algebraic manipulation without making any additional assumptions. If any reader of this letter is interested in seeing the details of the transformation they can be obtained upon request.

JOSEPH E. ROWE
Dept. of Elec. Eng.
University of Michigan
Ann Arbor, Mich.

Author's Comment[9]

V and I are respectively the transmission-line voltage and current of the equivalent circuit of the traveling-wave tube. Neither the power carried by the circuit nor the output power is necessarily equal to $\frac{1}{2}\mathrm{Re}\,[VI^*]$, when C is large. This has been discussed previously in the published letters by Wang and Pierce.[10]

P. K. TIEN

[8] Tien, *loc. cit.*
[9] Received by the IRE, October 18, 1956.
[10] C. C. Wang and J. R. Pierce, "Power flow and equivalent circuits of traveling-wave tubes," PROC. IRE, vol. 42, pp. 1701–1702; November, 1954.

Talking Drums and Binary Coding*

Communication by drums, the "jungle telegraph" as the white man has called it, is common among a number of African jungle tribes.[1] What kind of code is employed? It is anything but an exact phonetic code in which a certain set of beats represents a specific sound.

The code system is interrelated with the language of the tribe as follows. The meaning of a word depends not only upon phonetics but upon intonation. A given set of sounds may have totally different meanings depending upon the relative pitch at which each syllable is spoken. In one such language there are essentially two intonations, the higher and lower. The message drums are used in pairs of a lower-pitched "male" drum and a higher-pitched "female" drum. They are made to "talk" in the sense that they imitate the pitch and rhythm of speech.

But without phonetic differences, how can words of identical pitch and rhythm be distinguished? In drum language individual words are not used to represent an idea, but rather lengthy, redundant phrases. For example, not "cat" but "cat with long white whiskers that catches mice" might be transmitted. Standard phrases like the above example apparently become familiar to the listener and habitual with the drummer, comprising a code closely linked with the language and thus easily remembered by every member of the tribe.

The information content of the spoken language is in its intonation and rhythm as well as in its phonetics. Without phonetics, the rhythm and intonation alone, increased in quantity by redundant phraseology and repetition, suffice to transmit the same information in drum language. Since in the particular instance the intonation constitutes a binary code, only two drums or types of beat are necessary.

Message drums can be heard up to seven or eight miles through the jungle, and, some believe, as far as sixty miles under optimum conditions. Their low frequency probably facilitates long-distance transmission of the sound.

Standard sign-on, sender identification, and sign-off procedures are employed by the drummers, and by relaying, messages have been sent as far as a hundred miles in a few hours.

JOHN H. BORROWMAN
Box 1055, Ogden Dunes
Gary, Ind.

* Received by the IRE, August 30, 1956.
[1] J. F. Carrington, "Talking Drums of Africa," Carey Kingsgate Press, London, Eng., 1949.

The Magnetic Field in Wafer-Type Solenoids*

INTRODUCTION

To focus the electron beam inside a traveling-wave tube a magnetic field is required.

It is desired that this magnetic field be of uniform field strength along the axis of the tube. In wire wound solenoids a rather uniform field can easily be achieved by winding the solenoid in a uniform manner. Also, in a foil-wound solenoid with one foil winding, a very uniform field is obtained. Often it is desirable to cut a foil-wound solenoid into several sections called wafers. There are two advantages inherent in such a wafer type solenoid.

1) If the wafers are connected in series, it is possible to design high-voltage solenoids without using extremely thin foil. This is due to the possibility of choice between number of wafers and number of layers of the foil.[1]
2) Foil-wound solenoids have excellent heat transfer in an axial direction and very poor heat transfer in a radial direction. It is therefore desirable to cool the edge of the foil. The division of a long foil-wound solenoid into wafers increases the total edge surface available for cooling. If gaps are left between the wafers, air can be blown through the gaps to take advantage of this increased cooling surface.

It is the object of this report to analyze the nonuniformity of the magnetic field that will be caused by cutting a foil-wound solenoid into wafers, and leaving a gap between wafers.

DERIVATION OF AN EQUATION TO EXPRESS THE MAGNETIC FIELD OF A SOLENOID WAFER

Consider a ring of width a, with an inner radius r_1 and an outer radius r_2. In this wafer ring (see Fig. 1), the current density is

$$j=\frac{N_1I}{a(r_2-r_1)}, \tag{1}$$

where j = current density, assumed to be uniform, and N_1 = number of turns.

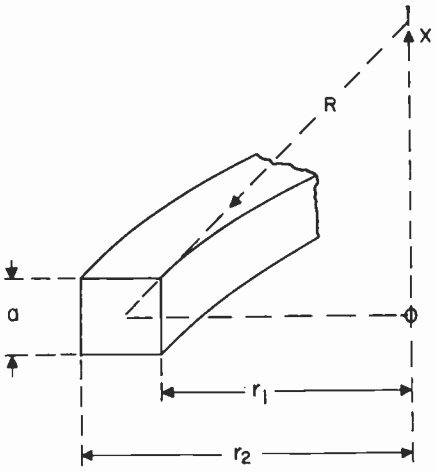

Fig. 1—Schematic of a wafer ring.

Applying the well-known equation of a circular current to this ring we find

$$dH=\frac{j}{2}\frac{r^2}{(r^2+x^2)^{3/2}}\,dxdr. \tag{2}$$

This together with (1) gives

$$H=\frac{N_1I}{2a(r_2-r_1)}\int_x\int_r\frac{r^2}{(r^2+x^2)^{3/2}}\,dxdr.$$

Integrating with respect to x,

$$H=\frac{N_1I}{2a(r_2-r_1)}\int_r\frac{x}{\sqrt{x^2+r^2}}\Bigg|_x^x dr.$$

Integrating with respect to r,

$$H=\frac{N_1I}{2a(r_2-r_1)}\left\|x\ln\left(\frac{r+\sqrt{x^2+r^2}}{x}\right)\right|_{x_1}^{x_2}\Bigg|_r^{r_2}$$

which is

$$H=\frac{N_1I}{2a(r_2-r_1)}\left\{x_2\ln\left(\frac{r_2+\sqrt{x_2^2+r_2^2}}{r_1+\sqrt{x_2^2+r_1^2}}\right)-x_1\ln\left(\frac{r_2+\sqrt{x_1^2+r_2^2}}{r_1+\sqrt{x_1^2+r_1^2}}\right)\right\}.$$

This is the magnetic field of one wafer

* Received by the IRE, April 23, 1956; revised manuscript received July 11, 1956.
[1] A. S. Gutman, "Design of Solenoids for Airborne Applications," Sylvania Waltham Labs., TR-14-2-13, April 18, 1955 (unclassified).

Determination of the Magnetic Field of a Wafer-Type Foil-Wound Solenoid

For the field on the center axis of the cylinder, $r_1 = \frac{1}{2}$ inner diameter of wafer; $r_2 = \frac{1}{2}$ outer diameter of wafer.

For the field at a point which is x inches from the center of the wafer on the axis of the cylinder, $x_1 = a/2 - x$; $x_2 = -a/2 - x$ where "a" is the length of the wafer. (See Fig. 2.)

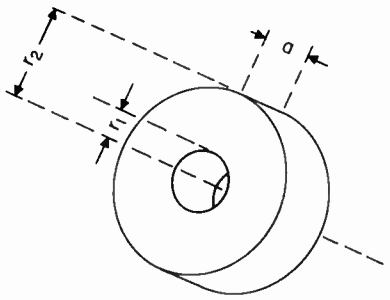

Fig. 2—Sketch of wafer.

With these equations it is possible to determine the magnetic field of one wafer as a function of x. This has been done for one wafer of a specific solenoid. (See Fig. 2.) The field of N_2 wafers spaced together with an axial gap g can be obtained by graphical superposition of N_2 field curves.

Analytically the field of N_2 wafers is

$$H = \sum_{i=1}^{i=N_2} \frac{N_1 I}{2a(r_2 - r_1)} \left\{ x_2 \ln \left(\frac{r_2 + \sqrt{x_2^2 + r_2^2}}{r_1 + \sqrt{x_2^2 + r_1^2}} \right) - x_1 \ln \left(\frac{r_2 + \sqrt{x_1^2 + r_2^2}}{r_1 + \sqrt{x_1^2 + r_1^2}} \right) \right\}$$

where

$$x_1 = \frac{a}{2} + (i-1)(a+g) - x$$

$$x_2 = -\frac{a}{2} + (i-1)(a+g) - x.$$

The amount of ripple in the magnetic field can be obtained by setting in the above formula, first, $x=0$ and evaluating H; second, $x=(a+g)/2$ and evaluating H'. The ripple is then the ratio H/H'.

For a foil-wound wafer, of 160 turns with $1\frac{7}{8}$-inch inside diameter, $4\frac{3}{4}$-inch outside diameter, 0.400 inch width, the magnetic field, when operated with 16-ampere current, was numerically evaluated by R. Gammerman.[1] The fields of 16 of such wafers spaced 0.040-inch apart from each other were superimposed on each other, to obtain the magnetic field distribution for the entire solenoid. (See Fig. 3.) No ripple could be detected from this curve. Therefore the ripple was determined for the condition where the gaps-between-wafers were much larger than the 0.040-inch actual gap. (See Fig. 4.) The ripple was evaluated in per cent and plotted vs gap width. (See Fig. 4.) The result shows clearly that the magnetic field is uniform for a solenoid with small air gaps.

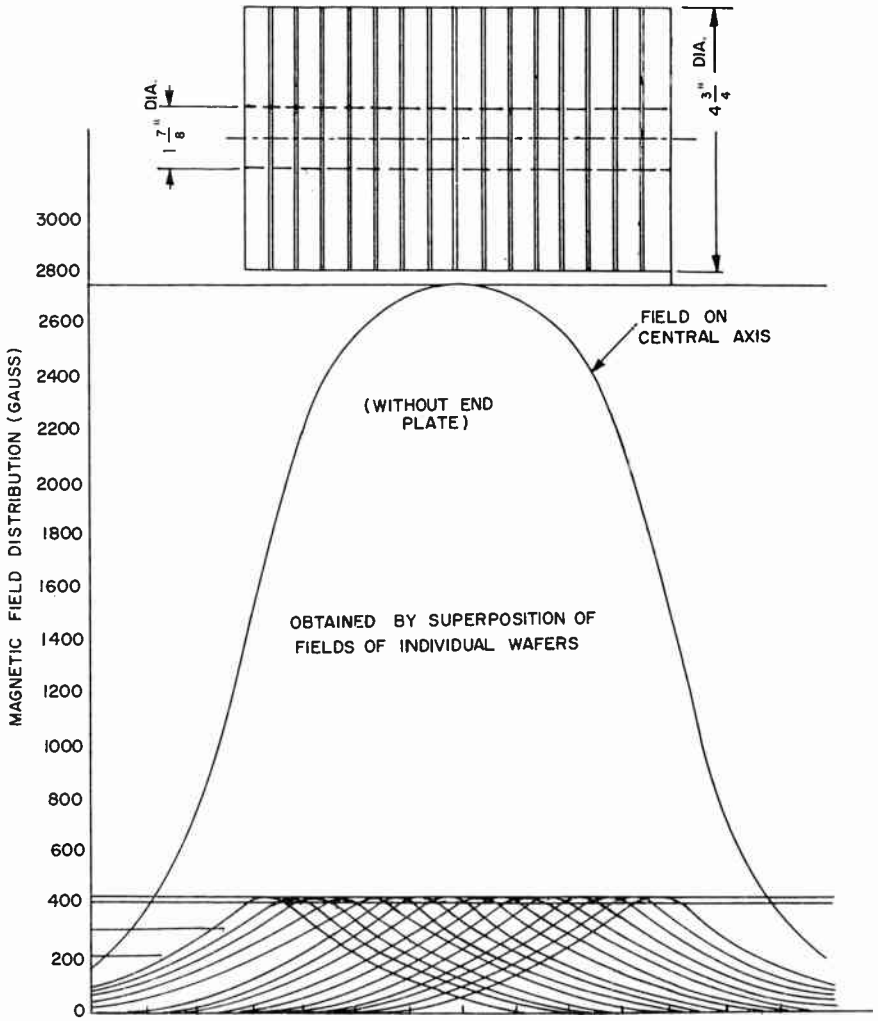

Fig. 3—Magnetic field distribution for a solenoid—16 wafers spaced 0.040-inch apart.

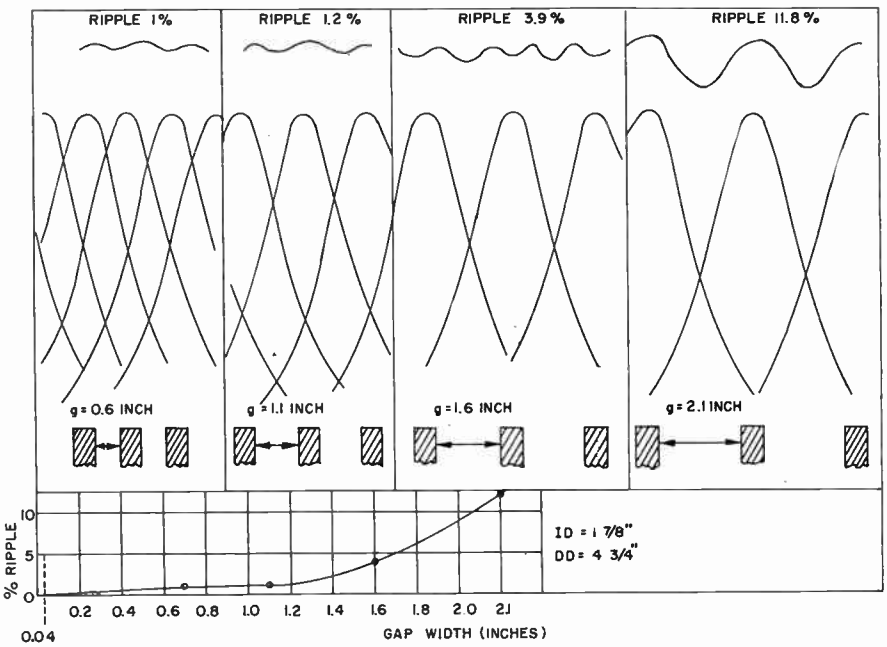

Fig. 4—Ripple of magnetic field at different wafer spacings.

[1] R. Gammerman, "Design of a 2800 Gauss Solenoid 5½" Long," Sylvania Waltham Labs., TR-14-2-30, November 21, 1955 (unclassified).

A. S. Gutman
Sylvania Elec. Prods., Inc.
Waltham, Mass.

Accurate Measurement of Emitter and Collector Series Resistances in Transistors*

In both grown junction and diffused base transistors, appreciable collector and emitter series resistances may be encountered. They may be a source of unnecessary power dissipation and of unnecessary and perhaps disqualifying voltage drops in certain types of logic circuits. The accurate measurement of these resistances is a prerequisite to their control and minimization.

This measurement is accomplished by measuring the voltage across the transistor from collector to grounded emitter as a function of base current with the collector current constrained to be zero (see Fig. 1).

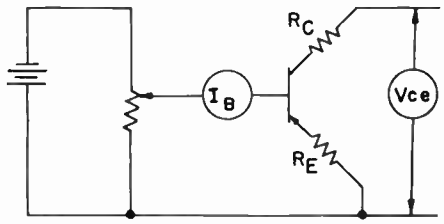

Fig. 1—Circuit for measurement of emitter and collector series resistances.

Ebers and Moll[1] have shown that

$$V_{CE} = (\pm)\frac{kT}{q}\ln\frac{\alpha_I\left[1-\frac{I_C}{I_B}\left(\frac{1-\alpha_N}{\alpha_N}\right)\right]}{1+\frac{I_C}{I_B}(1-\alpha_I)} \quad (1)$$

for a transistor in this general type of operation when voltage drops in emitter and collector series resistances are negligible. In this measurement $I_C=0$ and it is assumed that a measurable series resistance is present in the emitter.

Eq. (1) then becomes

$$V_{CE} = \frac{kT}{q}\ln\alpha_I + I_B R_E \quad (2)$$

where R_E is the series emitter resistance.

Thus V_{CE} vs I_B should plot as a straight line with y intercept kT/q ln α_I and slope R_E. If the transistor is inverted, that is if the emitter and collector are interchanged, the plot will of course have intercept kT/q ln α_N and slope R_C, the collector series resistance. Figs. 2 and 3 give typical plots obtained by this method for respectively a developmental silicon diffused base p-n-p transistor and a silicon grown n-p-n transistor.

This method of measurement can be readily modified to allow an oscilloscope display of V_{CE} vs I_B for a large number of approximate measurements.

An interesting by-product of this measurement is a confirmation of a theoretical prediction made by Ebers and Moll.[1] A re-examination of the derivation of (1) shows that the intercept in (2) is more directly given by

$$\frac{kT}{q}\ln\frac{\alpha_N I_{E0}}{I_{C0}}.$$

Since this intercept experimentally agrees closely with the measured value of α_I it confirms the relation $\alpha_I I_{C0}=\alpha_N I_{E0}$ theoretically derived by Ebers and Moll. Ordinarily the saturation currents observed for the reverse biased junctions do not conform to this relationship too well.

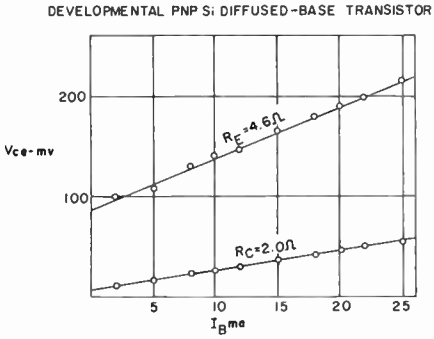

Fig. 2—Result of measurements on a diffused-base transistor. This type of transistor generally has a very low inverted α.

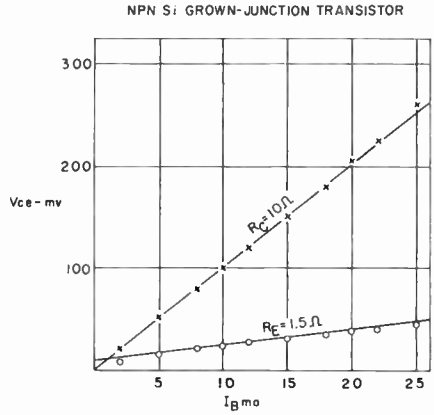

Fig. 3—Result of measurements on a grown-junction transistor.

In the case of transistors with complicated geometrical configurations, the values of R_E and R_C obtained in the manner described above are subject to some interpretation since the series resistances can be a function of the way in which the transistor is operated. During these measurements the series resistances are determined while their respective junctions are forward biased.

In regions where α_I or α_N are strong functions of current there can be considerable departure from the type of straight-line plots depicted in Figs. 2 and 3. This generally occurs at very low or very high current densities.

B. Kulke and S. L. Miller
Bell Telephone Labs., Inc.
Murray Hill, N. J.

* Received by the IRE, August 2, 1956.

[1] J. J. Ebers and J. L. Moll, "Large signal behavior of junction transistors," Proc. IRE, vol. 42, pp. 1761–1772; December, 1954.

Alternative Construction for Conjugate-Image Point*

Communications by Mathis, Altschuler, and most recently Bolinder[1] indicate the present interest in geometrical constructions on the reflection coefficient plane which yield the point Γ_a corresponding to the input conjugate-image impedance from loss circle data. A report[2] by the writer describes two additional constructions one of which may be cited here because of its naturalness and transparency from the standpoint of projective geometry.

The family of coaxal circles, of which the unit circle and the loss circle are members, determine on their common line of centers a hyperbolic involution of points; one of the double points of this involution (that one internal to the unit circle) is the point Γ_a. Now it is simple to locate the double points of an involution of points on a conic. The points of contact of the tangents from the center of the involution (located by drawing two lines) to the conic are just these double points.[3] The essence of the construction

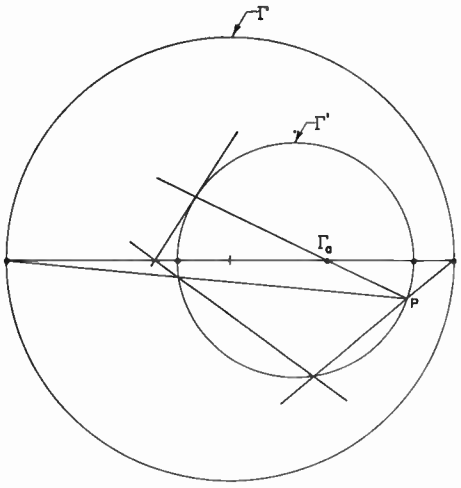

Fig. 1—Construction for Γ_a from loss circle data.

shown in Fig. 1 is: 1) project the involution on the line of centers onto a conic (in particular onto the loss circle which is already drawn on the diagram and through the arbitrarily chosen point P). 2) locate the double point; 3) project the desired point back onto the line of centers. This construction may also be carried out entirely within the confines of the unit circle.

Walter K. Kahn
Microwave Research Institute
Polytechnic Institute of Brooklyn
Brooklyn, N. Y.

* Received by the IRE, August 29, 1956.

[1] E. F. Bolinder, "Maximum efficiency of four terminal networks," Proc. IRE, vol. 44, p. 941; July, 1956. For additional references and definition of symbols see this communication.

[2] W. K. Kahn, "Impedance Maps," Wheeler Labs. Rep. 521. Wheeler Labs., Great Neck, N. Y.; March, 1954.

[3] See for example: B. C. Patterson, "Projective Geometry," John Wiley Sons, Inc., New York. N. Y., ch. 13, theorem 4, 1937.

Approximating the Alpha of a Junction Transistor*

The purpose of this note is to point out the usefulness and simplicity of a second-order power series approximation to the alpha of a junction transistor. The writer has used this approximation for some time and had assumed that it was well known in the field. A recent paper on the subject, however, makes no mention of it.[1]

If the emitter efficiency and collector multiplication factor are taken as unity, the forward short-circuit current gain of a junction transistor can be written as:

$$\alpha = \beta = \operatorname{sech}\left[(1+p\tau)\frac{w_0^2}{D\tau}\right]^{1/2}, \qquad (1)$$

where D is the diffusion constant and τ the diffusion time for the minority carriers in the base region, w_0 is the width of the base region, and p is the complex frequency variable. Expanding (1) in a power series gives:

$$\beta = \frac{1}{1+(1+p\tau)\frac{1}{2!}\frac{w_0^2}{D\tau}+(1+p\tau)^2\frac{1}{4!}\left(\frac{w_0^2}{D\tau}\right)^2+\cdots}. \qquad (2)$$

Retaining only the first two terms in the dedominator of (2) gives:

$$\beta \approx \frac{1}{1+\frac{1}{2}\frac{w_0^2}{D\tau}+p\frac{w_0^2}{2D}} \approx \frac{\beta_0}{1+\frac{p}{\omega_\alpha}} \qquad (3)$$

where

$$\beta_0 = 1-\frac{1}{2}\frac{w_0^2}{D\tau} \qquad (4)$$

and

$$\omega_\alpha = \frac{2D}{w_0^2\beta_0}. \qquad (5)$$

This is the well-known approximate expression for β; it is simple and is frequently useful to $\omega=\omega_\alpha$.[2,3] Plots of the errors introduced by using (3) instead of (1) for the cases of $\beta_0=0.99$ and $\beta_0=0.9$ are given by the dashed curves in Fig. 1. In calculating these curves the measured value of ω_α was used in (3) rather than the value given by (5). Although the magnitude error is less than 0.2 db out to $\omega=2\omega_\alpha$ the phase angle error is seen to be 13.0 to 14.4 degrees even at $\omega=\omega_\alpha$. In some design problems this phase error is of considerable importance.

A much better approximation to (1) is obtained by retaining the first two terms in (2). This leads to the expression:

$$\beta \approx \frac{1}{1+\frac{w_0^2}{2D\tau}+\frac{w_0^4}{24D^2\tau^2}+p\frac{w_0^2}{2D}\left(1+\frac{w_0^2}{6D\tau}\right)+p^2\frac{w_0^4}{24D^2}} \qquad (6)$$

$$\approx \frac{\beta_0}{1+\frac{p}{\omega_0}+\frac{p^2}{6\omega_0^2}} \qquad (7)$$

where

$$\beta_0 = 1-\frac{w_0^2}{2D\tau}-\frac{w_0^4}{24D^2\tau^2} \qquad (8)$$

and

$$\omega_0 = 2\frac{D}{w_0^2}. \qquad (9)$$

Factoring the denominator of (7) gives

$$\beta \approx \frac{\beta_0}{\left(1+\frac{p}{1.268\omega_0}\right)\left(1+\frac{p}{4.732\omega_0}\right)}. \qquad (10)$$

It is convenient to rewrite (10) in terms of the frequency at which β is 3 db below β_0.

$$p = j1.192\omega_0 = \omega_\alpha. \qquad (11)$$

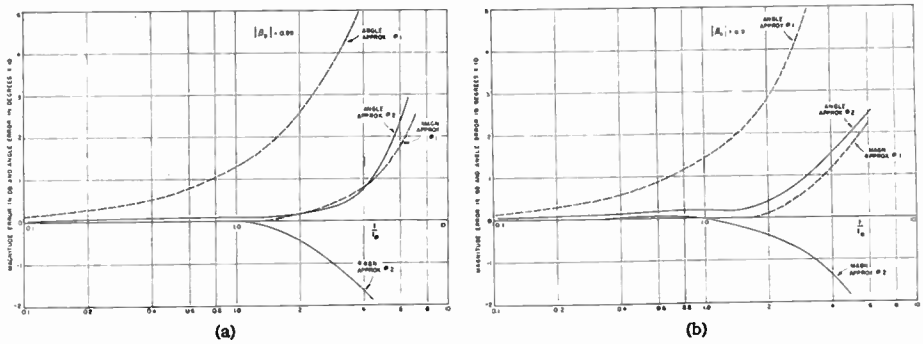

(a) (b)

Fig. 1—Errors of rational approximations to the alpha of a junction transistor, (a) $\beta_0=0.99$, (b) $\beta_0=0.90$, as a function of ω/ω_α.

This leads to

$$\beta = \frac{\beta_0}{\left(1+0.94\frac{p}{\omega_\alpha}\right)\left(1+0.252\frac{p}{\omega_\alpha}\right)} \qquad (12)$$

which can be compared directly with the exact expression (1) and the simplest approximation (3). This is done in Fig. 1; the solid curves represent the magnitude and phase error introduced by using (12) instead of (1). For the two values of β_0 considered one sees that the phase angle of approximation (12) is much better than (3). Even at $3\omega_\alpha$ the error is only 10 degrees (or 10 per cent) for the poorer case of $\beta_0=0.9$.

The magnitude error introduced by (12) is greater than that due to (2) although it is less than 1 db out to three times the cutoff frequency ω_α.

Since the additional pole of (12) overcompensates the magnitude while only partially correcting the phase shift of (1), it is clear that a nonminimum phase function can be used to give a better approximation without additional poles. The approximation

$$\beta = \frac{\beta_0}{\left(1+\frac{p}{\omega_\alpha}\right)} \times \frac{1-.134\frac{p}{\omega_\alpha}}{1+.134\frac{p}{\omega_\alpha}} \qquad (13)$$

gives the same magnitude agreement as our conventional expression (3) together with a better angle approximation than (12).

Another approach to approximating (1) is to expand it as an infinite product and retain only the first few terms. This leads to the approximation,

$$\beta = \frac{\beta_0}{\left(1+\frac{p}{\omega_0}\right)\left(1+\frac{p}{9\omega_0}\right)} \qquad (14)$$

when

$$\omega_0 = \frac{\pi^2}{4} \times \frac{D}{w_0^2}. \qquad (15)$$

This gives a better magnitude approximation than (12) but a somewhat poorer angle approximation.

The numerical values in (12) are somewhat inconvenient to use in day-to-day circuit analysis. The writer has found the cruder approximation

$$\beta = \frac{\beta_0}{\left(1+\frac{p}{\omega_\alpha}\right)\left(1+\frac{p}{4\omega_\alpha}\right)} \qquad (16)$$

somewhat easier to remember and use. It is still accurate enough for use in the design of feedback amplifiers having reasonable phase and gain margins.

A. B. Macnee
University of Michigan
Ann Arbor, Mich.

* Received by the IRE, August 8, 1956.

[1] R. D. Middlebrook and R. M. Scarlett, "An approximation to alpha of a junction-transistor," IRE Trans., vol. ED-3, pp. 25–29; January, 1956.

[2] J. M. Early, "Design theory of junction transistors," *Bell Sys. Tech. J.*, vol. 32, pp. 1271–1312; November, 1953.

[3] R. F. Shea, "Principles of Transistor Circuits," John Wiley and Sons, New York, N. Y., pp. 190–192; 1953.

Quantum Mechanical Amplifiers*

Recent work[1,2] in engineering a quantum mechanical oscillator seems to be restricted to the use of molecular beams and ammonia gas. For the past year the writer has been interested in enlisting engineering effort in the realization of a quantum mechanical amplifier or oscillator by the use of other quantum state preparation methods and the use of other quantum states and materials.

The *sine qua non* of a molecular amplifier is the creation of a nonequilibrium thermodynamic state so that net energy can be extracted from the system. The lifetime for the existence of a departure from thermal equilibrium is generally measured in terms of a relaxation time.[3] The aim of the game is to establish a condition of thermal nonequilibrium which has a survival time or relaxation time that is longer than the period in which one wishes to use this condition for oscillator or amplifier purposes. Consider the ammonia maser from this point of view. The electrostatic selector enhances the population in the higher energy state that is used, so that it exceeds the population in the lower energy state. This is not a state of thermal equilibrium. The molecules emerging from the electrostatic selector will approach a condition of thermal equilibrium due to collisions, spontaneous emission, and induced emission. Under the operating conditions of the ammonia maser collisions are very rare. The process of spontaneous emission is not probable; the lifetime for this process is of the order of thousands of seconds. In existent ammonia masers the lifetime for induced emission is arranged by adjusting cavity Q and power level to be the passage time of the molecules through the output cavity. This interaction time is of the order of milliseconds.

Consider the system of a proton in a magnetic field. It is a simple one, being visualized as a magnetic moment that can align itself with or against the magnetic field. The actual energy difference between these two steady states is the nuclear magnetic absorption frequency, which is given as

$$\nu = g_N \beta_N B$$

where $g_N\beta_N = 762.3$ cps/gauss. As workers in the field of nuclear resonance and induction have so adequately demonstrated, the relaxation times for proton states can vary over an extreme region from many seconds to microseconds, depending upon the proton surroundings (the physical and chemical state of the proton-containing material). In other words, a situation of thermal nonequilibrium in the proton states in a magnetic field could be made to last long enough for quite leisurely experiments aimed at coherently extracting the available energy.

A free, or nearly free, electron spin, interacting with a magnetic field also has two available states. These states can be visualized as being those in which the electron spin is aligned with or against the magnetic field. The energy difference associated with these two states of the electron spin in a magnetic field is

$$\nu = g e \beta_e B$$

where $g_e\beta_e = 2.8$ mc/gauss. There is experimental evidence of relaxation times as long as 16 seconds for such electronic paramagnetic states.[4] Here again by a suitable choice for the surroundings of the electrons, the electronic paramagnetic spin states can be so designed that the relaxation from thermal nonequilibrium to equilibrium can be any convenient time that will allow experiments involving the extraction of energy from these quantum mechanical states.

Other quantum states can also be used. But it is apparent that the use of these two systems alone offers certain marked advantages over the ammonia maser. In the first place, ammonia beams present a difficult vacuum pumping problem. The beam density must be low to reduce collision relaxation and scattering. The material-handling problem is especially grievous because ammonia is difficult to pump, even on cold surfaces, once a monomolecular layer of ammonia has formed. Thus, with the ammonia maser, one is restricted by pumping problems to beam densities of the order of 10^{13} particles per second. Proton or electron spin densities of 10^{18} spins/cc are readily available. Samples of proton or electron spins of tens of cc cycled through from thermal equilibrium to thermal nonequilibrium with a millisecond period (a number typical of a radar prf period) would be equivalent to beams of intensity $10^{22}\,\rho$, where ρ is the fraction of the spin state available for emission.

Let us consider one of the many methods available for state preparation in spin systems.[5] At the outset it is important to realize that total elimination of the lower energy state is not necessary in achieving net emission possibilities. All that is necessary is that the higher energy state shall have a population greater than that of the lower energy state. Such a two-level system has been analyzed in the past.[6] The populations of the

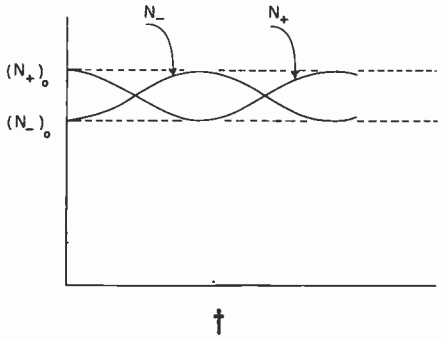

Fig. 1—Time dependent population of a two-quantum state system interacting with an electromagnetic field. N_+ is the population of spins aligned with the field; N_- is the population of spins aligned against the field; $(N_+)_0$ represents the equilibrium values,

$$(N_+)_0 = (N_-)_0 \exp\left(\frac{-h\nu}{kT}\right) \approx (N_-)_0\left(1 - \frac{h\nu}{kT}\right).$$

two spin states under the influence of a pulse of coherent radiation of duration t is indicated in Fig. 1. The equilibrium distribution of population is given by the Boltzmann distribution in terms of the frequency difference between the two levels. Thus, if the radiation is terminated at a time when the populations are inverted, an excess population in the upper state is available for amplifier and oscillator experiments. In this case ρ would be computed as:

$$\rho = \frac{h\nu}{kT}$$

where h is Planck's constant, k is Boltzmann's constant, and T is the equilibrium temperature in degrees Kelvin. At room temperature, $T = 300°\text{K}$, $\rho = 1.6\nu \times 10^{-7}$, where ν is the frequency in megacycles. Thus, even at $\nu = 1$ mc, the cycled spin systems provide a possible source of energy that is much greater than that of normal ammonia beams.

The gain and power possibilities are exciting. With $N\rho$ spins state-selected at a pulse recurrence frequency Ω and operating at a radiofrequency ν with a photon energy $h\nu$, the power which may be induced from them by the feeble signal radiation field is

$$P_{\text{available}} = \tfrac{1}{2} N\rho\Omega h\nu \text{ watts.}$$

Since ρ also depends on ν, this power increases as ν^2. At X-band, however, using the values given above, we have

$$P_{\text{available}} = 100\ \mu \text{ watts.}$$

With a 10-mc bandwidth, this implies an allowable gain of 100 db with a source with an effective noise temperature of 1°K.

It is instructive to compare these figures with those pertaining to beam systems. As we pointed out above, the ammonia maser has been operated with a beam flux of 10^{13} effective molecules/sec. This number corresponds to our $N\rho\Omega$. The writer feels that by using refractory materials, which can easily be pumped on cold surfaces, this figure might be increased to 10^{15} states/sec. Using X-band again, we obtain for the best beam an available power of

$$(P_{\text{available}})\ \text{future beam} = 7 \times 10^{-3}\ \mu \text{ watts.}$$

* Received by the IRE, August 24, 1956; revised manuscript received, September 28, 1956. This work was supported in part by the U. S. Army (Signal Corps), the Air Force (Office of Scientific Research, Air Research and Development Command), and the Navy (Office of Naval Research), in part by Hughes Research and Development Laboratories, and in part by Cornell Aeronautical Laboratories.

[1] N. G. Basov, A. M. Prokhrov, "Theory of the molecular generator," *Zh. Eksp. Teor. Fiz.*, vol 30, p. 560; March, 1956.

[2] J. P. Gordon, *et al.*, "The maser," *Phys. Rev.*, vol, 99, p. 1264; August 15, 1955.

[3] By convention two relaxation times, T_1 and T_2 are of interest. We lack the space to do justice here to this point. Suffice it to say that T_1 is the time constant for establishing the equilibrium population distribution between the separate energy levels, and that T_2 is the time constant for establishing phase incoherence among members of a state, *i.e.*, for reducing net oscillating dipole moment to zero. By thermal relaxation we mean T_1, and it will be our main interest here. T_2 is of interest in discussing line width or circuit Q and would be considered in a detailed analysis of the response of the quantum mechanical system to electromagnetic radiation. In gas (beam) spectroscopy the simplification $T_1 = T_2$ appears.

[4] A. Honig, "Polarization of arsenic nuclei," *Phys. Rev.*, vol. 96, p. 234; October 1, 1954; A. Honig and J. Combrisson, "Paramagnetic resonance in As-doped silicon," *Phys. Rev.*, vol. 102. p. 917; May 1, 1956; and A. M. Portis, "Rapid passage effects in electron spin resonance," *Phys. Rev.*, vol. 100, p. 219; November 15, 1955.

[5] For other methods, see N. G. Basov and A. M. Prokhrov, "Possible methods of obtaining active molecules," *Zh. Eksp. Teor. Fiz.*, vol. 28, p. 249; February, 1955; and J. Combrisson, *et al.*, "Utilisation de la résonance de spins," *Compt. Rend.*, vol. 242, p. 2451; May 14, 1956.

[6] H. R. Johnson and M. W. P. Strandberg, "Broadening of microwave absorption lines," *Phys. Rev.*, vol. 86, p. 811; June 1, 1951.

This optimistic comparison is quite spectacular.

The preceding discussion serves to underline the second important advantage of using paramagnetic spin states: they are simply tunable by means of magnetic field. The use of electric or magnetic fields to vary the ammonia resonance frequency has been suggested. The ammonia magnetic tuning rate is about 10^{-4} as great as that of an electron spin: it is about one-sixth the proton tuning rate. Consideration of electric field homogeneity and breakdown in the maser cavity for electric field tuning would certainly limit the use of electric tuning to a few megacycles around 23,870 mc. Certainly it was only in the attitude of a wishfulness that such a suggestion was made in the past.

Some thought should probably be given to the problem of actually transporting the prepared or separated spin states from the region in the laboratory where state preparation or separation is performed to the region in the laboratory where the thermal nonequilibrium spins are used for amplification. Possibly these two functions will take place in the same region through a system of time multiplexing. In other words, the spin states could be prepared with a short intense pulse of radiation, and after this preparation the weak electromagnetic energy to be amplified could be brought into contact with the prepared states. Or, state preparation could take place at one point in the laboratory and the sample transported, as on a rotating disk or wheel, into a nearby region where emission or amplification could take place. While these two methods are certainly feasible and experimentally realizable, it is the author's fervent hope that they do not serve to circumscribe the imagination of those who are interested in applying the general principles that have been discussed.

The most enticing aspect of quantum mechanical amplifiers is the possibility that they offer of achieving essentially noise-free amplification. An amplifier having a signal source at a temperature much lower than room temperature—for example, a scatter communication receiver looking at the cold interplanetary region—should not be limited by room-temperature noise, but by noise with an effective temperature of a few degrees Kelvin. A receiver with a limiting sensitivity of a few degrees Kelvin is indeed achievable with a quantum mechanical amplifier. The transmission system that transfers the radiation to be amplified to the prepared quantum states will not be observable by means of its thermal radiation if it has a low insertion loss. This is just another way of saying that a good absorber is a good emitter and, conversely, a poor absorber is a poor emitter. Hence, a transmission system with low loss in the absence of the quantum mechanical energy levels and with strong interaction with electromagnetic radiation in the presence of the quantum mechanical levels can be made to have a power gain and yet to display an effective noise temperature of the source rather than that of the transmission system. Thus, with reasonable gains of, and with low-loss matching elements one may approach a noise figure of 1 for any source temperature with a quantum mechanical amplifier.

This by no means defines all of the attributes of a quantum mechanical amplifier that should make the electrical designer's eyes sparkle. These amplifiers will provide circuit elements at any frequency with Q's that are unrealizable with today's conventional elements. Quantum mechanical amplifiers would relieve the communications and radar transmitter designers from trying to create and work with higher and higher transmitter powers to obtain greater sensitivity. With near theoretical operation of the receiving amplifiers, the system could at least obtain a factor of 20 db in improved sensitivity and probably a factor of 25–30 db in the microwave region.

General work in this almost-unexploited field is in progress in the writer's Laboratory.

MALCOM W. P. STRANDBERG
Res. Lab. of Electronics
Mass. Inst. Tech.
Cambridge, Mass.

Japanese Technical Captions*

In view of the interest in the Russian technical glossaries that have recently been appearing on these pages, one may assume that there would also be interest in learning to decipher the captions on Japanese technical illustrations, labels, advertisements, *etc.* This is not at all as difficult for an Occidental as it sounds, for the vocabulary that the Japanese use for these purposes is almost entirely taken from the English (with an occasional French, German, or Latin word) and all that remains is to "read" the Japanese characters. This again need cause no alarm because, for this purpose, the Japanese use neither Chinese ideographs nor their syllabary of "51" cursive characters, but a rather simple syllabary, with only 45 different angular symbols, set up especially for "foreign" words.

These symbols are listed in Table I, and together with a few simple rules, one can begin at once to read Japanese technical words like the examples in Table II. The procedure is rather entertaining, as well as instructive.

The characters in Table I represent syllables consisting, in general, of one consonant plus one vowel, formed by combinations of nine consonants with five vowels. (The four important irregularities are marked with an asterisk.) Additional consonant sounds are formed by placing two short strokes to the upper right of the character, which changes K, S, T, and H to G, Z, D, and B, respectively. A small circle in the same position changes H to P. Words can be written horizontally (as in English) or vertically; in the latter case, one starts from the right side of the page. Five quick rules are:

1) A *dash* (written vertically in vertical words) means *lengthen* the preceding vowel.
2) A *small TSU* means *shorten* the preceding vowel, but is then silent itself.
3) When *YA, YU, YO,* or any vowel is written *small,* it should supplant the original vowel of the preceding syllable.
4) *U* is a weak vowel and tends to become silent; also, sometimes, the *O* in *TO* or *DO.*
5) *L, V,* and *TH* sounds don't exist in Japanese, and have to be written as *R, B,* and *S,* respectively.

A. KARP
Bell Telephone Labs., Inc.
Holmdel, N. J.

* Received by the IRE, August 31, 1956.

TABLE I

JAPANESE SYLLABARY FOR "FOREIGN WORDS"

	A	I	U	E	O
-	ア A	イ I	ウ U	エ E	オ O
K	カ KA *GA	キ KI *GI	ク KU *GU	ケ KE *GE	コ KO *GO
S	サ SA *ZA	シ *SHI *JI	ス SU *ZU	セ SE *ZE	ソ SO *ZO
T	タ TA *DA	チ *CHI *JI	ツ *TSU *ZU	テ TE *DE	ト TO *DO
N	ナ NA	ニ NI	ヌ NU	ネ NE	ノ NO
H	ハ HA *BA *PA	ヒ HI *BI *PI	フ *FU *BU *PU	ヘ HE *BE *PE	ホ HO *BO *PO
M	マ MA	ミ MI	ム MU	メ ME	モ MO
Y	ヤ YA	I	ユ YU	E	ヨ YO
R	ラ RA	リ RI	ル RU	レ RE	ロ RO
W	ワ WA	I	U	E	O
		ン N			

TABLE II

EXAMPLES OF JAPANESE TECHNICAL VOCABULARY

	syllables	English
オシロスコープ*	O SHI RO Su KO- Pu	Oscilloscope
クロロマイセチン	Ku RO RO MA I SE CHI N	chloromycetin
アマチュア	A MA CH' YU A	amateur
プレート	Pu RE- To	plate
コイル	KO I Ru	coil
スポット	Su PO/ To	spot
ビーム	BI- Mu	beam
エレクトロン ガン	E RE Ku To RO N GA N	electron gun
カソード	KA SO- Do	cathode
スペーサー	Su PE- SA-	spacer
スプリング*	Su Pu RI N Gu	spring
ヒーター	HI- TA-	heater
グリッド	Gu RI/ Do	grid
フルオレッセント	Fu RU O RE/ SE N To	fluorescent
スクリーン	Su Ku RI- N	screen
フィラメント	F'I RA ME N To	filament
スリーブ*	Su RI- Bu	sleeve
レンズ*	RE N Zu	lens
コンクール	KO N KU- Ru	concours (Fr.)
ハッピ*	HA/ PI	happy •
ミラクル	MI RA KU Ru	miracle •
ネオパン	NE O PA N	Neopan •
グレイ フェイス	Gu RE I F'E I Su	gray face
ラジオ	RA JI O	radio

• trade names

Phase Stability of Frequency Multipliers*

Tests are reported on a conventional frequency multiplier from 100 kc to 10 mc (using class C multiplication). Oscilloscope techniques were employed for measuring its phase stability. The phase of the output was directly compared with the phase of the input by the following two methods: 1) The 10 mc output was examined on an oscilloscope with sweep triggered by a 100 kc signal from the same crystal oscillator which fed the multiplier. 2) The 10 mc output and the 100 kc input formed a Lissajous pattern with a 100:1 ratio. The phase stability of the multiplier could then be directly studied by observing the oscilloscope pattern.

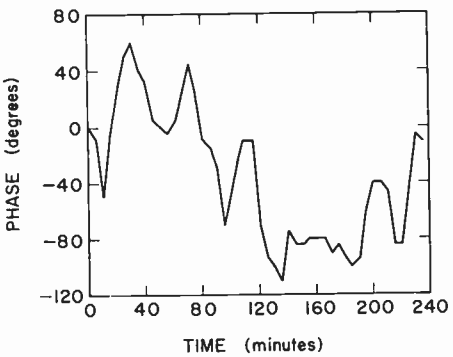

Fig. 1—Random phase changes with time in a 100-kc to 10-mc frequency multiplier. The slope of the curve gives the significant frequency change, where in a slope of 6.5° per minute corresponds to a frequency change of 3 parts in 10^{11}.

Fig. 1 shows the results obtained from one such test using method 1). All equipment used was fed by constant voltage transformers. Test variations in line voltage showed a negligible phase effect. All equipment had a minimum warming-up period of 20 hours, and was shock-mounted in a temperature controlled room. A weak correlation between the input amplitude to the multiplier and the measured phase changes indicated that the input amplitude may be responsible for a small fraction of the observed changes. A separate test, made using both of the above methods simultaneously, showed agreement to well within 10 per cent of the observed changes. These phase drifts are interpreted in terms of frequency as follows: A shift of 10.8° at the 10-mc stage over a period of 5 minutes corresponds to a frequency deviation of $10.8/360\times300\times10^{7}=10^{-11}$; *i.e.* 1 part in 10^{11}.

The frequency errors introduced by a multiplier chain as studied here are distinct from the short-time phase jitter due to phase modulation of the carrier by noise. These long-time phase drifts were also observed in a commercially made frequency multiplier. Other observers[1] have noticed random phase drifts in stabilized oscillators involving multiplier chains that are of the same order of magnitude.

There is at present some confusion existing in the field of frequency multiplication as regards the errors introduced by a multiplier chain. This may be due to loose terminology and lack of accurate data. These errors become particularly important when high precision measurements in the microwave region are required. By taking a random five minute interval for frequency comparison errors up to about $1:10^{10}$ may result. Even though Fig. 1 shows that over a long interval of several hours the accumulated phase error may be centered about a mean, this is not always the case.

S. N. Kalra and E. J. Woods
Division of Applied Physics
National Research Council
Ottawa, Canada

* Received by the IRE, July 16, 1956.
[1] Symposium on Generation, Frequency-Stabilization and Amplification of Electromagnetic Oscillations by Atomic and Molecular Resonances, Asbury Park, N. J.; February, 29–March 1, 1956.

Frequency Modulation Noise in Oscillators*

In a recent paper Stewart[1] pays attention to the fact that it is extremely difficult to make a direct measurement of the width of the oscillator power spectrum resulting from frequency modulation by shot noise. The first difficulty is the smallness of this width. The second (and the principal one) is the additional broadening of the spectrum due to various relatively slow random processes. This additional broadening results in a much wider power spectrum than that due to the shot noise. It is convenient to distinguish between *natural* spectrum width[2] due to shot (and eventually Johnson) noise and the *instrumental* width[3] due to flicker effect, microphonics, drift *etc.*, mentioned above as the slow random processes.

A method of measurement of the natural width avoiding both difficulties pointed out by Stewart was developed by one of us some years ago.[4]

The difference of two voltages, u_1 and u_2, both taken from the oscillator—the first directly and the second through a delay line—is fed to a detector. The output voltage of the oscillator is a random process

$$u(t)=[U+\Delta U(t)]\cos[2\pi f_0 t-\phi(t)].$$

[The fluctuations of the phase $\phi(t)$ are related to the frequency modulation by shot noise and other random processes mentioned above.] The phase difference of u_1 and u_2 is then

$$\psi+\Delta\phi=\psi+\phi(t)-\phi(t-\tau),$$

where ψ is a constant, and τ the delay time of the line (assumed to have no dispersion).

A proper adjustment of the amplitude ratio of u_1 and u_2, and of ψ, makes the amplitude of u_1-u_2 almost insensitive to the amplitude fluctuations $\Delta U(t)$ and equal to $a+b\Delta\phi$, a and b being constants.

The phase deviation $\Delta\phi$ may be represented as a sum of two terms:

$$\Delta\phi=\Delta\phi_1+\Delta\phi_2$$

corresponding respectively to the natural and the instrumental widths of the oscillator power spectrum. These terms are statistically independent. Thus

$$\overline{(\Delta\phi)^2}=\overline{(\Delta\phi_1)^2}+\overline{(\Delta\phi_2)^2}.$$

According to the theory[2]

$$\overline{(\Delta\phi_1)^2}=D\tau$$

where the "phase diffusion coefficient" D is linked to the natural spectrum width Δf by

$$D=2\pi\Delta f.$$

If τ is small compared with the correlation time of the "instrumental" frequency drift $\delta f=F(t)$ there is an obvious equation

$$\overline{(\Delta\phi_2)^2}=4\pi^2\overline{F^2}\tau^2.$$

Thus, the delay line being short enough

$$\overline{(\Delta\phi_2)^2}\ll\overline{(\Delta\phi_1)^2}.$$

In this case the output noise power measurement of the detector will give D if intrinsic detector noise is negligible.

So far the situation has been somewhat simplified. It was actually the *spectral density* of noise power at the detector output that was measured in the experiments. As may be shown this spectral density is proportional to

$$\left(\frac{\sin\pi f\tau}{f}\right)^2[D+2\pi^2B(f)],$$

where $B(f)$ is the spectral density of $\overline{F^2}$. It approaches zero as f increases, what makes possible the determination of D.

The measurements were performed at $f_0=18$ mc. The delay line time was about 3 microseconds. $B(f)$ was practically zero when f exceeded 10–20 kc. The experiment gave Δf of the order of 10^{-6} cycles per second in agreement with the theory.

The theory shows that the delay line may be replaced by a high Q resonance system with resonance frequency equal to f_0. In this case the spectral density of noise power at the detector output is proportional to

$$\frac{1}{(f_0/Q)^2+4f^2}[D+2\pi^2B(f)].$$

I. Berstein
Inst. for Tech. Physics
Gorki University
Gorki, USSR

G. Gorelik
Inst. for Radio and Electronics
Academy of Sciences of the USSR
Moscow, USSR

* Received by the IRE, July 7, 1956.
[1] J. L. Stewart, "Frequency modulation noise in oscillators," Proc. IRE, vol. 44, pp. 372–376; March, 1956.
[2] I. L. Berstein, "Fluctuations in autooscillating systems and the natural width of oscillator frequency spectrum," *J. Tech. Phys. (USSR)*, vol. II, pp. 305–316; 1941.
[3] G. Gorelik, "On the instrumental and the natural line width of oscillators," *J. Exp. & Theoret. Phys. (USSR)*, vol. 20, pp. 351–355; 1950.
[4] I. L. Berstein, "Amplitude and phase fluctuations in oscillators," *Izvest. Akad. Nauk (USSR)*, ser. phys., vol. 14, pp. 145–173, 1950.

The Waveguide Mode Theory of VLF Ionospheric Propagation*

It has been proposed by Budden,[1] Bremmer,[2] Schuman,[3] and others that the propagation of very low frequency radio waves can be described in terms of the mode theory. In this case, the ionosphere and the ground are regarded as the upper and lower surfaces, respectively, of a parallel-plate waveguide. While the lower boundary (the ground) can be represented by a sharply bounded isotropic medium, the upper boundary (the ionosphere) is diffuse and the medium is anisotropic. However, for frequencies of the order of 16 kc and less it is usually permissible to assume the ionosphere is a sharply-bounded isotropic medium if attention is restricted to the vertically-polarized field at large ranges. With this simplification, the equation to solve for the possible waveguide modes is

$$\left[\frac{(L-i)C-\sqrt{C^2L^2-iL}}{(L-i)C+\sqrt{C^2L^2-iL}}\right] \cdot \left[\frac{(KG-i)C-\sqrt{(K-1)G^2-iG+C^2G^2}}{(KG-i)C+\sqrt{(K-1)G^2-iG+C^2G}}\right] = e^{4\pi ihC/\lambda}e^{-2\pi in} \quad (n=0,1,2,3,\cdots) \quad (1)$$

where C is the cosine of the complex angle of incidence of the rays in the guide;

$$L=\frac{\omega\nu}{\omega_0^2},$$

ω is the angular frequency, ν is the collision frequency and ω_0 is the ionospheric plasma frequency;

$$G=\frac{\epsilon_0\omega}{\sigma}, \qquad \epsilon_0=8.854\times10^{-12},$$

σ is the conductivity of the ground in mhos /meter; $K=\epsilon/\epsilon_0$, ϵ is the dielectric constant of the ground; h is the height of the ionosphere, and λ is the wavelength.

The two factors on the left-hand side of the preceding equation are the reflection coefficients of a wave incident on the ionosphere and on the ground, respectively, at a complex angle whose cosine is C. The exponent $4\pi ihC/\lambda$ on the exponential on the right-hand side can be regarded as a complex phase difference between a direct upgoing ray and one that has been reflected once at the ionosphere and the ground. Consistent modes are then determined by the complex values of C that will satisfy (1) for integral values of n, the mode number. The form of (1) is modified slightly to account for earth curvature but this does not change any essential features of the results.

Using methods based on the calculus of residues, it can be shown that these modes correspond to the contributions from the poles of the contour integral for the distant field of a dipole source. This "Watson-type" residues series yields the following expression for the vertical field E at range d:

$$\frac{E}{E_0}\cong\left[\frac{d/a}{\sin(d/a)}\right]^{1/2}\frac{(d/\lambda)^{1/2}}{(h/\lambda)^{1/2}}e^{-i\pi/4}e^{i2\pi d/\lambda}\cdot\sum_{n=0}^{\infty}S_n^{3/2}e^{-i2\pi S_n(d/\lambda)} \quad (2)$$

where a is the radius of the earth, E_0 is the unattenuated free-space field and $S_n^2=1-C_n^2$ where $C_n(n=0,1,2\cdots)$ are the solutions of (1). For d/a small, it is seen that the attenuation of the modes is determined mainly by the real part of the exponent $i2\pi S_n(d/\lambda)$. The attenuation rate is then proportional to $-ImS_n$ where Im signifies that the imaginary part is to be taken. Values of $-ImS_n$ are shown plotted in Fig. 1

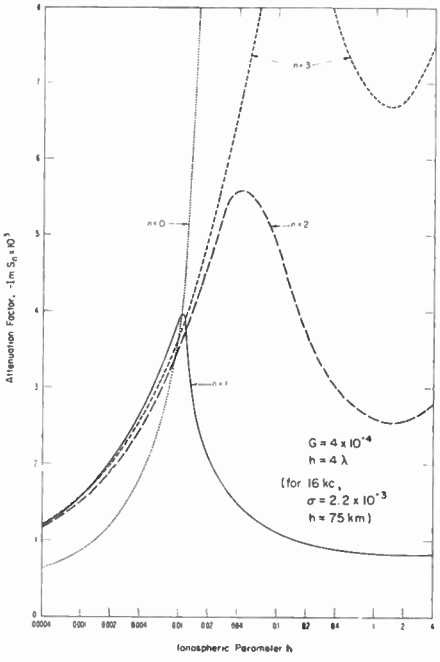

Fig. 1—The attenuation rate as a function of the reciprocal of the ionospheric conductivity for the first four modes.

for mode numbers $n=0$, 1, 2 and 3 as a function L for $G=4\times10^{-4}$, $K=15$, and $h=4\lambda$. At 16 kc this corresponds to a ground conductivity $\sigma=2.2\times10^{-3}$ mhos/meter and the ionospheric height, $h=75$ km. L, which is defined above, can be regarded as a factor proportional to the reciprocal of the conductivity of the ionosphere. At 16 kc it is known to be of the order of 0.4 for the daytime and somewhat smaller for the night.

It is most interesting to note that the zero-order mode has an attenuation which becomes prohibitively high for the larger L values. From the perturbation theory[4] of waveguides with finitely conducting walls, it can be deduced that for small L

$$-\mathrm{Im}\,S_n\cong\frac{\sqrt{G}+\sqrt{L}}{4\sqrt{2\pi}}\left(\frac{\lambda}{n}\right)\cdot\epsilon_n\left[1-\left(\frac{n\lambda}{2h}\right)^2\right]^{-1/2} \quad (3)$$

where $\epsilon_0=1$ and $\epsilon_n=2(n\neq1)$. It can be seen that curves in Fig. 1 are in good agreement with this simple formula if L is less than about 0.004. Beyond this point the curves must be computed from (1) using iterative procedures which will not be described here. For large values of L the attenuation for the modes 1, 2, and 3 becomes somewhat smaller. In the region from $L=0.1$ to 4 and higher, the dominant mode is of order one and not zero as is commonly supposed.

To illustrate the effect of ground conductivity, which is usually assumed infinite, the attenuation coefficient $-ImS_1$ is plotted in Fig. 2 as a function of L for $G=4\times10^{-4}$,

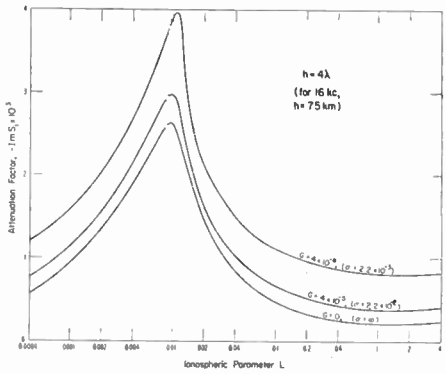

Fig. 2—The attenuation rate for the mode of order one for different ground conductivities.

4×10^{-5} and 0. These correspond to ground conductivities of 2.2×10^{-3}, 2.2×10^{-2}, and ∞, respectively, for 16 kc. The difference between the attenuation rates is most striking. It is significant to observe that the experimental value of the attenuation coefficient deduced by Budden[1] from Weekes' experiment for a daytime path from Cairo to London is 0.00048 which would correspond to $G=0.0004$ and L about 0.3. This conductivity of 0.022 mhos/meter would not be at all unreasonable as an average value for the path. Recent experimental studies of the spectrum of radio atmospherics indicate that the average attenuation rate of frequency components in the 10-kc region is, indeed, higher over an all-land path than for an all-sea path.[5] The ratio between the attenuation rates is of the order of 2.

The detailed calculations for the attenuation and phase constants of the modes for larger orders and a range of ionospheric heights and frequencies will be reported at a later date. It is believed that these extensive results shed considerable light on the behavior of waveguides with "lossy" walls. The conductivity of the ground seems to be a very important parameter in the propagation of vlf waves to great distances. Furthermore, it is believed that the dependence of radio atmospheric waveforms on the geographical location of the source can be explained by the marked influence of ground conductivity on the dominant mode.

J. R. Wait and H. H. Howe
Natl. Bur. of Standards
Boulder, Colo.

* Received by the IRE, September 17, 1956.

[1] K. G. Budden, "The propagation of radio waves to great distances," *Phil. Mag.*, vol. 44, ser. 7, pp. 504–513; May, 1953.

[2] H. Bremmer, "Terrestrial Radio Waves," Elsevier Publishing Co., Amsterdam, Netherlands; 1949.

[3] W. O. Schumann, "Uber die oberfelder bei der aubreitung langer, elecktrischer wellen in system erde-luft-ionosphare und 2 andwendunger," *Z. angew. Phys.* vol 6, pp. 35–43; January, 1954.

[4] H. R. L. Lamont, "Wave Guides," Methuen and Co., Ltd., London, England, ch. 3; 1942.

[5] Personal communications from E. T. Pierce and F. W. Chapman.

Review of Industrial Applications of Heat Transfer to Electronics*

The above article by Professor Kaye[1] has been read with much interest by my associates and myself who have been working on related problems of thermal design here at The Ohio State University during the past eight years. We are pleased that the Editor has invited this contribution in which many significant aspects of component and equipment design are presented.

Professor Kaye's effort to cover an extremely broad field in one article is most commendable. The scope of his presentation may have prompted him to limit himself to a discussion of the so-called "cold-plate technique" in dealing with equipment thermal design, as related to the packaging of groups of components with the incorporation of heat transfer means of predictable performance. I fear that this may give the uninitiated designer the impression that this technique is optimal and universally applicable. In fact, it is superior to others only under a limited number of design conditions and has many disadvantages in respect to cost, manufacturing tolerances, temperature control, and over-all systems penalty in airborne applications. The thermal performance of equipment incorporating other techniques of component heat transfer which do not have these shortcomings is quite as predictable.

Since the publication of Professor Kaye's article, we have received many requests for those of our reports which he has referenced. We should like to bring to the attention of your readers that in recent years about thirty comprehensive reports related to cooling of aircraft electronic and electrical equipment have been prepared at The Ohio State University under Air Force sponsorship. These reports should be of interest to equipment designers since they contain information on cooling systems, component heat transfer, and examples of the application of advanced cooling techniques to airborne equipment. While these reports can be obtained from government agencies only, we shall be glad to supply a list of them, and information on how to procure them, to all interested persons who would direct their requests to the writer.

WALTER ROBINSON
Mechanical Engineering Dept.
The Ohio State University
Columbus 10, Ohio

* Received by the IRE, November 5, 1956.
[1] Joseph Kaye, PROC. IRE, vol. 44, pp. 977–991; August, 1956.

Contributors

Dean F. Babcock (S'43–A'47–M'55–SM'56) was born in Minneapolis, Minn., on March 14, 1924. He attended the University of Minnesota, where he received the B.E.E. degree in 1944. From 1942 to 1946 he served in the U. S. Navy.


D. F. BABCOCK

Mr. Babcock was employed by Engineering Research Associates, Inc., from 1946 until 1951 in the fields of radio communications equipment and digital computer techniques. After joining Collins Radio Company, Western Division, in Burbank, Calif., he became a research and development group manager on communications equipment and systems. At present he is head of the electronic countermeasures group.

He is a member of Tau Beta Pi and Eta Kappa Nu.

❖

Robert G. Baron (A'53) was born in New Haven, Conn., on June 23, 1926. After serving in the U. S. Navy for two years during World War II, he enrolled at the University of Connecticut and received the B.S. degree in electrical engineering in 1950. He received the M.S. degree in electrical engineering from Columbia University in 1955.

His first employment in 1950 was with the M. W. Kellogg Co., Jersey City, N. J., where he was primarily concerned with rocket engine feedback control systems. In December, 1951, he joined the staff of Columbia University Electronic Research Laboratories, New York, N. Y., where he participated in various electronic and electromechanical special purpose computer research programs. Since December, 1955, Mr. Baron has been with the Airborne Computer Laboratory of the International Business Machines Co., Owego, N. Y., where he has been concerned with inertial navigation and digital control systems.


R. G. BARON

❖

Hubert M. Bath was born in Omaha, Neb. on November 22, 1929. He received the degree of bachelor of arts in 1950 from the College of the University of Chicago, and transferring to Purdue University, he received the B.S. and M.S. degrees, both in physics, in 1951 and 1953. During 1952–1953 he held a research fellowship from the Purdue Research Foundation, doing work on the heat treatment of germanium.


H. M. BATH

Since 1953, Mr. Bath has been associated with the Semiconductor Laboratory of Hughes Aircraft Company, engaged in the study of diode characteristics, and in the measurement of the electrical properties of semiconductors.

He is a member of the American Physical Society.

❖

For a photograph and biography of Kern K. N. Chang, see page 104 of the January, 1955 issue of PROCEEDINGS.

❖

For a photograph and biography of John P. Costas, see page 1882 of the December, 1956 issue of PROCEEDINGS.

❖

Melvin Cutler was born in Beaumont, Tex., on December 18, 1923. He received the B.S. degree in chemistry from City College of New York in 1943. His graduate studies in physical chemistry at Columbia University led to the A.M. degree in 1947 and the Ph.D. degree in 1951.


M. CUTLER

He has been engaged in semiconductor research and development at Hughes Aircraft

Company from 1951 to the present time. His main fields of activity have been semiconductor surfaces and device theory.

Dr. Cutler is a member of Sigma Xi, Phi Beta Kappa, the American Chemical Society, and the American Physical Society.

❖

James C. Hathaway (A'50–M'55) was born in Chisholm, Minn., on July 14, 1925. He received the B.E.E. degree at the University of Minnesota in 1946, and the M.S. degree at Harvard University in 1949.

J. C. HATHAWAY

He was employed by the Collins Radio Company in Cedar Rapids, Iowa, from 1946 to 1948. During this period, he worked on the development of vhf communications equipment. After receiving the Master's degree in 1949, he joined the Western Division of Collins Radio Company, in Burbank, Calif.

Here he has been engaged in development work on guided missile control receivers, ideal detection receivers for aircraft data transmission systems, and electromechanical components.

At present he is head of the research and development department concerned with development of mechanical filters, and special components and materials for communications equipment.

Mr. Hathaway is a member of Tau Beta Pi and Eta Kappa Nu.

❖

William H. Huggins (S'39–A'44–SM'55–F'57) was born on January 11, 1919, at Rupert, Idaho. He received the B.S. and M.S. degrees in electrical engineering from Oregon State College in 1941 and 1942, respectively, where he subsequently served as a research associate, studying precipitation-static radio interference, and as an instructor in electrical engineering. In 1944 he joined the Radio Research Laboratory, Harvard University. From 1946 to 1954, Mr. Huggins served as a civilian engineer with the Air Force Cambridge Research Center. In 1953, he received the Science Doctorate from Massachusetts Institute of Technology with a dissertation on "A Theory of Hearing." Since 1954, he has been a Professor of Electrical Engineering at The Johns Hopkins University and a consultant to the RAND Corporation.

W. H. HUGGINS

Dr. Huggins received the Browder J. Thompson Memorial Award for 1948 for his papers on broad-band microwave short-circuits, and (as co-author with David Middleton) the 1955 Annual Award of the National Electronics Conference. In 1954, he received the Air Force Decoration for Exceptional Civilian Service.

He is currently editor of IRE TRANSACTIONS ON CIRCUIT THEORY.

❖

Martin Katzin (J'27–A'29–M'42–SM'43–F'55) was born in New York, N. Y. on February 17, 1908. He received the B.S.E. degree in electrical engineering in 1928 and the degrees of M.S.E. in electrical engineering and B.S.E. in mathematics in 1929 from the University of Michigan. He was a research engineer with RCA Communications, Inc. from 1929 to 1941, during which time he was engaged in the development of high-frequency receiving systems, and in wave propagation and antenna studies. He was employed at the Naval Research Laboratory as an electronics consultant from 1941 to 1955, where he engaged in basic radar, countermeasures, antenna and wave propagation studies, and also organized and headed the wave propagation branch.

M. KATZIN

Since 1955, Mr. Katzin has been engaged in a consulting engineering practice in Washington, D. C. He recently founded the Electromagnetic Research Corporation, of which he is President.

Mr. Katzin holds membership in the American Physical Society, American Meteorological Society, American Geophysical Union, American Association of Physics Teachers, Acoustical Society of America, Association for Computing Machinery, Society for Industrial and Applied Mathematics, Armed Forces Communications and Electronics Association, Sigma Xi, and the Arctic Institute of North America. He is a registered professional engineer in the State of Maryland in the District of Columbia.

❖

E. L. Maxwell was born in Fort Collins, Colo., on December 24, 1930. He acquired his first training in electronics through work with amateur radio. In 1950 he obtained his First-Class Radiotelephone License and worked in broadcast radio for a total of about three and a half years. From May, 1951 to August, 1952, he was on active duty with the Air Force as a Radio Maintenance Technician. During this period he attended the advanced Radio Technician School at Scott Field, Ill.

E. L. MAXWELL

He has at present partially completed his undergraduate work toward the B.S. degree in electrical engineering at Colorado University.

In 1955 he joined the National Bureau of Standards Central Radio Propagation Laboratory in Boulder, Colo., where he has been working on noise studies and radio system problems.

❖

Herbert P. Raabe (A'51–SM'54) was born in Halle, Germany, on August 15, 1909. He received the Dipl.Ing. degree in 1936, and the Dr.Ing. degree in 1939, both from the Technical University of Berlin.

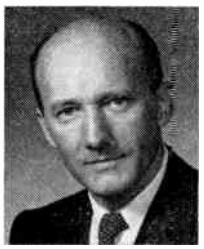

H. P. RAABE

From 1936 to 1945, he was employed in research and teaching in the communication technique department of the same University. From 1938 to 1945 he also conducted research work at the Heinrich Hertz Institut für Schwingungsforschung.

During 1946 he was employed by the Bureau of Communication Technique in Berlin.

From 1947 to 1956 he was a consultant to the Wright Air Development Center in Dayton, Ohio, in the fields of microwave circuitry and radar systems.

In September, 1956, Dr. Raabe joined General Mills, Inc., Mechanical Division, Minneapolis, Minn.

❖

Arthur D. Watt (SM'54) was born in Cedar Lake, Ind., on November 2, 1920. He received the B.S.E.E. degree from Purdue University in 1942. From 1942 to 1951 he was employed at the Naval Research Laboratory where he worked on transmitters, receivers, antennas, facsimile, television, communication theory, and communication system design problems. While at NRL, he took graduate work at the University of Maryland.

A. D. WATT

In 1951 he joined the National Bureau of Standards Central Radio Propagation Laboratory in Boulder, Colo., where he has worked on modulation and radio system problems including studies to optimize utilization of the frequency spectrum and signal to noise studies.

Mr. Watt is a member of HKN, a charter member of the Boulder RESA branch, and is active in URSI and CCIR work.

IRE News and Radio Notes

Calendar of Coming Events

Symposium on Communication Theory and Antenna Design, Hillel House, Boston Univ., Boston, Mass., Jan. 9–11

New York Section Winter Symposium on Engineering Management, Eng. Soc. Bldg. Auditorium, New York City, Jan. 11

Symposium on Reliability & Quality Control in Elec., Statler Hotel, Wash., D. C., Jan. 14–15, 1957

Symposium on VLF Waves, Boulder Labs., Boulder, Colo., Jan. 23–25

Automatic Coding Symposium, Franklin Institute, Philadelphia, Pa., Jan. 24–25

IAS Convention, Sheraton-Astor Hotel, New York City, Jan. 28–31

Electronics in Aviation Day, New York City, Jan. 30

Operations Research Symposium, U. of Pa., Philadelphia Pa., Feb. 7

West Coast Convention of Audio Eng. Soc., Ambassador Hotel, Los Angeles, Calif., Feb. 7–8

PGME Symposium on Recording of Heart Sounds, Univ. of Buffalo Medical School, Buffalo, N. Y., Feb. 14

Conference on Transistor Circuits, Philadelphia, Pa., Feb. 14–15

Western Joint Computer Conference, Statler Hotel, Los Angeles, Calif., Feb. 26–28

National Biophysics Conference, Columbus, Ohio, March 4–6

EJC Second Annual Nuclear Science and Engineering Congress, Philadelphia, Pa., March 11–14

IRE National Convention. Waldorf-Astoria and New York Coliseum, New York City, March 18–21

British Radio & Electronic Component Show, Grosvenor House and Park Lane House, London, England, Apr. 8–11

Industrial Electronics Educational Conference, Ill., Inst. of Tech., Chicago, Ill., April 9–10

Ninth Southwestern Regional Conference & Show, Shamrock-Hilton Hotel, Houston, Tex., April 11–13

National Simulation Conference, Shamrock-Hilton Hotel, Houston, Tex., April 11–13

PGTRC National Telemetering Symposium, Philadelphia, Pa., April 14–16

Symposium on Role of Solid State Devices in Electric Circuits, Engrg. Society Bldg., New York City, April 23–25

Region Seven Technical Conference & Trade Show, San Diego, Calif., April 24–26

Eleventh Annual Spring Television Conference, Engrg. Society Bldg., Cincinnati, Ohio, April 26–27

Electronic Components Conference, Morrison Hotel, Chicago, Ill., May 1–3

PGMTT National Meeting, Western Union Auditorium, New York City, May 9–10

IRE Announces Annual Awards

The IRE has announced the recipients of three of its annual awards for 1957. The actual presentation of these awards will be made during the IRE National Convention, which will be held March 18–21 in New York City.

The Morris Liebmann Memorial Prize Award will go to O. G. Villard, Jr., Professor at Stanford University, Stanford, Calif., "for his contributions in the fields of meteor astronomy and ionosphere physics which led to the solution of outstanding problems in radio propagation." The award is made annually to a member of the IRE for a recent important contribution to the radio art.

Donald Richman, Supervising Engineer at Hazeltine Corp., Little Neck, N. Y., will be the recipient of the Vladimir K. Zworykin Prize Award "for contributions to the theory of synchronization, particularly that of color subcarrier reference oscillator synchronization in color television." This award is made annually for outstanding contributions to electronic television.

The Harry Diamond Memorial Prize Award will be given to Georg Goubau, Physicist at the Signal Corps Engineering Labs., Ft. Monmouth, N. J., "for his many contributions in ionospheric research and circuit theory and for his discovery of the surface wave transmission principle." The award is given annually to a person in government service for outstanding contributions in the field of radio or electronics as evidenced by publication in professional journals.

IRE Elects Officers for 1957

At its meeting on November 14, 1956, the Board of Directors announced the election of the following IRE officers and directors:

President, 1957: John T. Henderson, Principal Research Officer of the National Research Council, Ottawa, Canada.

Vice-President, 1957: Yasujiro Niwa, President of Tokyo Electrical Engineering College, Tokyo, Japan.

Directors-Elected-at-Large, 1957–1958: D. E. Noble, Vice-President in Charge, Communications and Electronics Division of Motorola, Inc., Chicago, Ill.; and Samuel Seely, Professor and Head of the Department of Electrical Engineering, Case Institute of Technology, Cleveland, Ohio.

Regional Directors, 1957–1958: Region Two, F. A. Polkinghorn, Bell Telephone Laboratories, Whippany, N. J.; Region Six, Kenneth Newton, Bendix Aviation Corp., Kansas City, Mo.; Region Eight, A. B. Oxley, RCA Victor Company, Ltd., Montreal, Canada.

In Region Four, the nominee receiving the greatest number of qualified votes for Regional Director was disqualified by moving from the Region. Therefore, the Board of Directors voted to hold a second election in Region Four.

IRE National Convention Meets at Waldorf & Coliseum

Plans are under way for the 1957 IRE National Convention, which will be held at the Waldorf-Astoria Hotel and the New York Coliseum, New York City, March 18–21. Because of the increased IRE membership of 55,000 and many new developments in the radio-electronics field, the convention is again expected to draw a huge gathering of engineers and scientists, and a record-breaking display of 840 informative technical exhibits.

A comprehensive program of fifty-five technical sessions is being set up by the Technical Program Committee with the assistance of all the IRE Professional Groups. Thirty-three sessions will be held at the Waldorf; the remainder, at the Coliseum. The evening of the 19th will be devoted to a special session on "Future Use of Air Space" and "Microminiaturization—The Ultimate Technique." Full program details will be announced in the March issue of the PROCEEDINGS OF THE IRE.

All registration will take place on arrival either at the Waldorf or at the Coliseum. Registration fees are $1.00 for each IRE member, $3.00 for each non-member. Payment of the fee enables attendance at all sessions and exhibits.

During the convention the annual meeting will take place. Haraden Pratt, IRE Secretary, and W. R. G. Baker, IRE Treasurer, will present their annual reports. The guest speaker will be Donald G. Fink, Director of Research of the Philco Corporation and Editor of the IRE, who will discuss "Electronics and the IRE—1957."

This year the exhibition will be held in the recently opened New York Coliseum, conveniently located at Columbus Circle in midtown Manhattan. All four floors will be set aside for the use of the exhibitors at the Radio Engineering Show. For registrants' convenience, computers and communications exhibits will be grouped together on the first floor; component parts exhibits on the second; instruments, microwave and components exhibits on the third; and production tools, materials and services exhibits on the fourth floor.

The "get-together" cocktail party during the afternoon of the 18th will head the list of social events, climaxed by the annual banquet in the Grand Ballroom of the Waldorf on the evening of the 20th. The banquet will feature the IRE award winners for 1957. On this occasion, newly-elected IRE Fellows will also be honored and Maj. Gen. J. D. O'Connell, Chief Signal Officer, U. S. Army Signal Corps., will speak on their behalf. The toastmaster will be Rear Admiral C. F. Horne of Convair.

A guided tour of a modern art gallery, a choice of two popular Broadway plays, a trip to nearby West Point, a visit to *Living for Young Homemakers* magazine, a sightseeing tour of New York City, and a luncheon-fashion show will provide a varied and interesting schedule for members' wives and families.

Grants Are Available to High School Science Teachers

Grants totaling $4,065,000 have been awarded by the National Science Foundation to sixteen colleges and universities in the United States to support academic-year institutes designed to help high-school science teachers improve their knowledge of science subject matter.

In announcing the awards, A. T. Waterman, Director of the Foundation, an independent agency of the federal government, said that an estimated 750 high-school science and mathematics teachers would be enrolled in the institutes, beginning September, 1957. Each teacher will pursue a program of study in the sciences and mathematics planned especially for him and conducted by leaders noted not only for competence in their fields but for skill in presentation. The grants will provide stipends of $3,000 each to approximately fifty teachers in each institute. Additional allowances for dependents and travel will also be provided.

A list is appended showing the institutes receiving grants, and the persons to whom inquiries or applications should be addressed: Dean Francis Keppel, Graduate School of Education, Harvard University, Cambridge, Massachusetts; Professor J. S. Richardson, College of Education, Ohio State University, Columbus 10, Ohio; Professor J. H. Zant, Department of Mathematics, Oklahoma Agricultural and Mechanical College, Stillwater, Oklahoma; Professor S. E. Williamson, Department of Science Education, Oregon State College, Corvallis, Oregon; W. H. Powers, Arts and Sciences Extension, Pennsylvania State University, University Park, Pennsylvania; Professor H. M. Bacon, Department of Mathematics, Stanford University, Stanford University, California; Dean T. F. Hall, Washington University, St. Louis, Missouri; Professor E. P. Northrop, Mathematics Staff, University of Chicago, Chicago 37, Illinois; Professor W. E. Briggs, Department of Mathematics, University of Colorado, Boulder, Colorado; Professor Joseph Landin, Department of Mathematics, University of Illinois, Urbana, Illinois; Professor F. D. Miller, Department of Astronomy, University of Michigan, Ann Arbor, Michigan; Professor E. C. Markham, Department of Chemistry, University of North Carolina, Chapel Hill, North Carolina; Professor R. C. Anderson, Department of Chemistry, University of Texas, Austin 12, Texas; Professor T. J. Parmley, Department of Physics, University of Utah, Salt Lake City, Utah; Professor J. W. Cole, Department of Chemistry, University of Virginia, Charlottesville, Virginia; Professor C. H. Sorum, Department of Chemistry; University of Wisconsin, Madison 6, Wisconsin.

National Symposium on Telemetering

The Professional Group on Telemetry and Remote Control will sponsor a National Symposium on Telemetering, April 14–16, 1957, at the Sheraton Hotel, Philadelphia, Pa.

For information regarding exhibits and papers, write to L. P. Clark, Tele-Dynamics Inc., 32 & Walnut St., Philadelphia 4, Pa.

Third East Coast Conference Features Student Symposium

Fifteen hundred persons registered for the Third Annual East Coast Conference on Aeronautical and Navigational Electronics, held in Baltimore, Md., October 29–30, 1956. The conference, sponsored by the IRE Baltimore Section and the Professional Group on Aeronautical and Navigational Electronics, was held during the week of October 29–November 4, a week proclaimed as "Airborne Electronics Week" by the governor of Maryland and the mayor of Baltimore.

One of the highlights of the conference, which contained seven technical sessions, was a student symposium on "The Engineer in Airborne Electronics," an innovation at this conference. Undergraduate students from Johns Hopkins University, University of Maryland, George Washington University and the Naval Academy participated in a panel round table discussion with S. W. Herwald, Westinghouse Electric Corp.; G. J. Strickroth, Glenn L. Martin Co.; D. M. Allison, Bendix Radio Division; Joel Jacobsen, Aircraft Armaments, Inc.; and J. M. Pearce, Hoover Electronics Co. The discussion was moderated by Ferdinand Hamburger of Johns Hopkins University.

Four hundred persons attended the conference banquet, at which R. E. Horner, Acting Assistant Secretary of the Air Force (Research and Development) was the principal speaker. K. C. Black, banquet toastmaster, introduced Joanne Alford of Glenn L. Martin Co. as "Miss Airpower of 1956."

Ladies' activities featured a tour of historic Annapolis.

Baruch Is Named Outstanding Young Electrical Engineer

The Jury of Award for the Eta Kappa Nu Recognition of Outstanding Young Electrical Engineers met in New York on October 20, 1956 and named J. J. Baruch (S'48–M'50), of Boston, Mass., winner for the year of 1956. Honorable mention was awarded to R. B. Seidel of Wayne, Pa.

Dr. Baruch, a graduate of M.I.T., is Vice-President and Director of New Products Development for Bolt, Beranek and Newman Inc., a consulting firm in Cambridge Mass. He is also associated with M.I.T. in a part-time teaching capacity.

During World War II Dr. Baruch served in the European and Pacific theaters in chemical warfare, explosives and demolitions instruction, and in carrier-radio operation.

In 1946 he enrolled in the cooperative course in electrical engineering at M.I.T., majoring in instrumentation. His M. S. thesis, "The Photoelastic Analysis of Dynamic Stresses," was conducted jointly under the mechanical and electrical engineering Departments. He was awarded the S.B. and S.M. degrees simultaneously in June, 1948. He received fellowships in acoustics for the years 1948–1950 from Celotex Corp. and Armstrong Cork Corp., and completed work for his Sc.D. degree with the thesis, "Instrumentation for Acoustic Transmission," at M.I.T. He served as assistant professor in electric instrumentation at M.I.T. until 1955.

Dr. Baruch is a member of Sigma Xi, Tau Beta Pi, and Eta Kappa Nu, an Associate of the American Institute of Management, and a Fellow of the Acoustical Society of America. He holds patents on nine devices and systems, principally in the field of acoustics.

He was chairman of the IRE Professional Group on Audio in 1952–1953.

PGVC Held National Conference at Detroit

One conference session consisted of a panel discussion on "Single Side Band AM for Mobile Communications." *Standing, left to right*—Austin Bailey, moderator of the discussion; J. E. Keller and Henry Magnuski, participants. *Seated, left to right*—C. B. Plummer, K. L. Neumann and J. S. Smith, also panel participants. E. L. White of Microwave Services, Inc. spoke on radio communications at the annual banquet.

Physics Journal Will Appear

Annals of Physics, a new monthly journal of physics, under the editorship of P. M. Morse, Professor of Physics, Massachusetts Institute of Technology, has been announced by Academic Press, New York.

Original articles on research in any branch of physics will be welcome. *Annals of Physics* hopes to provide a medium for the publication of important articles which are internally complete and thus are generally understandable to professional physicists working in other fields.

The first issue is scheduled for release in April, 1957. Manuscripts should be submitted to the Editor, Professor P. M. Morse, Department of Physics, Massachusetts Institute of Technology, Cambridge 39, Massachusetts. Those received up to December, 1956 will be considered for inclusion in the initial issue.

IRE Sponsors Three Sessions at IAS New York Convention

The Institute of Aeronautical Sciences will hold its convention at the Sheraton-Astor Hotel January 28–31. The IRE Professional Group on Aeronautical and Navigational Electronics, and the Radio Technical Commission for Aeronautics will sponsor several sessions at the convention.

The Professional Group on Aeronautical and Navigational Electronics will sponsor a session on electronics during the morning of January 30, a session on air space utilization for air traffic control and national defense on the afternoon of the same day, and a session on self-contained air navigation systems during the morning of January 31.

D. S. Little of American Airlines will be the chairman for the session on electronics. H. K. Morgan, Bendix Aviation Corp., will open the session with a paper on common system standards. V. I. Weihe, Air Transport Association of America, will discuss how and why airborne computers will reduce cockpit workload, and Luther Davis, Jr., Raytheon Manufacturing Co., will deliver a paper entitled *Components Development Influencing Aviation Electronics*. F. W. Bushman, Boeing Airplane Co., will deliver the concluding paper of the session on antenna system problems with high speed aircraft.

The afternoon session on air space utilization will be presided over by James Anast, Systems Planning Advisor to the President for Aviation Facilities Planning. D. D. Thomas, Office of Air Traffic Control, Civil Aeronautics Administration, will speak on *Air Space Use for Air Traffic Control and Air Defense. Common or Uncommon Systems: Air Traffic Control and Air Defense?* will be the topic of D. R. Israel and Herbert Sherman, Lincoln Laboratory. John Dickie, Ministry of Transport and Civil Aviation, will also present a paper.

Chairman of the following day's session on self-contained air navigation systems will be L. I. Davis of Holloman Air Development Center at Holloman Air Force Base. During this session R. W. West, DCS/D, United States Air Force Headquarters, will speak on *Operational Needs and Use for Self-Contained Navigation Systems;* Walter Wrigley, R. B. Woodbury and John Hovorka, M.I.T. Instrumentation Lab., on *Inertial Guidance;* W. J. Tull, General Precision Lab., on *Doppler Navigation;* and V. E. Carbonara, Kollsman Instrument Corp., on *Automatic Celestial Navigation.*

Professional Group News

IRE Annexes Five Chapters

The following chapters of Professional Groups were approved by the IRE Executive Committee at its meeting of November 13th: PG on Audio, Baltimore Section; PG on Broadcast Transmission Systems, San Francisco Section; PG on Component Parts, Buffalo-Niagara Section; PG on Electron Devices, Joint New York, Northern New Jersey and Long Island Section; and PG on Military Electronics, Boston Section.

Over One Thousand Register at PGED Washington Meeting

The Second Annual Technical Meeting of the IRE Professional Group on Electron Devices was held at the Shoreham Hotel in Washington, D. C., October 25–26, 1956. 1050 persons registered at the meeting.

Following the custom adopted the preceding year, a single session was held on the morning of the first day. This session was given over to a series of four invited papers on recent developments in electron devices. Speakers and their topics were: R. Kompfner, Bell Telephone Laboratories, *Microwave Devices;* D. W. Epstein, RCA, *Display and Storage Devices;* C. L. Hogan, Harvard, *Ferroelectric and Ferromagnetic Devices;* H. L. Owens, Texas Instruments, *Transistors in 1956.*

Following the first session a luncheon was held at which William Shockley, a recent Nobel Prize winner, gave an informal talk during which he compared graphically the ratio of growth, in terms of commercial production, between tubes and transistors from their beginnings. Extrapolation of production curves indicate that the annual production of transistors will equal that of tubes in about three years.

W. Shockley, who recently was named a Nobel Prize winner for his part in the development of the transistor, compares the electron device with a fifty-year old audion radio tube held by T. Liimatainen (*left*), general chairman of the PGED technical meeting.

On Thursday afternoon three technical sessions were held simultaneously, on the subjects of microwave tubes, materials and techniques, and high-frequency semiconductor devices. That evening a cocktail party and informal dinner were held in the hotel.

The program on Friday consisted exclusively of technical meetings. Those in the forenoon were on microwave tubes, two-terminal solid-state devices, and advances in electron tube design. In the afternoon, sessions were held on microwave tubes, semiconductor power devices and analysis, and display tubes and related circuits. The total number of contributed papers was sixty.

The general committee in charge of the technical meeting consisted of T. M. Liimatainen, *Chairman;* H. L. Owens, *Vice-Chairman;* R. L. Pritchard, *Technical Program Chairman;* A. K. Wing, *Secretary;* E. L. Steele, *Publiactions;* P. Colviner, *Publicity.* J. H. Wright served as Chairman of the Local Arrangements Committee, assisted by H. D. Arnett, R. W. Grantham, T. E. Hanley, C. P. Marsden, H. J. Peake, and W. E. Waters.

Magnetic Amplifiers Conference Posts Call for Papers

The IRE Professional Group on Industrial Electronics and the AIEE Magnetic Amplifier Committee will sponsor a Special Technical Conference on Magnetic Amplifiers at the Hotel Penn Sheraton Hotel in Pittsburgh, Pa., September 4–6, 1957.

The technical program will consist of four sessions devoted to basic problems and techniques of design, development, manufacturing and testing; magnetic amplifier applications; computing and switching applications of saturation magnetic devices and circuits; papers of general interest which fall outside the above topics (such as ferrite devices, frequency multipliers, reference devices, etc.).

The deadline for receipt of papers is January 15, 1957. This should include a 200-word abstract. The deadline for final manuscripts will be June 11, 1957. Papers should be submitted to the Technical Program Chairman: G. F. Pittman, Jr., Westinghouse Electric Corp., P.O. Box 10596, Pittsburgh 35, Pa.

It is expected that a "Proceedings" of the papers presented at this conference will be published.

PGMTT Plans Annual Meeting

The 1957 annual meeting of the IRE Professional Group on Microwave Theory and Technique will take place at the Western Union Auditorium, New York City, May 9–10, 1957. The meeting will serve to report on recent advances in the microwave art with special emphasis on microwave ferrite devices and their applications, nonreciprocal propagation in gas media and microwave solid-state devices. A round-table discussion on design limitations of microwave ferrite devices is scheduled for the last day of the meeting.

The deadline date for those wishing to contribute papers to the meeting is March 1, 1957. All papers should be sent to S. Weisbaum, Technical Program Chairman, Bell Telephone Laboratories, Murray Hill, N. J.

PGPT Plans First Symposium—Subject: Automation

The First National Symposium on Production Techniques will be held at the Hotel Willard, Washington, D. C., June 6–7. The

symposium on "Production Techniques at a Glance" will be sponsored by the IRE Professional Group on Production Techniques. The program will consist of technical sessions and panel discussions, and exhibits will be displayed on the ballroom floor of Hotel Willard.

Heading symposium committees are: A. A. Lawson, Melpar, General Chairman; J. M. Lee, Bureau of Ordnance, Vice-Chairman; S. Levine, Melpar, F. Israel, Aerovox, and G. Shapiro, NBS, Technical Program and Exhibits; J. P. Nigro, NBS, and F. Israel, Aerovox, Local Arrangements and Finance; and H. S. Wolf, Martin-Balto, Publicity and Publications. The advisory board consists of R. R. Batcher, J. M. Bridges, L. M. Clement, R. I. Cole, R. L. Henry, and A. R. Gray.

Call for Papers, Electronic Components Symposium

Authors wishing to present papers at the 1957 Electronic Components Symposium, May 1–3, Chicago, Ill., should submit 150 to 200 word abstracts by January 16 to V. H. Disney, Electrical Engineering Dept., Armour Research Foundation, 10 W. 35 St., Chicago, Ill.

Obituary

J. T. Filgate, Sr., former president of the Rand Electronics, Inc. of Stamford, Connecticut, died recently. He had been a paraplegic for over a year.

Mr. Filgate, who studied at George Washington University and received a master's degree in communications engineering from Yale University, had been employed, successively, by the U. S. Signal Corps at Washington, D. C., Hawaii and Fort Monmouth, N. J.; National Carbon Company; General Motors Radio Corporation; United American Bosch Company; and Westinghouse Electric & Manufacturing Company. His work was primarily with mobile radio receivers.

Mr. Filgate, who rose from Associate to Senior Member rank in the IRE, was an active member of the Professional Groups on Instrumentation, Medical Electronics and Nuclear Science.

Technical Committee Notes

The **Audio Techniques** Committee met at IRE headquarters on October 30 with Chairman Iden Kerney presiding. The committee continued reviewing the Proposed Standards on Audio Techniques: Definitions of Terms.

Chairman W. A. Lynch presided at a meeting of the **Circuits** Committee on October 19 at IRE Headquarters. The entire meeting was devoted to review of the Proposed Standard on Linear Active Networks: Definitions of Terms Related to Basic Feedback Theory.

The **Information Theory and Modulation Systems** Committee met at IRE Headquarters on November 2 with Chairman J. G. Kreer, Jr. presiding. The major portion of the meeting was devoted to review of the proposed definitions of terms.

Chairman H. R. Mimno presided at a meeting of the **Navagation Aids** Committee held at IRE Headquarters on October 15. The Proposed Standard on Navigation Aids: Methods of Testing the VHF Omni-Directional Radio Range (VOR) was discussed and amended. Having nearly completed all formally scheduled projects, the committee undertook a very brief exploratory discussion of related devices and systems. The following list of topics received introductory mention: TACAN (including components of VORTAC); airborne VOR receiving-equipment; vhf and uhf direction-finders; automatic direction finders; ILS; airborne ILS receiving-equipment; LORAN; CONSOLAN; DECCA; and long-distance aids. It should be understood that this list is not a proposed program of Navigation Aids Committee activity.

The **Radio Transmitters** Committee met at IRE Headquarters on November 9 with Vice-Chairman A. E. Kerwien presiding. It was announced that at the request of the Radio Transmitters Committee the Standards Committee has now appointed M. R. Briggs as chairman of an Ad Hoc Committee (20.10) for Transmitter-Receiver Standards Coordination. This Ad Hoc Committee is charged with the determination of whether a technical committee should be established to resolve common questions in this area, particularly regarding microwave relay systems. Representation on this committee will be from the Radio Receivers, Radio Transmitters, Information Theory and Modulation Systems, Antennas and Waveguides, and Wave Propagation Committees. It is expected that the committee will be organized and operating shortly.

Chairman D. E. Maxwell presided at a meeting of the **Recording and Reproducing** Committee on October 18 at IRE Headquarters. R. C. Moyer, Chairman of Subcommittee 19.1 on Magnetic Recording, reported that some 180 definitions were about ready for consideration by the full subcommittee.

L. Thompson, Chairman of Subcommittee 19.2 on Mechanical Recording, reported that his subcommittee plans to complete the standards proposal on mechanically-recorded frequency records for submission to the main committee at their December meeting.

T. G. Veal, Chairman of Subcommittee 19.3 on Optical Recording, reported that his subcommittee is reviewing 81 terms on optical recording and hopes to submit them to the main committee at their November meeting.

H. E. Roys, Chairman of Subcommittee 19.5 on Flutter, reported that his subcommittee is planning to review the IRE Standard on Recording and Reproducing: Methods for Determining Flutter Content.

The **Solid State Devices** Committee met at IRE Headquarters on October 24 with J. P. Jordan presiding. J. M. Early reported that the Proposed Standards on Methods of Test for Semiconductor Devices for Large Signal Applications should be ready shortly for consideration by the main committee. The remainder of the meeting was devoted to the reports of the various subcommittees on their present and future activities.

Chairman M. W. Baldwin presided at a meeting of the **Standards** Committee at IRE Headquarters on November 8. The Proposed Standards on Piezoelectric Crystals: The Piezoelectric Vibrator: Definitions and Methods of Measurement was discussed, amended and unanimously approved.

The Proposed Standard on Electron Tubes: Cathode Ray Tube Definitions was discussed, amended and unanimously approved.

Books

Vacuum-Tube Circuits and Transistors by L. B. Arguimbau with Transistor Contributions by R. B. Adler

Published (1956) by John Wiley & Sons, Inc., 440 Fourth Ave., N. Y. 16, N. Y. 637 pages+8 index pages+vii pages. 612 figures+484 problems. 5¾×8¼. $10.25.

This book is a rather extensive revision of the 1948 book by Mr. Arguimbau which was reviewed on p. 1272 of the October, 1948 issue of the PROCEEDINGS. Although the number of pages are about the same, two chapters on transistors have been added, and transistor material has also been interspersed through the other chapters. The main emphasis of the book is on tube and transistor circuits as employed for communications. Related communication material on amplitude modulation, frequency modulation, and television are also included. Circuits as employed in instrumentation and industrial control are not included.

Mr. Arguimbau's provocative style of writing has been retained in this edition and is intended to help the reader to see through the fundamental processes treated. The authors have made a "strong effort to get clear and simple yet satisfying answers to difficult questions." This effort has been aided by extensive use of figures, problems, and examples.

This book will be valuable to those who wish to supplement their knowledge of communications with additional reading and study. As a textbook it will be useful for a general treatment of the field as contrasted with detailed authoritative presentations found in other books.

L. J. GIACOLETTO
Scientific Laboratory
Ford Motor Company
Dearborn, Michigan

Communication Engineering, 3rd ed. by W. L. Everitt and G. E. Anner

Published (1956) by McGraw-Hill Book Co., Inc., 330 W. 42 St., N. Y. 36, N. Y. 625 pages+8 index pages+9 pages of appendix+xi pages. Illus. 9¼×6¼. $9.00.

After a lapse of almost twenty years, one of the classic electrical-engineering textbooks of the prewar era has appeared in a new third edition. One has only to reflect briefly on the astonishing growth of the field of communications engineering since 1937, the date of the previous edition, to appreciate some of the revision problems which must have confronted Dr. Everitt and his co-author, Professor Anner. Those who know the second edition (and this must include an impressive number of persons) will recall that roughly half the book was devoted to networks and lines, and the remainder to vacuum circuits that are basic to receiver and transmitter practice. The subject field then was reasonably well rounded out with a chapter on radiation and one on electromechanical devices.

In the current edition, the sole remaining material on electronic circuits is a new chapter called "Linear Amplifiers," which serves to introduce broadband amplifiers. The main theme of the book is now concentrated in the area of networks and lines in the steady state. Thus a strong resemblance prevails between the new edition and the first half of the previous edition. Although considerable rewriting has been done, and new material added, the chapter headings remain unchanged for the most part, and an appreciable amount of material in the retained chapters is carried over from the second edition. A chapter on basic circuit theory is followed by the familiar headings: "Resonance," "Bridge Networks," and "Wave Filters." This selection of topics is rounded out to good advantage with a new chapter dealing with iterative networks. The material on lines is separated out of the network sequence and the old chapters entitled "The Infinite Line and Reflection" are augmented by a new chapter titled "Lines of Low Loss." A large amount of valuable new material has been assembled in the area of impedance transformation. The old chapter bearing this title is retained and two new chapters are added, one dealing with stub matching and the other with various aspects of broadband matching. The book concludes with three chapters bearing the headings: "Equalization," "Linear Amplifiers," and "Electromechanical Coupling," two of which appeared in the second edition.

It is observed that the scope of communications engineering subject matter encompassed is considerably smaller than in the previous edition. In the preface of the new edition, the authors take note of the "explosive" expansion of the subject field during the past two decades, and express some doubt about the appropriateness of the title, but nevertheless, decide to retain it. The desire to preserve identity with the well-known second edition is entirely understandable, but the present scope of coverage does not seem, to this reviewer, to begin to represent what the title implies. The authors state as their objective concentration on the area that is basic to all other divisions of communications, "namely, the fundamentals of linear-network analysis and synthesis, including the use of unilateral elements." This statement, together with the title, is quite likely to lead a reader to expect more than the book actually covers. One does not succeed in finding any organized treatment of modern network synthesis, nor is any use made of unilateral elements, for the chapter concerned with amplifier material treats only the passive aspects of interstage coupling networks.

The chief criticism of the book as a whole, however, in this reviewer's opinion, is that the viewpoints and the over-all philosophy remain essentially what they were in the previous edition. Despite an introductory chapter that surveys some of the modern methods of analysis that have been developed during the past decade or so, one detects no systematic use being made of them in the core of the book. The most disappointing example of this is the failure to develop effectively the unifying concept of the complex frequency and to exploit the countless advantages of the complex-plane representations of network functions. Here is a beautiful tool for unifying and simplifying linear network theory—one that is simple in concept but which can afford the student real depth of insight. It is true that zeros and poles are mentioned in scattered parts of the book, namely, in the survey chapter and in the chapter on amplifiers; but no organized use is made of the complex plane in the main theme of steady-state analysis. An associated aspect of this criticism concerns the heavy emphasis on the steady state to the neglect of time-domain concepts.

This book is very well written and the ideas that it expresses are carefully and rigorously developed. For the reader seeking a traditional treatment of communications networks and lines, this is an excellent choice. It will not, however, satisfy the needs of a reader seeking a treatment, at the undergraduate level, of network theory from a modern point of view.

W. A. Lynch
Polytechnic Institute of Brooklyn
Brooklyn, N. Y

Spectroscopy at Radio and Microwave Frequencies by D. J. E. Ingram

Published (1956) by Philosophical Library, Inc., 15 East 40 St., N. Y. 16, N. Y. 302 pages+7 appendix pages+xii pages. 73 figures. 9×5½. $15.00. (Also published (1955) by Butterworth's Scientific Publications London. 45s.)

An author who presents a broad survey of a young, rapidly growing field of science has performed a real service. Dr. Ingram has produced a very coherent and readable account of the techniques, the accomplishments, and the problems of microwave and radio frequency spectroscopy, achieving this in a comparatively small book. His book supplements rather than competes with the three principal works extant on this subject (all entitled *Microwave Spectroscopy:* the monograph by Strandberg; the book of Gordy, Smith, and Trambarulo; and that by Townes and Schawlow).

It is only natural that the breadth of this survey should be achieved at some cost to the depth, particularly in the details of gas spectroscopy. This is not a disadvantage to the reader for whom the book is primarily intended, the scientist or engineer who is not a practicing microwave or radio spectroscopist. To a large degree the lack of detail is compensated by the extensive references to periodical literature included in each chapter. In the chapters dealing with Ingram's own field of special interest, paramagnetic and electron resonance, the coverage is more complete. Both theory and details of experimental work are well presented in a manner which imparts to the reader a "feel" for the subject. The final chapter is a very interesting summary of possible applications, of both scientific and practical nature, for the methods of radiowave spectroscopy.

Because of its high price the American edition will probably not enjoy the wide sales to individuals which it deserves. Since this book does not contain the extensive tables of mathematical and experimental data incorporated in earlier volumes it will not find great favor as a handbook for practicing spectroscopists. Those interested in obtaining a first view of this field will tend to borrow the book from a library. It is most unfortunate that a price increase of 240% over the British price was necessary in the U. S. A. Nevertheless every scientific library, both educational and industrial, should make this volume available to its clientele and publicize it as an excellent summary of this new and fruitful field of research.

W. C. King
General Electric Co.
Philadelphia, Pa.

Recent Books

Bell, D. A., *Information Theory and Its Engineering Applications*, 2nd ed. Pitman Pub. Corp., 2 W. 45 St., N. Y. 36, N. Y. $5.00.

Bitter, Francis, *Currents, Fields and Particles*. Technology Press of M.I.T., and John Wiley and Sons, 440 Fourth Ave., N. Y. 16, N. Y. $8.50.

Computer Development at the National Bureau of Standards. U. S. Government Printing Office, Washington 25, D.C. $2.00.

Haas, A. and Hallows, R. W., *The Oscilloscope at Work*. Philosophical Library, Inc., 15 E. 40 St., N. Y. 16, N. Y. $10.00.

McLachlan, N. W., *Ordinary Non-Linear Differential Equations*, 2nd ed. Oxford University Press, Amen House, London E. C. 4, England. 35s.

Numerical Analysis, ed. by J. H. Curtiss. Proceedings of the Sixth Symposium in Applied Mathematics of the American Mathematical Society, Volume VI. McGraw-Hill Book Co., Inc., 330 W. 42 St., N. Y. 36, N. Y. $9.75.

Oldfield, R. L., *Radio-Television and Basic Electronics*. American Technical Society, 848 E. 58 St., Chicago 37, Ill. $4.95.

Proceedings of the Conference on Radio Interference Reduction, Volumes I and II. Complete text of papers presented at the 1954 and 1956 conferences. Armour Research Foundation, Dept. E, 10 W. 35 St., Chicago 16, Ill. $6.00 for the set of two volumes.

Vajda, S., *The Theory of Games and Linear Programming*. John Wiley and Sons, 440 Fourth Ave., N. Y. 16, N. Y. $1.75.

Professional Groups†

Aeronautical & Navigational Electronics—Joseph General, 6019 Highgate Dr., Baltimore 15, Md.

Antennas & Propagation—H. G. Booker, School of Physics and Elec. Engrg., Cornell Univ., Ithaca, N. Y.

Audio—D. W. Martin, The Baldwin Piano Company, 1801 Gilbert Ave., Cincinnati 2, Ohio.

Automatic Control—J. C. Lozier, Bell Tel. Labs., Whippany, N. J.

Broadcast & Television Receivers—L. R. Fink, Research Lab., General Electric Company, Schenectady, N. Y.

Broadcast Transmission Systems—O. W. B. Reed, Jr., Jansky & Bailey, 1735 DeSales St., N.W., Washington, D. C.

Circuit Theory—H. J. Carlin, Microwave Res. Inst., Polytechnic Inst. of Brooklyn, 55 Johnson St., Brooklyn 1, N. Y.

Communications Systems—F. M. Ryan, American Telephone and Telegraph Co., 195 Broadway, New York 7, N. Y.

Component Parts—R. M. Soria, American Phenolic Corp., 1830 S. 54 Ave., Chicago 50, Ill.

Electron Devices—R. R. Law, CBS-Hytron, Danvers, Mass.

Electronic Computers—J. D. Noe, Div. of Engineering Research, Stanford Research Institute, Stanford, Calif.

Engineering Management—Rear Adm. C. F. Horne, Jr., Convair, Pomona, Calif.

Industrial Electronics—C. E. Smith, Consulting Engineer, 4900 Euclid Ave., Cleveland 3, Ohio.

Information Theory—M. J. Di Toro, Polytech. Research & Dev. Corp., 200 Tillary St., Brooklyn, N. Y.

Instrumentation—F. G. Marble, Boonton Radio Corporation, Intervale Road, Boonton, N. J.

Medical Electronics—V. K. Zworykin, RCA Labs., Princeton, N. J.

Microwave Theory and Techniques—H. F. Englemann, Federal Telecommunication Labs., Nutley, N. J.

Military Electronics—C. L. Engleman, 2480 16 St., N.W., Washington 9, D. C.

Nuclear Science—W. E. Shoupp, Westinghouse Elec. Corp., Commercial Atomic Power Activities, P.O. Box 355, Pittsburgh 30, Pa.

Production Techniques—R. R. Batcher, 240-02—42nd Ave., Douglaston, L. I., N. Y.

Reliability and Quality Control—Victor Wouk, Beta Electric Corp., 333 E. 103rd St., New York 29, N. Y.

Telemetry and Remote Control—C. H. Hoeppner, Stavid Engineering, Plainfield, N. J.

Ultrasonics Engineering—J. F. Herrick, Mayo Foundation, Univ. of Minnesota, Rochester, Minn.

Vehicular Communications—Newton Monk, Bell Labs., 463 West St., N. Y., N. Y.

† Names listed are group Chairmen.

Sections*

Akron (4)—C. O. Lambert, 1144 Roslyn Ave., Akron 20, Ohio; M. L. Kult, 1006 Sackett Ave., Cuhahoga Falls, Ohio.

Alamagordo-Holloman (7)—O. W. Fix, Box 915, Holloman AFB, N. M.; T. F. Hall, Box 824, Holloman AFB, N. M.

Albuquerque-Los Alamos (7)—G. A. Fowler, 3333—49 Loop, Sandia Base, Albuquerque, N. M.; S. H. Dike, Sandia Corp., Dept. 5120, Albuquerque, N. M.

Atlanta (3)—M. D. Prince, 3821 Stoland Dr., Chamblee, Ga.; P. C. Toole, 605 Morningside Dr., Marietta, Ga.

Baltimore (3)—M. I. Jacob, 1505 Tredegar Ave., Catonsville 28, Md.; P. A. Hoffman, 514 Piccadilly Rd., Baltimore 4, Md.

Bay of Quinte (8)—R. L. Smith, Northern Electric Co., Ltd., Box 400, Belleville, Ont., Canada; M. J. Waller, R.R. 1, Foxboro, Ont., Canada.

Beaumont-Port Arthur (6)—J. G. Morgan, 508 Garland St., Beaumont, Tex.; B. J. Ballard, Box 2831, Rm. 608, Beaumont, Tex.

Binghamton (1)—Arthur Hamburgen, 926 Glendale Drive, Endicott, N. Y.; Y. M. Hill, 2621 Smith Dr., Endwell, N. Y.

Boston (1)—R. L. McFarlan, 20 Circuit Rd., Chestnut Hill 67, Mass.; T. F. Jones, Jr., 62 Bay St., Squantum, Mass.

Buenos Aires—A. H. Cassiet, Zavalia 2090 1 "B," Buenos Aires, Argentina; O. C. Fernandez, Transradio Internacional, 379 San Martin, Buenos Aires, Argentina.

Buffalo-Niagara (1)—G. F. Buranich, Route 1, Lewiston, N. Y.; Earl Whyman, 375 Mt. Vernon Rd., Snyder 21, N. Y.

Cedar Rapids (5)—A. H. Wulfsberg, 3235—14 Ave., S.E., Cedar Rapids, Iowa; W. B. Bruene, 2769 Franklin Ave., N.E., Cedar Rapids, Iowa.

Central Florida (3)—K. A. West, 1345 Indian River Dr., Eau Gallie, Fla.; J. M. Kaeser, 1453 Thomas Barbour Dr., Loveridge Heights, Eau Gallie, Fla.

Chicago (5)—R. M. Soria, 1830 S. 54th Ave., Chicago 50, Ill.; G. H. Brittain, 3150 Summit Ave., Highland Park, Ill.

China Lake (7)—H. W. Rosenberg, 217-B Fowler St., N.O.T.S., China Lake, Calif.; C. E. Hendrix, 2-A Wasp Rd., China Lake, Calif.

Cincinnati (4)—F. L. Weidig, Jr., 3819 Davenant Ave., Cincinnati 13, Ohio; H. E. Hancock, R.R. 4, Branch Hill Box 52, Loveland, Ohio.

Cleveland (4)—J. F. Keithley, 22775 Douglas Rd., Shaker Heights 22, Ohio; C. F. Schunemann, 2021 Sagamore Dr., Euclid 17, Ohio.

Columbus (4)—T. E. Tice, 2214 Jervis Rd., Columbus 21, Ohio; G. R. Jacoby, 78 N. James Rd., Columbus 13, Ohio.

Connecticut Valley (1)—B. R. Kamens, 94 Admiral Dr., New London, Conn.; J. D. Lebel, Benedict Hill Rd., New Canaan, Conn.

Dallas (6)—G. K. Teal, Texas Instruments Inc., 6000 Lemmon Ave., Dallas, Texas; John Albano, 4134 Park Lane, Dallas, Texas.

Dayton (4)—R. W. Ittelson, 724 Golfview Dr., Dayton 6, Ohio; Yale Jacobs, 310 Ryburn Ave., Dayton 5, Ohio.

Denver (6)—R. C. Webb, 2440 S. Dahlia St., Denver 22, Colo.; S. B. Peterson, 1295 S. Jackson, Denver 10, Colo.

Detroit (4)—M. B. Scherba, 5635 Forman Dr., Birmingham, Mich.; R. H. Reust, 20078 Westbrook, Detroit 19, Mich.

Egypt—H. M. Mahmoud, Faculty of Engineering, Fouad I University, Giza, Cairo, Egypt; El Garhi I El Kashlan, Egyptian Broadcasting, 4, Shari Sherifein, Cairo, Egypt.

Elmira-Corning (1)—J. P. Hocker, Pilot Plant No. 2, Corning Glass Works, Corning, N. Y.; J. H. Fink, 26 Hudson St., Bath, N. Y.

El Paso (6)—J. H. Maury, 328 Olivia Circle, El Paso, Tex.; W. A. Toland, 912 Brazil St., El Paso, Tex.

Emporium (4)—D. A. Dander, 22 S. Cherry St., Emporium, Pa.; R. J. Bisso, 99 Meadow Rd., Emporium, Pa.

Evansville-Owensboro (5)—D. D. Mickey, Jr., Engineering Department, General Electric Co., Owensboro, Ky.; C. L. Taylor, 2301 N. York, Owensboro, Ky.

Florida West Coast (3)—E. L. White, 460 Coffee Pot Riviera, St. Petersburg, Fla.; R. Murphy, 12112 N. Edison Ave., Tampa 4, Fla.

Fort Huachuca (7)—J. H. Homsy, Box 123, San Jose Branch, Bisbee, Ariz.; R. E. Campbell, Box 553, Benson, Ariz.

(*Sections cont'd*)

* Numerals in parentheses following Section designate region number. First name designates Chairman, second name, Secretary.

Fort Wayne (5)—T. L. Slater, 1916 Eileen Dr., Waynedale, Ind.; F. P. Smith, Windsor Rd., R.R. 15, Fort Wayne, Ind.

Fort Worth (6)—G. C. Sumner, 3900 Spurgeon, Fort Worth, Texas; C. W. Macune, 3132 Forest Park Blvd., Fort Worth, Texas.

Hamilton (8)—A. L. Fromanger, Box 507, Ancaster, Ont., Canada; C J. Smith, Gilbert Ave., Dancaster Courts, Sub. Serv. 2, Ancaster, Ont., Canada.

Hawaii (7)—R. R. Hill, 219 Uilma St., Lanikai, T. H.; L. R. Dawson, 432 A Kalama St., Lanikai, T. H.

Houston (6)—R. L. Ransome, 1705 Huge Oaks, Houston 24, Tex.; T. N. Whitaker, 3801 Cullen Blvd., Houston 4, Tex.

Huntsville (3)—T. L. Greenwood, 1709 La Grande St., Huntsville, Ala.; W. J. Robinson, 20 Polk Dr., Huntsville, Ala.

Indianapolis (5)—V. V. K. French, 1636 Pennsylvania St., Indianapolis, Ind.; J. V. Dunn, 1614 N. Alton Ave., Indianapolis 22, Ind.

Israel—Franz Ollendorf, Box 910, Hebrew Inst. of Technology, Haifa, Israel; A. A. Wulkan, P.O. B. 1, Kiryat Motzkin, Haifa, Israel.

Ithaca (1)—R. L. Wooley, 110 Cascadilla St., Ithaca, N. Y.; W. H. Murray, General Electric Co., Ithaca, N. Y.

Kansas City (6)—R. W. Butler, Bendix Aviation Corp., Kansas City Division, Kansas City 10, Mo.; Mrs. G. L. Curtis, Radio Industries, Inc., 1307 Central Ave., Kansas City 2, Kan.

Little Rock (6)—D. L. Winn, 10th and Spring Sts., Little Rock, Ark.; F. J. Wilson, Rt. 7, Box 500-J, Little Rock, Ark.

London (8)—E. R. Jarmain, 13 King St., London, Ont., Canada; W. A. Nunn, Radio Station CFPL-TV, London, Ont., Canada.

Long Island (2)—David Dettinger, Wheeler Laboratories, Inc., Great Neck, Long Island, N. Y.; T. C. Hana, 59-25 Little Neck Parkway, Little Neck, Long Island, N. Y.

Los Angeles (7)—V. J. Braun, 2673 N. Raymond Ave., Altadena, Calif.; J. N. Whitaker, 323—15th St., Santa Monica, Calif.

Louisville (5)—O. W. Towner, WHAS Inc., 525 W. Broadway, Louisville 2, Ky.; F. M. Sweets, 114 S. First St., Louisville 2, Ky.

Lubbock (6)—J. B. Joiner, 2621—30th St., Lubbock, Texas; E. W. Jenkins, Jr., Shell Oil Co., Admin. Dept., Box 1509, Midland, Tex.

Miami (3)—E. C. Lockwood, 149 N.W. 105th St., Miami 50, Fla.; E. W. Kimball, 209 Alhambra Circle, Coral Gables 34, Fla.

Milwaukee (5)—W. A. Van Zeeland, 4510 N. 45th St., Milwaukee 16, Wis.; L. C. Geiger, 2734 N. Farwell Ave., Milwaukee 11, Wis.

Montreal (8)—F. H. Margolick, Canadian Marconi Co., 2442 Trenton Ave., Montreal, Quebec, Canada; A. H. Gregory, 170 Fieldcrest Ave., Point Claire, P. Q., Canada.

Newfoundland (8)—Col. J. A. MacDavid, Hgtrs. Dir. Comm., Northeast Air Command, APO 862, N. Y., N. Y.; J. A. Willis, Can. Marconi Co., Ltd., Pinetree—NEAC Depot, Pepperill AFB, St. John's, Newfoundland, Can.

New Orleans (6)—M. F. Chapin, General Electric Co., 236 Lee Circle Bldg., New Orleans 12, La.; G. A. Hero, 1102 Lowerline St., New Orleans 18, La.

New York (2)—H. S. Renne, Bell Telephone Laboratories, Inc., Publication Department, 463 West St., New York 14, N. Y.; O. J. Murphy, 410 Central Park W., New York 25, N. Y.

North Carolina-Virginia (3)—M. J. Minor, Route 3, York Rd., Charlotte, N. C.; A. L. Comstock, 1404 Hampton Dr., Newport News, Va.

Northern Alberta (8)—J. E. Sacker, 10235—103rd St., Edmonton, Alberta, Canada; Frank Hollingworth, 9619—85th St., Edmonton, Alberta, Canada.

Northern New Jersey (2)—A. M. Skellett, 10 Midwood Terr., Madison, N. J.; G. D. Hulst, 37 College Ave., Upper Montclair, N. J.

Northwest Florida (3)—F. E. Howard, Jr., 573 E. Gardner Dr., Fort Walton, Fla.; W. W. Gamel, Canoga Corp., P.O. Box 188, Shalimar, Fla.

Oklahoma City (6)—C. M. Easum, 3020 N.W. 14th St., Oklahoma City, Okla.; Nicholas Battenburg, 2004 N.W. 30th St., Oklahoma City 6, Okla.

Omaha-Lincoln (5)—J. S. Petrik, 760 S. 70 St., Omaha, Neb.; H. W. Becher, 1214 N. 34 St., Omaha, Neb.

Ottawa (8)—C. F. Pattenson, 3, Braemar, Ottawa 2, Ont., Canada; J. P. Gilmore, 1458 Kilborn Ave., Ottawa, Ont., Canada.

Philadelphia (3)—M. S. Corrington, RCA Victor TV Division, Cherry Hill 204-2, Camden 8, N. J.; I. L. Auerbach, 1243—65th Ave., Philadelphia 26, Pa.

Phoenix (7)—Everett Eberhard, 30 E. Colter St., Phoenix, Ariz.; R. V. Baum, 1718 East Rancho Dr., Phoenix, Ariz.

Pittsburgh (4)—Gary Muffly, 715 Hulton Rd., Oakmont, Pa.; H. R. Kaiser, WIIC-WWSW, Sherwyn Hotel Pittsburgh 22, Pa.

Portland (7)—R. R. Po ley, 3153 N.E. 83 Ave., Portland 20, Ore.; S. D. James, 5531 S.W. Brugger, Portland 19, Ore.

Princeton (2)—J. L. Potter, Rutgers Univ., New Brunswick, N. J.; P. K. Weimer, RCA Laboratories, Princeton, N. J.

Regina (8)—William McKay, 2856 Retallack St., Regina, Saskatchewan, Canada; J. A. Funk, 138 Leopold Crescent, Regina, Saskatchewan, Canada.

Rio de Janeiro—W. W. L. Heininger, Rua Anchieta 5, Apt. 1001—LEME, Rio de Janeiro, Brazil; J. C. B. Frederico, AV Atlantica 586, Apt. 1101—LEME, Rio de Janeiro, Brazil.

Rochester (1)—W. F. Bellor, 186 Dorsey Rd., Rochester 16, N. Y.; R. E. Vosteen, 473 Badkus Rd., Webster, N. Y.

Rome-Utica (1)—M. V. Ratynski, 205 W. Cedar St., Rome, N. Y.; Sidney Rosenberg, 907 Valentine Ave., Rome, N. Y.

Sacramento (7)—E. W. Berger, 3421—5th St., Sacramento 20, Calif.; P. K. Onnigian, 4003 Parkside Ct., Sacramento, Calif.

St. Louis (6)—F. W. Swantz, 16 S. 23rd St., Belleville, Ill.; Gilbert Pauls, 1108 Pembroke Dr., Webster Groves 19, Mo.

Salt Lake City (7)—V. E. Clayton, 1525 Browning Ave., Salt Lake City, Utah. A. L. Gunderson, 3906 Parkview Dr., Salt Lake City 17, Utah.

San Antonio (6)—W. H. Hartwig, Dept. of Elec. Eng., University of Texas, Austin 12, Tex.; E. L. Hixson, Dept. of Elec. Eng., University of Texas, Austin 12, Tex.

San Diego (7)—R. A. Kirkman, 3681 El Canto Dr., Spring Valley, Calif.; A. H. Drayner, 4520—62 St., San Diego, Calif.

San Francisco (7)—J. S. McCullough, 1781 Willow St., San Jose 25, Calif.; E. G. Goddard, Stanford Research Institute, Menlo Park, Calif.

Schenectady (1)—J. S. Hickey, Jr., General Electric Co., Box 1088, Schenectady, N. Y.; C. V. Jakowatz, 10 Cornelius Ave., Schenectady 9, N. Y.

Seattle (7)—K. R. Wilson, 1100—17th Ave 206, Seattle 22, Wash.; W. J. Siddons, 6539—39th N.E., Seattle 15, Wash.

South Bend-Mishawaka (5)—J. L. Colten, Bendix Aviation Corp., Missile Section, 400 S. Beiger St., Mishawaka, Inc.; P. Cox, 400 S. Beiger St., Mishawaka, Ind.

Southern Alberta (8)—W. Partin, 448—22nd Ave. N.W., Calgary, Alberta, Canada; R. W. H. Lamb, Radio Station CFCN, 12th Ave. and Sixth St. E., Calgary, Alberta, Canada.

Syracuse (1)—P. W. Howells, General Electric Co., H.M.E.E. Dept., Bldg. 3, Industrial Park, Syracuse, N. Y.; G. M. Glasford, Elec. Eng. Dept., Syracuse University, Syracuse 10, N. Y.

Tokyo—Hidetsugu Yagi, Musashi Kogyo Daigaku, 2334 Tamagawa Todoroki 1, Setagayaku, Tokyo, Japan; Fumio Minozuma, 16 Ohara-Machi, Meguro-Ku, Tokyo, Japan.

Toledo (4)—M. E. Rosencrantz, 4744 Overland Parkway, Apt. 204, Toledo, Ohio; L. B. Chapman, 2459 Parkview Ave., Toledo 6, Ohio.

Toronto (8)—F. J. Heath, 830 Lansdowne Ave., Toronto 4, Ont., Canada; H. F. Shoemaker, Radio College of Canada, 86 Bathurst St., Toronto, Ont., Canada.

Tucson (7)—R. C. Bundy, Department 15, Hughes Aircraft Co., Tucson, Ariz.; Daniel Hochman, 2917 E. Malvern St., Tucson, Ariz.

Tulsa (6)—J. D. Eisler, Box 591, Tulsa 2, Okla.; J. M. Deming, 5734 E. 25th St., Tulsa, Okla.

Twin Cities (5)—J. L. Hill, 25—17 Ave., N.E., North St. Paul 9, Minn.; F. C. Wagner, 16219 Tonkaway Rd., Wayzata, Minn.

Vancouver (8)—J. S. Gray, 4069 W. 13th Ave., Vancouver, B. C., Canada; L. R. Kersey, Department of Electrical Engineering, Univ. of British Columbia, Vancouver 8, B. C., Canada.

Washington (3)—R. I. Cole, 2208 Valley Circle, Alexandria, Va.; R. M. Page, 5400 Branch Ave., Washington 23, D. C.

Wichita (6)—J. W. Patterson, 300 N. Broadway, Wichita 2, Kan.; H. C. Davis, 1908 S. Parkwood Lane, Wichita 18, Kan.

Williamsport (4)—F. T. Henry, 1345 Pennsylvania Ave., Williamsport, Pa.; W. H. Bresee, 818 Park Ave., Williamsport, Pa.

Winnipeg (8)—H. T. Wormell, 419 Notre Dame Ave., Winnipeg, Manitoba, Canada; T. J. White, 923 Waterford Ave., Fort Garry, Winnipeg 9, Manitoba, Canada.

Subsections

Berkshire (1)—A. H. Forman, Jr., O.P. 1-203, N.O.D., General Electric Co., 100 Plastics Ave., Pittsfield, Mass.; E. L. Pack, 62 Cole Ave., Pittsfield, Mass.

Buenaventura (7)—O. La Plant, 325 N. "J" St., Oxnard, Calif.; W. L. MacDonald, 65 Glen Ellen Dr., Ventura, Calif.

Centre County (4)—R. E. Skipper, 276 Ellen Ave., State College, Pa.; S. A. Bowhill, 315 W. Beaver Ave., State College, Pa.

Charleston (3)—W. L. Schachte, 152 Grove St., Charleston 22, S. C.; Arthur Jonas, 105 Lancaster St., North Charleston, S. C.

East Bay (7)—H. F. Gray, Jr., 2019 Mira Vista Dr., El Cerrito, Calif.; D. I. Cone, 1257 Martin Ave., Palo Alto, Calif.

Erie (1)—J. D. Heibel, 310 W. Grandview, Erie, Pa.; D. H. Smith, 3025 State St., Erie, Pa.

Gainesville (3)—Officers to be elected.

Hampton Roads (3)—R. L. Lindell, 2731 Jason Ave., Norfolk 9, Va.; J. E. Eller, Waterview Apts., Apt. E-3, Portsmouth, Va.

Lancaster (3)—W. T. Dyall, 1415 Hillcrest Rd., Lancaster, Pa.; P. W. Kaseman, 405 S. School Lane, Lancaster, Pa.

Las Cruces-White Sands Proving Grounds (6)—Officers to be elected.

Memphis (3)—R. N. Clark, Box 227, Memphis State College, Memphis, Tenn. (Chairman)

Mid-Hudson (2)—J. C. Logue, IBM Eng. Lab. Annex, Poughkeepsie, N. Y.; R. R. Blessing, IBM South Rd., Poughkeepsie, N. Y.

Monmouth (2)—W. M. Sharpless, Box 107, Bell Tel. Labs., Red Bank, N. J.; A. P. King, Bell Tel. Labs., Box 107, Red Bank, N. J.

New Hampshire (1)—Officers to be elected.

Orange Belt (7)—J. Tampico, 2709 N. Garey Ave., Pomona, Calif.; R. E. Beekman, 1133 N. Lillie, Fullerton, Calif.

Palo Alto (7)—W. B. Wholey, 342 Verano Dr., Los Altos, Calif.; A. M. Peterson, 14846 Manuella Ave., Los Altos, Calif.

Panama City (3)—Officers to be elected.

Pasadena (7)—R. M. Ashby, 3600 Fairmeade Rd., Pasadena, Calif.; J. L. Stewart, Department of Electrical Engineering, California Institute of Technology, Pasadena, Calif.

Piedmont (3)—H. H. Arnold, 548 S. Westview Dr., Winston-Salem, N. C.; C. A. Norwood, 830 Gales Ave., Winston-Salem, N. C.

Quebec (8)—R. E. Collin, 590 Avenue Mon Repos, Ste. Foy, Quebec, Can.; R. M. Vaillancourt, 638 Avenue Mon Repos, Ste. Foy, Quebec, Canada.

Richland (7)—W. G. Spear, 1503 Birch, Richland, Wash.; P. C. Althoff, 1800 Thompson, Richland, Wash.

San Fernando (7)—J. C. Van Groos, 14515 Dickens St., Sherman Oaks, Calif.; F. E. La Fetra, 22700 Erwin St., Woodland Hills, Calif.

Shreveport (6)—E. D. Nuttall, Box 1407, Shreveport, La.; R. W. Bains, 827 Martha Lane, Shreveport, La.

USAFIT (5)—L. D. Williams, USAF Institute of Technology, MCLI, Box 3039, Wright-Patterson AFB, Ohio; G. P. Gould, Box 3274, USAFIT, Wright-Patterson AFB, Ohio.

Westchester County (2)—F. S. Preston, Norden Laboratories, 121 Westmoreland Ave., White Plains, N. Y.; R. A. LaPlante, Philips Laboratories, Inc., S. Broadway, Irvington, N. Y.

Western North Carolina (3)—Officers to be elected.

Automatic Coding Symposium

FRANKLIN INSTITUTE, PHILADELPHIA, PA., JANUARY 24–25

The two-day symposium on automatic coding at the Franklin Institute will include the presentation of eight technical papers, two luncheons, cocktails and dinner, and a demonstration of the Institute's UNIVAC Computing Center, announced D. B. Houghton, Program Chairman. Registration arrangements, preferably in advance, and detailed information are available from Automatic Coding Symposium, Franklin Institute, 20th and Parkway, Philadelphia 3, Pa. The registration fee is $35.00.

The following papers will be read:

Print I—An Automatic Coding System for the IBM 705, R. N. Bemer, IBM.

Automatic Coding Experience at the General Electric Company's UNIVAC Installation in Louisville, R. M. Peterson, Major Appliance Div., G. E. Co.

Debugging Automatic Coding, Charles Katz, Remington Rand UNIVAC Div., Sperry Rand Corp.

Omnicode, A Common Language Programming System, R. C. McGee, Automatic Programming, G. E. Co.

A Mathematical Language Compiler, A. J. Perlis, Computation Center, Carnegie Inst. of Technology.

The Procedure Translator, A System of Automatic Programming, H. H. Kinsler, Electronic Installations, Metropolitan Life Ins. Co., and M. Moskowitz, Electronic Research Bureau.

A Mechanized Approach to Automatic Coding, E. C. Yowell, Nat'l Cash Register Co.

A Matrix Compiler for UNIVAC, L. C. McGinn, Analysis Section, Franklin Institute Labs.

Symposium on the Present Status of Heart Sound Production and Recording

UNIVERSITY OF BUFFALO, BUFFALO, NEW YORK, FEBRUARY 14, 1957

TENTATIVE PROGRAM

Morning

Introductory Remarks, Chancellor Furnas, S. Kimball, P. Mohn, J. Patterson, and G. Buranich.

History and Present Status of Phonocardiography, Howard Sprague, M.D.

Physiological-Auscultatory Correlations, D. G. Greene, M.D.

Physics and Instrumentation to Date, M. B. Rappaport.

Paper to be announced, L. Dunn, M.D.

Does Cavitation Play a Role in the Genesis of Cardiovascular Sounds?, Samuel Boyer, M.D.

Generation of Musical Murmurs, Victor McKusick, M.D.

Afternoon

The Calibration of Heart Sound Intensity, M. B. Rappaport and D. Larue, M.D.

Estimation of Absolute Loudness of Heart Sounds and Murmurs by Means of Quantitative Ausculation with Internal Calibration, Eugene Lepeschkin, M.D. and D. Larue, M.D.

High Sensitivity Capacitance Pickup for Heart Sounds, Dale Groom, M.D. and Y. T. Sihvonen.

Studies in Intracardiac Phonocardiography, David Lewis, M.D. and John Wallace.

Evaluation of the Spectral Phonocardiographic Analysis, George Webb.

Newer Studies of Selective Phonocardiography Including a New Method for the Identification of the Frequency Range of Extra Sounds, Aldo Luisada, M.D.

The Generation of Heart Sounds and Murmurs by Recurrent Transients, Simon Rodbard, M.D.

Instrumentation Problems in a High Frequency Heart Sound Analyzer, Wilson Greatbatch.

Evening

Joint Buffalo-Niagara IRE Section—PGME Chapter meeting.

Round table discussion.

1957 Transistor and Solid-State Circuits Conference

SPONSORED BY IRE, AIEE, AND UNIVERSITY OF PENNSYLVANIA, UNIVERSITY OF PENNSYLVANIA, PHILADELPHIA, PA., FEBRUARY 14–15

The 1957 Transistor and Solid State Circuits Conference is sponsored jointly by the Philadelphia Section of the IRE, the Science and Electronics Technical Division of the AIEE, the IRE Professional Group on Circuit Theory, and the University of Pennsylvania. Patterned after the previous conferences held at the same location for the past several years, this conference will include information on both linear and nonlinear transistor circuits. Also, one session will be devoted to other solid-state circuits, including ferroelectrics and magnetic cores. Two tutorial sessions are aimed at surveying recent advances in the subject and will provide the practicing engineer in solid-state circuitry with a broader picture of the state of the art.

Although no conference transactions will be published, a technical addendum to the program booklet will be available at the time of registration, containing reproductions of all slides, including mathematical expressions.

The Bellevue-Stratford Hotel, Broad and Chestnut Streets, has reserved a block of rooms for those attending the conference.

Registration and hotel reservation forms are being mailed to members of the sponsoring groups. Others may obtain them from F. W. Anderson, General Electric Company, Missile and Ordnance Systems Department, 3198 Chestnut Street, Philadelphia 4, Pennsylvania. Fees for the conference are as follows: advance registrations made before February 7, $3.00; Thursday luncheon, $2.50; cocktail buffet, $6.00; and Friday luncheon, $2.50—registration at conference, $4.00; Thursday luncheon, $3.00; cocktail buffet, $6.50; Friday luncheon, $3.00.

Because of limited facilities, and to assist the Local Arrangements Committee, advance registration is urged.

THURSDAY, FEBRUARY 14

8:00 a.m.

Irvine Auditorium

Registration

9:30 a.m.—Noon

Irvine Auditorium

SWITCHING CIRCUITS

Chairman, J. L. Walsh, IBM Engineering Laboratory.

A Decade Ring Counter Using Avalanche-Operated Junction Transistors, J. E. Lindsay, Radio Corp. of America.

Transistor Circuits for Magnetic Drum Recording, Gordon Kuster, Ferranti Elec. Ltd.

Large Scale Testing of Switching Speeds of Junction Transistors, Irwin Dorros, Bell Telephone Laboratories.

Effects of Low Temperatures on Transistor Characteristics, A. B. Credle, IBM.

9:30 a.m.—Noon

University Museum Auditorium

TUTORIAL—A

Chairman, T. H. Bonn, Sperry Rand Univac.

A Survey of Solid-State Devices for Control and Information Handling Systems, J. A. Rajchman, RCA Laboratories.

Thermal Considerations in Transistor Circuit Design, S. K. Ghandi, Gen. Elec. Co.

Noon—2:00 p.m.

University Museum Egyptian Gallery

Lunch

2:00 p.m.—2:20 p.m.

Irvine Auditorium

Formal Opening of Conference and Presentation to University of Pennsylvania by A. L. Samuel, Chairman of Conference; G. L. Haller, Past Chairman of Conference; and J. G. Brainerd, University of Pennsylvania.

2:30 p.m.—5:30 p.m.

Irvine Auditorium

Computer Switching

Chairman, R. E. McMahon, MIT Lincoln Laboratory.

Millimicrosecond Transistor Current Switching Circuits, H. S. Yourke, IBM Laboratory.

DCTL Complementing Flip-Flop Circuits, E. G. Clark, Burroughs Research Center.

A New Bistable Transistor Element Suitable for Digital Computers, N. F. Moody, Defense Research Board.

An Analysis of the Complementary Pair Trigger Circuit, C. D. Florida, Defense Research Board.

A Complementary Symmetry Monostable Multivibrator, C. F. Chong and A. I. Aronson, Radio Corp. of America.

The Design of Dual-Range Transistor Circuits for Minimum Standby-Current Systems, H. E. Tompkins, Univ. of Pa.

2:30 p.m.—5:30 p.m.

University Museum Auditorium

Linear Amplifiers

Chairman, A. P. Stern, General Electric Company.

Transistor Low Noise Preamplifier with High Input Impedance, A. E. Bachmann, General Electric Company.

Wide Band Feedback Amplifiers, F. D. Waldhauer, Bell Telephone Laboratories.

A Transistorized High Voltage Push-Pull Sweep Generator Using High Impedance Techniques, P. J. Anzelone, Radio Corp. of America.

Series Tuned Methods in Transistor Radio Circuitry, W. F. Chow and D. A. Paynter, General Electric Company.

A New Approach to Transistor Receiver Design, A. Proudfit, K. M. St. John, C. R. Wilhelmsen, and R. J. Farber, Hazeltine Research Corp.

6:00 p.m.

Bellevue-Stratford Hotel

Cocktail buffet

8:00 p.m.

Bellevue-Stratford Hotel Conference Rooms

Informal group discussions

Friday, February 15

8:30 a.m.

Registration opens

9:00 a.m.—Noon

Irvine Auditorium

Power Circuits

Chairman, H. T. Moores, Minneapolis-Honeywell.

Some Solutions to Problems of Operating Germanium Transistor Servo Amplifiers at High Ambient Temperatures, P. M. Thompson and J. Mitchell, Defense Research Board.

Phase Controlled Transistor Power Supply Regulation, D. E. Deuitch, Radio Corp. of America.

Transistor DC Amplifier Utilizing "Firing-Angle" Control, H. R. Lowry, General Electric Company.

An Improved Square-Wave Oscillator Circuit, J. L. Jensen, Minneapolis-Honeywell.

Three-Phase Static Inverter, T. M. Corry and R. P. Putkovich, Westinghouse Electric Corp.

A New Tramag Oscillator, A. J. Meyerhoff and R. M. Tillman, Burroughs Research Center.

9:00 a.m.—Noon

University Museum Auditorium

Tutorial—B

Chairman, F. H. Tendick, Bell Telephone Laboratories.

Characteristics and Application of New High Frequency Transistors, R. L. Pritchard, General Electric Research Laboratories.

Design of High Frequency Amplifiers, G. T. Lake, Defense Research Board.

Noon—2:00 p.m.

University Museum Egyptian Gallery

Lunch

Irvine Auditorium

2:00 p.m.—4:30 p.m.

Special Device Circuits

Chairman, Chaang Huang, Sylvania.

Temperature Compensation of Transfluxors, H. W. Abbot and J. J. Suran, General Electric Company.

Counting Circuits Using Ferroelectric Devices, R. M. Wolfe, Bell Telephone Laboratories.

Switching Characteristics of Magnetic Cores as Circuit Elements, R. D. Torrey, A. Krell, and C. Meyer, Sperry Rand Univac.

Transient and Frequency Response Characteristics of Field Effect Unijunction Transistors, J. J. Suran and B. K. Eriksen, General Electric Company.

1957 Western Joint Computer Conference

HOTEL STATLER, LOS ANGELES, CALIFORNIA, FEBRUARY 26–28, 1957

The 1957 Western Joint Computer Conference, which will be held at Hotel Statler in Los Angeles, California, February 26–28, is sponsored by the IRE, the American Institute of Electrical Engineers, and the Association for Computing Machinery. Emphasis will be on reliability techniques in the thirty-eight papers scheduled for presentation during the ten sessions of the conference.

Inspection tours of the Jet Propulsion Laboratory, ElectroData Corporation, Ramo-Wooldridge Corporation, UCLA, Telemeter Magnetics, Inc., Litton Industries, Rand Corporation, and National Cash Register will also be arranged. Meanwhile, women's activities will include sightseeing tours of movie and television studios. The conference cocktail party will be held on the evening of February 26, and a luncheon is planned for the afternoon of February 28.

The Los Angeles chapter of the ACM is sponsoring a symposium at the Statler Hotel, March 1, on the subject "New Computers—A Report from the Manufacturers."

TUESDAY, FEBRUARY 26

Morning

Registration.

Welcome: J. L. Barnes, Conference Chairman.

Keynote Address: J. H. Bridges, Chief of Electronics, Office of the Assistant Secretary of Defense.

Afternoon

MATHEMATICS OF RELIABILITY

Mathematics of Reliability, M. Boldyreff, Rand Corp.

Design of Experiments, J. Hofmann, System Laboratories Corp.

On Prediction of System Performance from Information on Component Performance, J. R. Rosenblatt, National Bureau of Standards.

Evaluation of Failure Data, H. I. Zagor, Arma Div., American Bosch Arma Corp.

NEW SYSTEMS—A

A Digital System Simulator, W. E. Smith, Aeronutronic Systems Inc.

Factors Influencing the Design of the New High Speed Input-Output System for the Florida Automatic Computer (FLAC), C. F. Sumner, RCA Service Co.

The IBM RAMAC System-Memory Unit Operation, D. Royse, IBM.

The IBM RAMAC System-Inquiry Station Operation, H. A. Reitfort, IBM.

WEDNESDAY, FEBRUARY 27

Morning

APPLICATIONS

Reliability in Business System, H. T. Glantz, John Diebold & Associates.

Panel Discussion: A Report from the Users.

NEW COMPONENTS

A RCA High Performance Tape Transport System, S. Baybrick and R. E. Montijo, RCA.

A Medium Speed Magnetic Core Memory, G. E. Valenty, Remington Rand UNIVAC.

Millimicrosecond Transistor Switching Techniques, E. J. Slobodzinski and H. S. Yourke, IBM Research Center.

New High Speed Magnetic Phenomena, E. L. Newhouse, RCA.

Afternoon

COMPONENT RELIABILITY

Packaging Techniques, W. E. Dombert, Burroughs Corp.

Accuracy Control Systems for Magnetic Core Memories, A. Katz, A. G. Jones and G. Rezet, RCA.

Design of a Basic Computer Building Block, J. Alman, P. Phipps and D. Wilson, Remington Rand UNIVAC.

Error Detection in Redundant Systems, S. Schneider and D. H. Wagner, Burroughs Research Center.

ANALOG COMPUTER EQUIPMENT

Analog Logarithmic and Antilogarithmic Circuits Using Switching Transistors, A. J. Schiewe and K. Chen, Westinghouse Elec. Corp.

High Speed Digital-to-Analog Conversion by Integration of a Variable Rate Pulse Train, A. D. Glick, Minneapolis-Honeywell Regulator Co.

A Reliable Method of Drift Stabilization and Error Detection in Large Scale Analog Computers, E. E. Eddey, Goodyear Aircraft Corp.

A New Method of Verifying Analog Computer Problems and Performance, W. C. Meilander, Goodyear Aircraft Corp.

THURSDAY, FEBRUARY 28

Morning

PROGRAMMING FOR RELIABILITY

Diagnostic Techniques Improve Reliability, M. Grems, M. Smith and A. Stadler, Boeing Airplane Company.

Error Detection and Error Correction in Real Time Digital Computers, A. Ralston, Bell Tel. Labs.

The FORTRAN Automatic Coding System—A Description and Users' Reports, IBM.

NEW SYSTEMS—B

The Lincoln TX-2 System—The Lincoln TX-2 Computer, W. A. Clark, Lincoln Lab., M.I.T.

Functional Description of the TX-2, J. M. Frankovitch, Lincoln Lab.

The TX-2 Input-Output System, J. W. Forgie, Lincoln Lab.

Memory Units of the TX-2, R. L. Best, Lincoln Lab.

Standardized Circuitry of the TX-2, K. H. Olsen, Lincoln Lab.

Afternoon

SYSTEMS RELIABILITY

The Interpretation and Attainment of Reliability in Industrial Data Systems, B. K. Smith, Beckman Instruments, Inc.

Accuracy Control in the RCA BIZMAC System, I. Cohen, J. G. Smith and A. M. Spielberg, RCA.

Continuous Computer Operational Reliability, R. D. Briskman, U. S. Army.

Field Performance of a New Automatic Fault Locating Means, J. F. Scully and L. P. Colangelo, Rome Air Development Center.

PROGRAMMING

The Variable Word and Record Length Problem and the Combined Record Approach on Electronic Data Processing Systems, N. J. Dean, Ramo-Wooldridge Corp.

The RCA BIZMAC Sorter, B. Adler, H. P. Guerber, J. C. Hammerton and J. F. Page, RCA.

Empirical Exploration of the Logic Theory Machine, A. Newell, J. C. Shaw and H. A. Simon, Rand Corp.

Programming the Logic Theory Machine, A. Newell and J. C. Shaw, Rand Corp.

Abstracts of IRE Transactions

The following issues of "Transactions" have recently been published, and are now available from the Institute of Radio Engineers, Inc., 1 East 79th Street, New York 21, N. Y. at the following prices. The contents of each issue and, where available, abstracts of technical papers are given below.

Sponsoring Group	Publication	Group Members	IRE Members	Non-Members*
Broadcast Transmission Systems	PGBTS-6	$ .80	$1.20	$2.40
Communications Systems	Vol. CS-4, No. 3	1.05	1.55	3.15
Component Parts	Vol. CP-3, No. 3	1.75	2.60	5.25
Microwave Theory & Techniques	Vol. MTT-4, No. 4	1.85	2.75	5.55

* Public libraries and colleges may purchase copies at IRE Member rates.

Broadcast Transmission Systems

PGBTS-6, October, 1956

Some Aspects of Tropospheric Radio Wave Propagation—A. P. Barsis (p. 1)

The Tropospheric Propagation Research Section of the Radio Propagation Engineering Division, National Bureau of Standards, has conducted extensive measurements of programs in the 100–1000 mc frequency range. A variety of transmitting and receiving antenna heights was used, and long-term recordings are available over distances ranging from well within to far beyond the radio horizon.

Some results of this measurement program are evaluated to provide estimates for power requirements and interference problems concerning broadcasting services in this frequency range.

The Vitascan, Live Flying-Spot Color Scanner—J. H. Haines and G. R. Tingley (p. 11)

The DuMont "Vitascan" color TV system produces live color television pictures of high quality without the use of expensive and complicated color television cameras or highly trained and skilled camera and maintenance crews. It is, in fact, a modern all-electronic version of the earliest forms of mechanical live television pickup which employed the flying-spot scanning principles.

While the Vitascan cannot displace storage-type color TV cameras, it is expected that the unique advantages of the Vitascan will earn it a modest place in color TV programming. It is the purpose of this paper to explain its virtues and shortcomings.

On an historical level, it is our hope to explain how the present technical state of the art has allowed this revitalization of the old flying-spot principle. The basic principles are discussed and the evolution of a workable system leading to the present commercially available equipment is traced.

The RETMA Color Television Test Stripe Signal—R. J. Farber (p. 26)

In a television receiver installation, reflections on the antenna feeder line or multipath transmission to the receiving antenna can give rise to selective reinforcement and cancellation throughout any given channel, so that a relatively non-uniform transmission characteristic results. When a monochrome television receiver is involved, this response characteristic is generally only of secondary interest. Since a color television receiver makes more complete use of the available spectrum, it becomes more important in this latter case to have a more or less flat transmission characteristic from the transmitter to the receiver terminals if satisfactory performance is to be had.

By observing the relative transmission of sideband components due to modulation by frequencies in the neighborhood of the color subcarrier, the usefulness of an antenna for a color television receiver can be determined. A color test stripe signal has been devised so that this observation can be made when only monochrome program material is being transmitted. This paper describes the test stripe and its application to color television receivers.

Communications Systems

Vol. CS-4, No. 3, October, 1956

Systems Engineering—F. M. Ryan (p. 1)

Design of FM Radio Relay Systems for Multi-Channel Telephone Service—J. W. O. Halina (p. 3)

Design Consideration for a Linear VHF Transmitter—D. G. Gallagher (p. 14)

The Printing Telegraph Signal Normalizer—E. N. Dingley, Jr. (p. 18)

An Impulse Interference Blanker for Communications Receivers—Robert Engels (p. 21)

The necessity for adequate and reliable communications for military operations has always existed. Today, with the trend toward ever-increasing specializations of military forces and the continued growth of complex systems of radar, fighter control, etc., this requirement has become more urgent. Since items of communication apparatus are often in close physical proximity to facilitate coordination, the equipment has almost invariably been subjected to detrimental effects from mutual interference.

When communications receivers are placed close to radars, impulse interference may occur, which is at times severe enough to cause complete loss of intelligibility. Such interference may be introduced into a receiver through various channels: (a) shock excitation of the tuned circuits of the receiver by the large modulator-generated d-c pulses; (b) direct pick-up of the radiated r-f radar pulses; (c) feed-back through common power supplies; (d) non-linear detection of the r-f pulse.

As a remedial measure, the ground communications equipment has often been located as far as one-half mile from the radar sites. Such physical separation naturally increases the problems of remoting, maintenance, real estate procurement, additional buildings, heating, etc. Where airborne equipment is involved, such remoting possibilities obviously cannot be plausibly considered. Therefore, as the most effective method of reducing the effects of pulse interference to a minimum or negligible value, the impulse interference blanker for communications receivers was developed.

Study and investigation by engineers of the Interference Analysis and Control Section of the General Engineering Laboratory, RADC, have shown that (a) above is the most common type of interference. However, the impulse interference blanker as developed will eliminate impulse interference no matter how it is introduced into the receiver. The blanker facilitates close-in operation of communications receivers with high-power pulsed equipments of present and projected design. It is so synchronized with the interfering pulse that it generates a blanking gate which is applied to the local oscillator of the affected receiver. Such a measure greatly attenuates the interfering impulse.

Spectrum of Frequency-Shift Radio Photo-Transmissions—A. D. Watt (p. 27)

The spectrum of frequency-shift and subcarrier frequency-shift radio-photo transmissions are obtained from the general expression for the spectrum of a carrier which is frequency modulated with a triangular pulse. A simplified asymptotic expression for rapidly determining the high order sideband amplitudes is developed along with expressions for the interfering bandwidths of radio-photo transmissions. The effect of shaped apertures in the radio-photo scanner upon the output frequency spectrum is discussed. Experimentally determined values for triangular wave spectra are compared with calculated values.

Reduction of Adjacent-Channel Interference from On-Off Keyed Carriers—A. D. Watt, R. M. Coon and V. J. Zurick (p. 41)

The well-known reduction of sideband interference by filtering in the keying circuit of transmitter is examined in detail to determine the amounts of sideband reduction which can be obtained with practical filters and still retain desirable keying waveforms. It is found that reductions in interfering bandwidths by 100 to 1 or more over unfiltered keying at sideband levels of 70 db or more below the carrier are possible by employing filters having specified frequency response characteristics in the keying circuit of linear transmitters. Design criteria are given for a filter which results in the greatest practical interference reduction and also retains a very desirable transient response. The overshoot when employing this type of filter is less than two per cent of the mark to space voltage and at the same time a high out-of-band rejection ratio is obtained. A practical design of a relatively simple four-section low-pass filter which meets these requirements is presented. The effects of receiver linearity on the amount of bandwidth reduction realizable are also considered.

Contributors to this Issue (p. 59)

Component Parts

Vol. CP-3, No. 2, September, 1956

Design and Performance of Air-Cooled Chassis for Electronic Equipment—M. Mark and M. Stephenson (p. 38)

A method of cooling certain types of electronic equipment incorporates in the chassis a simple plate-fin heat exchanger, sometimes called a cold plate or cooled chassis. To deter-

theoretical basis for design is established by first considering the theory of coupled transmission lines. Several designs which utilize a quarter-wavelength or shorter loops and which have very desirable features with regard to coupling, directivity, and bandwidth are illustrated. Typical performance of couplers having couplings of 20–40 db and directivities of over 30 db are presented.

Improved Rectangular Waveguide Resonance Isolators—M. T. Weiss (p. 240)

The early resonance isolators, using nearly full waveguide height ferrite slabs, gave a high reverse loss per unit length but a disappointingly low reverse-to-forward loss ratio. By substantially reducing the height of the ferrite slabs, the reverse-to-forward loss ratio can be increased at the expense of reverse loss per unit length. More recently, it has been found that the addition of certain dielectric loading in rectangular waveguide resonance isolators results in generally improved performance. Thus, the reverse-to-forward loss ratio of these isolators is high (150 to 1 at X band) and the reverse loss per unit length is also high (20 db/inch at X band). The broad-banding problem is also briefly discussed.

An Automatic Gain Control System for Microwaves—J. P. Vinding (p. 244)

This paper describes a system which can keep the power level in a microwave set-up constant with good accuracy in spite of variations of the input power level.

The system uses a variable attenuator based on the Faraday rotation in magnetized ferrite, and thereby achieves a frequency response up to about 500 cps with the present equipment and much better potential response.

Variations in input power are reduced by a factor varying from 10 to 400 depending on available power and on the detector used to detect the output power.

A Method of Analysis of Symmetrical Four-Port Networks—J. Reed and G. J. Wheeler (p. 246)

An analysis of four-arm symmetrical networks such as a branched directional double stub coupler or the hybrid ring (rat race) is presented. The input wave is broken into an even and an odd mode and the vector amplitude out the various arms is computed from the sums or differences of the reflection or transmission coefficients for the two modes. A zero decibel directional coupler is described and its possible use as a duplexer is proposed. The design of multiple stub directional couplers for any degree of coupling is discussed. A method of computing the bandwidth of all these couplers is outlined, and the bandwidth curves, the power out the various arms with respect to frequency of the zero decibel coupler, are computed. A tabulation is made for six different 3 db couplers (even-power split) and their standing wave ratio, evenness of power split and isolation of the fourth arm as a function of frequency assuming perfect performance at the band center.

Broad-Band Waveguide Series *T* for Switching—J. W. E. Griemsmann and G. S. Kasai (p. 252)

By use of properly proportioned half-wavelength transformer sections in the arms of a waveguide series *T* broadband performance can be obtained for switching applications. Over the frequency band 8200 to 9765 megacycles per second, corresponding to a bandwidth of 17.4 per cent, an experimental model showed an insertion vswr of less than 1.15 for transmission through the aligned arms and 1.30 for transmission around the bend. Further bandwidth improvement is possible with the use of a special arrangement of quarter-wave transformer sections but at the expense of further impairment of power-carrying capacity.

A Traveling-Wave Directional Filter—F. S. Coale (p. 256)

A new type of microwave filter is presented in which resonance occurs in the form of a traveling wave rather than in the conventional form of a standing wave. This device is a constant-resistance circuit, and therefore presents a very low input vswr. Formulas for loaded *Q* and insertion loss are given. Experimental results verify the theoretical approach. This filter, which is constructed of a transmission-line loop and two directional couplers, finds application in multiplexing filters as well as in matched band-pass and band-rejection filters.

Miniaturization of Microwave Assemblies—Leonard Lewin (p. 261)

A method of construction is described in which waveguides are arranged in a single plane with adjacent walls common. An assembly is made from a top and bottom plate between which partition walls are arranged to constitute the transmission region. A hybrid-*T* is made from a 3 db coupler, and a microwave repeater is described consisting of five band-pass filters, two hybrid-*T*'s, an isolator, and several other component aspects.

Setting up in situ is achieved by the use of a Bethe hole coupler to monitor the reflection or transmission at a number of specially located check ports.

No electric coupling can be measured across a soldered fabricated waveguide wall.

Recent Advances in Finline Circuits—S. D. Robertson (p. 263)

Detailed studies of transmission properties of the finline coupler have revealed existence of certain phenomena which adversely affect the transmission characteristics. A discussion of the origin and successful elimination of such effects is described.

New applications for the finline coupler have been found in the design of hybrid junctions, twists and bends in multimode waveguide, and other polarization selective devices.

The paper concludes with a presentation of theoretical and experimental results in the application of finline techniques to low-pass microwave filters.

Recent Advances in Waveguide Hybrid Junctions—P. A. Loth (p. 268)

Design techniques for waveguide hybrid tee junctions, resulting in convenient structures and simple internal matching elements for increased bandwidth and power-handling capacity are described, and experimental data are given.

Abstracts and References

Compiled by the Radio Research Organization of the Department of Scientific and Industrial Research, London, England, and Published by Arrangement with that Department and the *Wireless Engineer*, London, England

NOTE: The Institute of Radio Engineers does not have available copies of the publications mentioned in these pages, nor does it have reprints of the articles abstracted. Correspondence regarding these articles and requests for their procurement should be addressed to the individual publications, not to the IRE.

The number in heavy type at the upper left of each Abstract is its Universal Decimal Classification number and is not to be confused with the Decimal Classification used by the United States National Bureau of Standards. The number in heavy type at the top right is the serial number of the Abstract. DC numbers marked with a dagger (†) must be regarded as provisional.

The Index to the Abstracts and References published in the PROC. IRE from February, 1955 through January, 1956 is published by the PROC. IRE, April, 1956, Part II. It is also published by *Wireless Engineer* and included in the March, 1956 issue of that journal. Included with the Index is a selected list of journals scanned for abstracting with publishers' addresses.

ACOUSTICS AND AUDIO FREQUENCIES

534.232 3599

Variable Resonant Transducer—D. H. Robey. (*J. Acoust. Soc. Amer.*, vol. 28, pp. 700–704; July, 1956.) Variation of the resonance frequency of a composite system, such as a crystal plate associated with a backing plate, is effected by applying a force which varies the friction between the two plates.

534.232:534.64 3600

Transducer Calibration by Impedance Measurements—G. A. Sabin. (*J. Acoust. Soc. Amer.*, vol. 28, pp. 705–710; July, 1956.)

534.24 3601

Reflection of a Plane Acoustic Wave from a Surface of Nonuniform Impedance—H. S. Heaps. (*J. Acoust. Soc. Amer.*, vol. 28, pp. 666–671; July, 1956.) Theory is presented for surfaces with 1) random and 2) nonrandom nonuniformity. In case 1), the reflection obeys Lambert's cosine law if the surface is at approximately zero pressure; perfectly diffuse scattering is obtained if the surface is approximately rigid. In case 2), the scattered radiation is contained in a beam whose axis lies in the direction of specular reflection.

534.24 3602

Reflection of Plane Sound Waves from an Irregular Surface—J. G. Parker. (*J. Acoust. Soc. Amer.*, vol. 28, pp. 672–680; July, 1956.) Analysis is presented in which the reflected field is regarded as formed by superposed plane waves with unequal amplitudes. The method is used to investigate scattering from a surface with sinusoidal corrugations in one dimension. The results are compared with those given by Rayleigh's theory and with measurements made by LaCasce and Tamarkin (1938 of 1956).

534.413:534.115 3603

Gaseous and Liquid Jets Sensitive [to sound]—M. Dubois. (*Ann. Télécommun.*, vol. 11, pp. 111–116; May, 1956.) Results of measurements on air and water jets are presented graphically to show the frequency ranges over which jets with given diameter and flow velocity are sensitive.

534.414:534.833 3604

The Degree of Sound Absorption by Cavity Resonators and its Dependence on the Arrangement—E. Kohlsdorf. (*Hochfrequenztech. u. Elektroakust.*, vol. 64, pp. 162–164; April, 1956.) Results of calculations are compared with measurements by the Kundt's tube and reverberation-room methods. Point, line, and area distributions of the resonators are considered.

534.612.2 3605

Acoustic Wattmeter—T. J. Schultz. (*J. Acoust. Soc. Amer.*, vol. 28, pp. 693–699; July, 1956.) Equipment is described comprising a small probe containing a pair of microphones with their preamplifiers, connected by cable to the unit containing amplifiers, equalizers, phase-shifters and measuring circuits. Direct readings of acoustic intensity are obtained over a 50-db range at frequencies up to 10 kc. Theory and measurement results are given.

534.7 3606

Effect of attenuating One Channel of a Dichotic Circuit upon the Word Reception of Dual Messages—G. C. Tolhurst and R. W. Peters. (*J. Acoust. Soc. Amer.*, vol. 28, pp. 602–605; July, 1956.) Experiments indicate that the improvement in the reception of the unattenuated message is more pronounced with a noisy than with a quiet background.

534.7:534.86 3607

Articulation Reduction by Combined Distortions of Speech Waves—D. W. Martin, R. L. Murphy, and A. Meyer. (*J. Acoust. Soc. Amer.*, vol. 28, pp. 597–601; July, 1956.) The effects on intelligibility of the following four types of distortion were studied individually and in combination, with different levels of background noise: attenuation of high-frequency components; multiple echo; random amplitude modulation; irregular frequency-response characteristic.

534.7:621.39 3608

Speech Communication Research Symposium—(*J. Acoust. Soc. Amer.*, vol. 28, pp. 531–591; July, 1956.) The full or summarized text is given of a number of papers presented at the symposium held at San Diego in November, 1955. The material was grouped under the headings: Temporal Factors in Speech Reception; Speech Communication in Noise; Speech Analysis and Synthesis Systems.

534.7:621.396.822 3609

Detection of Signals in Noise: a Comparison between the Human Detector and an Electronic Detector—C. W. Sherwin, F. Kodman, Jr., J. J. Kovaly, W. C. Prothe, and J. Melrose. (*J. Acoust. Soc. Amer.*, vol. 28, pp. 617–622; July, 1956.) Recorded signals mixed with noise were presented to 1) four observers and 2) a detector system comprising filter with 60-cps pass band, square-law detector, and integrator. Incomplete correlation between the responses of the observers and the detector can be explained by assuming that the observers' threshold fluctuates about a mean value, or that noise is generated internally within the observers. The false-alarm rate is about an order of magnitude lower for the observers than for the detector system.

534.75 3610

Masked Threshold and its Relation to the Duration of the Masked Stimulus—E. J. Thwing. (*J. Acoust. Soc. Amer.*, vol. 28, pp. 606–610; July, 1956.)

534.75 3611

Masking of Tones by Bands of Noise—R. C. Bilger and I. J. Hirsh. (*J. Acoust. Soc. Amer.*, vol. 28, pp. 623–630; July, 1956.)

534.771 3612

Study of Audiometer Standardization—R. Lehmann. (*Onde Élect.*, vol. 36, pp. 466–477; May, 1956.) The determination of the mean threshold of hearing, and measurement techniques for air and bone conduction, are discussed, with a description of progress in various countries in the construction of artificial ears. 39 references.

534.78:621.39 3613

Bandwidth and Channel Capacity necessary to transmit the Formant Information of Speech—J. L. Flanagan. (*J. Acoust. Soc. Amer.*, vol. 28, pp. 592–596; July, 1956.)

534.78:621.39 3614

The Intelligibility of Amplitude-Limited Speech—H. Schneider. (*Frequenz*, vol. 10, pp. 97–106 and 152–161; April/May, 1956.) Various known limiter systems are compared; the problem of improving signal-to-noise ratio by amplitude limiting and level regulating, without impairing intelligibility, is discussed. Experimental results indicate that the dynamic range of single tones is at least as significant as the formant structure of the spectrum. A new theoretical explanation is given for the success of the limiting system in which the signal spectrum is predistorted and later restored. Systems involving frequency transposition of the speech band are superior as regards freedom from distortion. Separate limiting in sub-bands gives better results again. Intelligibility losses with the less satisfactory

systems may amount to 50 per cent, but are only about 10 per cent with the two last-mentioned systems.

534.83/.84 3615
Architectural Acoustics—J. Matras. (*Onde Élect.*, vol. 36, pp. 384–415; May, 1956.) A survey covering sources of noise and modes of propagation of sound in buildings, measurement of noise levels, and factors affecting the acoustics of large and small interiors.

534.83 3616
Acoustic Insulation of Heavy Structures—J. Pujolle. (*Onde Élect.*,vol. 36, pp. 435–440; May, 1956.) Research on wall materials and methods of construction is carried out in a laboratory consisting of two rooms separated by the test wall. Measurements are reported on some composite structures made of brick and/or cement; the structure selected as satisfactory for insulating studios comprised a three-leaved cement wall with glass wool in the intervening spaces, providing a mean insulation of 94 db. The importance of avoiding indirect transmission of sound is emphasized.

534.833:534.414 3617
Coupled Vibrations in (acoustic) Cavity Resonators with Grids—E. Kohlsdorf. (*Hochfrequenztech. u. Elektroakust.*, vol. 64, pp. 160–162; April, 1956.) Calculations are made for resonators faced with perforated panels, taking account of resonance of the panel on its own as well as resonance of the whole cavity system. The results are in good agreement with measurements on several systems.

534.833.4:621.395.623.54 3618
Noise Bands *versus* Pure Tones as Stimuli in measuring the Acoustic Attenuation of Ear Protective Devices—J. C. Webster, P. O. Thompson, and H. R. Beitscher. (*J. Acoust. Soc. Amer.*, vol. 28, pp. 631–638; July, 1956.)

534.84:621.374.32 3619
New Acoustic Characterization of Rooms and the Development of a Multipurpose Electronic Counter—R. Lamoral and R. Trembasky. (*Onde Élect.*, vol. 36, pp. 441–449; May, 1956.) The importance of the diffusion characteristics for the acoustic quality of a room is emphasized. An index of diffusion is defined in general terms and apparatus for determining it is described, including details of a specially developed four-decade counter. The index is measured over a range of frequencies up to 4 kc as the number of peaks whose value exceeds a given mean level. The apparatus may be used for measuring reverberation time and other acoustic properties.

534.843 3620
Sound Level in the Corners and near the Walls of Closed Rooms in the Presence of Noise—W. Wöhle. (*Hochfrequenztech. u. Elektroakust.*, vol. 64, pp. 158–160; April, 1956.) A simple method of calculation is presented; the results are confirmed by measurements on a room of volume 63 m³, using noise band of 200–400 and 37.5–75 cps. The greatest difference in sound level between the corners and the middle of the room was about 9 db.

534.845 3621
Visual Display of Sound and Ultrasonic Waves—F. Canac. (*Onde Élect.*, vol. 36, pp. 422–427; May, 1956.) See 2291 of 1954.

534.845 3622
The Acoustic Properties of Materials—T. Vogel. (*Onde Élect.*, vol. 36, pp. 428–434; May, 1956.) The analogy between acoustic and electrical phenomena is used to derive an expression for the coefficient of absorption; a method of determining this coefficient is described, based on measurements of incident and reflected sound fields in a specially constructed chamber (see also 2197 of 1953). Comparison with the original work of Sabine relating acoustic quality with reverberation time shows that Sabine's formula is applicable to conditions involving higher absorption coefficients than are encountered in practice.

534.846 3623
Acoustics of the Auditorium at the State Opera House, Berlin, Unter den Linden—W. Reichardt. (*Hochfrequenztech. u. Elektroakust.*, vol. 64, pp. 134–144; April, 1956.) Details are given of tests made in connection with the rebuilding of this opera house; diffusivity, clarity, and reverberation time were investigated. Measurements made on models were confirmed by the final results. The reverberation time was made as long as possible, and is longer than that of the building in its previous form.

534.86:546.82 3624
Application of Metal Titanium to the Acoustic Instruments, in Japan—T. Hayasaka, K. Masuzawa, S. Nagai, and M. Suzuki. (*Rep. Elect. Commun. Lab., Japan*, vol. 4, pp. 39–54; April, 1956.)

534.86:621.396.712.3 3625
Modern Broadcasting Studios: Marseilles—J. Pujolle. (*Onde. Élect.*, vol. 36, pp. 419–421; May, 1956.) A brief description is given of the acoustic treatment of these studios, which include one with a volume of 3000 m³, having a reverberation time of about 1.5 s, and four smaller studios having reverberation times from 0.5 to 0.8 s.

534.861:621.396.813 3626
The Receiving Side of a Radio Broadcast Transmission and its Influence on the Audio-Frequency Bandwidth—Ebert. (See 3881.)

621.395.616 3627
Full-Range Electrostatic Loudspeakers—H. J. Leak and A. B. Sarkar. (*Wireless World*, vol. 62, pp. 486–488; October, 1956. Correction, *ibid.*, vol. 62, p. 528; November, 1956. Discussion of a design using two parallel plastic diaphragms, with resistive coatings on the faces turned away from each other, and a parallel conducting electrode fixed midway between them. With this arrangement there is no need for a high resistance in the lead to the charged middle electrode. Other advantages are that the diaphragms need not be unreasonably large, and that they form a dust-proof protection for the middle electrode.

621.395.623.8 3628
Experimental Investigation of Sound Coverage of an Open Space by a Distributed System of Loudspeakers—B. D. Tartakovski. (*C.R. Acad. Sci. U.R.S.S.*, vol. 108, pp. 636–639; June 1, 1956. In Russian.) The results indicate that the required coverage can be achieved using 20-w loudspeakers with nondirectional characteristics in the horizontal plane, mounted at a height of 5 m and spaced at about 20 m.

ANTENNAS AND TRANSMISSION LINES

621.372.029.6:621.318.134 3629
Waveguide Components with Nonreciprocal Properties—Brown and Clarricoats. (See 3666.)

621.372.2+621.396.677.3]:512.3 3630
Application of Chebyshev [Tchebycheff] Polynomials in the Calculation of Step Transitions—Ya. M. Turover and N. I. Strutinski. (*Radiotekhnika i Elektronika*, vol. 1, pp. 143–161; February, 1956.) Applications to the theory of transmission lines and antenna arrays are discussed.

621.372.2:621.315.212 3631
On the Theory of a Coaxial Transmission Line consisting of Elliptic Conductors—J. Y. Wong. (*Canad. J. Phys.*, vol. 34, pp. 354–361; April, 1956.) Analysis using elliptic-cylinder wave functions is presented for a line in which the inner and outer conductors have confocal cross sections. The theory is applicable to the shielded-strip line and the rectangular coaxial line as special cases.

621.372.21:621.3.015.3 3632
The Capacitor Discharge on the Infinitely Long Line with Uniform Distribution of Resistance and Capacitance—F. Böttcher. (*Frequenz*, vol. 10, pp. 120–125; April, 1956.) Analysis is presented based on a finite source resistance, corresponding to a finite value of current at the instant when the line is connected to the capacitor. Expressions are derived for the voltage and current at any subsequent instant at any point along the line.

621.372.8 3633
Curved Waveguides with Constant Cross-Section—B. Z. Katsenelenbaum. (*Radiotekhnika i Elektronika*, vol. 1, pp. 171–185; February, 1956.) Propagation in a waveguide comprising a straight and a curved section is considered theoretically. If the radius of curvature is sufficiently large, the solution for the field can be obtained approximately by considering a series of straight sections in place of the actual curved guide. The coefficients for the modes satisfy a system of ordinary differential equations of the first order.

621.372.8 3634
Conditions at the Boundary of Imperfectly Conducting Waveguides—M. L. De Socio. (*R.C. Accad. naz. Lincei*, vol. 20, pp. 469–476; April, 1956.) Analysis is presented; expressions derived are compared with those obtained by Baudoux (3151 of 1955).

621.372.8 3635
Transmission Loss due to Resonance of Loosely Coupled Modes in a Multi-mode System—A. P. King and E. A. Marcatili. (*Bell Syst. Tech. J.*, vol. 35, pp. 899–906; July, 1956.) "In a multimode transmission system the presence of spurious modes which resonate in a closed environment can produce an appreciable loss to the principal mode. The theory for the evaluation and control of this effect under certain conditions has been derived and checked experimentally in the particularly interesting case of a TE_{01} transmission system, where mode conversion to TE_{02}, TE_{03} . . . is produced by tapered junctions between two sizes of waveguide."

621.372.8:538.221:538.63 3636
Polarimetric Study of a Ferrite in the 2000-Mc/s Frequency Band—P. Loudette and A. Charru. (*C.R. Acad. Sci., Paris*, vol. 243, pp. 251–254; July 16, 1956.) Measurements were made on a system comprising three ferrite rods arranged along the axis of a circular waveguide. The rotation of the plane of polarization on application of a longitudinal magnetic field H, and the square of the ellipticity, are plotted 1) as functions of H with λ as parameter, and 2) as functions of λ with H as parameter. Corresponding points of inflection are noted.

621.396.67:537.226 3637
Some Investigations on Dielectric Aerials: Part 1—R. Chatterjee and S. K. Chatterjee. (*J. Indian Inst. Sci.*, vol. 38, pp. 93–103; April, 1956.) The radiation field intensity at a distant point due to a circular-section dielectric rod antenna excited in the HE_{11} mode is derived theoretically. General expressions are given for the radiation patterns in two planes of particular interest, and are evaluated for a polystyrene rod of length 3λ and diameter 0.46λ.

621.396.67:621.396.822 3638
Induced Thermal Noise in Aerials—M. L. Levin. (*Zh. Tekh. Fiz.*, vol. 25, pp. 2313–2318; November, 1955.) Induced fluctuation cur-

rents in a thin antenna due to external heated bodies are discussed. Considerable mathematical difficulties arise in the calculation of these currents, owing to the fact that the fluctuation field is not δ-correlated along the antenna. These difficulties are largely avoided by use of the electrodynamic theory of reciprocity. The general formulas so obtained are applied to the following two cases: 1) antenna in an equilibrium radiation field; 2) thermal noise induced by remote bodies.

621.396.67.029.62:621.397.7 3639
The Crystal Palace Television Transmitting Station—McLean, Thomas, and Rowden. (See 3895.)

621.396.674.3 3640
Some Comments on Wide-Band and Folded Aerials—E. O. Willoughby. (*J. Brit. Instn. Radio Engrs.*, vol. 16, pp. 455–462; August, 1956.) Reprint. See 2622 of 1956.

621.396.677:621.397.26 3641
Deviating Aerial Installations for Television Coverage—H. Hesselbach. (*Frequenz*, vol. 10, pp. 116–120; April, 1956.) Antenna systems for ensuring reception in obscured or marginal areas are discussed; they are termed active or passive according as they are or are not associated with amplifiers; the passive class includes both simple reflectors and systems with separate receiving and transmitting antennas.

621.396.677.012.12 3642
End-Fire Arrays of Magnetic Line Sources mounted on a Conducting Half-Plane—R. A. Hurd. (*Canad. J. Phys.*, vol. 34, pp. 370–377; April, 1956.) Expressions are derived for the radiation patterns of arrays of sources such as slots in a perfectly conducting half-plane. The problem is made two-dimensional by assuming the sources to run parallel to the edge of the plane. The variation of beam tilt, beam width, and side-lobe level with the array parameters is studied. The theory gives a reasonable representation of the behavior of corrugated surface radiators embedded in a finite ground plane, provided the distance from the array to the edge is about equal to the array length.

621.396.677.029.6.012.12 3643
Microwave Aerial Testing at Reduced Ranges—D. K. Cheng. (*Wireless Engr.*, vol. 33, pp. 234–237; October, 1956.) Three methods are presented for determining the appropriate amount of defocus of the primary source for simulating Fraunhofer patterns within the Fresnel zone. The results are plotted and compared.

621.396.677.3:523.7 3644
The Multiple-Aerial Interferometer at the Nançay Station—É. J. Blum, A. Boischot, and M. Ginat. (*C.R. Acad. Sci., Paris*, vol. 243, pp. 19–22; July 2, 1956.) A system for locating centers of solar rf radiation comprises eight parabolic mirrors of 5-m diameter on an east-west base of length 700 m; it operates on 169 mc and has a resolving power of 7.5′. Some records of the passage of rf sources are reproduced. A system of 32 antennas on a 1500-m base is projected, which is to include the present system.

621.396.677.3.012.12 3645
Aerial Pattern Synthesis—H. E. Salzer. (*Wireless Engr.*, vol. 33, pp. 240–244; October, 1956.) When the Dolph-Tchebycheff distributions are used to determine the feeding coefficients required to produce sharp beams with broadside arrays, the numerical work increases with the number of sources. An alternative method is described which uses a special case of a general formula due to Poisson to synthesize extremely sharp patterns. A simple explicit expression is derived for the amplitude of the feeding coefficients which is just as easy to calculate for a large number of terms as for a small number.

621.396.677.83 3646
Theory of Periscopic Aerial Systems—L. B. Tartakovski and A. M. Pokras. (*Radiotekhnika i Elektronika*, vol. 1, pp. 186–196; February, 1956.) A system comprising a parabolic radiator and a plane elliptical deflector is investigated theoretically by a method similar to that used previously by Jakes (1243 of 1953). The solution for the field gain n_E of the system is obtained in terms of infinite series of Bessel functions; the expression is considerably simplified in the cases of 1) a point source, and 2) uniform distribution of amplitudes over the aperture and coincidence of the radiator aperture with the circular projection of the deflector. n_E is plotted as a function of a dimensionless parameter m for three different amplitude distributions over the aperture and five different ratios of the diameter of the radiator aperture to that of the deflector projection; the effect of the amplitude distribution is shown to be small. The results obtained are in good agreement with those calculated by Jakes and the experimental results of Drexler (2565 of 1954).

621.396.677.83 3647
Aerial System with [raised] Reflector—V. D. Kuznetsov. (*Radiotekhnika, Moscow*, vol. 11, pp. 4–15; March, 1956.) The radiation characteristics of various arrangements of the type used at microwave relay stations, comprising a reflector-type antenna and a raised deflecting reflector, are considered theoretically.

621.396.677.833 3648
The Electromagnetic Field of a Dipole Radiator located inside a Paraboloidal Reflector—I. P. Skal'skaya. (*Zh. Tekh. Fiz.*, vol. 25, pp. 2371–2380; November, 1955.) The case of a dipole arranged perpendicular to the axis of the paraboloid is considered. The solution given by Pinney (2687 of 1947) in the form of series of Laguerre polynomials is not justified mathematically. A new solution applicable to the whole region inside the paraboloid is obtained which gives the desired field components in the form of complex integrals. This solution is used to determine the field in the limiting case when the wavelength is much smaller than the focal length of the paraboloid.

621.396.677.833:523.16 3649
The George R. Agassiz Radio Telescope of Harvard Observatory—Bok. (See 3715.)

621.396.677.833.1 3650
Electromagnetic Field of a Linear Radiator located inside an Ideally Conducting Parabolic Screen [reflector]—G. A. Grinberg, N. N. Lebedev, I. P. Skal'skaya, and Ya. S. Uflyand. (*Zh. Eksp. Teor. Fiz.*, vol. 30, pp. 528–543; March, 1956.) The field problem considered earlier (2867 of 1954) is re-examined a more rigorous solution is derived. This is shown to agree with the geometrical-optics solution at frequencies tending to infinity.

621.396.677.833.2 3651
The Far Field of a Paraboloid of Revolution with Hertzian Dipole Normal to the Plane of the Aperture—F. Müller. (*Hochfrequenztech. u. Elektroakust.*, vol. 64, pp. 155–158; April, 1956.) Calculations show that the power density and field direction are rotationally symmetrical about the axis of the paraboloid; the transverse electric field has zero intensity on the axis.

621.396.677.85:621.372.43 3652
Reflection and Transmission at a Slotted Dielectric Interface—R. E. Collin. (*Canad. J. Phys.*, vol. 34, pp. 398–411; April, 1956.) Theory presented by Collin and Brown (2293 of 1956) is extended to the problem of matching a microwave lens to free space for waves incident obliquely. Calculations show that the reflection coefficient can be reduced from 23 per cent to 5 per cent for angles of incidence up to 30°, for waves of 3–3.28 cm λ, the dielectric constant of the slotted medium being 2.56.

AUTOMATIC COMPUTERS

681.142 3653
Trends in Computer Input/Output Devices—J. M. Carroll. (*Electronics*, vol. 29, pp. 142–149; September, 1956.)

681.142 3654
Design of Computer Circuits for Reliability—W. Renwick. (*Electronic Eng.*, vol. 28, pp. 380–384; September, 1956.) Factors influencing the choice of components, and precautions taken during the initial circuit design and mechanical construction of the EDSAC II machine are described.

681.142 3655
A Circuit for Analogue Formation of xy/Z—M. J. Somerville. (*Electronic Eng.*, vol. 28, pp. 388–389; September, 1956.) "A quarter squares multiplier, using a triangle carrier waveform in the squaring circuits is extended to give division simultaneously with multiplication. This is achieved by controlling the slope of the triangle carrier waveform so as to be proportional to the divisor Z."

681.142:621.317.729.1 3656
An Automatic Electron Trajectory Tracer—Pizer, Yates, and Sander (See 3833.)

681.142(083.7) 3657
IRE Standards on Electronic Computers: Definitions of Terms, 1956—(Proc. IRE, vol. 44, pp. 1166–1173; September, 1956.) Standard 56. IRE 8.S1.

CIRCUITS AND CIRCUIT ELEMENTS

621.3.002.2 3658
High-Temperature Components—G. W. A. Dummer. (*Wireless World* vol. 62, pp. 510–512; October, 1956.) New materials and methods of production to meet Service demands are briefly described.

621.3.049.75 3659
Printed Circuits—(See 3902.)

621.318.4.045 3660
Winding Method for Coils with Parallel Windings—P. von Belatini. (*Bull. Tech. Univ. Istanbul* vol. 9, pp. 10–21; 1956. In German.) Theory is presented indicating the purposes for which parallel-wound coils are suited, and practical examples are described.

621.318.57:621.314.7 3661
***P-N-P-N* Transistor Switches**—Moll, Tanenbaum, Goldey, and Holonyak. (See 3899.)

621.318.57:621.385 3662
Ten-Channel Time-Division Multiplexer—H. Moss and S. Kuchinsky. (*Tele-Tech and Electronic Ind.*, vol., 15, pp. 80–82, 154; May, 1956.) A "magnetron" beam-switching tube [3434 of 1955 (Fan)] forms the basis of a 10-contact, single-channel circuit giving switching times of about 0.2 μs. The tube is used in conjunction with a gating system; a gate circuit is described which permits the examination of signals in the microvolt range.

621.319.4:621.373.4 3663
Non-linear D.C.-Tuned Capacitors—T. W. Butler, Jr., H. Diamond, and L. W. Carr. (*Tele-Tech and Electronic Ind.*, vol. 15, pp. 68–69, 135; May, 1956.) The design and production of very small tuning capacitors using Ba-Sr titanate ferroelectric dielectrics is described. Examples are given of applications to oscillators for the frequency range 25–400 mcs, with cw power outputs of 50 mw–3 w.

621.372.011.1 3664
Formulae relating some Equivalent Networks—R. J. Duffin and E. Keitzer. (*J. Math. Phys.*, vol. 35, pp. 72–82; April, 1956.) Explicit formulas are obtained for the elements of a network without transformers which has the same driving-point impedance as an arbitrary two-loop passive network.

621.372.011.2 3665
An Existence Theorem for Driving-Point Impedance Functions—N. DeClaris. (*J. Math. Phys.*, vol. 35, pp. 83–88; April, 1956.)

621.372.029.6:621.318.134 3666
Waveguide Components with Nonreciprocal Properties—J. Brown and P. J. B. Clarricoats. (*Electronic Eng.*, vol. 28, pp. 328–332, 376–379; August/September, 1956.) The mechanism of the nonreciprocal effects occurring when an e.m. wave is propagated through a magnetized material, particularly a ferrite, is discussed; the gyrator, the isolator and the circulator are described.

621.372.029.64:538.569.4 3667
Further Aspects of the Theory of the Maser—Shimoda, Wang, and Townes. (See 3710.)

621.372.412 3668
Variation of the Quality Factor of Piezoelectric Crystals as a Function of Pressure—H. Mayer. (*C.R. Acad. Sci., Paris*, vol. 243, pp. 246–249; July 16, 1956.) Measurements were made on a 100-kc quartz crystal and on a Rochelle-salt crystal, using apparatus described in *J. Phys. Radium*, vol. 17, June, 1956. Supplement to *Phys. Appl.* pp. 104A–107A. Results are presented as $Q/\log p$ curves for values of $\log p$ up to 4, where p is in mm Hg. Decrease of pressure below about 10^{-2} mm Hg does not affect Q value.

621.372.413 3669
Design of a Toroidal Cavity Resonator by the Method of Curvilinear Coordinates—V. L. Patrushev. (*Radiotekhnika i Elektronika*, vol. 1, pp. 162–170; February, 1956.) The application of the formulas derived is illustrated by a calculation of the resonance frequency of a cavity of given dimensions. The calculated value of $\lambda = 23.0$ cm agrees well with the experimental value of 23.2 cm.

621.372.5 3670
Restrictions on the Shape Factors of the Step Response of Positive Real System Functions—A. H. Zemanian. (PROC. IRE vol. 44, pp. 1160–1165; September, 1956.) Extension of previous analysis of the transient response of networks (1577 of 1955).

621.372.5:537.227 3671
Theory of Nonlinear Coupling in a Novel Ferroelectric Device—W. H. Higa. (*J. Appl. Phys.* vol. 27, pp. 775–777; July, 1956.) A device which can be used as a modulator or as a frequency divider or multiplier comprises a block of ferroelectric material with electrodes arranged on two pairs of facing sides. On connecting an inductance across one pair of electrodes a resonant circuit is provided in which the capacitance varies periodically, oscillations being sustained when the frequency of this parametric excitation is twice the resonance frequency of the circuit. Analysis is presented using the Mathieu equation.

621.372.54 3672
The Analysis of Three-Terminal Null Networks—T. H. O'Dell. (*Electronic Eng.*, vol. 28, pp. 398–400; September, 1956.) A simple method of analysis is presented; the twin-T and bridged-T networks are treated as examples.

621.372.54 3673
By-Pass Filters—R. O. Rowlands. (*Wireless Eng.*, vol. 33, pp. 238–240; October, 1956.) "By-pass filters are described having three pairs of terminals and in which all frequencies are passed, without distortion, between two of the pairs but only a limited band of frequencies is transmitted between either of these pairs and the third pair of terminals."

621.372.543.3 3674
An Improved Crystal Band-Elimination Filter—R. C. Leigh. (*A.T.E. J.*, vol. 12, pp. 101–106; April, 1956.) An all-pass network consisting of two filters in parallel is described, suitable for applications in which it is required to transmit a wide frequency range while suppressing one or more narrow frequency bands within the range. Internal impedance transformations eliminate the need for high-ratio transformers.

621.372.56.029.6:621.372.8:621.318.134 3675
The Field Displacement Isolator—S. Weisbaum and H. Seidel. (*Bell. Syst. Tech. J.*, vol. 35, pp. 877–898; July, 1956.) A nonreciprocal device with forward loss about 0.2 db and reverse loss about 30 db over a wide band at about 6 kmc is based on use of a single ferrite slab spaced from the wall of a rectangular waveguide and having a resistive strip on one face. Optimum field conditions in the waveguide are discussed.

621.372.57:621.374.34 3676
Operation of an Amplitude Limiter—M. E. Zhabotinski and Yu. L. Sverdlov. (*Radiotechnika i Elektronika* vol. 1, pp. 205–212; February, 1956.) Theoretical analysis and experimental evidence suggest that the stray capacitance shunting the nonlinear element causes a parasitic phase modulation of the output signal and limits the efficiency. A neutralized circuit is shown and design formulas are given.

621.372.632:621.314.63 3677
Two-Terminal *P-N* Junction Devices for Frequency Conversion and Computation—Uhlir. (See 3894.)

621.373.421.1 3678
Mutual Synchronization of Three Coupled Oscillators with Weak Coupling—V. N. Parygin. (*Radiotekhnika i Elektronika*, vol. 1, pp. 197–204; February, 1956.) The system investigated theoretically and experimentally comprises three triode tube oscillators coupled by small capacitors between the grids of the first and second and second and third tubes. Approximate expressions are derived for the frequency and amplitude of the oscillations in each oscillator. The regions where mutual synchronization takes place are shown in a Δ_2/Δ_1 graph, where Δ_1 and Δ_2 are respectively the frequency differences between the first and second and the third and second oscillators.

621.373.421.13:621.396.96 3679
Stable Local Oscillator for S-Band Radar—W. J. Dauksher. (*Electronics*, vol. 29, pp. 179–181; September, 1956.) A continuous frequency range of 1.3 per cent is obtained using six crystal oscillators tunable over overlapping ranges of 0.25 per cent. The desired output frequency is obtained by means of harmonic amplifiers.

621.374.3 3680
A Possible Construction of Amplitude Analysers—A. M. Bonch-Bruevich. (*Zh. Tekh. Fiz.*, vol. 25, pp. 2397–2398; November, 1955.) A circuit is described by means of which pulses with amplitudes exceeding or lying within certain limits can be counted.

621.374.3:621.396.822 3681
Influence of Large Fluctuations on an Electronic Relay—V. I. Tikhonov. (*Radiotekhnika i Elektronika*, vol. 1, pp. 213–224; February, 1956.) The probability of untimely triggering by fluctuation voltages is considered theoretically. The cases discussed include the effect of fluctuations on a relay with or without inertia both in the presence and in the absence of regular pulses; the effect on a coincidence-type circuit is also discussed.

621.375.13 3682
Effect of Component Tolerances in Low-Frequency Selective Amplifiers: some Experimental Results—N. S. Nagaraja and V. Rajaraman. (*J. Indian Inst. Sci.*, vol. 38, pp. 81–92; April, 1956.) Results obtained previously by analysis [1339 of 1956 (Nagaraja)] have been verified experimentally, using the operational amplifiers of the PREDA analog computer [24 of 1956 (Biswas *et al.*)].

621.375.232.3:621.3.018.75 3683
Trailing Edge of Pulse in Cathode Follower with Capacitive Load—M. L. Volin. (*Radiotekhnika, Moscow*, vol. 11, pp. 63–69; March, 1956.) The decay time of a rectangular pulse at the output of a cathode follower can be shortened by connecting a triode in parallel with the cathode resistor and capacitor and controlling the triode grid voltage via a RC coupling from the anode of the cathode-follower tetrode tube. The circuit constants are such that the triode impedance decreases momentarily at the end of each pulse.

621.375.4:621.314.7 3684
The Design of Tetrode Transistor Amplifiers—J. G. Linvill and L. G. Schimpf. (*Bell Syst. Tech. J.*, vol. 35, pp. 813–840; July, 1956.) Methods are discussed for determining suitable loads when the two-port parameters of the transistor are known. Charts are presented for determining power gain and input impedance as functions of load. Circuits described as examples include a common-base 20-mc video amplifier, a common-emitter 10-mc video amplifier, and IF amplifiers centered at 30 mc and 70 mc respectively. Predicted and measured gains are compared.

621.375.4:621.314.7 3685
Servo Amplifiers use Power Transistors—B. M. Benton. (*Electronics*, vol. 29, pp. 153–155; September, 1956.) High efficiency in a class-B-type amplifier using Ge power transistors is obtained by providing the collector power by full-wave rectification of the ac power supply.

621.375.4:621.314.7:546.28 3686
Micro-power Operation of Silicon Transistors—Keonjian. (See 3898.)

GENERAL PHYSICS

535.33-1:535.417:538.569.4 3687
Interferometric Spectroscopy in the Far Infrared—H. A. Gebbie and G. A. Vanasse. (*Nature, Lond.*, vol. 178, p. 432; August 25, 1956.) The response of a thermal detector to the resultant of two interfering infrared beams was measured using a reflection interferometer with the path difference varied up to 7 mm. The spectral information is displayed in a Fourier transform obtained by analysis of the resultant-intensity/path-difference curve. An instrument with 30-cm aperture has been made for studying atmospheric transmission at submillimeter wavelengths.

537.2 3688
An Extension of the Circle and Sphere Theorems—G. Power. (*Brit. J. Appl. Phys.*, vol. 7, pp. 218–221; June, 1956.) Theory relating to cylinders and spheres immersed in two- and three-dimensional electric fields (*e.g.*, 3555 of 1955) is extended to include certain other boundaries along which either the electric potential or the current function takes a constant value.

537.311.1 3689
On the Bohm-Pines Theory of a Quantum-

discussed previously [*e.g.*, 403 of 1956 (Gordon *et al.*)] are examined; various types of noise and oscillator frequency shift are considered. The theoretical minimum detectable beam intensity when the maser is used as a spectrometer for the 3-3 ammonia line is about 10^9 molecules/sec under typical experimental conditions.

621.318.3 3711

A General-Purpose Electromagnet—W. Sucksmith and S. P. Anderson. (*J. Sci. Instrum.*, vol. 33, pp. 234–236; June, 1956.) Details are given of a magnet for laboratory purposes, with a soft iron yoke having low residual magnetism and poles of diameter 10 cm, together with a table showing the variation of the field in the center of the gap with excitation and gap length.

GEOPHYSICAL AND EXTRATERRESTRIAL PHENOMENA

523.16 3712

Distribution of Radio Stars—J. G. Bolton. (*Observatory*, vol. 76, pp. 62–64; April, 1956.) A tentative explanation is given of discrepancies between the distribution derived by Ryle from interferometer measurements at 81 mc and that derived by Pawsey from Mills Cross measurements, also at 81 mc, as discussed at the recent Jodrell Bank symposium.

523.16 3713

The Radio Source near the Galactic Centre—B. Y. Mills. (*Observatory*, vol. 76, pp. 65–67; April, 1956.) Recent observations on 3.5 m λ with the "cross" antenna are discussed in relation to earlier observations on 9.4 cm and 21 cm λ. The position of the dominant source is shown on a contour map of equivalent brightness temperatures. Alternative models accounting for the observations and involving absorbing H II regions are mentioned; whichever model is assumed, the nucleus of Type-II stars in the Galaxy is not itself detectable as a rf source.

523.16 3714

Polarization Measurements on Three Intense Radio Sources—R. H. Brown, H. P. Palmer, and A. R. Thompson. (*Mon. Not. R. Astr. Soc.*, vol. 115, pp. 487–492; 1955.) Measurements have been made on radiation of wavelength 1.9 m from sources in Cygnus, Cassiopeia, and Taurus. The results indicate that there is no plane polarized component >1 per cent and no circularly polarized component >4 per cent in the flux from the first two of these sources; the corresponding figures for the source in Taurus are $2\frac{1}{2}$ per cent and 4 per cent respectively.

523.16:621.396.677.833 3715

The George R. Agassiz Radio Telescope of Harvard Observatory—B. J. Bok. (*Nature Lond.*, vol. 178, pp. 232–234; August 4, 1956.) The antenna of this 60-ft instrument is a paraboloid of expanded aluminium-wire mesh with a horn collector at the focus. At a wavelength of 21 cm the angular resolution is about 0.7°, thus the accuracy of setting and following is more than sufficient for research on discrete radio sources. The receiver is a double-conversion superheterodyne comparison radiometer with a 20-channel comb filter at the second conversion frequency. The instrument is to be used both for research and training.

523.5 3716

Some Factors affecting the Radio Determination of Meteoric Velocities—D. W. R. McKinley. (*Naturwissenschaften*, vol. 43, pp. 221–222; May, 1956. In English.) Questions raised by Hoffmeister (409 of 1956) are discussed further. Deceleration of meteors along the path prior to the point of measurement may be an important factor; techniques for measuring the deceleration over an appreciable path length by the radio amplitude/time method require to be developed. Existing techniques may be failing to detect faint meteors with hyperbolic orbits.

523.5:621.396.96 3717

Radar Echoes from Meteor Trails under Conditions of Severe Diffusion—G. S. Hawkins. (PROC. IRE, vol. 44, p. 1192; September, 1956.) An expression is derived indicating that the power of the echo is proportional to λ^6 and to R^{-4}, where R is the range. For a given meteor velocity there is a critical height above which the effects of diffusion become serious. A graph shows the critical-height/velocity curves for values of λ between 0.5 and 16 m.

523.7:621.396.677.3 3718

The Multiple-Aerial Interferometer at the Nançay Station—Blum, Boischot, and Ginat. (See 3644.)

523.72:523.78 3719

Radio-Frequency Observations of the Solar Eclipse of June 30, 1954,—G Eriksen, Ø. Hauge, and E. Tandberg-Hanssen. (*Astrophys. Norveg.*, vol. 5, pp. 131–152; August, 1955.) "Radio-frequency power received from the sun at wavelengths of 60 cm and 1.5 m was measured during the solar eclipse of June 30, 1954. The sun was essentially free from active areas, and the eclipse curves obtained have been used to derive models of the radio sun at the two wavelengths. These models give predicted eclipse curves in good agreement with the observed ones. Comparison has been made with models derived by other investigators on the same wavelengths."

523.746 3720

The Constancy of the Scale of the Relative Sunspot Numbers—W. Gleissberg. (*Naturwissenschaften*, vol. 43, p. 196; May, 1956.) Comparison of sunspot numbers with the Greenwich data for sunspot areas over several cycles indicates that the proportionality factor between total sunspot area and relative sunspot number increases with the latter, but there is no significant variation of the scale of the relative sunspot number.

550.38:523.165 3721

Effective Geomagnetic Equator for Cosmic Radiation—J. A. Simpson, K. B. Fenton, J. Katzman, and D. C. Rose. (*Phys. Rev.*, vol. 102, pp. 1648–1653; June 15, 1956.) The distribution of the geomagnetic field extending far from the surface of the earth is investigated by using cosmic-ray particles as probes. Measurements using the neutron intensity from the nucleonic component indicate wide discrepancies between the observations and geomagnetic coordinates derived from surface magnetic-field measurements. Some anomalous observations of cosmic rays can be explained as due to the interaction of the rotating and inclined magnetic dipole field with a highly ionized interplanetary medium. See also 2371 of 1956 (Simpson *et al.*).

550.385:523.78 3722

Theory of Solar-Eclipse Effects on the Earth's Magnetic Field—H. Volland. (*J. Atmos. Terr. Phys.*, vol. 9, pp. 131–143; August/September, 1956. In German.) "The deformation of the S_q current during a solar eclipse is represented by a current function S_e, which is superposed on the S_q system and moves with the eclipse. The magnetic field components of S_e are computed, and the influence of the part induced in the earth's crust is discussed."

551.5 3723

Upper-Air Density and Temperature by the Falling-Sphere Method—F. L. Bartman, L. W. Chaney, L. M. Jones, and V. C. Liu. (*J. Appl. Phys.*, vol. 27, pp. 706–712; July, 1956.) Technique and results are described of a method for investigating the atmosphere at heights up to 100 km. A 4-ft nylon sphere with a transponder and antenna is ejected from a rocket near the peak of its trajectory.

551.510.5:621.396.11 3724

Turbulent Mixing Theory applied to Radio Scattering—Silverman. (See 3853.)

551.510.534 3725

An Experimental Investigation of the 9.6-μ Band of Ozone in the Solar Spectrum—C. D. Walshaw and R. M. Goody. (*Quart. J. R. Met. Soc.*, vol. 82, pp. 177–186; April, 1956.) Mean heights of atmospheric ozone have been investigated over a period of two years, using Strong's method (1297 of 1941). A seasonal variation is observed, with a minimum height in summer and a range of 3.4 km.

551.510.534 3726

Determination of the Vertical Distribution of Ozone from Emission Spectra—R. M. Goody and W. T. Roach. (*Quart. J. R. Met. Soc.*, vol. 82, pp. 217–221; April, 1956.)

551.510.535 3727

Electron Density in a Nonisothermal Ionosphere—F. Mariani. (*Ann. Geofis.*, vol. 9, pp. 43–62; January, 1956.) Continuation of work noted previously (749 of 1956). The difference in the calculated values of electron density when the earth's curvature is taken into account may be appreciable, especially for the winter; the corresponding difference in critical frequency may amount to 20–25 per cent for the for the period just after sunrise. Comparison of calculated and observed values of f_0F_1 suggests that a representative model of an F region can be based on the assumption that the temperature varies linearly with height up to the F_1/F_2 interface and then remains constant. The parabolic law of variation of electron density is acceptable only for heights corresponding to reflection frequencies not less than 0.7–0.8 times the critical frequency. A general expression is derived relating temperature, electron density, density of matter, recombination coefficient, and absorption coefficient.

551.510.535 3728

Resonance Scattering by Atmospheric Sodium: Part 1—Theory of the Intensity Plateau in the Twilight Airglow—J. W. Chamberlain. (*J. Atmos. Terr. Phys.*, vol. 9, pp. 73–89; August/September, 1956.) Numerical results based on theory of radiative transfer are compared with observations by various workers, for a layer scattering solar D-line radiation, observed in the zenith or at zenith distance 75°. Winter observations indicate an absolute brightness slightly greater than given by the theory. Abundance of Na appears to vary between 10^9 (summer) and 10^{10} (winter) atoms/cm² (column).

551.510.535 3729

The Effect of Ambipolar Diffusion in the Night-Time F Layer—J. W. Dungey. (*J. Atmos. Terr. Phys.*, vol. 9, pp. 90–102; August/September, 1956.) The effect is examined in the light of recent low estimates of the density of neutral particles in the F layer [*e.g.*, *Rocket Exploration of the Upper Atmosphere*, p. 347, 1954 (Cates)] and assuming that the rate of loss of electrons is proportional to the electron density, N. With certain other simplifying assumptions, N may be expressed as a sum of functions which decay exponentially with time; an approximately parabolic (Chapman) model based on the most slowly decaying of these is discussed. Correlation is found between both f_0F_1 and the magnetic C figure and the sunspot-cycle variation of the F-region temperature.

551.510.535 3730
Observation at Akita of Ionospheric Drift—Y. Ogata. (*J. Radio Res. Labs, Japan*, vol. 3, pp. 135–140; April, 1956.) Simultaneous observations of the variations with time of the virtual heights of the E, E_s and F layers were made at three observatories in Japan, during the period July–August, 1955, mainly at night. Drift velocities of the layers are deduced; the results are presented in the form of histograms.

551.510.535:[523.3+523.7 3731
Lunar Variations of the F_1 Layer at Ibadan—R. A. Brown. (*J. Atmos. Terr. Phys.*, vol. 9, pp. 144–154; August/September, 1956.) Analysis of h_m, $y_m f_0$ and h' determinations for the F_2 layer, made at Ibadan from December 1951 to April 1954, shows semidiurnal lunar variations of considerable amplitude; these variations in turn exhibit marked variations of amplitude and phase with season and with time of solar day. Values of the recombination coefficient in the layer, deduced from the luni-solar variations, decrease exponentially with increasing height.

551.510.535:523.78 3732
Behaviour of the Ionosphere at Rome during the Partial Solar Eclipse of 30th June 1954—P. Dominici. (*Ann. Geofis.*, vol. 9, pp. 107–131; January, 1956.) Observed eclipse effects are compared with effects calculated on the assumption that the electrons are produced by photo-ionization and removed by ionic recombination or attachment to neutral atoms and molecules, and that the ionizing radiation is distributed uniformly over the visible disk of the sun. It is deduced that the electron loss rate is consistent with an ionic recombination process in the E and F_1 layers and with an attachment process in the F_2 layer. The attachment and recombination coefficients decrease with increasing height; their variations during the eclipse are related to the vertical movements of the ionosphere. Seasonal variations between effects observed in a number of eclipses are explained in terms of different degrees of superposition of the F_1 and F_2 layers. The existence of secondary minima of electron density is interpreted as indicating that a distinction must be drawn between the "ionizing" sun and the visible sun. Eclipse effects in the E_s layer are also discussed. 62 references.

551.510.535:523.78 3733
Recombination and Attachment in the F_1 and F_2 Layers during the Solar Eclipse of 25 December, 1954—M. E. Szendrei and M. W. McElhinny. (*J. Atmos. Terr. Phys.*, vol. 9, pp. 118–130; August/September, 1956.) Examination of the variations of electron density at Grahamstown in relation to actual, rather than virtual, heights in the F region during the annular eclipse of December 25, 1954 suggests that the recombination process is predominant in the F_1 region; in the F_2 region, recombination and attachment coefficients decrease regularly with height. Possible explanations of the separation of the F_1 and F_2 layers are advanced.

551.510.535:537.533.1:621.396.11 3734
Theory of Nonlinear Effects in the Ionosphere—Zhevakin and Fain. (See 3856.)

551.510.535:621.3.087.4 3735
Ionospheric Sounding Equipment—J. O. Cardus. (*Rev. Geofis., Madrid*, vol. 14, pp. 285–312; October/December, 1955.) The characteristics of the ionosphere are briefly reviewed and some soundings obtained at the Tortosa station, inaugurated in 1955, are reproduced. The sounding equipment installed is identical with that used by the Bureau Ionosphérique Français.

551.510.535:621.396.11 3736
Ionospheric Prediction Methods and the Probable Sources of Error—Baral. (See 3854.)

551.510.535:621.396.11 3737
Equatorial Ionospheric Absorption—Skinner and Wright. (See 3855.)

551.510.535:621.396.812.3 3738
Study of the Selective Fading appearing on the *fct*-Traces—Uyeda and Nakata. (See 3863.)

551.594.5 3739
Height Distribution of Auroral Emissions—L. Harang. (*J. Atmos. Terr. Phys.*, vol. 9, pp. 157–159; August/September, 1956.)

551.594.5:551.508:621.397.424 3740
Measurement of Auroral Radiation 3200 Å with a Photon Counter (Geiger Tube)—E. V. Ashburn. (*J. Atmos. Terr. Phys.*, vol. 9, pp. 156–157; August/September, 1956.) A copper-cathode G-M counter is satisfactory for measuring this radiation.

551.594.6:621.396.821 3741
The Level of Interference due to Atmospherics in the Very-Long-Wave Range, and its Diurnal and Seasonal Variations—Lauter. (See 3868.)

LOCATION AND AIDS TO NAVIGATION

621.396.96 3742
Radar Echoes from Birds and Insects—L. L. Bonham and L. V. Blake. (*Sci. Mon.*' vol. 82, pp. 204–209; April, 1956.) General discussion and report of observations confirming Crawford's view (2300 of 1949) that certain otherwise unexplained echoes are in fact due to birds and insects. The quantitative aspects of the phenonena are briefly touched on.

621.396.96:621.396.62:621.396.822 3743
Technical Possibilities for Noise Reduction in the Reception of Weak Radar Signals—H. Borg. (*Ann. Télécommun.*, vol. 11, pp. 90–110; May, 1956.) Known systems for detecting a weak signal in the presence of noise are critically reviewed. The optimum-filter method is most generally useful. Correlation methods are not directly applicable to the detection of moving targets, but are best for detecting very weak periodic signals. 40 references.

621.396.96:621.397.2 3744
The Transmission of Radar Displays with Compressed Bandwidth—H. Meinke and H. Groll. (*Nachrichtentech. Z.*, vol. 9, pp. 214–221; May, 1956.) Methods using cr tubes with line-storage techniques are discussed; the bandwidth can be reduced to 12 kc. The requirements in respect of scanning precision are stringent, but much less so than with area storage. Special pulses are used for distortion testing. Photographs show original and transmitted displays obtained at Munich using Decca radar equipment on a tower. The possibility of storing the display on magnetic tape is also discussed.

621.396.96.001.362 3745
A Synthetic Radar Trainer—F. W. Cook. (*A.T.E.J.*, vol. 12, pp. 89–100; April, 1956.)

621.396.962.2:621.376.3 3746
A Precise New System of F. M. Radar—M. A. W. Ismail. (PROC. IRE, vol. 44, pp. 1140–1145; September, 1956.) A system for measurement of both range and speed of the target uses a sinusoidal rather than a symmetrical triangular frequency-modulating waveform. Relatively small frequency deviations are required, and there is no fixed error, hence short ranges can be measured accurately. Brief details are given of an altimeter based on the principles discussed.

621.396.962.3 3747
Maximum Angular Accuracy of a Pulsed Search Radar—P. Swerling. (PROC. IRE, vol. 44, pp. 1146–1155; September, 1956.) "Using a result in the theory of statistical estimation, a lower bound is derived for the standard deviation of regular unbiased estimates of target angular position, for a large class of methods of angular position determination; the lower bound depends on scan rate, pulse repetition rate, beamwidth, beam shape, and signal-to-noise ratio. A similar analysis is made of the limits on angular accuracy imposed by a combination of receiver noise and one particular type of target cross section fluctuation. . . . The relation between the estimation of angular position and the problem of target detection is discussed. A graphical presentation of the main results is given."

MATERIALS AND SUBSIDIARY TECHNIQUES

533.5 3748
Ionic Pump with Cold Electrodes, and its Characteristics—E. M. Reikhrudel', G. V. Smirnitskaya, and A. I. Borisenko. (*Radiotekhnika i Elektronika*, vol. 1, pp. 253–259; February, 1956.) The characteristics of an ionic pump using both an electric and a magnetic field were investigated. Pressures down to 5×10^{-8} mm Hg have been obtained in particular cases, the normal working range being 10^{-2}–10^{-7} mm Hg with air, Ne and He.

535.215:537.311.33 3749
Optical and Electrical Measurements on Caesium-Antimony Layers of Different Composition—G. Wallis. (*Ann. Phys., Lpz.*, vol. 17, pp. 401–416; April 30, 1956.) Measurements are reported of the optical absorption and temperature dependence of conductivity for Cs-Sb layers produced by a method giving rise to a stratified structure. The absorption measurements were extended beyond the region of photosensitivity into the infrared. Values are derived and discussed for the activation energy. The nature of the particular compound formed and the influence of the crystal structure on the results are considered. The absorption of films of pure Sb and Cs at wavelengths of 400–1800 mμ was also measured.

535.215+535.37]:546.482.21 3750
Photoconductivity and Luminescence of Polycrystalline CdS(Cu)—N. A. Tolstoi, B. T. Kolomiets, O. I. Golikova, and M. Ya. Tsenter. (*Zh. Eksp. Teor. Fiz.*, vol. 30, pp. 575–576; March, 1956.) Brief report on results of measurements on nine CdS specimens containing up to 10^{-3} g/g Cu and one specimen containing 10^{-3} g/g Cu and 10^{-5} g/g Fe. The results are discussed in relation to the degenerate bimolecular recombination mechanism and the two-step excitation mechanism.

535.215:546.817.221:539.234 3751
Photosensitization of PbS Films—R. H. Harada and H. T. Minden. (*Phys. Rev.*, vol. 102, pp. 1258–1262; June 1, 1956.) Experiments are reported in which evaporated PbS films were treated with O_2 and the resulting changes in the photoconductive response were observed. The variations of conductance in the absence and in the presence of illumination are found to be correlated. The photoconduction response time increases monotonically as the film changes from *n*- to *p*-type. The results are interpreted in terms of two oxygen surface states.

535.37 3752
Excitation and Destruction of Phosphors by H^+ Ions—H. P. Gilfrich. (*Z. Phys.*, vol. 145, pp. 241–248; April 17, 1956.) Measurements have been made of the reduction of luminescence intensity in various inorganic and organic phosphors bombarded by 10-kV H^+ ions. The reduction can be expressed by the formula $I/I_0=1/1+CN$, where N is the number of ions and C is the "destruction constant." The value of C drops to about a tenth for each step of the series constituted by organic phosphors,

MATHEMATICS

517.632 3819
Inverse Laplace Transforms expressed as Neumann Series—E. Cambi. (*J. Math. Phys.*, vol. 35, pp. 114–122; April, 1956.)

517.9 3820
On the Classification of the Ordinary Differential Equations of Field Theory—P. Moon and D. E. Spencer. (*Quart. Appl. Math.*, vol. 14, pp. 1–10; April, 1956.)

517.9:681.142 3821
Extension of Field of Application of Relaxation Methods of Computation—B. E. Knight and D. N de G. Allen. (*Nature, Lond.*, vol. 178, pp. 433–434; August 25, 1956.) The possibilities of solving linear and nonlinear partial differential equations by relaxation methods, using computers, are discussed.

MEASUREMENTS AND TEST GEAR

53.087.9 3822
A Semi-automatic Pen-Recorder Chart Analyser—C. W. Spencer and G. H. Bazzard. (*J. Sci. Instrum.*, vol. 33, pp. 228–229; June, 1956.) The contact arm of a multicontact switch connected to a pulse generator is made to follow the chart trace. Counters brought into circuit by the moving switch arm record pulse counts proportional to the time the trace is between preselected levels.

531.761+529.7+621.3.018.41(083.74) 3823
Standards of Time and Frequency—G. M. Clemence. (*Science*, vol. 123, pp. 567–573; April 6, 1956.) Basic concepts are reviewed. Problems involved in the concurrent use of an atomic and an astronomical standard are discussed. See also 1153 of 1956.

621.317.3:537.311.33 3824
Contactless Method for the Estimation of Resistivity and Lifetime of Semiconductors—H. K. Henisch and J. Zucker. (*Rev. Sci. Instrum.*, vol. 27, pp. 409–410; June, 1956.)

621.317.3.029.63:621.396.822 3825
Noise Measurements in the 3-cm Waveband using a Hot Source—H. Sutcliffe. (*Proc. IEE*, vol. 103, pp. 673–677; September, 1956.) "The method discussed uses the noise power produced in a waveguide termination at temperatures up to 600°C. as a standard source of low-level power. A suitable type of hot source and associated waveguide and detecting circuits are described. Some experimental results are given of measurements on the effective temperature of a gas-discharge tube used as a secondary standard source."

621.317.32:621.396.621:621.376.3 3826
Measurements of Interference Radiation from F.M. Receivers, carried out in Switzerland by a Group of Experts of the International Electrotechnical Commission Subcommittee 12-1 (Radio Communications—S.C. Measurements)—J. Meyer de Stadelhofen. (*Tech. Mitt. Schweiz. Telegr.-Teleph Verw.*, vol. 34, pp. 158–166; April 1, 1956. In French.) Measurements were made on 14 fm receivers from six different countries, using various methods, the main features of which are tabulated. Measurements at distances of 30, 10, and 3 m give practically equivalent results. The Seright-Anderson method, in which the measurements are made at a distance of 3 m, is probably most suitable for standardization.

621.317.6:519.272.1 3827
Technique for Approximate Measurement of Correlation Coefficients—T. P. Goodman. (*J. Appl. Phys.*, vol. 27, pp. 773–775; July, 1956.) "This method makes use of simple analog-computing elements to obtain the coefficient of linear regression of one variable on the other. Its use in connection with an oscilloscope display of the two variables is described, and the relation between these displays and the Lissajous figure formed by two sinusoids is discussed. A possible design for a direct-reading correlation meter is suggested."

621.317.6:621.396.822 3828
Calculating Noise Level in Radar Receivers—D. W. Haney. (*Tele-Tech. and Electronic Ind.*, vol. 15, pp. 74–75; 123; May, 1956.) For a receiver in which the second detector is a tube diode, the rms noise level is derived simply in terms of equivalent input voltage from the rf-input/second-detector-output characteristic. The method is based on the theory of Rice for nonlinear detectors (2168 and 2169 of 1945); its application to the present case is justified theoretically, and an experimental verification is described.

621.317.7.029.63:537.54:621.396.822 3829
Absolute Calibration of a Standard-Temperature Noise Source for Use with S-Band Radiometers—V. A. Hughes. (*Proc. IEE*, vol. 103, pp. 669–672; September, 1956.) "To provide a standard-temperature noise source for use with S-band radiometers, the noise power from the argon discharge tube CV1881 has been calibrated at 2860 mc using radiometer techniques. The absolute value of the effective temperature of the tube with a discharge current of 180 ma, when mounted across a waveguide parallel to the E-plane and properly matched, is 11 140°K (15.73 db) with a maximum error of 260°K (0.10 db), and represents a considerable improvement in accuracy over previous measurements. Since this tube shows a high degree of stability and consistency it is suggested that it could be used as an absolute standard of noise source for the measurement of the noise factor of receivers."

621.317.7.087.6 3830
Servo-Operated Recording Instruments—A. J. Maddock. (*Proc. IEE*, vol. 103, pp. 617–632; September, 1956.) A historical review of these instruments is presented, followed by a detailed discussion of the principal modern types, classified according to the circuit component which is varied to produce balance; this may be a resistor, a capacitor, or an electromagnetic device. Function plotters, scanning recorders, and other special types are included.

621.317.715.087 3831
Wide-Amplitude String Galvanometer for Direct Recording—L. B. Browder. (*Rev. Sci. Instrum.*, vol. 27, pp. 363–368; June, 1956.) The use of compliant end supports for the string makes possible an extended frequency range; a string 10-cm long, having a resonant frequency of 230 cps, can be made to vibrate with an amplitude of 2.5 cm.

621.317.725/.726 3832
The Modern Valve Voltmeter and its Uses—G. Hitchcox. (*Brit. Commun. Electronics*, vol. 3, pp. 238–242; May, 1956.) The short survey presented includes descriptions of seven modern types of instrument and a guide to the selection of instruments for various applications. The characteristics of 27 instruments, mainly of British manufacture, are tabulated.

621.317.729.1:681.142 3833
An Automatic Electron-Trajectory Tracer—J. G. Yates and K. F. Sander. (*J. Electronics*, vol. 2, pp. 65–86; July, 1956.) Field measurements are made using an electrolytic tank, and the equations of electron motion are hence derived using a specially designed digital computer. The results of the computation are fed back to the tank so that the measuring probes automatically trace the required trajectory.

621.317.74:621.397.6.001.4 3834
Portable Color-Signal Generator—J. R. Popkin-Clurman. (*Electronics*, vol. 29, pp. 170–172; September, 1956.) The circuit described provides a signal including a horizontal synchronizing pulse, a 3.58-mc reference burst and black, color, and white bars.

621.317.77 3835
A Fast-Acting Phase-Conscious Indicator—D. L. Davies. (*Electronic Eng.*, vol. 28, pp. 385–387; September, 1956.) A phase-sensitive rectifier circuit consists of two similar cathode followers connected in parallel and gated by applying to the grids rectangular-waveform voltages of signal frequency, 180° out of phase. In an instrument designed to operate over the frequency range 60 cps–24kc, second- and third-harmonic rejection and quadrature-signal rejection were all >100/1.

OTHER APPLICATIONS OF RADIO AND ELECTRONICS

531.768:551.51 3836
Transit-Time Accelerometer—L. M. Jones. (*Rev. Sci. Instrum.*, vol. 27, pp. 374–377; June, 1956.) A device is described for measuring the drag acceleration of spheres dropped from rockets, thus permitting the density and temperature of the upper atmosphere to be determined. A bobbin is periodically held and released within a cavity contained in the following sphere; the time taken for the released bobbin to reach the cavity wall is measured. A range from 5×10^{-3} *g* to 5 *g* is covered.

535.82:621.397.6 3837
Television Microscopy—W. Köhler. (*Optik, Stuttgart*, vol. 13, pp. 186–191; 1956.) Apparatus combining an ordinary microscope with electronic pickup and reproduction of the image is discussed. Both photoemissive and photoconductive pickup tubes have been used. One of the advantages of the system over the usual optical projection system is that contrast can be controlled to some extent, leading to improved resolution in some cases.

539.172.4:621.317.7:621–52 3838
Control of Nuclear Reactors—(*Proc. IEE*, vol. 103, pp. 564–616; September, 1956.) Four papers and discussion dealing with experimental reactors are presented:—

The Control and Instrumentation of a Nuclear Reactor—A.B. Gillespie (pp. 564–576).

The Control of Nuclear Reactors—R. J. Cox and J. Walker (pp. 577–589).

Nuclear-Reactor-Control Ionization Chambers—W. Abson and F. Wade (pp. 590–596).

Some Design Aspects of Nuclear-Reactor Control Mechanisms—G. E. Lockett (pp. 597–607).

Discussion (pp. 607–616).

550.837:538.566.2.029.42 3839
Possibility of using the Intrinsic Electromagnetic Field Impedance of the Earth for investigating its Upper Layers—A. N. Tikhonov and D. N. Shakhsuvarov. (*Bull. Acad. Sci. U.R.S.S., Sér. Géophys.*, pp. 410–418. April, 1956. In Russian.) The use of vlf em waves for investigating stratified conducting media is considered theoretically and some quantitative calculated results are given.

621.316. 825:616–7 3840
Thermistor Hypodermic Needle for Subcutaneous Temperature Measurement—J. Krog. (*Rev. Sci. Instrum.*, vol. 27, pp. 408–409; June, 1956.)

621.317.39:531.77 3841
Potentiometer Tachometer has High Sensitivity—G. M. Davidson and M. Pavalow. (*Electronics*, vol. 29, pp. 158–161; September, 1956.) By using a linear potentiometer transducer to feed a differentiating operational amplifier a direct output voltage proportional to

the input rate is obtained. Rotation in either direction may be measured by using duplicate channels suitably switched. An accuracy within about 0.5 per cent is obtained without special temperature compensation; the minimum speed measurable is 1/200 rev/min, with a range of 16,000:1.

621.327.43:535.376 3842
The Voltage Drop through Phosphor Screens and its Bearing on Performance of Cathodoluminescent Lamps—Koller. (See 3756.)

621.365.55 3843
The Electric Field of a Dielectric Heating Work Circuit—N. H. Langton and E. E. Gunn. (*J. Brit. Instn. Radio Engrs.*, vol. 16, pp. 414–424; August, 1956.) A theoretical investigation is made of work circuits in which the lower capacitor plate is larger than the upper; the fringing effect and the relation between specimen and capacitor-plate dimensions are studied. Some experiments on field plotting using an electrolytic analog are described.

621.383.5:531.745 3844
Balloon-Borne System for tracking the Sun—H. D. Edwards, A. Goddard, Jr., M. Juza, T. Maher, and F. Speck (*Rev. Sci. Instrum.*, vol. 27, pp. 381–385; June, 1956.) Photoelectrically controlled apparatus weighing 125 lb is described, capable of pointing a 20-lb load at a predetermined evaluation and azimuth with an accuracy of $\pm 15'$. Results of balloon flights attaining an altitude $> 100{,}000$ ft are given.

621.384.6:621.319.339 3845
Some Problems on the Design and Construction of Nuclear-Physics Particle Accelerators for Particle Energies of a few MeV—K. Simonyi. (*Nuovo Cim.*, vol. 3, Supplement, pp. 345–362; 1956. In German.) Particles of energies down to 0.03 mev are useful for research and practical applications. The range of applications corresponding to different ranges of energy values is shown graphically; for energies up to a few mev, direct accelerators with cascade or Van de Graaff generators are used. A model with a Van de Graaff generator developed at Budapest is described. The same material is presented in two consecutive papers, in German, in *Acta Tech. Acad Sci. hungaricae*, vol. 15, pp. 191–204; 1956.

621.384.612 3846
Storage-Ring Synchrotron: Device for High-Energy Physics Research—G. K. O'Neill. (*Phys. Rev.*, vol. 102, pp. 1418–1419; June 1, 1956.) Increased energy is made available, in an accelerator with a strong, well focused external beam, by means of two "storage rings" comprising focusing magnets with straight sections built near the accelerator and operated at a high fixed field strength. Each ring contains a set of foils shaped so as to prevent the beams striking the inflectors.

621.385.83:621.386.1 3847
Electron Optics of X-Ray Tubes and the Design of Unbiased Sharply-Focusing Cathodes—A. R. Lang and D. A. G. Broad. (*Brit. J. Appl. Phys.*, vol. 7, pp. 221–226; June, 1956.)

621.385.833 3848
Investigation of Nonrotationally Symmetrical Electrostatic Electron Optical Lenses—R. F. Whitmer. (*J. Appl. Phys.*, vol. 27, pp. 808–815; July, 1956.) Analysis is presented for a two-cylinder lens.

621.385.833 3849
Practical Realization of a Magnetic Four-Pole Lens for Very-High Frequency Particles—A. Septier, (*C.R. Acad. Sci.*, Paris, vol. 243, pp. 132–135; July 9, 1956.) A lens for focusing 50-mev protons, with a focal length variable between 0.8 and 3 m, uses an electromagnet with four-pole pieces formed by portions of circular cylinder.

621.387.4:621.374.32 3850
A Direct-Reading Counting-Rate Ratio Meter—H. Miwa. (*J. Phys. Soc. Japan*, vol. 11, pp. 458–462; April, 1956.) A nonlogarithmic instrument for determining the ratio between two radiation-counting rates comprises a sawtooth voltage generator whose output is proportional to the period of one pulse train and is used to modulate the height of rectangular pulses synchronized with the second pulse train.

621.398 3851
Bandwidth Requirements of F.M./F.M. Telemetering—J. C. Carpenter, Jr. (*Tele-Tech. and Electronic Ind.*, vol. 15, pp. 79, 147; May, 1956.)

621.385.833 3852
Handbuch der Physik, Band 33: Korpuskularoptik [Book Review]—S. Flügge (Ed.). Springer, Berlin, 702 pp., D.M. 122.50. 1956. (*Nature, Lond.*, vol. 178, pp. 285–286; August 11, 1956.) A comprehensive treatment of the optics of charged particles and of the electron microscope.

PROPAGATION OF WAVES

621.396.11:551.510.5 3853
Turbulent Mixing Theory applied to Radio Scattering—R. A. Silverman. (*J. Appl. Phys.*, vol. 27, pp. 699–705; July, 1956.) Scattering due to refractive-index fluctuations in the troposphere and ionosphere is discussed using statistical theory developed by Obukhov (1928 of 1949) and applied by Krasil'nikov (2024 of 1949). For the ionospheric case, the theoretical results are in order-of-magnitude agreement with the observed scattered power if the refractive-index fluctuations are attributed to electron-density fluctuations produced by turbulent mixing at the lower edge of the E layer. For the tropospheric case, order-of-magnitude agreement is obtained, except for the summer months, by attributing the refractive-index variations to temperature variations. Humidity and its fluctuations are important during the summer and at low scattering heights. The results are compared with those obtained by Villars and Weisskopf (244 of 1956).

621.396.11:551.510.535 3854
Ionospheric Prediction Methods and the Probable Sources of Error—S. S. Baral. (*Indian J. Phys.*, vol. 30, pp. 189–205; April, 1956.) Methods in current use for forecasting ionospheric characteristics are reviewed. An indication is given of the reduction of errors to be expected as greater accuracy is achieved in forecasting sunspot numbers and diurnal and seasonal variations, and in estimating geographical variations.

621.396.11:551.510.535 3855
Equatorial Ionospheric Absorption—N. J. Skinner and R. W. Wright. (*J. Atmos. Terr. Phys.*, vol. 9, pp. 103–117; August/September, 1956.) Vertical-incidence absorption measurements made at Ibadan during the period December 1953–December 1954 are studied. Nonderivative absorption appears to vary inversely with frequency; total absorption varies as $(\cos \kappa)n$, where κ is the sun's zenith distance and n is about 0.7. These variations are accounted for by assuming that the nonderivative absorption takes place in a Chapman-type D layer at a level where the electron collision frequency is of the same order as the angular frequency of the exploring signal. The frequency and seasonal variations at Singapore are similar to those at Ibadan.

621.396.11:551.510.535:537.533.1 3856
Theory of Nonlinear Effects in the Ionosphere—S. A. Zhevakin and V. M. Fain. (*Zh. Eksp. Teor. Fiz.*, vol. 30, pp. 518–527; March, 1956.) A theory of the Luxemburg and other nonlinear effects is developed on the basis of work noted in 79 of 1956 (Fain). The self-demodulation effect [*e.g.*, 1167 of 1954 (Cutolo)] could be utilized in an experimental determination of the effective electron-collision frequency.

621.396.11.029.51.08 3857
Low-Frequency Ground Waves. Equipment for the Measurement of the Phase Change with Distance—G. E. Ashwell and C. S. Fowler. (*Wireless Eng.*, vol. 33, pp. 245–250; October, 1956.) "The equipment described was developed to investigate the phase change with distance of a low-frequency wave passing over ground of finite conductivity and, in particular, the changes that occur near a boundary between grounds of different conductivities or across a coastline. The method employs an uhf link between a fixed monitor station and a mobile measuring station to provide a reference signal against which the phase of the low-frequency signal is compared at the measuring station. The equipment is capable of operating over distances of up to 50 km and measures the phase to an accuracy of 2° at a frequency of 127.5 kc."

621.396.11.029.53/.55:523.78 3858
Sweep-Frequency Oblique-Incidence Experiments over a Distance of 1320 km—H. G. Möller. (*J. Atmos. Terr. Phys.*, vol. 9, pp. 155–156; August/September, 1956.) A preliminary note giving the main results of an investigation into the effects of the solar eclipse of June 30, 1954 on propagation between Lindau and Helsinki.

621.396.11.029.55 3859
An Estimate of the Size of the Antipodal Area in Short-Wave Radio Propagation—H. A. Whale. (*J. Atmos. Terr. Phys.*, vol. 9, pp. 159–161; August/September, 1956.) From measurements made at Seagrove, Auckland, N.Z., of the elevation and bearing angles of arrival of transmissions on a frequency of 14.975 mc from Slough, England, it is deduced that the antipodal area was about 550 km in radius, centered on the geometric antipodal point.

621.396.11.029.6 3860
Extended Transmission Ranges at Metre, Decimetre and Centimetre Wavelengths—H. Poeverlein. (*Z. Angew. Phys.*, vol. 8, pp. 244–254; May, 1956.) A survey of typical modes of propagation giving rise to extended-range reception; over 60 references.

621.396.11.029.64 3861
Radio Transmission Experiments of Microwaves over the Sea—M. Onoue, M. Nenohi, R. Usui, and H. Irie. (*J. Radio Res. Labs, Japan*, vol. 3, pp. 141–147; April, 1956.) Measurements of signal strength and direction of arrival for transmissions on a frequency of 9.375 kmc, over a distance of 77 km during the period September 1954–September 1955 are reported. Duct propagation is indicated.

621.396.11.029.65:535.343.4 3862
Measurement of Atmospheric Attenuation at Millimeter Wavelengths—A. B. Crawford and D. C. Hogg. (*Bell Syst. Tech. J.*, vol. 35, pp. 907–916; July, 1956.) Technique is described in which a variable-frequency oscillation from a klystron generator is radiated from a horn antenna and reflected back by a pair of spaced corner reflectors whose relative reflecting properties are known. Absorption measurements in the wavelength range 5–6 mm are reported; the results are in good agreement with Van Vleck's theory of oxygen absorption (3098 of 1947).

621.396.812.3:551.510.535 3863
Study of the Selective Fading appearing on the *fct*-Traces—H. Uyeda and Y. Nakata. (*J. Radio Res. Labs, Japan*, vol. 3, pp. 119–133; April, 1956.) Records of the variation of critical frequency with time for the F_2 and E_s layers show evidence of selective fading caused by interference between waves reflected from the sides of riples in the layers. The mechanism of the fading and its bearing on layer structure are discussed.

RECEPTION

621.396.621:621.376.3:621.317.32 3864
Measurements of Interference Radiation from F.M. Receivers, carried out in Switzerland by a Group of Experts of the International Electrotechnical Commission Subcommittee 12-1 (Radio Communications—S. C. Measurements)—Meyer de Stadelhofen. (See 3826.)

621.396.621:621.376.33 3865
F.M. Receiver Design—L. W. Johnson. (*Wireless World*, vol. 62, pp. 497–502; October, 1956.) Methods are reviewed for improving the capture ratio of fm receivers, with the object of overcoming multipath, co-channel and other types of interference. The bandwidth required in the circuits following the limiter depends on the desired capture ratio as well as on the frequency deviation. Principles developed at the Massachusetts Institute of Technology are explained and their application in receiver design is illustrated. Desirable characteristics can be obtained by use of wide-band modifications of the ratio detector in conjunction with preceding limiters. Use of the Type-6BN6 gated-beam tube simply as a limiter is recommended. Locked-oscillator and counter-type detectors are also discussed.

621.396.621.54 3866
Alignment Problems with Tuned Circuits in Superheterodyne Receivers—W. Rotkiewicz. (*Hochfrequenztech. u. Elektroakust.*, vol. 64, pp. 144–154; April, 1956.) Design formulas are derived for the rf and oscillator circuits. A method is developed in which the alignment errors are analyzed first and the tuned circuits are then calculated. The interaction between a fixed-tuned primary and a variable-tuned secondary circuit is considered in relation to the alignment.

621.396.82+621.397.82 3867
Radio and Television Interference—M. Smith. (*J. Brit. Instn Radio Engrs*, vol. 16, pp. 444–449. Discussion, pp. 449–452; August, 1956.) "A survey is given of the principal causes of interference to domestic radio and television; methods of detection and suppression of the various types of interference are also described, with particular reference to the work of the British Post Office investigating branch."

621.396.821:551.594.6 3868
The Level of Interference due to Atmospherics in the Very-Long-Wave Range, and its Diurnal and Seasonal Variations—E. A. Lauter. (*Z. Met.*, vol. 10, pp. 110–121; April, 1956.) Measurement procedure and definitions are discussed on the basis of observations of the frequency distribution of atmospherics at Kühlungsborn and the geographical distribution of the sources. Observations made over the period 1952–1954 on frequencies of 14, 27 and 48 kc are analyzed and correlated with ionospheric propagation conditions. Results indicate that in winter the frequency dependence of the propagation conditions is the predominating influence on the diurnal variation of the atmospherics level, whereas in summer the approach of the disturbance centers is is more important. Interdiurnal variations, twilight effect, and solar-flare effect are mentioned briefly.

621.396.822:621.317.6 3869
Calculating Noise Level in Radar Receivers—Haney. (See 3828.)

621.396.822:621.396.96:621.396.62 3870
Technical Possibilities for Noise Reduction in the Reception of Weak Radar Signals—Borg. (See 3743.)

STATIONS AND COMMUNICATION SYSTEMS

621.39:534.7 3871
Speech Communication Research Symposium—(See 3608.)

621.39:534.78 3872
The Intelligibility of Amplitude-Limited Speech—Schneider. (See 3614.)

621.39:534.78 3873
A Development of the Collard Principle of Articulation Calculation—D. L. Richards and R. B. Archbold. (*Proc. IEE*, vol. 103, pp. 679–691; September, 1956.)

621.39:534.78 3874
Bandwidth and Channel Capacity Necessary to transmit the Formant Information of Speech—J. L. Flanagan. (*J. Acoust. Soc. Amer.*, vol. 28, pp. 592–596; July, 1956.)

621.39.001.11 3875
A New Interpretation of Information Rate—J. L. Kelly, Jr. (*Bell Syst. Tech. J.*, vol. 35, pp. 917–926; July, 1956.)

621.39.001.11 3876
Interference Stability of Systems with Correcting Codes—V. I. Siforov. (*Radiotekhnika i Elektronika*, vol. 1, pp. 131–142; February, 1956.) Relations are derived connecting the interference stabiility of communication systems with the parameters of the correcting codes used.

621.395.97:621.395.82 3877
The Influence of Long-Wave Transmissions on High-Frequency Diffsusion of Programs on Overhead Telephone Lines—R. Kallen. (*Tech. Mitt. Schweiz. Telegr.-Teleph-Verw.*, vol. 34, pp. 145–157; April 1, 1956. In German.) An investigation was made of the possibility of improving signal/noise ratio while retaining the use of ordinary unstranded conductors. Both from theoretical considerations and from measurements, it appears that artificial balancing of the overhead lines would be ineffective. Arrangements for obtaining the best inherent symmetry are indicated.

621.396.41:621.376.55 3878
New Developments in Time-Sharing Multiplex Systems for Regional [radio] Telephone Links—L. J. Libois. (*Électronique*, pp. 18–23; April, 1956.) For short-distance links, time-sharing systems with up to 24 channels are suitable. An AM carrier of 2 km cps or a fm carrier of 7 km cps is used in conjunctoin with p.p.m. The pulse waveform is symmetrical about zero, thus there is no dc component; this waveform is advantageous as regards signal /noise ratio. Appropriate transmitting and receiving equipment is outlined; a common antenna is used. The performance is adequate for transmission over some hundreds of km, using a number of sections. Systems of this type have been provisionally standardized by the C.C.I.R.; a link is installed between Bagnères-de-Bigorre and the Pic du Midi, about 15 km away.

621.396.65.029.62:621.396.41 3879
A Long-Distance V.H.F. Radio Link—P. Brocklesby and P. Robinson. (*A.T.E. J.*, vol. 12, pp. 78–88; April, 1956.) Four separate radio links on frequencies between 40 and 50 mc are provided over a 200-mile path between the Shetlands and Norway, the path attenuation being 155 db with 20 db fading. Twelve fm carrier channels and four service channels are available, with a maximum modulation frequency of 12.2 kc.

621.396.712.3:534.86 3880
Modern Broadcasting Studios: Marseilles—Pujolle. (See 3625.)

621.396.813:534.861 3881
The Receiving Side of a Radio Broadcast Transmission and its Influence on the Audio-Frequency Bandwidth—W. Ebert. (*Tech. Mitt. Schweiz. Telegr.-TelephVerw.*, vol. 34, pp. 166–171; April 1, 1956. In German.) The effect of the different parts of the transmission chain on reproduction quality, previously discussed by Furrer *et al.* (1787 of 1949), is reassessed in relation to fm vhf systems. The loudspeaker still constitutes the most critical element from the point of view of bandwidth. It seems unlikely that any substantial improvement of quality would result if the af transmission band were increased from 10 to 15 kc, except in the case of receivers equipped with suitable loudspeaker combinations.

621.396.93:621.396.6 3882
Generation of Transmission and Local-Oscillator Frequencies in [mobile] Transmitters and Receivers—F. Läng. (*Bull. Schweiz. Elektrotech. Ver.*, vol. 47, pp. 458, 467–475; May 12, 1956.) Frequency-stability requirements are formulated on the basis of an examination of the effects of instability on signal/noise ratio and transmission quality. Only fm and phm systems for the frequency band 30–500 mc are considered. Methods of deriving the transmission frequency from quartz oscillators are outlined. Problems connected with channel switching and with the production of parasitic frequencies are discusssed.

621.396.93.029.51:621.314.7 3883
Transistor-Operated Personnel Paging System—(*Brit. Commun. Electronics*, vol. 3, pp. 252–253; May, 1956.) The system comprises a 25-w transmitter, crystal-controlled on any one of up to 50 channels and feeding a loop surrounding the building, together with up to 50 pocket-size selective transistor receivers. The frequency band used is 75–87 kc; channel separation is 250 cps. Apparatus serving a similar purpose is described in *Wireless World*, vol. 62, pp. 520–521; November, 1956.

621.396.931.029.62 3884
Mobile Radio Development—J. R. Humphreys. (*Wireless World*, vol. 62, pp. 481–485; October, 1956.) The problem of channel congestion in the 71.5–88 and 156–184-mc bands in the U.K. is reviewed with reference to the impending reduction of the upper limit to 174 mc. Frequency stability, permitted power, geographical spacing of stations and the use of split channels are discussed in relation to equipment design for a suggested basic channel spacing of 25 kc.

621.396.933 3885
Symposium on Aeronautical Communications—(IRE TRANS., vol. CS-4, pp. 3–143; May, 1956.) The text is given of 17 papers presented at a symposium held at Utica, N. Y., in November, 1955. Abstracts of most of these papers are given in PROC. IRE, vol. 44, pp. 954–955; July, 1956.

SUBSIDIARY APPARATUS

621.311.6:537.311.33:535.215 3886
Theoretical Considerations governing the Choice of the Optimum Semiconductor for Photovoltaic Solar-Energy Conversion—Loferski. (See 3769.)

621.311.6:621.373.52:621.397.6 3887
C.R.T. Power Supply uses Transistor Oscillator—P. M. Toscano and J. B. Heffner.

(*Electronics*, vol. 29, pp. 162–165; September, 1956.) A 12.5-kc positive-feedback oscillator using a Ge transistor provides an output voltage which is doubled, rectified and stabilized at 10 kv. A collector supply of −30 v is the only external power required. For 1-ma output current the over-all efficiency is 64 per cent.

621.314.6 3888

Characteristics for Half-Wave Rectifier Circuits—H. A. Enge. (*Electronic Eng.*, vol. 28, pp. 401–406; September, 1956.) "Voltage regulation characteristics, form factor, first harmonic, and peak current values are given for half wave rectifiers with common type loads. All in nondimensional variables."

621.314.63:546.28 3889

Silicon Junction Power Diodes—D. E. Mason, A. A. Shepherd, and W. M. Walbank. (*J. Brit. Instn. Radio Eng.*, vol. 16, pp. 431–441; August, 1956.) Simplified semiconductor theory is presented and a description is given of three main methods of making *p-n* junction diodes and of the properties of the diodes. Advantageous features and appropriate applications of these rectifiers are indicated.

621.316.722.1:621.311.6 3890

Wide-Range Voltage Stabilizers—F. A. Benson and L. J. Bental. (*Electronic Eng.*, vol. 28, pp. 390–394; September, 1956.) A unit is described, based on a circuit by Admiral (863 of 1954), which gives a stabilized output voltage adjustable within the range 0–300 v, with maximum load current of 180–200 ma; the stabilization ratio is about 2000.

TELEVISION AND PHOTOTELEGRAPHY

621.397.242 3891

The Broadcasting House Crystal Palace Television Link—A. R. A. Rendall and S. H. Padel. (*Proc. IEE*, vol. 103, pp. 644–650. Discussion, pp. 663–666; September, 1956.) This 9-mile link uses two 0.975-in. coaxial cables and provides two channels in each direction, only one of which is required initially. The system is dsb AM, and the carrier frequency is 15 mc. The performance of the link is given in terms of the amplitude and differential-delay characteristics, transient response, linearity and signal/noise ratio.

621.397.6.001.4:621.317.74 3892

Portable Color-Signal Generator—Popkin-Clurman. (See 3834.)

621.397.62:535.623:621.385.832 3893

The "Apple" Television System—(PROC. IRE, vol. 44; September, 1956.) Fuller details of the receiver described previously (3232 of 1956) are given in the following there papers:

A New Beam-Indexing Color-Television Display System—R. G. Clapp, E. M. Creamer, S. W. Moulton, M. E. Partin, and J. S. Bryan (pp. 1108–1114).

A Beam-Indexing Color Picture Tube—the Apple Tube—G. F. Barnett, F. J. Bingley, S. L. Parsons, G. W. Pratt, and M. Sadowsky (pp. 1115–1119).

Current Status of Apple Receiver Circuits and Components—R. A. Bloomsburgh, W. P. Boothroyd, G. A. Fedde, and R. C. Moore (pp. 1120–1124).

621.397.621.2:535.623:621.385.832 3894

An Analysis of Focusing and Deflection in the Post-Deflection-Focus Color Kinescope—C. P. Carpenter, C. W. Helstrom, and A. E. Anderson. (IRE TRANS., vol. ED-2, pp. 1–7; October, 1955.) Color-television picture tubes are considered in which an array of parallel wires close to the phosphor screen is used for focusing the beam and for deflecting it up and down to produce the color changes. Expressions are derived for the deflection sensitivity and the focusing properties; the variation over the grid plane is shown by contour maps. The theoretical results are supported by observations.

621.397.7:621.396.67.029.62 3895

The Crystal Palace Television Transmitting Station—F. C. McLean, A. N. Thomas, and R. A. Rowden. (*Proc. IEE*, vol. 103, pp. 633–643. Discussion, pp. 663–666; September, 1956.) Factors underlying the siting, planning, and design of the station are indicated and an account is given of steps taken to attain a high standard of reliability. The self-supporting antenna tower has a total height of 668 ft; the radiating elements are single dipoles for the upper half of the antenna and double dipoles for the lower half; antenna performance figures are given. For a shorter account see 2896 of 1956.

621.397.82+621.396.82 3896

Radio and Television Interference—Smith. (See 3867.)

TUBES AND THERMIONICS

621.314.63:621.372.632 3897

Two-Terminal *P-N* Junction Devices for Frequency Conversion and Computation—A. Uhlir, Jr., (PROC. IRE, vol. 44, pp. 1183–1191; September, 1956.) "Design principles for semiconductor diodes are derived from the analysis of idealized *p-n* junctions. The analysis gives the superheterodyne conversion matrix and the large-signal admittance in terms of the small-signal diffusion admittances. Structures that minimize minority-carrier storage give minimum conversion loss under matched conditions in converting a high frequency to a low frequency, and are useful in logic circuits of computers. Examples are the emitter-base diode of a transistor and a small bonded or point contact. Amplification and improved power-handling capabilities can be obtained in converting a low frequency to a high frequency, if the geometry favors storage of minority carriers near the junction. Such structures can also be used as pulse amplifiers."

621.314.7:546.28:621.375.4 3898

Micro-power Operation of Silicon Transistors—E. Keonjian. (*Tele-Tech and Electronic Ind.*, vol. 15, pp. 76–78, 142; May, 1956.) Characteristics are presented for Si transistors at power levels of a few μW over the temperature range −25° to +75°C. An experimental two-stage audio amplifier is described having an output power of 10 μW, with over-all gain of 37 db within ± 3 db over the range 20 cps–20 kc; current consumption is 65 μA from a supply of 1.5 v.

621.314.7:621.318.57 3899

***P-N-P-N* Transistor Switches**—J. L. Moll, M. Tanenbaum, J. M. Goldey, and N. Holonyak. (PROC. IRE vol. 44, pp. 1174–1182; September, 1956.) Discussion of the design, manufacture, and electrical characteristics of Si transistors with $\alpha > 1$, for switching purposes. Over the high-impedance portion of the characteristic the impedance depends chiefly on the capacitance of the junctions, which is of the order of tens of $\mu\mu$f. Over the low-impedance portion, the slope resistance is a few ohms. Suitable methods of manufacture include combinations of solid diffusion and alloying. Possible applications to function generators, relays, etc. are mentioned.

621.385.832:621.397.62:535.623 3900

The "Apple" Television System—(See 3893.)

621.385.832:621.397.621.2:535.623 3901

An Analysis of Focusing and Deflection in the Post-Deflection-Focus Color Kinescope—Carpenter, Helstrom, and Anderson. (See 3894.)

MISCELLANEOUS

621.3.049.75 3902

Printed Circuits—(*Tele-Tech and Electronic Ind.*, vol. 14, pp. 68, 149; December, 1955.) This issue is a special one devoted largely to printed circuits; papers are given on the production of individual components and subassemblies, edge-dip soldering, assembly systems and special laminates; a directory of U.S.A. firms manufacturing printed circuits and related products is included.